

https://dspace.org/

Synthesis and performance evaluation of Polyethersulphone membrane infused with Chitosan and coated with Polyamide layer for acid mine drainage treatment

Jeremia, Mathaba Machodi

2020

https://hdl.handle.net/10539/31331

Jeremia, Mathaba Machodi. (2019). Synthesis and performance evaluation of Polyethersulphone membrane infused with Chitosan and coated with Polyamide layer for acid mine drainage treatment. University of the Witwatersrand, https://hdl.handle.net/10539/31331

Downloaded from a DSpace repository. https://dspace.org/



Synthesis and Performance Evaluation of Polyethersulphone Membrane Infused with Chitosan and Coated with Polyamide Layer for Acid Mine Drainage Treatment

Mathaba Machodi Jeremia

A dissertation submitted to the faculty of Engineering and the Built Environment, University of the Witwatersrand, Johannesburg, in fulfilment of the requirements for the degree of Doctor in Philosophy in Engineering

Supervisor: Professor M.O Daramola

March 2020

Declaration

I declare that this dissertation is my own unaided work. It is being submitted for the degree of Doctor of Philosophy in Engineering to the University of the Witwatersrand, Johannesburg, South Africa. It has not been submitted for any degree or examination to any other University

……

(Signature of candidate)

……day of……2020

(Day) (Month) (Year)

Abstract

Membrane technology has emerged as an alternative technology for the treatment of acid mine drainage (AMD) over conventional methods because they either produce large volume of toxic sludge and pose a secondary pollution or they achieve partial treatment. Polymeric materials have gained enormous attention for membrane synthesis application due to their non-toxic and biodegradable properties. Polyethersulphone (PES) and polysulphone (PSf) based membranes have gained significant progress in AMD treatment because of their high chemical and thermal resistance, mechanical stability in hot and wet conditions and high permeability. Although PES exhibits higher degree of hydrophilicity compared to PSf, its inherent hydrophobic character generated by the sulfonyl group linking the two phenyl rings results in serious membrane fouling which leads to deterioration in permeation flux, shortening of the membrane lifespan and producing unpredictable separation efficiencies. To this effect, several interventions have been made to increase PES membrane's hydrophilicity to avoid quick membrane deterioration, enhance low fouling character and the ability to restore water flux after cleaning during wastewater treatment.

This study proposed infusing chitosan within PES membrane by blending chitosan with PES suspension and coating the surface with polyamide layer via the co-solvent assisted interfacial polymerization technique to enhance its antifouling character and permselectivity. This modification aims to localize the hydrophilic materials on the membrane surface and within the pores to positively influence membrane flux and selectivity. The study investigated the effect of chitosan content inside the PES membrane matrix on its performance during synthetic AMD treatment. It further explored the effect of coating polyamide layer on the PES membranes infused with chitosan. The fouling and operational stability of the optimized PES/chitosan and PES/chitosan/PA membranes were evaluated.

Chitosan used in the study was derived from chitin through deacetylation process, which is treating chitin with a strong alkaline solution. Chitin is the second most abundant polymer after cellulose and is naturally occurring in the exoskeletons of arthropods. Chitosan contains one primary amino and two free hydroxyl functional groups which can act as contaminate binding sites. Effect of temperature and strength sodium hydroxide solution on chitosan's degree of deacetylation was investigated. The experimental results showed that higher NaOH concentration (40% NaOH) promotes degradation of acetyl group and exposure of amine groups, thus increasing chitosan's degree of deacetylation. They further showed that temperature of 100 ^{o}C was enough to induce enough energy to cause degradation of acetyl groups. As such, higher degree of deacetylation of 96% was achieved with NaOH concentration of 40% and temperature of 100 ^{o}C.

The research also investigated the influence of chitosan content on the performance of the synthesised membranes during synthetic AMD treatment. Permeate flux of pristine PES membrane was increased from 97 to 102 and 133L/m^2.hr when chitosan content was 0.5 and 0.75 wt%, respectively. This was attributed to the increased hydrophilic character of chitosan used to modify the membrane. When chitosan was increased further to 1wt%, it induced a flux decline to 116 L/m^2.hr. Chitosan loading of 0.75 wt% was selected for further investigations. Coating polyamide layer on the PES/chitosan membrane revealed that permeability increased with increasing chitosan content. This behaviour was attributed to the fact that, the interaction of chitosan's amine group and PA active layer's unreacted acylchloride group created a thin layer on the membrane surface. Moreover, amine groups which could not interact with unreacted acylchloride groups favoured sorption of water molecules by the membrane. This behaviour showed that higher chitosan's degree of deacetylation enhanced membrane permeability and selectivity.

Influence of operational parameters was also investigated. Literature has shown that pH values corresponding to a peak in flux reporting the lowest rejection of ions by a membrane indicates the isoelectric point (IEP) or zero potential charge of the membrane. Similar behaviour for both PES/chitosan and PES/chitosan/PA membranes was observed at a pH of around 5.5. Therefore, it was concluded that the IEP of the membranes was at a pH of 5.5. Moreover, it was concluded that the surface charge of both PES/chitosan and PES/chitosan/PA membranes becomes positive at pH lower than 5.5 and at pH above 5.5 have negative charges. It was observed that cation rejection was high when pH was lower than IEP and anion removal was high at pH values higher than IEP. Coating polyamide layer onto the PES/chitosan membrane to produce PES/chitosan/PA membrane introduced amide, amines, carboxylic and alcoholic functional groups. It was observed that, rejection of ions by PES/chitosan/PA membranes was slightly higher than that of PES/chitosan membranes and this was due to increased number of available functional groups provided by polyamide. Investigation of initial feed concentration and pressure is very essential to assess the applicability range and determine optimum conditions for an efficient membrane separation operation. The experimental results showed that membrane flux was increasing with increasing pressure and this was due to increased forces which forces water molecules through the membrane. Moreover, solutions with low concentration reported high permeated flux due to low number of ions being trapped on the membrane surface and subsequently blocking the pores and forming a layer obstructing flow. Rejection experimental tests showed that rejection increased with increasing pressure and significantly reduced with increasing initial ions concentrations.

Lastly, after optimizing chitosan loading and its degree of deacetylation to synthesise PES/chitosan and PES/chitosan/PA membranes, operational stability and fouling potential of the membranes were investigated using real industrial AMD. When pure water was filtered through the membranes after AMD permeation, the new pure water flux reported 14 and 27%

loss of the initial flux for PES/chitosan and PES/chitosan/PA membrane, respectively. After backwashing, it was evidently clear that the initial flux of the membranes was almost restored with only 1.7 and 2% loss of flux compared to the original fluxes of PES/chitosan and PES/chitosan/PA membranes, respectively. The fouling experimental data confirmed superior characteristics of PES/chitosan and PES/chitosan/PA membranes against fouling. Hermia's filtration models fitted with the experimental deduced that the dominating fouling mechanisms taking place during filtration of AMD through PES/chitosan and PES/chitosan/PA membranes are complete and cake or gel layer formation blocking models.

The results obtained from this research demonstrated outstanding antifouling and permselectivity properties of PES membranes infused with chitosan and coated with polyamide layer. These findings further provide a basis for scale-up operation to test the membranes against the traditional technologies for AMD treatment.

Acknowledgement

Firstly, I would to thank the Lord Almighty for the gift of life and all opportunities he has given me.

I am very grateful for the unconditional support afforded to me by my supervisor Prof. M.O Daramola and for allowing me to purse my doctoral studies under his supervision. Thank you for the tremendous dedication and knowledge during the course of this research work. I am truly grateful, and may God continue to bless him in abundance.

Thank you to the University of the Witwatersrand for allowing me to register my doctoral degree with their institution.

Many thanks to the Department of Chemical Engineering and Applied Chemistry at the University of Johannesburg for all the support offered. Thank you for availing your facilities and laboratories to conduct experiments and analysis.

My very warm thanks to my family for the moral support offered as and when I needed it. Special appreciation to my mother, who supported me from childhood as a single parent after the passing of my late Father in 1995. She inspired me to prioritize education and God at all times. This PhD is dedicated to her commitment and dedication in fulfilling her parental duties. I thank friends and mentors for their support and belief in my ability to succeed in all my endeavours.

This research was made possible by the funding provided by the National Research Foundation (NRF) organization. I would like to express my sincere humble appreciation and gratitude.

Last but not least, I also thank colleagues in my research group for the constructive criticism of my work which aided me to improve, their support and friendship

Dedication

This dissertation is dedicated to my mother Maria Mamokone Mathaba

Thank you for always believing in me and seeing beyond my best at all times. Your words of encouragement and always giving me hope to make you proud inspire my ability to always be better than my best.

Publications from the study

Few publication which have emanated from this research project are listed below

1. **Machodi, M.,** Daramola, M.O. (2019) Sodalite and Chitosan based Composite Membrane Materials for Treatment of Metal-containing Wastewater in Mining Operations In: Water Management: Social and Technological Perspectives (I Mutjaba, M .K. Amosa and T. Majozi, eds.), CRC Press, pp.169-189 (978-1-1380-6724-0).

2. **Mathaba, M.J,** Daramola, M.O (2019). Synthesis and performance evaluation of PES/chitosan membranes coated with polyamide for acid mine drainage treatment. *Sci Rep*, 9: 17657 doi:10.1038/s41598-019-53512-8

3. **Mathaba, M.J,** Daramola, M.O (2020). Synthesis of PES and PES/Chitosan membranes for acid mine drainage treatment. Water SA, 46(1):114-122

4. **Mathaba, M.J,** Daramola, M.O (2020). Antifouling property and operational stability of PES membrane infused with chitosan and coated with polyamide during AMD treatment, Membrane(in press).

Table of Contents

Declaration i
Abstract ii
Acknowledgement vi
Dedication vii
Publications from the study viii
List of Figures xiii
List of Tables xviii
Abbreviations xix
Chapter 1 Introduction 1
1.1 Background and Motivation 1
1.2 Research questions 7
1.3 Research aim and objectives 7
1.4 Research outputs and outcomes 8
1.5 Thesis outline 9
Chapter 2 Literature review 11
2.1 Introduction 11
2.2 History of gold mining in South Africa 11
2.3 Gold Extraction 13
2.4 Mining tailings 16
2.5 Ground water pollution and AMD seepage 17
2.6 Acid mine drainage (AMD) 19
2.6.1 Formation of AMD 19
2.6.2 Effect of AMD 22
2.6.3 AMD in Johannesburg 23
2.6.4 AMD in Tweelopies Spruit River 25
2.7 Treatment of AMD 31
2.7.1 Active treatment 31
2.7.2 Passive treatment 33
2.7.3 Ion exchange technology 34
2.8 Membrane technology 35
2.8.1 Membrane types 35
2.8.2 Membrane aspects 38
2.8.3 Membrane material 40
2.8.4 Membrane preparation methods 41

2.8.5 Membrane Modification 43
2.8.6 Polyethersulphone membrane 45
2.9 Hermia's models adapted to crossflow filtration 59
2.10 Summary 66
Chapter 3 Experimental Procedure and Materials 68
3.1 Introduction 68
3.2 Material and Chemicals 69
3.3 Apparatus 69
3.4 Experimental methodology summary 70
3.5 Chitosan production from chitin 72
3.6 Membrane synthesis 74
3.6.1 Synthesis of Pure PES 74
3.6.2 Synthesis of PES membrane infused with chitosan (PES/chitosan membrane) 75
3.6.3 Fabricating Polyamide layer 77
3.7 Characterization of physicochemical properties of synthesized chitosan particles, pure PES, PES/chitosan and PES/chitosan/PA membranes 78
3.7.1 Thermogravimetric Analysis (TGA) 78
3.7.2 Particle size distribution (PSD) 78
3.7.3 Fourier-Transform Infrared (FTIR) spectroscopy 79
3.7.4 Scanning Electron Microscopy (SEM) 80
3.7.5 Contact angle analysis 80
3.7.6 Mechanical strength analysis 81
3.7.7 Bulk porosity 81
3.8 Membrane performance evaluation 82
3.8.1 Dead-end filtration setup 82
3.8.2 Crossflow filtration tests 85
3.9 Fouling and operational stability experiments 87
Chapter 4 Effect of chitosan and polyamide layer on the quality and performance of the synthesized PES/chitosan and PES/chitosan/PA membranes 89
4.1 Introduction 89
4.2 Chitosan production from chitin 90
4.3 Characterization 91
4.3.1 FTIR 91
4.4 Effect of chitosan loading on the quality and performance of produced PES/chitosan and PES/chitosan/PA membranes during AMD treatment 92
4.4.1 Physicochemical properties of the synthesized PES/chitosan and PES/chitosan/PA membranes 92

4.4.2 Membrane Performance Investigation 108
4.5 Summary 121
Chapter 5: Effect of chitosan's degree of deacetylation on the performance of the synthesized PES/chitosan and PES/chitosan/PA membranes 124
5.1 Introduction 124
5.2 Synthesis of chitosan with different degree of deacetylation 125
5.3 Characterization 125
5.3.1 Yield (%) 125
5.3.2 FTIR analysis 127
5.3.3 PSD of chitosan samples 130
5.4 Effect of chitosan synthesis process on the degree of deacetylation (DD) 131
5.5 Effect of chitosan degree of deacetylation (DD) on the quality and performance of PES/chitosan and PES/chitosan/PA membranes 134
5.5.1 Characterization of the synthesized membranes 134
4.5.2 Evaluation of membrane performance 145
5.6 Summary 162
Chapter 6: Operational stability and antifouling property of the membranes 166
6.1 Introduction 166
6.2 Membrane synthesis 166
6.3 AMD sampling and characterization 167
6.4 Fouling experiments 180
6.4 Summary 191
Chapter 7: General conclusions and recommendations 194
7.1 Conclusions 194
7.2 Recommendations 199
References 201
Appendices 231
Appendix A: Synthesis and characterization of chitosan 231
A1: Calculation for chitosan percentage yield 231
A2: FTIR graphs of the synthesized chitosan samples 233
A3: PSD results for the synthesized chitosan samples 236
Appendix B: Membrane synthesis and characterization 239
B1: FTIR graphs for synthesized PES/chitosan membranes 239
B2: FTIR graphs for synthesised PES/chitosan/PA membranes 244
B3: TGA Raw data for the PES/chitosan samples 249
B4: TGA Raw data for the PES/chitosan/PA samples 251

Appendix C: Information about membrane performance evaluation 254
C1: Effect of chitosan degree of deacetylation on rejection of PES/chitosan membranes 254
C2: Effect of chitosan degree of deacetylation on rejection of PES/chitosan membranes 256
C3: Effect of feed pH on the rejection of PES/chitosan membranes 258
C4: Effect of feed pH on the rejection of PES/chitosan/PA membranes 259
C5: Effect of feed pH on the flux of PES/chitosan membranes 262
C6: Effect of feed pH on the flux of PES/chitosan/PA membranes 263
C7: Effect of initial concentration and feed pressure for PES/chitosan membrane 263
C8: Effect of initial concentration and feed pressure for PES/chitosan/PA membrane 265
C9: The pumping station in western basin which real industrial AMD was collected 266
Appendix D: Plagiarism report 267
Appendix E: Permission to use Material in the thesis 269
Appendix F: Publications 278

List of Figures

Figure 1.1: Acidic water level rise in Randfontein, West Rand ……..3

Figure 2.1: Location map of the Witwatersrand Basin and its major goldfields...……...13

Figure 2.2: Typical mineral processing operation flow-chart ……14

Figure 2.3: Manual hydraulic monitor on a tailing facility in South Africa…...…….16

Figure 2.4: Mine tailings storage dams in Johannesburg…….....17

Figure 2.5: Stream contaminated with AMD……..23

Figure 2.6: Scientific publication (books, book Chapters, articles and conference proceedings) on acid mine drainage in South Africa…….....24

Figure 2.7: Map showing the river network in South Africa……...……...26

Figure 2.8: Google Map showing the Black Reef Incline, 18 and 17……...….…….26

Figure 2.9: Map showing the location of the survey sites and watercourses…….....28

Figure 2.10: Spatial changes observed for selected parameters between the survey sites……..30

Figure 2.11: Pressure driven membranes…….……36

Figure 2.12: Schematic illustration of interfacial polymerization…….……..43

Figure 2.13: Polyethersulphone structure (PES)…….....46

Figure 2.14: Structure of (a) Chitin and (b) Chitosan…….49

Figure 2.15: Conventional Interfacial polymerization and modification with chitosan…….……...57

Figure 2.16: Schematic representation of conventional IP and CAIP using acetone…….59

Figure 2.17: Schematic of membrane fouling mechanisms of the filtration laws……..60

Figure 3.1: Overall flow diagram showing the summary of the experimental procedure…….....71

Figure 3.2: Steps followed to synthesis Pure PES membrane……...……..75

Figure 3.3: Steps followed to synthesis PES membrane infused with chitosan….....76

Figure 3.4: Steps followed to synthesis PES membrane infused with chitosan….....77

Figure 3.5: Dead end filtration setup……...85

Figure 3.6: Fouling experiments procedure…….……....88

Figure 4.1: FTIR spectrum of chitosan synthesised from chitin……...…….91

Figure 4.2: Particle size distribution of the synthesised chitosan…….....94

Figure 4.3: SEM images showing surface morphology and cross-section of (a and b) PES, (c and d) PES/ 0.5 wt% chitosan, (e and f) PES/0.75 wt% chitosan and (g and h) PES/1 wt% chitosan membranes……..……...96

Figure 4.4: SEM images showing surface morphology and cross-section of (a and b) PES/PA, (c and d) PES/ 0.5 wt% chitosan/PA, (e and f) PES/0.75 wt% chitosan/PA and (g and h) PES/1 wt% chitosan/PA membranes…….....99

Figure 4.5: FTIR spectra of (a) PES/1wt% chitosan, (b) PES/0.75wt% chitosan, (c) PES/0.5wt% chitosan and (d) Bare PES membranes…….……101

Figure 4.6: FTIR spectra of PES/1wt% chitosan/PA (a), PES/0.75wt% chitosan/PA (b), PES/0.5wt% chitosan (c) and PES (d) membranes…….……...103

Figure 4.7: Static water contact angle and bulk porosity of the (a) PES/chitosan and (b) PES/chitosan/PA membranes…….....106

Figure 4.8: Effect of chitosan loading on the Tensile Strength of PES/chitosan and PES/chitosan/PA membranes……..…….....108

Figure 4.9: Membrane (a) pure water flux and (b) AMD flux of PES/chitosan membranes…….111

Figure 4.10: Membrane (a) pure water flux and (b) AMD flux of PES/chitosan/PA membrane…….....114

Figure 4.11: Rejection (%) of metal and sulphates ions using PES/chitosan membranes having various chitosan loading……..…….....117

Figure 4.12: Metal ion rejection against flux of the prepared PES/chitosan membranes…….117

Figure 4.13. Rejection (%) of metal and sulphates ions using PES/chitosan membranes coated with polyamide layer having various chitosan loading……..…….119

Figure 5.1: FTIR spectra of selected chitosan (a) Samples 1A and 1B, (b) Samples 5A and 5B, (c) Samples 9A and 9B…….…….....129

Figure 5.2: Particle size distribution of synthesised chitosan of (a) Sample 1A and 1B (b), Samples 6A and 6B and (c) Samples 9A and 9B…….....131

Figure 5.3: FTIR spectra of (a) PES 1A and 1B, (b) PES 3A and 3B, (c) PA 1A and 1B and (d) PA 3A and 3B……..…….....138

Figure 5.4: Contact angle and porosity results of (a) PES/chitosan and (b) PES/chitosan/PA membranes……..…….....141

Figure 5.5: Thermal stability of the synthesised (a) PES/chitosan and (b) PES/chitosan/PA membranes……..…….....144

Figure 5.6: Membrane flux of (a) PES/chitosan membranes and (b) PES/chitosan/PA membranes……..…….....147

Figure 5.7: Rejection (%) of metal and sulphates ions using PES/chitosan membranes…….149

Figure 5.8: Rejection (%) of metal and sulphates ions using PES/chitosan membranes coated with polyamide layer (PES/chitosan/PA membranes)…….....149

Figure 5.9: Effect feed pH on rejection efficiency of (a) PES/chitosan and (b) PES/chitosan/PA membranes……..…….....151

Figure 5.10: Effect feed pH on AMD permeate flux of PES/chitosan and PES/chitosan membrane……...155

Figure 5.11: Fluxes versus feed pressure for solutions with various concentrations for (a) PES/chitosan and (b) PES/chitosan/PA membranes……..158

Figure 5.12: The effect of feed pressure on the rejection of iron (Fe^{2+}) solution on (a) PES/chitosan and (b) PES/chitosan/PA membranes……..161

Figure 5.13: The effect of feed pressure on the rejection of sulphates (SO_4^{2+}) solution on (a) PES/chitosan and (b) PES/chitosan/PA membranes……..161

Figure 6.1: AMD filtering with 0.45 µm filter paper…….....167

Figure 6.2: An image showing the cross-flow system used……...171

Figure 6.3: Pure water and AMD flux for both (a) PES/chitosan membranes and (b) PES/chitosan/PA membranes…….....173

Figure 6.4: Pure water and AMD permeability for (a) PES/chitosan membranes and (b) PES/chitosan/PA membranes……175

Figure 6.5. Rejection of selected AMD constituencies by (a) PES/chitosan membranes and (b) PES/chitosan/PA membranes…….....178

Figure 6.6. pH values of the permeate AMD solution against pressure…….....179

Figure 6.7: Permeate flux of pure water and AMD as a function of time for (a)PES/chitosan membranes and (b) PES/chitosan/PA membranes…….....181

Figure 6.8. Fouling experimental results for (a) PES/chitosan membranes and (b) PES/chitosan/PA membranes…….....183

Figure 6.9: Complete blocking model for cross flow predications for (a)PES/chitosan membranes and (b) PES/chitosan/PA membranes for individual foulant in the AMD feed solution…….…….....186

Figure 6.10: Intermediate blocking model for cross flow predicitons for (a)PES/chitosan membranes and (b) PES/chitosan/PA membranes for individual foulant in the AMD feed solution…….…….....187

Figure 6.11: Standard blocking model for cross flow predicitons for (a)PES/chitosan membranes and (b) PES/chitosan/PA membranes for individual foulant in the AMD feed solution……..…….....188

Figure 6.12. Gel layer formation blocking model for cross flow predicitons for (a) PES/chitosan membranes and (b) PES/chitosan/PA membranes for individual foulant in the AMD feed solution…….…….....189

List of Tables

Table 2.1: Common sulphide minerals associated with the production of AMD……...21

Table 2.2: Comparison of PES and PA membranes modified with chitosan……..54

Table 3.1: Chitosan synthesis process conditions from chitin…….....73

Table 3.2: Casting solution composition……..76

Table 3.3: Synthetic Feed composition……83

Table 3.2: AAS operating parameters……..84

Table 4.1: Performance comparison of this research with other studies in literature……120

Table 5.1: Chitosan yield…….....126

Table 5.2: Degree of deacetylation of chitosan under different synthesis conditions…….....133

Table 5.3: Coded names of the synthesised membranes……....135

Table 5.4: Feed composition to investigate effect of feed pressure and initial concentration……..157

Table 6.1: AAS operating parameters……....169

Table 6.2: AMD composition…….……....170

Table 6.3: Measures of fit, as per the R^2s, of Hermia's models for PES/chitosan membranes…….....190

Table 6.4: Measures of fit, as per the R^2s, of Hermia's models for PES/chitosan/PA membranes……..……...190

Abbreviations

AAS	Atomic absorption spectroscopy
AMD	Acid mine drainage
ARD	Acid rock drainage
BMWP	Biological Monitoring Working Party
CAIP	co-solvent assisted interfacial polymerization procedure
DD	Degree of deacetylation
DMF	Dimethyl formamide
DMSO	Dimethyl sulfoxide
DWAF	Department of water affairs and forestry
EPA	Environmental Protection Agency
EST	Ecotoxicological screening tool
FRR	Flux recovery ratio
FTIR	Fourier transform infrared
GDARD	Gauteng department of agriculture and rural development
IEP	Isoelectric point
IP	Interfacial polymerization
MF	Microfiltration
ML	Megaliters
MPDA	m-phenylenediamine

MSP	Membrane separation process
NF	Nanofiltration
PA	Polyamide
PAN	Polyacrylonitrile
PDA	Polydopamine
PES	Polyethersulphone
PEI	Polyethyleneimine
PIP	Piperazine
PSD	Particle size distribution
PSf	Polysulphone
PWF	Pure water flux
R_{ir}	Irreversible Resistance
RO	Reverse osmosis
R_r	Reversible Resistance
SBR	Sulphate-reducing bacteria
SEM	Scanning electron microscopy
TEA	Triethylenediamine
TGA	Thermo-gravimetric analyser
TMC	Trimesoyl chloride
TFC	Thin film composite

TMP	Transmembrane pressure
UF	Ultrafiltration
WHO	World health organization

Chapter 1 Introduction

1.1 Background and Motivation

Gold mining operation in South Africa commenced soon after the discovery of gold in Johannesburg Main Reef in 1886 by Mr. George Harrison (Naicker et al., 2003). A number of mines immediately developed and led to the establishment of Germiston and Boksburg to the East and Roodepoort, Randfontein and Klerksdorp to the West of Johannesburg (Durand, 2012). The gold bearing reefs of the Witwatersrand region contained various kinds of mineral ores such as native gold, uranium oxides and sulphide rocks with pyrite being the most abundant (Lusilao-Makiese et al., 2013). During the events of underground mining operation, ore is mined and brought to surface through conveyor belts, gold is extracted, and waste tailings are transported to dumps near the extraction plant. Initially, mercury amalgam method was used to extract the gold. The ore is crushed and milled to fine sand and is exposed to mercury film spread on copper plates to form mercury-gold amalgam which is distilled to recover the gold. As the mines became deeper, unoxidized rocks containing pyrite (FeS_2) were discovered and they interfered with the gold extraction (McCarthy and Venter, 2006). This led to the development of MacArthur-Forrest process of gold extraction, which used cyanide and was successfully applied to the Witwatersrand ores around 1890s. These processes did not fully recover all the gold completely, as such; small quantities at around 0.5 g/t remained in the tailings (Naicker et al., 2003). As the mines got deeper, groundwater aquifers were encountered and to allow continued mining operations, the mines had to be dewatered constantly. This saw millions of litres of groundwater with good quality being pumped from the mine voids to surface daily (Durand, 2012).

The mining operations were tended uneconomic at around 1960. Most of the mines have since ceased operation due to economic, liquidation and environmental non-compliance reasons

(Durand, 2012). When underground workings and unprofitable shafts were abandoned by mine operators, no rehabilitation was done on the shafts and waste tailings dump, slime dams and access portals were not sealed. Currently, diverse mining operations such as illegal exploration of the gold reefs (popularly known as Zama Zama, South African artisanal name miners) (Nhlengetwa and Hein, 2015) and reclamation of slime dams and old sands to recover remaining gold are taking place (Lusilao-Makiese et al., 2013). Until the last decades, the tailing dumps around Johannesburg have been left undisturbed and during this period, oxygenated rainwater has been percolating through and infiltrating the groundwater tables. This caused oxidation of sulphide bearing rocks, particularly pyrite since it was abundant in the area. Pyrite oxidation triggered acidification of water percolating through the tailing dumps and infiltrating into the groundwater aquifers (Naicker et al., 2003). The groundwater around the Johannesburg vicinity has been reported to be heavily contaminated with acid mine water or drainage (Ochieng et al., 2010). Overtime, the unrehabilitated mine voids have been filling up with acidic water until September 2002 when the contaminated water started spilling out of unused mines in Randfontein in the West Rand. Figure 1.1 shows water level rise monitored from 1996 prior to surface decant in Sep 2002 in the West Rand. Acid mine drainage (AMD) refers to seepage of high acidic water with very low pH, usually has high concentration of metals, sulphates and salts (Neculita et al., 2007). Its formed when sulphide containing rocks such as pyrite are exposed to oxygenated water and cause gradual decrease in water pH. The natural process of AMD formation can take up to 15 years, however, microbial catalysation by archaea and bacteria (e.g. acidophilic Thiobacillus Ferroxidans) (Rawlings and Kusano, 1994) shortens the reaction rate to about 8 minutes (Metesh et al., 1998)

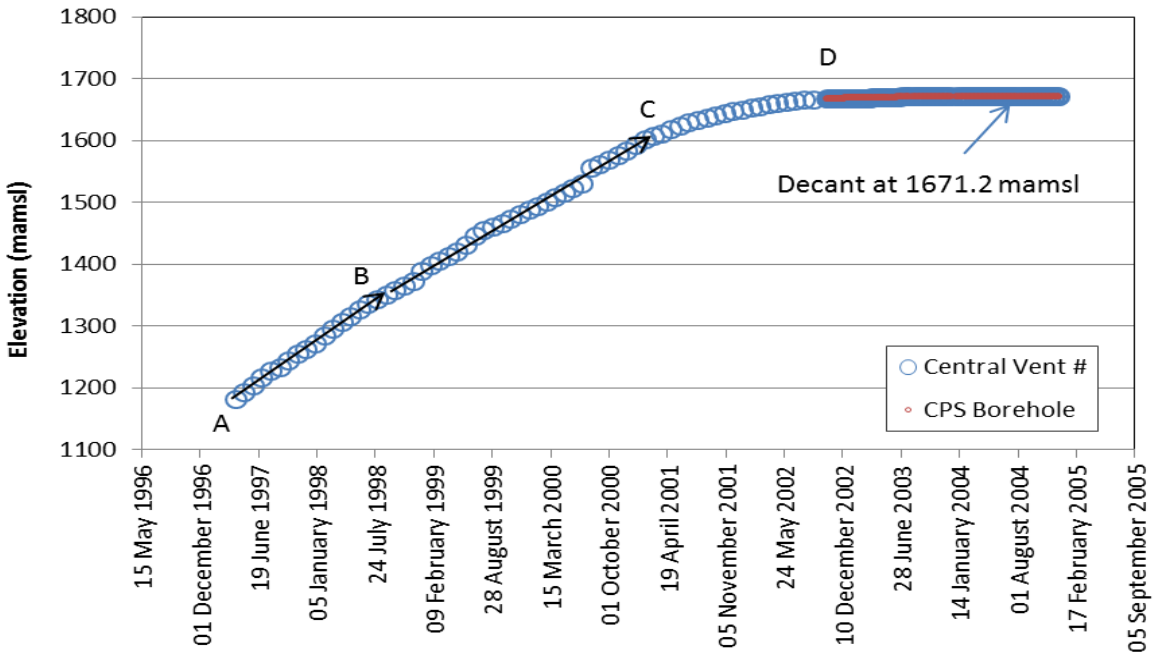


Figure 1.1: Acidic water level rise in Randfontein, West Rand (DWAF, 2013)

Traditional technologies which have been applied for decades to rehabilitate AMD are active and passive treatment processes. The former depends on addition of alkaline materials which neutralises the acidity of the AMD and precipitate dissolved metals (Masindi et al., 2015) and the latter relies on the biological, gravitational and geochemical processes (Tolonen et al., 2014). Other technologies which have been researched include Ion exchange and adsorption technique (Masukume et al., 2014 Ricci et al., 2015). Conventional treatment technologies have disadvantages of producing high volume of toxic sludge which poses secondary pollution; they require frequent maintenance and only achieve partial treatment. Membrane technology emerged as an eminent and promising alternative due to its high separation efficiency and does not require frequent maintenance (Hilal et al., 2005). Membrane is a thin layer of semi-permeable material which creates a barrier that traps and separate substances when a driving force is applied across (Daramola et al., 2015). Microfiltration (MF), ultrafiltration (UF), nanofiltration(NF) and reverse osmosis (RO) are common pressure driven membrane separation processes currently employed (Maphutha et al., 2014). Significant characteristics

of a good membrane include mechanical strength, chemical resistance and thermal stability and these are highly influenced by the material of construction and synthesis method.

Concentration polarisation and membrane fouling are vital problems associated with membrane technology as they limit full potential utilization of this technology (Shi et al., 2014). The former, refers to continual accumulation of rejected solutes near the membrane surface due to convective and driving force leading to solute concentration in the membrane vicinity being higher than in the bulk (Luis, 2018; Shi et al., 2019). The latter takes place when suspended or dissolved matter in the feed solution migrate from the liquid phase to form deposits either on the membrane surface, pore openings or within the membrane porous structure (Koros et al., 1996). Although these challenges are considered inevitable, their rate and extent are highly influenced by membrane properties, feed characteristics and operational conditions (Wei et al., 2010). Material of construction, membrane synthesis method, available functional groups and exposed operational conditions affect membrane properties and its antifouling nature (Aguiar et al., 2016). The effect of operational conditions such as the feed solution pH is vital as it affects the membrane charge which could either protonate or deprotonate membrane available functional groups (Carvalho et al., 2011). Temperature, feed flow rate and pressure influence the movement of foulants towards the membrane surface and the treatment capacity of the membrane (Wei et al., 2010). Membrane fouling needs to be effectively and efficiently controlled and minimized as it could result in increased operational costs and can shorten the membrane life.

Synthetic polymers are common materials used for membrane manufacturing, although other materials such as ceramic and metallic membrane could be available. Polymeric materials have attracted enormous attention for membrane synthesis application due to their non-toxic and biodegradable properties (Garni et al., 2017). Depending on the desired membrane properties, various materials used as polymeric membrane precursor includes polyvinylidene fluoride,

cellulose acetate, polypropylene, polyamide, polysulphone, polyethersulphone and polyacrylonitrile amongst others. Membrane properties such as surface charge, pH and oxidant tolerance, degree of hydrophobicity, strength and flexibility will dictate which membrane material could be used (Koltuniewicz, 2005). Polyethersulphone is one of the most important polymeric materials used for membrane manufacturing for water and wastewater treatment because it is stable in water and is an inert membrane. Phenylene rings connected by the sulfonyl groups offers polyethersulphone membranes high rigidity, chemical and thermal stability, oxidation resistance and high mechanical strength (Shen et al., 2011; Chen et al., 2013). The operating temperature for these membranes can reach up to 78 ^{o}C and have operating pH tolerance ranging from 1 to 13 (Baker, 2004a). It's commonly known that pure polymeric membranes are somewhat lacking in meeting complete requirements of a good membrane (Aroon et al., 2010a). Several studies concluded that membrane fouling is directly related to hydrophobicity as reviewed by Van der Bruggen (2009) and Khulbe et al. (2010). Its commonly known that most commercial nanofiltration membranes are constructed using polyethersulphone (Zhao et a., 2013). Nanofiltration is an intermediate membrane between UF and RO membrane with high permeate flux and can retain dissolved molecules with molecular weight of 200 to 300g/mol and ions through electrostatic interaction between the ions and membrane charge combined with size exclusion (Linde and Johnson. 1995; Carvalho et a., 2011).

To overcome hydrophobic and selectivity challenges which limits application of PES and PES based membranes, various alteration approaches such as blending, chemical, physical and surface modification approaches have been reported (Chen et al., 2013). The membrane modification technique aims to localize the hydrophilic material on the membrane surface and pores to positively influence membrane flux and selectivity and fouling reduction (Zhao et al., 2013). Addition of hydrophilic functional groups on to PES and PES based membranes through

surface grafting (Rahimpour, 2011), coating (Reddy et al., 2003) or blending with hydrophilic polymers (Peyravi et al., 2012) or nanoparticles (Ji et al., 2015) could modify the membranes. Introducing chitosan and polyamide as hydrophilic agents will improve the membrane's hydrophilic nature, antifouling property without compromising selectivity. Chitosan is characterised by large number of amino ($-NH_2$) and hydroxyl (-OH) groups which can act as contaminate binding sites and additional features such as high hydrophilicity, mechanical and chemical stability (Wan Ngaha, 2011). The reactive amino functional group on chitosan structure binds almost all group III and transition metals. In acidic medium, the amino group gets protonated and attract metal anions through ion exchange and repel cations through electrostatic repulsion (Anirudhan and Rijith, 2012). Polyamide offers numerous active functional groups such as amines, free carboxylic acid and unreacted acylchloride which are prone to modification and can act as binding sites (Zou et al., 2010; Ji et al., 2011). Although hydrophilic polymers containing polyamides and amines have been reported to be extremely effective in enhancing hydrophilic nature and selective properties of polymeric membranes, little information is available in open literature on the use of chitosan and/or polyamide to modify PES and PES based membranes. Most studies opted to coating these hydrophilic agents, but no information is available about infusing them within PES membrane matrix to not only modify the membrane surface but also within the membrane. It is against this background that this synthesised adsorptive polymeric PES membrane infused with chitosan by blending it with PES suspension and coated it with polyamide layer for AMD treatment.

1.2 Research questions

This work was devoted to synthesising polyethersulphone membrane infused with chitosan and coated with polyamide layer for the treatment of acid mine drainage by addressing the following research questions:

(i) What is the effect of blending chitosan having various ’s degree of deacetylation on the performance of PES membrane during AMD treatment?

(ii) What is the effect of coating polyamide layer on PES membrane infused with chitosan on the performance during AMD treatment?

(iii) What will the effect of operating variables such as pH, feed pressure and feed composition on the separation performance of the membranes be?

(iv) What will the fouling behaviour and operational stability of the membrane be during AMD treatment?

1.3 Research aim and objectives

The study synthesised polyethersulphone membrane infused with chitosan and coated with polyamide layer and evaluated synthesised membrane performance during AMD treatment. The following specific objectives were defined to address the above-posed research questions:

(i) To synthesize polyethersulphone membrane infused with chitosan and coated with polyamide layer for the treatment of AMD

(ii) Investigate the influence of chitosan content and chitosan’s degree of deacetylation of on the quality and separation performance (cation and anion binding) of the modified membrane coated with polyamide top active layer during AMD treatment

(iii) Investigate to understand the effect of operating variables such as pH, feed pressure and feed composition on the separation performance of the optimized membrane from (ii)

(iv) To investigate fouling behaviour and operational stability of the membrane towards enhancing the membrane integrity during real AMD treatment.

1.4 Research outputs and outcomes

(i) Chitosan was successfully synthesised from chitin

(ii) Information on the influence of synthesis variables on chitosan's degree of deacetylation from chitin

(iii) The effect of chitosan content and chitosan's degree of deacetylation on the quality and performance of PES membrane infused with chitosan and coated with polyamide layer for the treatment of AMD

(iv) The effect of operational conditions (feed pH, pressure and composition) on the performance of optimized membrane in (iii) during AMD treatment

(v) The antifouling behaviour and operational stability of the optimized membrane

(vi) Peer reviewed publications (journals and book Chapter) and documented report in the form of a thesis

1.5 Thesis outline

Chapter 1

This Chapter gives a general background and motivation of this research. It also gives the aim, objectives of the study and key questions

Chapter 2

This Chapter gives an overview of the literature review of gold mining, AMD formation and its associated problems with special emphasis in South Africa, Johannesburg. It further outlines conventional treatment technologies available to remediate AMD and application of membrane technology to treat AMD contaminated wastewater. It provides literature on polyethersulphone as material of membrane construction, different membrane preparation methods and Hermia's fouling models.

Chapter 3

This Chapter focuses on the experimental design and methodology which was followed to conduct the study. It presents procedures followed to synthesise chitosan samples and membranes and their characterizations. Lastly, it presents the steps followed to conduct the membrane performance tests.

Chapter 4

This Chapter reports the results and discussion of the effect of chitosan content which was infused within PES membrane by blending chitosan with PES suspension to produce a casting gel used to fabricate PES/chitosan membrane and coated polyamide layer on top to produce PES/chitosan/PA membrane. It further reports on the quality and performance of the synthesised membranes during synthetic AMD treatment.

Chapter 5

This Chapter reports the results of synthesis and characterisation of chitosan having various degree of deacetylation synthesised from chitin. It reports further the quality and performance of membranes infused with chitosan having different degree of deacetylation (PES/chitosan membranes) and coated with polyamide layer (PES/chitosan/PA membranes) during synthetic AMD treatment. Lastly, it presents results and discussion on the effect of feed pH, initial concentration and pressure on membrane water flux and rejection

Chapter 6

This Chapter presents the results pertaining to the operational stability and fouling behaviour of PES/chitosan and PES/chitosan/PA membranes during the treatment of real industrial AMD using a crossflow filtration setup.

Chapter 7

This Chapter provides conclusions of the whole research and recommendations.

Chapter 2 Literature review

2.1 Introduction

This Chapter discusses in detail the history of gold mining and acid mine drainage in the Witwatersrand region, Johannesburg South Africa. It further discusses the formation of acid mine drainage first and its impact if discharged untreated. The conventional treatment technologies and their disadvantages are presented. Membrane technology emerged as an alternative technology; therefore, membrane technology is discussed with special emphasis on polymeric membranes, specifically polyethersulphone membrane. Challenges confronting membrane technology and measures available to address those challenges are also presented. Lastly, chitosan and polyamide are recommended as potential hydrophilic co-polymers for modification of polyethersulphone membrane for improved antifouling property and selectivity.

2.2 History of gold mining in South Africa

The Witwatersrand region was transformed within few years from a farming community into the most populated and dense area with mining operations after the discovery of gold in 1886 by Mr George Harrison at Langlaagte farm, not too far from the current Johannesburg city center (Naicker et al., 2003). The region was subjected to mining activities, geological exploration, and industrial development and associated informal settlement to provide housing for miners which led to the establishment of Germiston and Boksburg to the East and Roodepoort, Randfontein and Klerksdorp to the West part of Johannesburg (Durand, 2012). In global gold mining history, the Witwatersrand Super group was known for its goldfield's abundance having the richest and expensive gold deposits in the world (McCarthy and Rubidge, 2005). The Witwatersrand Super group is in Gauteng province in the North-Eastern part of South Africa and extends in an East West direction of Johannesburg over a strike length

of 45 km. It connects the Orange Free State and the old provinces of Transvaal and is of the same period as the Bushveld Igneous Complex and Vredefort impact of 2.023 Ga ago. The mine voids in this area are possibly the deepest in the world (mining operations at 3600 m and exploration core-drilling up to 4600m). The Supergroup holds quartz pebbles conglomerates set in a matrix of quartz sand which contains about 3% of pyrite and variety of other sulphide and oxide minerals (Naicker et al., 2003). The gold bearing reefs of the Witwatersrand region contained various kinds of mineral ores such as native gold, uranium oxides and sulphide rocks with pyrite being the most abundant (Lusilao-Makiese et al., 2013).

The artisanal mining industry in the area expanded within few years into the largest producer of gold on Earth accounting to 40% of global production at the time (Robb, 2008). South Africa's gold export amounted to $3.8 billion making it the world's leading producer of gold in 2005 which accounted for 12% of global gold production and became Africa's powerful economy holding 24% of the continent's GDP (Yager, 2004). Gold mining in South Africa gave rise to the world known billionaires such as the German immigrant Ernest Oppenheimer who founded Anglo American Limited and Imperial mining magnate Cecil John Rhodes, the first chairman of De beers. During the mining process, East, West and Central goldfields were created in what currently is referred to as the Eastern, Western and Central basins of the Witwatersrand goldfields (see Figure. 2.1). The Western Basin is located in the Krugersdorp, Witpoortjie and Randfontein areas, the Central basin covers the current Johannesburg city center and Gold reef city amusement park and the Eastern basin stretches from Boksburg reaching towards Nigel and Springs (Nhlengetwa and Hein, 2015).

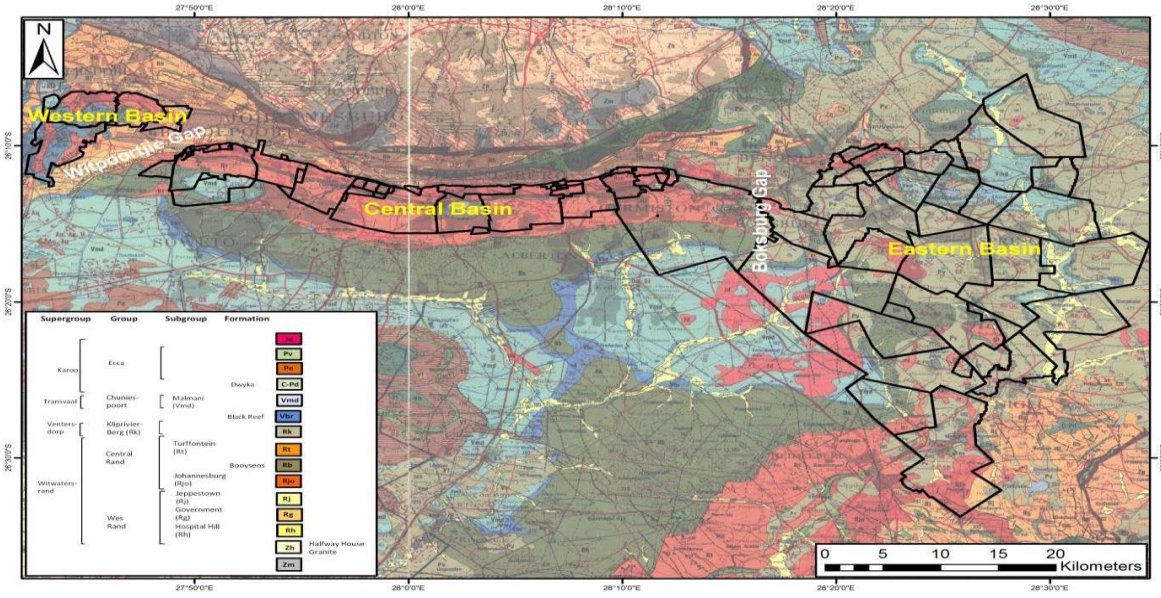


Figure 2.1: Location map of the Witwatersrand Basin and its major goldfields (DWAF, 2013)

2.3 Gold Extraction

During underground mining operation, the ore is mined and brought to surface through conveyor belts, gold is extracted, and waste tailings are transported to dumps near the extraction plant (Figure 2.2). Mercury amalgam method was originally used for the extraction of gold from ore but after the encounter of unoxidized ore containing pyrite, a new technology called MacArthur-Forrest was developed and applied to Witwatersrand operations using cyanide (Naicker et al., 2003). Gold extraction using mercury amalgamation is an inexpensive, uncomplicated and easily accessible procedure and was applied in the Randfontein area (Malehase et al., 2016). The ore is crushed and milled to fine sand and is exposed to mercury film spread on copper plate to form mercury-gold amalgam which is distilled to recover the gold. Mercury's unique capacity to react or amalgamate with most metals made it to be used in large quantities in the chemical and mining industry (Zolnikov and Ortiz, 2018). Apart from high levels of river siltation and mercury pollution, there are various degrees of chronic and acute adverse health effects associated with mercury exposure. Acute, low-dose exposure to mercury can cause respiratory complications such as chest pains, haemoptysis, dyspnoea,

coughs, interstitial pneumonitis and impairment of pulmonary functions. On the other hand, acute, high dose-exposure can cause permanent damage to the central nervous system. Chronic, low to moderate exposure is characterized by symptoms of fatigue, depression, irritability, vivid dreams and loss of memory (EPA, 2011).

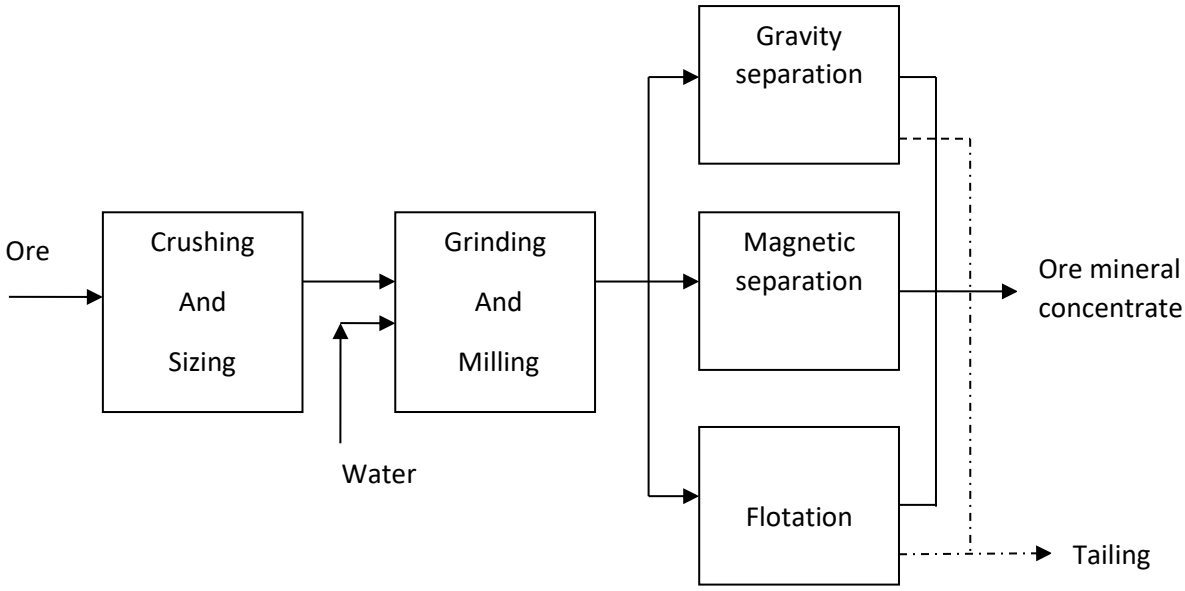


Figure 2.2: Simplified flow-chart of mineral processing operation (adapted and modified from Lottermoser, 2011).

When unoxidized ore which contained pyrite (FeS_2) was encountered, it interfered with the gold extraction process. It was for this reason and the adverse health effects related to mercury which caused mine operators to seek an alternative technology to continue extracting the gold. As such, at around 1890s, MacArthur-Forrest cyanidation process was phased in (McCarthy and Venter, 2006). The process required the ore to be milled into fine powder and treated with cyanide solution to dissolve the gold. The gold containing solution would then be further treated to recover the gold. Apart from the fact that gold extraction using cyanide is a rapid process, cyanide can bind to ionic gold (Au^+) and this leads to selective leaching of gold (Raphulu and Scurrell, 2015). The pH of about 10.5 was required for the efficient application of the process and therefore, lime was added to regulate the pH (Turton, 2013). Claims are

made in literature regarding gold extraction using cyanidation process as environmentally friendlier compared to mercury process. It can be degraded naturally and does not persist in the environment (Brüger et al., 2018).

These processes did not fully recover all the gold completely and small quantities at around 0.5 g/t remained in the tailings (Naicker et al., 2003). Over the past three decades and currently, diverse mining operations to reclaim the slime dams and old sands are taking place which includes illegal exploration of the gold reefs, artisanal and small-scale mining (Nhlengetwa and Hein, 2015; Lusilao-Makiese et al., 2013). Although the definition of artisanal and small-scale mining differs from region to region, generally it refers to the exploitation of mineral deposits by a group of 20 – 50 people using rudimentary tools. Commonly, artisanal operation is an option when the deposits are not profitable to mine using large-scale operation (Danielson and MacShame, 2003). Zvarivadza and Nhleko (2018) debunks challenges posed by artisanal and small-scale mining if not properly planned and regulated in much more details. The use of mercury and cyanide during artisanal and small-scale operations for gold processing threatens the ecosystem as in most cases it gets released into the environmental and cause adverse health effects. Normally, there is no proper and appropriate waste tailings facilities during artisanal operations, and these create potential for toxic substances to escape into the environment. The gold mining residues utilized are typically characterised by waste rock, slime (75% particle size <75µm) and sand (10-20% particle size <74 µm). The cost of gold mining residues is regarded as a relatively cheap source of gold since the cost of mining and size reduction has already been incurred (Muir et al., 2016). Hydraulic remining using high-pressure water-monitor guns is mostly preferred (currently applied at the Witwatersrand region) over mechanical and dredging reclamation in artisanal operations. It involves directing high-pressure water jet at the slime dam faces creating slurry which falls to the bottom of the dam where a pumping station is positioned (Figure 2.3).



Figure 2.3: Manual hydraulic monitor on a tailing facility in South Africa (*http://www.tailings.info/technical/hydraulic.htm*. Accessed on 22/02/2020)

2.4 Mining tailings

Mine tailings which sometimes referred to as mine dumps, slimes, refuse, culm dumps, tails, leach residue or slickens, are the left-over materials during the separation process of the valuable fraction from the uneconomic fraction (gangue) of an ore. Tailings are different from overburden, which is the materials or waste rock overlying an ore or mineral body that are removed during mining without being processed. At commencement, these residues are transported in slurry form to knowingly built facilities and stored as sediments across few kilometres from the mine. An estimated 468 million tons of mineral waste per annum was produced in South Africa in 1997. Malehase et al. (2016) estimated six billion cubic meters of surface area was covered by mineral waste and Oelofse et al. (2007) suggested that about 221 million tons or 47% of all mineral waste produced in South Africa was associated with gold mining making it the largest, single source of waste and pollution. Although the law requires that the tailings dams be vegetated to prevent wind erosion and precipitation, the mine dams around the Witwatersrand Basin have been exposed with no vegetation. Figure 2.4 shows an

aerial photograph of tailing storage facility taken by engineers from SKA consulting as part of their active monitoring program.



Figure 2.4: Mine tailings storage dams in Johannesburg (extracted from *http://www.mining.com/web/call-to-make-tailings-dams-safer/* on the 22/02/2020).

2.5 Ground water pollution and AMD seepage

As the mines got deeper, logistical challenges arose, such as supplying the shaft with fresh air, cooling of the operational tunnels and eventually the dewatering flooded shafts stopped. The Transvaal Supergroup overline the Witwatersrand Supergroup and the Ventersdorp Supergroup, which as a result many of the Central and East Rand gold mines are located beneath karst aquifers. Supergroup groundwater aquifers were encountered and to allow continued mining operations, the mines had to be dewatered constantly. This saw millions of litres of groundwater with good quality pumped from the mine voids to surface daily (Durand, 2012). Most of the mines have since ceased operation due to economic, liquidation and environmental non-compliance reasons (Durand, 2012). No rehabilitation was done on the shafts, waste tailings dump, and slime dams and access portals were not sealed when

underground workings and unprofitable shafts were abandoned by mine operators. Until the last decades, the tailing dumps around Johannesburg have been left undisturbed and during this period, oxygenated rainwater has been percolating through and infiltrating the groundwater tables. This caused oxidation of sulphide bearing rocks, particularly pyrite since it's in abundant in the area producing acidic water.

Pyrite oxidation triggered acidification of water percolating through the tailing dumps and infiltrating into the groundwater aquifers (Naicker et al., 2003). To provide scientific clarity after prevailing assumption that AMD is created in the mine void, Turton (2013) provided chemistry of AMD formation and its flow path into the underground void. **"Flow Pathway A",** referring to the oxidation of pyrite (FeS_2) by oxygenated rainwater to form ferrous iron and sulphates (Eq. (1)). This step happens on the surface of the tailings pile. The ferrous iron undergoes further oxidation to produce ferric iron, usually under very low pH (Eq. (2)). This was referred to as **"Flow pathway B",** which happens when the acidic water leaves the tailings piles. The ferric iron would then precipitate as iron hydroxide (Eq. (3)). This was termed **"Flow Pathway C"**. As previously described, a pH of 10.5 was required to ensure efficient MacArthur-Forrest cyanidation process for the extraction of gold. Therefore, the tailings piles were dumped at that pH, presumably. Although rainfall records do not include pH values, limited tests suggest that rainwater around mining operations is mostly acidic. As such, this creates conditions for reducing the pH and acidification of the tailing's dams' surface. Once the environment becomes conducive for AMD chemistry start, the process becomes self-propelling as ferric iron can either precipitate as iron hydroxide or act as an oxidizing agent and oxidize more pyrite (Eq. (4)). The infiltration of acidic water into the mine voids polluted the groundwater around the Johannesburg vicinity by acid mine water or drainage (Ochieng et al., 2010). For overtime, the unrehabilitated mine voids have been filling up with acidic water

until September 2002 when the contaminated water started decanting out of disused mine in Randfontein in the West Rand.

2.6 Acid mine drainage (AMD)

2.6.1 Formation of AMD

Acid mine drainage (AMD) and its associated contaminants have been reported to be the largest environmental problem facing the mining industry. It is commonly known as acid rock drainage (ARD) or acid mine drainage (AMD), here in the document to be referred to as AMD. AMD is formed when sulphide containing rocks are exposed to oxidizing environment and is characterized by low pH (< 5.0), high acidity, high concentration of metals, sulphides and salts (Neculita et al., 2007). The natural process of AMD formation can take up to 15 years, however, microbial catalysation by archaea and bacteria (e.g. acidophilic Thiobacillus Ferroxidans) (Rawlings and Kusano, 1994) and excavation of sulphide host rocks by mining activities shortens the reaction time to about 8 minutes (Metesh et al., 1998). Pyrite (FeS_2) is one of the most sulphide containing rock responsible for AMD generation due to its ease oxidation (Kefeni et al., 2017a) compared to other metal sulphide minerals (see Table 2.1). Pyrite will react with oxygen and water to produce acidic discharge which acts as a leaching agent of toxic metals and trace elements available in the host rocks (Kefeni et al., 2017a). Equations (1) to (4) shows the formation of acid mine drainage in the presence of air (oxygen), water and bacteria (Bwapwa et al., 2017, Othman et al., 2017, Kaur et al., 2018). Pyrite (FeS_2) oxidation by molecular oxygen and water under neutral conditions releases hydrogen (H^+), sulphates (SO_4^{2-}) and ferrous iron (Fe^{2+}) (Eq. (1)). The predominant source of oxygen during sulphide mineral dissolution is air which contains approximately 21% oxygen. Furthermore, with excess oxygen, oxidation of ferrous iron (Fe^{2+}) releases ferric iron (Fe^{3+}) (Eq. (2)) which either acts as an oxidizing agent and oxidizes more pyrite (Eq. (3)) or will precipitate as iron hydroxide ($Fe(OH)_3$) (Eq. (4)). Overall reaction summary is represented by Equation (5). Oxidation of

pyrite by ferric ion (Eq. (3)) is deemed faster than oxidation by oxygenated water (Eq. (1)) (Pierre Louis et al., 2015).

$$2FeS_{2(s)} + 2H_2O_{(l)} + 7O_{2(g)} \rightarrow 2Fe^{2+}_{(aq)} + 4SO_4^{2-}{}_{(aq)} + 4H^+_{(aq)} \quad (1)$$

$$2Fe^{2+}_{(aq)} + 4H^+_{(aq)} + O_{2(g)} \rightarrow 2Fe^{3+}_{(aq)} + 2H_2O_{(l)} \quad (2)$$

$$Fe^{3+}_{(aq)} + 3H_2O_{(l)} \rightarrow Fe(OH)_{3(s)} + 3H^+_{(aq)} \quad (3)$$

$$FeS_{2(s)} + 14Fe^{3+}_{(aq)}) + 8H_2O_{(l)} \rightarrow 15Fe^{2+}_{(aq)} + 2SO_4^{2-}{}_{(aq)} + 16H^+_{(aq)} \quad (4)$$

$$4\ FeS_{2(s)} + 15\ O_{2(g)} + 14\ H_2O_{(l)} \rightarrow 4\ Fe\ (OH)_{3(s)} + 8\ H_2SO_{4(aq)} \quad (5)$$

pH, temperature and oxygen content of the gas phase forms part of primary factors contributing to formation of AMD. The severity of AMD pollution is highly dependent on the geology of the mine sites or sources which determines the AMD composition and pH (Kefeni et al., 2017b). Other general features which also influences AMD formation includes oxygen concentration in the water phase, surface area of exposed metal sulphide, degree of oxygen saturation with water, chemical activity of Fe^{3+}, chemical activation energy required to initiate acid generation and bacterial activity (Akcil and Koldas, 2006). Formation and characteristics of AMD varies from site to site because of different mineralogy and other factors affecting formation of AMD and this makes predicting the potential for AMD formation more exceptionally challenging and very costly. The nature and size of associated risks and feasibility of mitigation options vary from site to site (Akcil and Koldas, 2006). The AMD in the Witwatersrand region is characterized by pH values between 2.0 to 6.65, 216 to 510 mS/cm for conductivity, sulphate content of 1037 to 4010 ppm, iron 38 to 1010 ppm, manganese 0.4 to 68.30, Nickel 0.5 to 71 ppm and cobalt 0.0012 to 17.11 ppm (Coetzee et al., 2010).

Table 2.1: Common sulphide minerals associated with the production of AMD (adapted and modified from National Rivers Authority, 1992, cited in Brown et al., 2002)

Mineral	**Composition**	**Aqueous end-products of complete oxidation**
Amorphous	FeS	Fe^{3+}, SO_4^{2-}, H^+
Arsenopyrite[a]	FeAsS	Fe^{3+}, AsO_4^{3-}, SO_4^{2-}, H^+
Bornite[a]	Cu_5FeS_4	Cu^{2+}, Fe^{3+}, SO_4^{2-}, H^+
Chalcocite[a]	Cu_2S	Cu^{2+}, SO_4^{2-}, H^+
Chalcopyrite[a]	$CuFeS_2$	Cu^{2+}, Fe^{3+}, SO_4^{2-}, H^+
Cinnabar	HgS	Hg^{2+}, SO_4^{2-}, H^+
Cobaltite[a]	CoAsS	Co^{2+}, AsO_4^{3-}, SO_4^{2-}, H^+
Galena[b]	PbS	Pb^{2+}, SO_4^{2-}, H^+
Mackinawite	FeS	Fe^{3+}, SO_4^{2-}, H^+
Marcasite[a]	FeS_2	Fe^{3+}, SO_4^{2-}, H^+
Molybdenite[a]	MoS_2	MoO_4^{2-}, SO_4^{2-}, H^+
Niccolite	NiAs	Ni^{2+}, AsO_4^{3-}, SO_4^{2-}, H^+
Orpiment[a]	As_2S_3	AsO_4^{3-}, SO_4^{2-}, H^+
Pentlandite	$(Fe,Ni)_9S_8$	Fe^{3+}, Ni^{2+}, SO_4^{2-}, H^+
Pyrite[a]	FeS_2	Fe^{3+}, SO_4^{2-}, H^+
Pyrrhotite[a]	$Fe_{1-x}S$	Fe^{3+}, SO_4^{2-}, H^+

Realgar	AsS	AsO_4^{3-}, SO_4^{2-}, H^+
Smythite	Fe_3S_4	Fe^{3+}, SO_4^{2-}, H^+
Sphalerite	ZnS	Zn^{2+}, SO_4^{2-}, H^+
Tetrahedrite	$Cu_{12}(Sb, As)_4S_{13}$	Cu^{2+}, SbO^{3-}, AsO_4^{3-}, SO_4^{2-}, H^+

Note: [a] Known to be oxidized by *Thiobacillus ferroxidans*.

[b] Known to be oxidized by iron-oxidizing bacteria

2.6.2 Effect of AMD

Mining operations have potential effects on all components of the environment and the impacts can be permanent/temporary, repairable/irreparable, beneficial/harmful, and reversible/ irreversible. Although there are numerous reasons for the toxicity of AMD to receiving water bodies, the major impact is because of the proton acidity of the AMD, which leads to a decrease in pH of the recipient water should it have insufficient neutralization capacity (Hallberg, 2010). Effluents generated from mining or associated operations contain heavy metals which have serious adverse effects on human health and ecological implications due to high concentration of toxic substances such as cyanide, toxic metals and sulphates (Akcil and Koldas, 2005). Conductivity, and sulphate concentrations and other pollutants associated with mine runoff, can directly cause environmental degradation, including disruption of water and ion balance in aquatic biota. Human health impacts may come from contact with streams or exposure to airborne toxins and dust (Palmer et al., 2010). Figure 2.5 shows a typical stream contaminates with AMD runoff.



Figure 2.5: Stream contaminated with AMD (extracted from *https://sites.google.com/a/gustavus.edu/sulfide-mining-in-the-boundary-waters/home/acid-mine-drainage* on 22/02/2020)

2.6.3 AMD in Johannesburg

Since the spilling out of AMD in the western basin in Sep 2002, it became a focus of intense studies (Lusilao-Makiese et al., 2013; Durand, 2012; Coetzee et al., 2010; Tutu et al., 2008) in recent years due to fears regarding the impact of acidic water contaminating large volumes of groundwater and sensitive surface water systems surrounding the area (Coetzee et al., 2010). Figure 2.6 shows scientific publications based on acid mine drainage in/by South Africa(ns) extracted from Scopus. Majority of the publications are research articles. According to Figure 2.7, there has been increased number of scientific researches around the topic of acid mine drainage.

During mining operations around the Witwatersrand, the mines became very deep and mine operators encountered underground aquifers which started flooding the mines making it difficult to continue mining and the gold mines had to be dewatered constantly to allow mining operations to continue. Closing of most of the mines in the East rand, Central and West rand worsened the threat of AMD as dewatering flooded shafts stopped and underground mine voids

started filling up with acidic water (Durand, 2012). Springs originally fed by clean groundwater started flowing but this time contained toxic and radioactive mixture of sulphuric acid, sulphates and heavy metals. In a study conducted by Fourie (2005), it was reported that 4500 mg/L of sulphates contained in mine water effluent from Harmony Gold's Randfontein Operations and 5055 mg/L was recorded in Robinson Lake which is a source of Tweelopies Spruit River. Sensitive individuals may endure vomiting and diarrhoea for consuming sulphate in excess of 200 mg/L while most individuals at 600 mg/L (Durand, 2012).

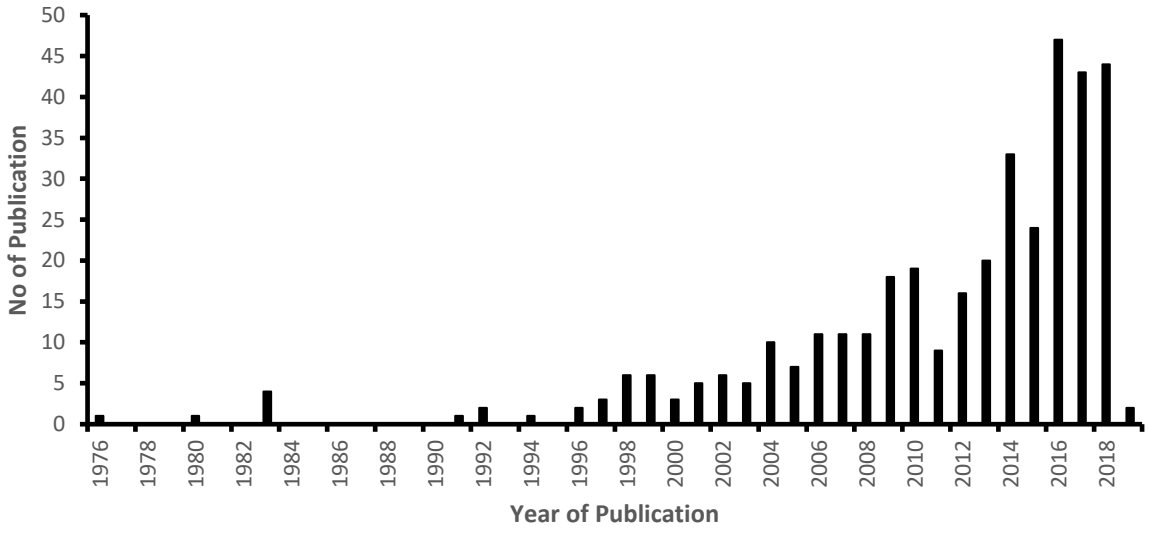


Figure 2.6: Scientific publication (books, book Chapters, journal articles and conference proceedings) on acid mine drainage in South Africa (obtained from *www.scopus.com* on 20/09/2019))

High concentration of metals such as manganese, iron, nickel, cobalt, copper, lead, aluminium, thorium, radium and uranium have been reported in AMD emanating from Gauteng and West rand gold mines (Coetzee et al.,2006). Exposure to any of these metals, depending on metal concentration and length of exposure, may be fatal to organisms including humans. Metals reach the groundwater and rivers systems through run-offs from slime dams and rock dumps and mine voids via seeps and decanting. Heavy metals have endocrine-disrupting effect

potential on organisms even at low concentrations (Durand, 2012). Uranium was reported to be in abundance than gold within the Witwatersrand Supergroup and most of it was dumped in slime dams littering Gauteng landscape (Coetzee et al., 2006). About 430 000 tonnes of uranium was produced during gold mine operations and most of it was discarded as waste (GDARD, 2011). The slime dams have potential to leach radioactive AMD and infiltrate the groundwater regimes. People living in the vicinity of these slime dams use groundwater as their source for drinking purpose, to irrigate their crops and water their livestock. Maximum limit of 30 µg/L (WHO, 2011) uranium has been recommended by the World Health Organization in drinking water and in South Africa is 70 µg/L (DWAF, 1996a). However, 14.9 mg/L uranium concentrations were reported in Robinson Lake in 2009 (Durand, 2010). Maximum allowable uranium concentration in water used for irrigation is 10 µg/L (DWAF, 1996b) because metal accumulation level in plants it's significantly higher than in water used for irrigation (Van Biljon, 2007).

2.6.4 AMD in Tweelopies Spruit River

The river drainage network in South Africa is very asymmetrical with the Vaal and Orange Rivers rising on the eastern incline and flowing across the whole country and discharging into the Atlantic Ocean. Two other major drainages are the Limpopo-Olifants River system, which stretches northern portion of the country and discharges into the Indian Ocean (see Figure 2.7). Bloubank stream is a tributary of the Crocodile River (an upper tributary of the Limpopo River) that drains the north-western portion of the Johannesburg, Gauteng Province, South Africa. The south-western portion (headwater) of the Bloubank stream system comprises the Riet stream and its tributary, the Tweelopies stream (Mccarthy, 2011). AMD started spilling out in September 2002 from Black Reef Incline Shaft and no.17 and 18 Winze Shafts into Tweelopies Spruit stream (see Figure 2.8) untreated and uncontrolled at a maximum of 60 ML/day with an average rate of approximately 25 ML/day, seasonally dependent (Hobbs & Cobbing, 2007).

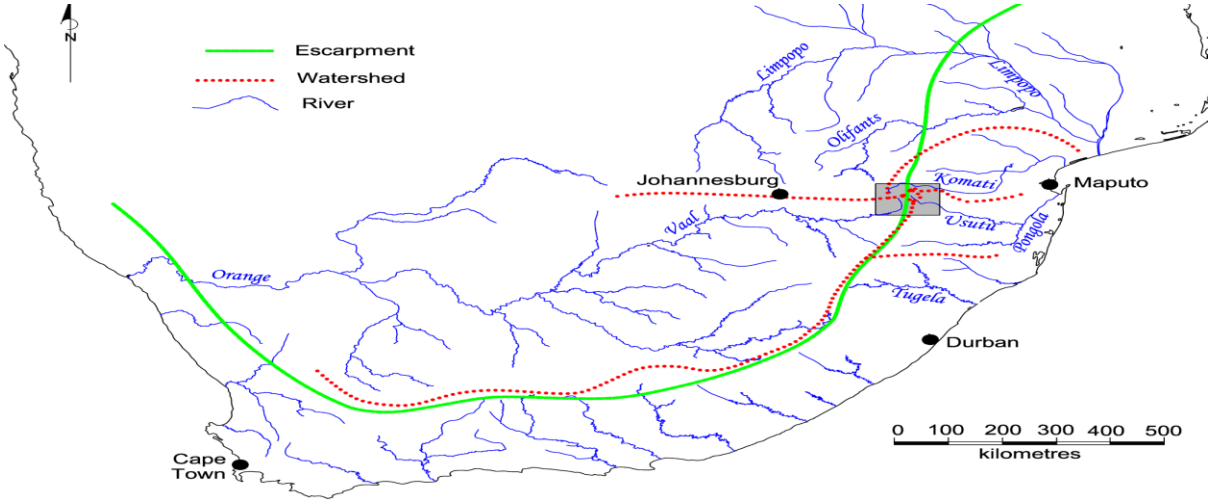


Figure 2.7: Map showing the river network in South Africa (DWAF, 2013)

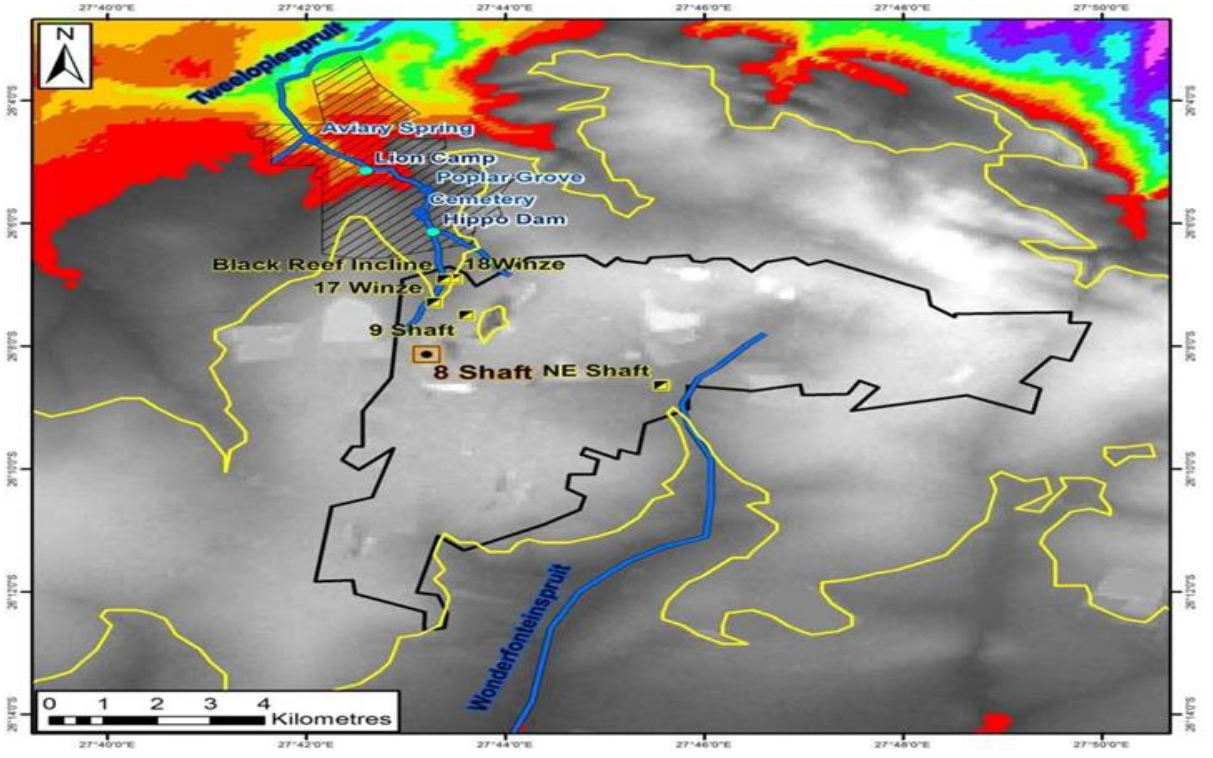


Figure 2.8: Google Map showing the Black Reef Incline, 18 and 17 (DWAF, 2013)

Oberholster et al. (2013) used physical, chemical and biological parameters to develop and evaluate an ecotoxicological screening tool that can be used to categorize AMD in impacted Tweelopies and Bloubank streams. The study incorporated investigating impacts posed in impacted streams and assessed downstream tributaries using the ecotoxicological screening to assess and prioritize future remediations plans. Several AMD studies to investigate adverse

impacts of mine water in streams and rivers made use of one or more biological indices (Jarvis and Young, 2000). In the United Kingdom more often Biological Monitoring Working Party (BMWP) score is used to assess impacts of mine water pollution. This index makes use of benthic macro invertebrates as bioindicators to determine AMD impacted stream sites. Its performance is based on the principle that different aquatic invertebrates have different tolerance to pollution. In South Africa, currently there is no screening tool specifically for AMD which employs both physicochemical and bioindicator parameters conjunctively. However, a study conducted by Oberholster et al., 2013, developed and evaluated an ecotoxicological screening tool (EST) to prioritise future remediation of streams impacted by AMD. According to Gray (1999), an Ecotoxicological screening tool (EST) integrates epilithic filamentous green algae biomass (chl-a mg m_2) and diatoms coinciding with physicochemical parameters and visual interpretation. Various organisms are employed as biological indicators of AMD impacted streams. For the identified study, selection of Epilithic filamentous green algae and diatoms was used because they are stationary and will directly indicate the physiochemical conditions of their habitat (Stevenson and White, 1995).

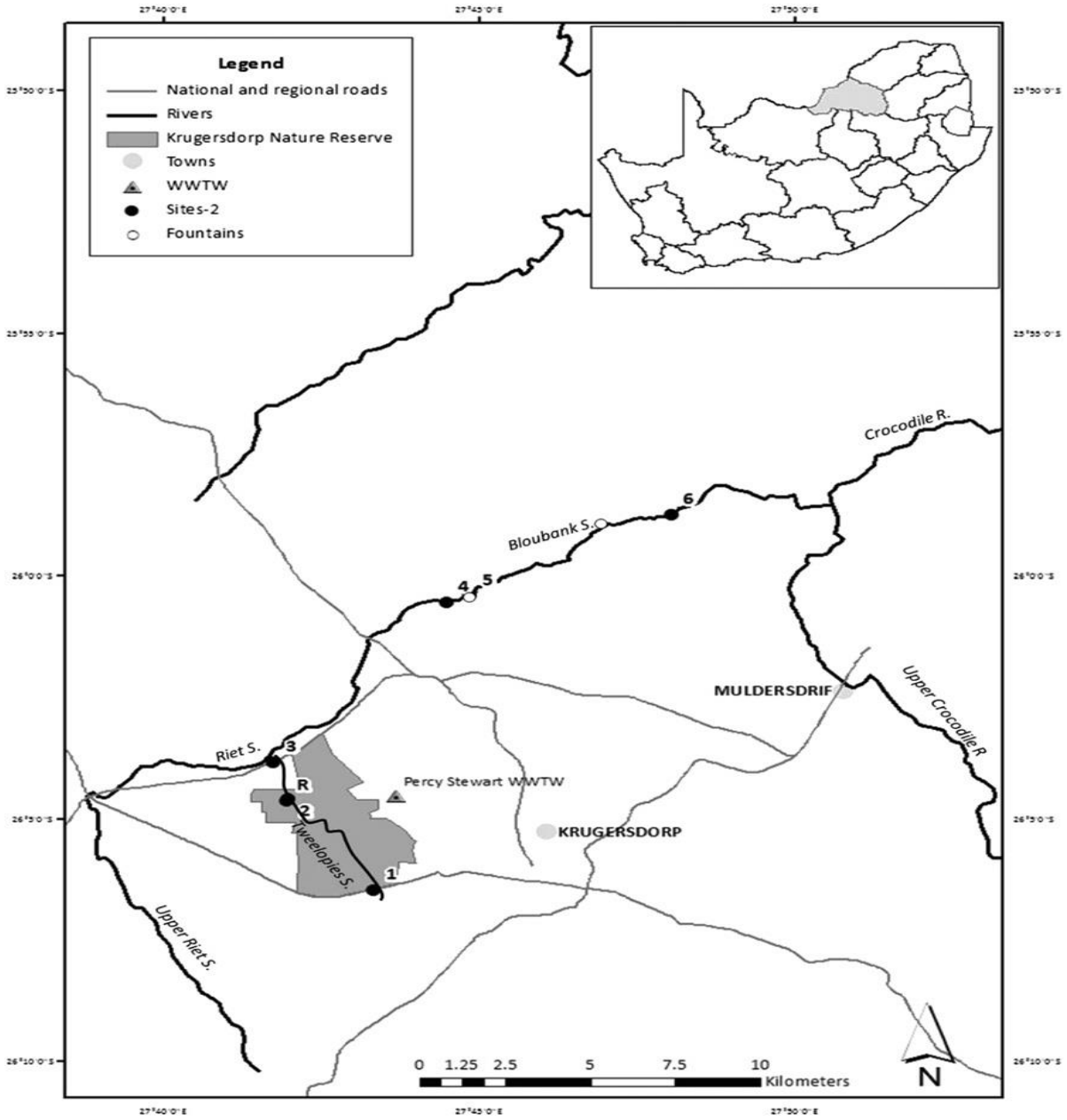


Figure 2.9: Map showing the location of the survey sites and watercourses (Oberholster et al., 2013, used with permission from Elsevier)

Figure 2.9 shows targeted survey sites used as sampling points. Basis for selecting the sites was on water chemistry (e.g. pH, conductivity and metal concentrations) and corresponding habitat characteristics (e.g. stream bank stability, substrate type and geology). Site 1 with a discharge of 24 ML/d is ± 500m downstream from the AMD drainage sources. Site 2 with 25 ML/d discharge and the reference (R) site at 0.9 ML/d are situated in the Krugersdorp Game

Reserve and the reference site which is natural wetland was not impacted by AMD. Site 3 is located few centimetres before confluence of the Tweelopies stream and the Riet stream discharging at 27.9 ML/d into Riet stream. Site 4 which open wider in area caused the discharge from site 3 to reduce to 17.9 ML/d and few meters downstream enters effluent from wastewater treatment plant. A karst spring discharging at 100 to 150 L/s is situated between site 4 and 5 and this together with the treatment plant effluent escalates site 5 discharge to 30.8 ML/d on the Bloubank stream. Another karst spring situated between site 5 and 6 discharging at 300 L/s increases discharge at site 6 which narrowed in shape and caused the discharge to be 61.9 ML/d.

Figure 2.10 presents the findings of the study. It can be noted that high metal concentration and low pH persisted within 6.5 km reach of Tweelopies stream between sites 1 to 2. The quality increased gradually at site 3 due to discharge from reference site not impacted by AMD. After the confluence with the Riet stream, metal concentration decreased dramatically due to dilution effect by the uncontaminated Riet stream and caused a rise in pH up to 7.5 at survey site 6. Benthic species range from site 1 to 6 revealed a generalized gradient of disruption by AMD discharge. Very low epilithic filamentous green algae was observed from site 1 to 3 which is within 5 km of Tweelopies and is directly affected by AMD discharge from the decanting sites, but gradual increase was observed in site 4 to 6 indicating decline in AMD strength. AMD has damaging effects on aquatic ecosystems and in lotic systems, a decrease in pH leads to a decrease in algal species diversity (Verb and Vis, 2000). High aluminium and iron concentration revealed adverse effect on biota showing decrease in metal concentration relationship with gradual increase in benthic diversity. Water samples from the 7 survey sites were collected and dispatched to the lab were Daphnia magna was subjected to this water to trace the animal's survival rates. Water from sites 1 to 3 produce 100% mortality rates because of suffocating condition of the water and site 4 water samples showed 35% survival rate. 80

and 90% survival rate were observed at site 5 and 6 showing increased water quality able to sustain life and justify dilution effect downstream and low AMD strength.

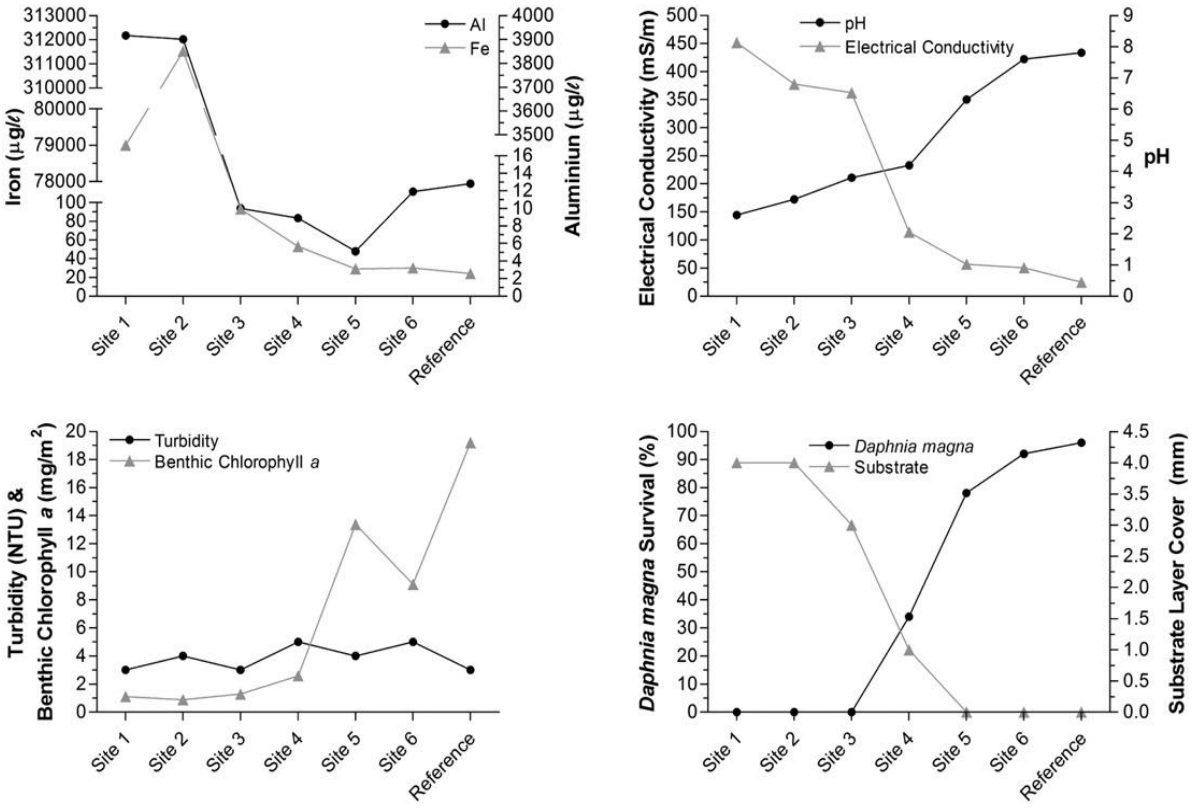


Figure 2.10: Spatial changes observed for selected parameters between the survey sites (Oberholster et al., 2013, used with permission from Elsevier)

2.7 Treatment of AMD

This study seeks to explore possibilities of polyethersulphone membranes infused with chitosan and coated with polyamide for AMD treatment. However, before discussing membrane technology in detail, an overview of various available treatment techniques for AMD is presented. Prevention is better than cure, generally it is preferable, although not always practical to prevent the formation of AMD in the first instance. Preventing or minimizing AMD formation requires excluding either oxygen or water or both from interacting with sulphide rocks as they are required to perpetuate the formation of AMD. However, most areas find it impossible to prevent formation or migration of AMD from its source and in such cases, it is only required to collect, treat, and discharge mine water (Johnson and Hallberg, 2005). Traditional technologies which have been applied for decades to rehabilitate AMD are active and passive treatment processes. The former depends on addition of alkaline materials which neutralises the acidity of the AMD and precipitate dissolved metals (Masindi et al., 2015) and the latter relies on the biological, gravitational and geochemical processes (Tolonen et al., 2014). Other active treatment technologies which have been researched include Ion exchange, adsorption and membrane technology amongst others (Masukume et al., 2014; Ricci et al., 2015).

2.7.1 Active treatment

Active treatment process involves addition of chemical-neutralizing agent (Johnson and Hallberg, 2005). The first reaction during AMD generation involves oxidation of pyrite into ferrous ion, which is soluble even at high pH. Further oxidation of the soluble ferrous iron gives off ferric iron which precipitates at pH greater than 3, 5. Addition of alkali materials (neutralizing chemicals) such as calcium carbonate, calcium oxide, calcium hydroxide or sodium hydroxide to AMD, causes a rise in pH. The dissolved ferric iron and other heavy metals will precipitate and be removed by sedimentation. The oxygen required for the entire

complete oxidation process from pyrite to ferric iron sometimes (oxygen transfer) becomes rate-limiting step as the amount required exceeds that present in AMD. For example, 9 mg/L of dissolved oxygen is required for AMD containing 63 mg/L (1.1 mM) ferrous iron for complete oxidation (Hustwit et al., 1992). Oxygen transfer can be a rate-limiting step because replenishment by diffusion is a relatively slow process. Any ferrous iron still existing in the treated water will cause oxidation of downstream water, producing further acidity and restoring the original problem. It then becomes necessary to incorporate water aeration procedure, or addition of a chemical oxidant such as hydrogen peroxide to completely oxidize ferric iron and this add to the costs of setting up and running a treatment plant. The last stage in conventional AMD treatment includes separation in settling ponds of the sludge produced, and discharge of the treated water to the receiving stream (Johnson, 1995). The disadvantage with this treatment technique is that the sulphate will sediment as gypsum ($CaSO_4.2H_2O$) sludge with high water content and still contains toxic metal hydroxides (Tolonen et al.,2014). Recovering the metal from the sludge has proven to be a difficult task and therefore, that makes the sludge to not have economic value. Thus, the sludge needs to be disposed of in an environmentally friendly manner to avoid leaching out of the metals and creating a secondary pollution (Chen et al., 2013; McDonald et al., 2006).

SAVMIN process is one of the active treatment technologies used to remove sulphates from AMD. The process consists of five sequential stages. Initially, lime is added to precipitate heavy metals as hydroxides. Then calcium and sulphate ions are removed by contact with gypsum crystals in stage 2. In stage 3, aluminium hydroxide is added to the saturated gypsum solution to form insoluble ettringite which gets optimized at relatively high pH. The solubility of the ettringite is sensitive to pH and requires control within a narrow pH range. In the fourth stage, the product water is stabilized by re-carbonation by adding CO_2 in order to reduce the pH which was elevated in the third stage. Finally, aluminium hydroxide is regenerated by

decomposing the ettringite with the help of sulphuric acid. The aluminium hydroxide is separated from the solution and the supersaturated gypsum solution is allowed to crystalize (Silva et al., 2012; Fernando et al., 2018; Guerrero-Flores et al., 2018)

2.7.2 Passive treatment

Passive treatment systems involve using sulphate-reducing bacteria or limestone or both to neutralize acidity and precipitate dissolved metals. Passive bioreactors rely on sulphate-reducing bacteria (SRB) that can be found in natural environments where anoxic conditions prevail (Neculita et al., 2007. As an alternative technology for acid mine drainage (AMD) treatment, sulphate-reducing bacteria received much attention. Activity of sulphate reducing bacteria (SRB) is controlled by the reactive mixture composition and this limit the long-term efficiency of the process (Neculita et al., 2007). Zhang et al. (2016) utilized novel immobilized sulphate-reducing bacteria beads for the treatment of synthetic AMD in an upflow anaerobic bioreactor. It was established that the bioreactor filled with SRB beads demonstrated high resistance to AMD containing high concentration of heavy metals with high removal efficiencies of over 99.9%. Removal of heavy metals and sulphates from synthetic AMD by Desulfovibrio desulfuricans, sulphate reducing bacteria and indigenous bacteria were studied by Hwang and Joh (2018). It was noted that the activity of SRB was inhibited by the presence of heavy metals in the synthetic AMD and the heavy metal removal process involved metal sulphide formation and biosorption.

Operating costs including labour, reagents and residual disposal and passive treatment with its typical requirement for acidity-dependent, land areas for bioreactors and aerated cells and ponds elevate the costs and make this technology less attractive. Adding alkaline materials such as lime cause the pH to increase and accelerate the chemical oxidation rate of ferrous iron (for which active aeration or addition of a chemical oxidizing agent such as hydrogen peroxide, is also necessary), and cause many of the metals present in solution to precipitates as

hydroxides and carbonates. This will result in the production of iron rich sludge that may also contain several metals depending on the chemistry of the mine water treated (Johnson and Hallberg, 2005). Mostly, the sludge produced is collected and disposed of through burial or injection into abandoned mine (Hedin, 2003). However; little effort has been focused on the beneficial use of precipitated metals in these systems, especially in passive systems as oxides, carbonates, or sulphides. Recovery of these minerals will not be as profitable as the mine itself, due to slow reaction kinetics of the process (Gusek and Clarke-Whistler, 2005).

2.7.3 Ion exchange technology

Ion exchange is a physical separation process which takes advantage of oppositely charged pollutant and employed solid resin to remove cation and anion from solutions (Manahan, 2005). The solid resin frameworks are characterized by either positively charged functional groups to interact with anions or negatively charged functional groups to interact with cations. The bonds formed are strongly bound but sometimes weakly bounds may result and get easily displaced through selectivity by stronger binding ions (Neumann and Fatula, 2009). The advantage of ion exchange is that it has shown high contaminants removal efficiency, it produces less volume of sludge and it has capability to recover the metal bounds. A high heavy metal ion uptake capability of this resin makes ion exchange an attractive technology but it's a desirable technology for low metal ion concentration. It then becomes a very expensive technology when dealing with high metal ion concentration solutions. The resins need to be regenerated when they are exhausted by chemicals and this regeneration can pose a secondary pollution and it elevates operational costs. Synthetic and natural resins are common resin materials used in ion exchange having ion exchanges sites classified as cationic, anionic and chelating exchange resin.

2.8 Membrane technology

Since current conventional methods only achieve partial treatment and have disadvantages of producing large volume of toxic sludge, have high energy consumption and require frequent maintenance (Ali et al., 2005), membrane technology has emerged as an eminent and promising alternative technology to substitute conventional methods for AMD remediation (Hilal et al., 2005). Advantages such as easy operation, inexpensiveness, low energy consumption, high separation efficiency and no need for integrated steps for further treatment, makes membrane technology an effective and attractive technology (Zhong et al., 2006).

2.8.1 Membrane types

Membrane is a thin layer of semi-permeable material which creates a barrier that traps and separate substances when a driving force is applied across (Daramola et al., 2015). Microfiltration (MF), ultrafiltration (UF), nanofiltration(NF) and reverse osmosis (RO) (Figure 2.11) are common pressure driven membrane separation processes currently employed with hollow fiber, flat sheets, spiral or tubular configurations (Maphutha et al., 2013). Advances in membrane technology development have significantly reduced the cost of membrane-based systems. Membrane pore-sizes, dimension of desired elements, solute diffusivity within the membrane matrix and associated electrostatic charges are part of key parameters when selecting a membrane (Cheryan, 1998). A significant characteristic of a good membrane includes mechanical strength, chemical resistance and thermal stability and this are highly influenced by the material of construction and the synthesis method.

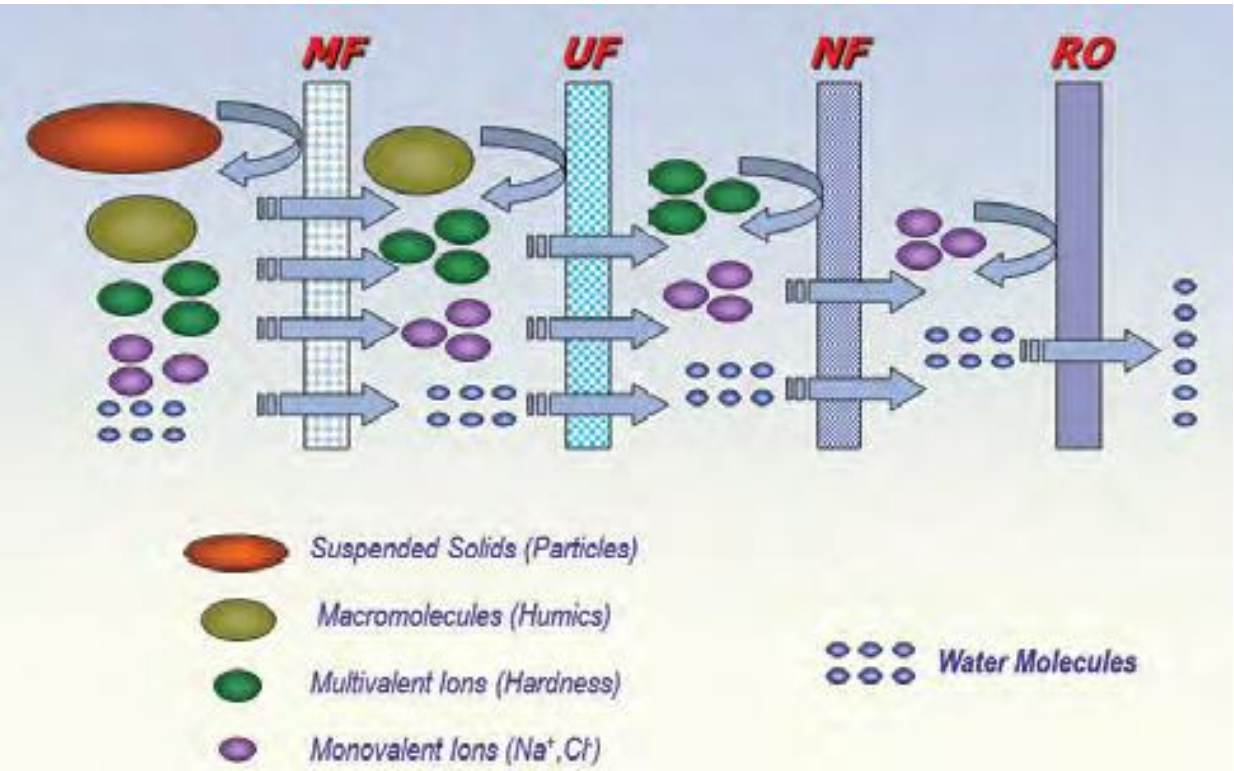


Figure 2.11: Pressure driven membranes (extracted from *https://www.wateronline.com/doc/nanofiltration-the-up-and-coming-membrane-process-0001* on 22/02/2020)

2.8.1.1 Microfiltration

Microfiltration is applied to remove suspended solids and living organisms but is unable to retain any type of dissolved solute. It is characterised by membrane pore sizes between 500 nm and 1 micron with operating pressure ranging from 0.2 to 3 bar (Ma et al., 2015). It removes material such as algae, bacteria except for viruses, sand, cysts and sand. It is usually applied as a pre-treatment to NF and RO membranes (Zhu et a., 2014a).

2.8.1.2 Ultrafiltration

Ultrafiltration membrane is a low-pressure membrane type consisting of pore sizes ranging from 2 to 20 nm and operating pressure range of 0.5 to 10 bar (Gao et al., 2014). The main disadvantage of this type of membrane is that it allows metal ions to pass through. It is suitable

for the rejection of groundwater viruses, colloids and most proteins. This type of membranes is usually applied as support material for enhancing metal ion removal and permeability (Leštan et al., 2008).

2.8.1.3 Nanofiltration

NF membranes which are intermediate membranes between UF, and RO membranes have higher permeate flux and can retain dissolved molecules with molecular weight greater than 200 to 300 g/mol and inorganic ions through electrostatic interaction between membrane charge and the ions combined with size exclusion (Carvalho et al., 2011). Membrane separation process (MSP) using Nanofiltration (NF) and reverse osmosis (RO) has been successfully applied to treat AMD due to their high salt and metal retention capacity (Ritchie and Bhattacharyya, 2002; Geise et al., 2010; Elimelech et al., 2011; Daramola et al., 2015). NF membrane is the most preferred because of its low required pressure and energy consumption, high selectivity and permeate flux. Although NF membranes have been reported as effective technologies to remove metals from wastewater, monovalent ions can still pass through (Gkotsis et al., 2014). The study conducted by Aguiar et al. (2016) showed NF membranes to be more suitable for gold AMD treatment than RO which had high permeate flux and solute rejection. Moreover, the study showed maximum water recovery of 60% with NF membrane under optimized conditions. Although the NF membrane had better results than RO membrane, its high fouling potential was worrying as it showed a sharper permeate flux decrease. Visser et al. (2001) employed NF membrane for the removal of calcium, sodium, chloride and sulphate ions from acidic water. It was established that under acidic conditions, sulphate removal was lower compared to 98% rejection under neutral pH. This behaviour was attributed to the likelihood of membrane charge changing from negative to positive and the availability of the HSO^-_4 ions.

2.8.1.4 Reverse Osmosis

Reverse osmosis is a type of membrane which can reject almost all materials including monovalent ions. They are characterised by very small pore sizes hence they require very high pressure of around 7 to 100 bar (Gkotsis et a., 2014). They have gained much attention as they are able to reach high rejection of 95 to 99.9% for metal ions. However, their high energy consumption as compared to other type of membranes makes them less attractive (Ma et al., 2015).

2.8.2 Membrane aspects

2.8.2.1 Concentration polarisation

Concentration polarisation and membrane fouling are vital problems associated with membrane technology as they limit full potential utilization of this technology. The former, is reversible but inevitable phenomenon which refers to continual accumulation and attachment of rejected solutes or particles on the membrane surface (Hughes et al., 2007). The latter takes place when suspended or dissolved matter in the feed solution migrate from the liquid phase to form deposits either on the membrane surface, pore openings or within the membrane porous structure (Koros et al., 1996). During membrane separation process, the inevitable natural consequence of semi-permeability and selectivity of a membrane result in accumulation of rejected solutes or particles on the membrane surface (Li et al., 2015). When the feed flow approaches the membrane surface, solvent molecules penetrates through the membrane, but the solute are rejected and retained on the surface. These rejected molecules are relatively slow to diffuse back into the bulk solution and causes concentration gradient just above the membrane surface. The accumulated molecules form a layer on the membrane surface which obstruct solvent flow through the membrane and create osmotic back pressure that reduces the effective transmembrane pressure (TMP) of the system (Cui et al., 2010). Although, concentration

polarisation is an inevitable but a reversible phenomenon, it does not affect fundamental properties of the membrane (Hughes et al., 2007).

2.8.2.2 Membrane fouling

In contrast to natural concentration polarisation, which is reversible, fouling may cause irreversible loss of permeability of a membrane. The relative resistance to cleaning is a distinguishing factor between reversible and irreversible fouling. Reversible fouling is the type that can be easily removed with certain cleaning methods, while irreversible fouling remains even after cleaning. The part of fouling that cannot be cleaned by hydraulic means is termed hydraulically irreversible fouling. Similarly, that left over after chemical cleaning is named chemically irreversible fouling (Kimura et al., 2004). Commonly trouble-causing substances termed foulants during membrane operation are roughly divided into four categories; particulates, macromolecules, ions and biological substances. Organic matter is the most challenging since it exists in natural waters and can cause both reversible and irreversible fouling (Zularisam et al, 2007: Guo et al., 2009). Although these challenges are considered inevitable, their rate and extent is highly influenced by membrane properties, feed characteristics and operational conditions (Wei et al., 2010). Material of construction, membrane synthesis method, available functional groups and exposed operational conditions affect membrane properties and its antifouling nature (Aguiar et al., 2016). The effects of feed characteristics such as the feed solution pH and feed solution initial concentration are vital since they affect the membrane charge which could either protonate or deprotonate functional groups on the membrane structure (Carvalho et al., 2011). Temperature, feed flow rate and pressure influence the movement of foulants towards the membrane surface and the treatment capacity of the membrane (Wei et al., 2010). Membrane fouling needs to be effectively and efficiently controlled and minimized as it could result in increased operational costs and

shortens the membrane life and have unpredictable separation performance (Agenson and Urase, 2007).

2.8.3 Membrane material

Choice of materials to fabricate membranes is important because they play an important role on the performance of the system (Qu et al., 2013). Depending on the material they are made of, membranes usually applied during wastewater treatment are classified as either organic or inorganic. Inorganic membranes are usually made of metals, glass or ceramics. Most ceramic membrane material includes alumina, zirconia, zeolites, silica and other nanoparticles. Inorganic membranes are more resistant to chemical and thermal attack during cleaning hence original water flux can be restored after extensive fouling (Labbez et al., 2003). Although inorganic membranes have desirable properties, their high cost of manufacturing and poor pore size distribution and control limit their full application in small-scale operations (Faibish and Cohen, 2001).

On the other hand, organic membranes are composed of natural or synthetic polymers such as tetrafluoroethylene, cellulose acetate, polyvinylidene fluoride, polysulphone and polyethersulphone just to name the few. Synthetic polymers are common materials used for membrane manufacturing, although other materials such as ceramic and metallic could be available (Nedzarek et al., 2015). Polymeric materials due to their non-toxic and biodegradable properties, attracted enormous attention for membrane synthesis application (Garni et al., 2017). Depending on the desired membrane properties, various materials used as polymeric membrane precursors include polyvinylidene fluoride, cellulose acetate, polypropylene, polyamide, polysulphone, polyethersulphone and polyacrylonitrile amongst others (Ahmad et al., 2013). Membrane properties such as surface charge, pH and oxidant tolerance, degree of hydrophilicity or hydrophobicity, strength and flexibility will dictate which membrane material could be used. Most commercial NF membranes available in the market are constructed using

Polyethersulphone (PES) material prepared through phase inversion method (Zhao et al., 2013).

2.8.4 Membrane preparation methods

There are several membrane methods and modification strategies to prepare different kinds of membranes. These methods include sol-gel, interfacial polymerization, dip-coating, phase inversion method, stretching, micro-filtration and extrusion (Lens and Kuenen, 2001). However, only interfacial polymerization and phase inversion methods will be discussed in this work. This is because phase inversion and interfacial polymerization methods are significant developments in the membrane science for synthesis of thin film composite membranes amongst the methods cited (Kong et al., 2011) and is the most preferred due to its simplicity (Liu et al., 2011). Polyamide membrane is one membrane which is prepared using interfacial polymerization technique (Lau and Ismail, 2011).

2.8.4.1 Phase Inversion method

Phase inversion technique is commonly used to develop membranes with desired composition, symmetry and morphology. It involves controlled conversion of homogenous polymer solution from liquid phase to a solid state facilitated by solvent and non-solvent exchange (Richards et al., 2012). Although other non-solvents such as n-methylpyrolidinone, methanol/water mixture could be used, water is commonly used as a non-solvent. The polymeric membrane forms due to the precipitation or solidification that takes place due to the mixing-demixing of the solvent and non-solvent after immersing the polymer solution inside coagulation bath containing the non-solvent (Wang et al., 2012).

The phase inversion method is comprised of several processes or stages before the final formation of the membrane. These steps include (but not limited to) thermally induced phase separation, solvent evaporation induced separation, immersion precipitation and vapour

induced phase separation (Gosh, 2008). The polymer solution or cast gel is cast on a suitable flat glass plate using a hand casting knife set at a desirable thickness, ideally 50 to 500 µm. Immediate solvent evaporation ensues in ambient temperature and subsequently immersed in a non-solvent coagulation bath. The resultant membrane is dried and stored until use. The type of polymer solvent/non-solvent and by varying the polymer concentration, membranes with different properties can be prepared (Misdan et al., 2013).

2.8.4.2 Interfacial polymerization

Interfacial polymerization is a technique commonly used to prepare thin film composite (TFC) membranes having various condensation polymers such as polyamides, polyurethanes, polycarbonates and polyureas (Freger, 2005). It involves a polymerization reaction between a polyfunctional amine dissolved in an aqueous solution and a polyfunctional acid chloride dissolved in an organic phase taking place at the water/organic phase (Roh et al., 2002).The TFC layer is developed on a porous layer supporting structures such as polysulphone or polyethersulphone amongst others. In the case of polyamide layers, two monomers such as m-phenylenediamine (MPDA) or triethylenediamine (TEA) are dissolved in an aqueous solution and react with trimesoyl chloride (TMC) dissolved in an organic phase (ideally hexane) at the water/organic phase. The properties of the organic solvent that govern the solubility of the amine monomer during reaction, as well as the diffusivity and reactivity of the monomers affect the morphology and network structure of the resultant membrane. Kim et al. (2002) demonstrated that the use of hexane as an organic solvent produced membranes with significantly smaller pores. The interfacial polymerization process is largely influenced by the diffusion of the amine monomer through the formed water/organic interface from the aqueous phase into the organic phase in order to react with the acid chloride (Tarboush et al., 2008). Initially, the membrane support (PSf or PES) is immersed in an aqueous solution with the polyfunctional amine (MPDA or TEA) monomer for few minutes and then afterwards, an

organic solution containing TMC in hexane solution is introduced and left for few seconds to allow interfacial polymerization to take place. Figure 2.12 shows mussel-inspired interlayer of polydopamine (PDA)/ polyethyleneimine (PEI) co deposited on polysulphone substrate to tune the interfacial polymerization of piperazine and trimesoyl chloride (Yang et al., 2017).

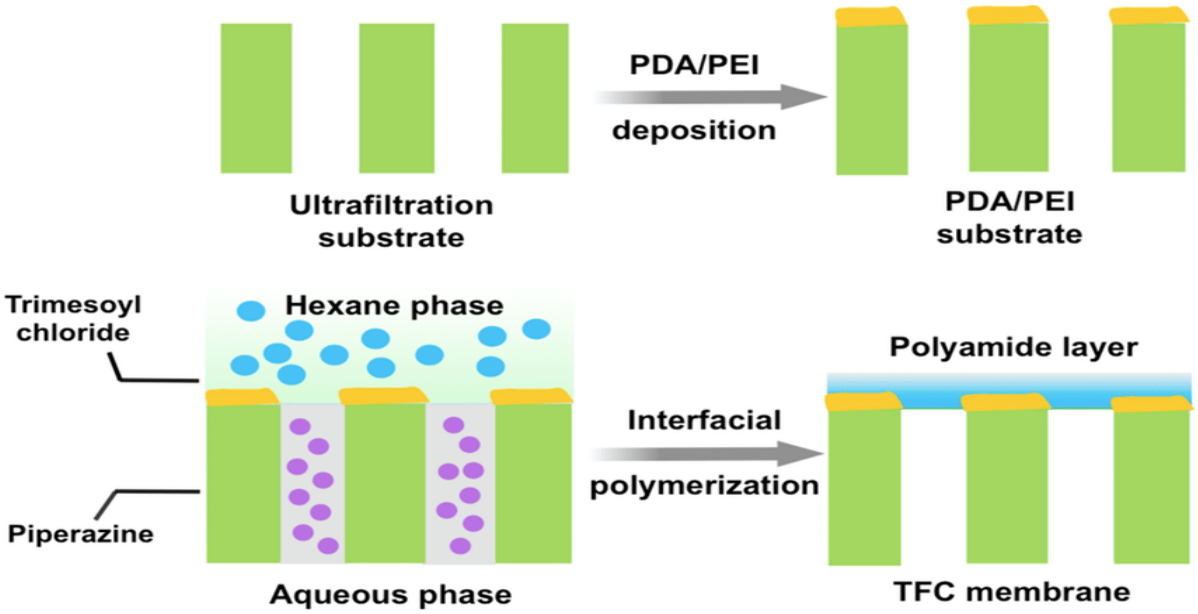


Figure 2.12: Schematic illustration of interfacial polymerization (Yang et al., 2017, used with permission from ACS publications)

2.8.5 Membrane Modification

Having been discussing challenges faced by membrane application such as membrane fouling and high degree of hydrophobicity which limit full application of polymeric membranes or reduce their lifespan, studies have been conducted to improve the performance of polymeric membranes through membrane modification. Amongst membrane modification techniques available, only surface modification of prepared membranes and blending will be discussed in this work. Surface modification methods can be classified as physical and chemical modification methods; however, only physical modification will be discussed (Cha and Yang, 2006). Physical modification method refers to the modification on the surface of polymeric

membranes by hydrophilic material due to physical interaction not through chemical reaction or covalent bonding (Bi et al., 2013).

2.8.5.1 Surface coating

Surface coating is a method which involves direct deposition of a thin layer on top of the membrane surface as a coating thin film layer. It is widely used to manipulate the surface chemistry of polymeric membranes. Surface coating is carried out by addition of hydrophilic materials that can lower the polymer-water interfacial energy which increases fouling resistance and water flux of the modified polymeric membrane (Xu et a., 2013). Coating hydrophilic materials on the membrane surface restrict movement and adsorption of foulants on to the membrane surface (Wu et al., 2010). Membrane modification using surface coating method, although it improves the salt rejection of the membrane, it sometimes compromises the flux. Additionally, the hydrophilic layer coated on the membrane surface will over time lose its durability and thus reduced the antifouling property of the membrane (Rana and Matsuura, 2010).

2.8.5.2 Blending method

Amongst other methods to modify polymeric membranes, blending with hydrophilic material is the simplest and most widely used. By directly blending hydrophilic polymers, polymeric membranes such as PES membranes are easily modified. The infused hydrophilic polymer helps to increase the hydrophilicity of the membrane and its antifouling property. Huang et al. (2011) modified the surface of PES membrane by blending methoxy poly(ethylene glycol)-polyurethane-methoxyl poly(ethylene glycol) triblock copolymers. The modified membrane showed to have good antifouling property. Polysulphone membrane was infused with sulfonated polyether-ethersulphone/polyethersulphone block copolymers by Knoell (1999). The produced membrane showed greater water flux and reduced biofouling potential.

2.8.6 Polyethersulphone membrane

Amongst other polymeric membranes, polyethersulphone (PES) and polysulphone (PSf) gained significant progress in acid mine drainage (AMD) treatment because of their high chemical and thermal resistance, high mechanical stability in hot and wet conditions and high permeability (Shockravi et al., 2017). Although PES exhibits higher degree of hydrophilicity compared to PSf, its inherent hydrophobic character result in serious membrane fouling which will lead to deterioration in permeation flux, shortening membrane lifespan and unpredictable separation efficiency (Agenson and Urase, 2007). PES and PES-based membranes have shown to have excellent thermal, oxidative and hydrolytic stability as well as good mechanical property. Membrane properties are highly influenced by the concentration, solvent, additives and temperature of the PES and PES-based membrane initial cast solution (Zhao et al., 2013: Barth et al., 2000).

Figure 2.13 shows the structure of PES. Phenylene rings connected by the sulfonyl groups offers polyethersulphone membranes high rigidity, chemical and thermal stability, oxidation resistance and high mechanical strength (Shen et al., 2011; Chen et al., 2013). The operating temperature for these membranes can reach up to 78 ^{o}C and have operating pH tolerance ranging from 1 to 13 (Baker, 2004b). Its commonly known that pure polymeric membranes are somewhat lacking in meeting complete requirements of a good membrane (Aroon et al., 2010b). Although PES and PES based membranes have been widely used, the main disadvantage is related to their hydrophobic character (Zhao et al., 2013). The high degree of hydrophobicity generated by the sulfonyl group linking the two phenylene rings leads to attachment of particles in the membrane pores and surface and this has consequential effects of reduced permeability as a result of fouling (Arkhagelsky et al., 2007). In a study, Mthethwa (2014) investigated the potential treatment of AMD by polyethersulphone hollow fibre nanofiltration membrane purchased commercially. The membrane reported a poor flux even

though the membrane had a larger surface area of 2 m^2. The hydrophobic nature of the membrane was concluded to have been responsible for various forms of fouling which contributed to the poor flux.

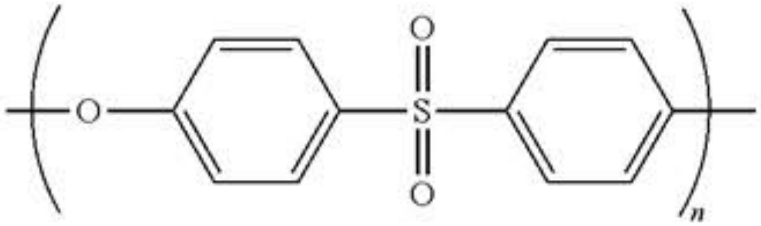


Figure 2.13: Polyethersulphone structure (PES) (Arkhagelsky et al., 2007, used with permission from Elsevier)

Several studies reviewed by Van der Bruggen (2009) and Khulbe et al. (2010) concluded that membrane fouling is directly related to hydrophobicity. Several interventions have been made to increase PES membrane's hydrophilicity during wastewater treatment to avoid quick membrane replacement due to irreversible internal and surface fouling (Louie et al., 2006). Pure polymeric and modified membranes that feature low fouling character and ability to restore water flux after cleaning would lower the replacement and maintenance cost of the technology during wastewater treatment. To overcome hydrophobic and selectivity challenges which limits the application of PES and PES based membranes, various alteration approaches such as blending, chemical, physical and surface modification approaches have been reported (Chen et al., 2013). The membrane modification technique aims to localize the hydrophilic material on the membrane surface and within the pores to positively influence membrane flux and selectivity and reduce fouling (Zhao et al., 2013). Addition of hydrophilic functional groups on to PES and PES based membranes through surface grafting (Rahimpour, 2011), coating (Reddy et al., 2003) or blending with hydrophilic polymers (Peyravi et al., 2012) or nanoparticles (Ji et al., 2015) could modify the membranes. Several attempts such as blending

nanoparticles in the membrane casting solution to modify PES membrane have been reported. Commonly introduced nanoparticles include TiO_2, (Sotto et al., 2011, Razmjou et al., 2011) Al_2O_3 (Maximous et al., 2010) and SiO_2 (Shen et al., 2011). Biofouling, which is initiated by bacterial activity which attach and grow on the surface of the membrane limit PES membranes application in water treatment (Zhu et al., 2010). Incorporating self-antibacterial materials within the membrane's matrix helps inhibiting development of biofilm (Yang et al., 2017). Several anti-bacterial agents such as silver ions/nanoparticles, TiO_2 and copper ions have been introduced to prepare antibacterial membranes (Zhu et al., 2010). However, most of these anti-bacterial agents such as silver, suffer from leaching problem due to poor compatibility with the polymer. Therefore, it requires introduction of carrier materials to release silver slowly (Chen et al., 2013). This makes modification with nanoparticle materials somewhat complex and costly.

PES membrane was embedded with polyaniline modified iron oxide nanoparticles to remove ions from solution (Darei et al., 2012). The adsorptive performance of polymeric membranes can be improved and/or optimized by introducing nanoparticles during preparation as an additive. As observed by Darei et al. (2012), Iron oxide showed great affinity towards heavy metals as compared to other metal oxides. The study also revealed improved adsorptive properties of Fe_3O_4 nanoparticles due to the presence of nitrogen atoms introduced by NH groups of the polyaniline. Membrane flux of the nanocomposite membrane reported to be low and this attested to be due to the hydrophobic nature of polyaniline. These revelations provoked Ghaemi et al. (2015) to investigate hydrophilic materials to modify the iron oxide nanoparticles to improve the flux. Nano-enhanced polyethersulphone mixed matrix membrane was fabricated by adding different types of iron oxide nanoparticles with silica, metformin and amine. The PES polymer and modified Fe_3O_4 blend led to an increased hydrophilicity and water

flux of the membrane with highly efficient copper removal. The study proved that incorporating hydrophilic materials have positive effect on the membrane flux and rejection.

Introducing chitosan and polyamide polymers as hydrophilic agents will improve the membrane's hydrophilic nature, anti-fouling property and selectivity. The advantage of blending PES with chitosan is that modification does not only take place on the membrane surface but also inside the pores (Ghiggi et al., 2017). Polyamide offers numerous active functional groups such as amines, free carboxylic acid and unreacted acylchloride groups which are prone to modification and can act as binding sites (Zou et al., 2010). Although hydrophilic polymers containing chitosan and polyamides have been reported to be extremely effective in enhancing hydrophilic nature and selective properties of polymeric membranes, little information is available in open literature on the use of chitosan and/or polyamide to modify PES and PES based membranes. This study seeks to introduce hydrophilic chitosan polymer by blending it with PES suspension and polyamide layer by coating it on top of the synthesised PES/chitosan membrane.

Chitosan is widely known as a sorbent for the removal of heavy and transition metals and dyes (Vieira and Beppu, 2006). Chitosan is a naturally occurring bio-compatible, bio-degradable, bio-renewable and non-toxic co-polymer composed of glucosamine and acetyl glucosamine derived from chitin, a natural polysaccharide (Shukla et al., 2013). Chitin, which is a high molecular weight linear polymer of 2-acetamide-2-deoxy-glucopyranose units connected by 1.4 glycosidic bonds (Figure 2.14 (a)), is the second most abundant natural fiber after cellulose. Chitin is produced by many different living organisms such as insects, shellfish, crabs, fungi, arthropods and crustacean shells (Rinaudo, 2006). Naturally, chitin occurs as three types ($\alpha, \beta \; and \; \gamma - structures$). The third type ($\gamma - chitin$) seems to just be a combination of the $\alpha -$ structure and $\beta -$structure rather than a third allomorph. $\alpha -$chitin is the most abundant and it is found in walls of yeast and fungal cells, shrimp cells, crab tendons and cells as well as

insect cuticle. β −chitin is rare and is found in association with proteins in squid pens (Rinaudo, 2006). Chitosan which is a biopolymer obtained through partial N-deacetylation of chitin, it contains one primary amino and two free hydroxyl functional groups for each C_3 and C_6 building unit (Figure 2.14 (b)) (Juang and Shiao, 2002). The large number of amino (-NH_2) and hydroxyl (-OH) groups which can act as contaminate binding sites and additional features such as high hydrophilicity, mechanical and chemical stability makes it attractive as membrane material and modifier. The reactive amino functional groups on chitosan structure binds almost to all group III and transition metals. In acidic medium, the amino group gets protonated and attract metal anions through ion exchange and repel cations through electrostatic repulsion (Anirudhan and Rijith, 2012).

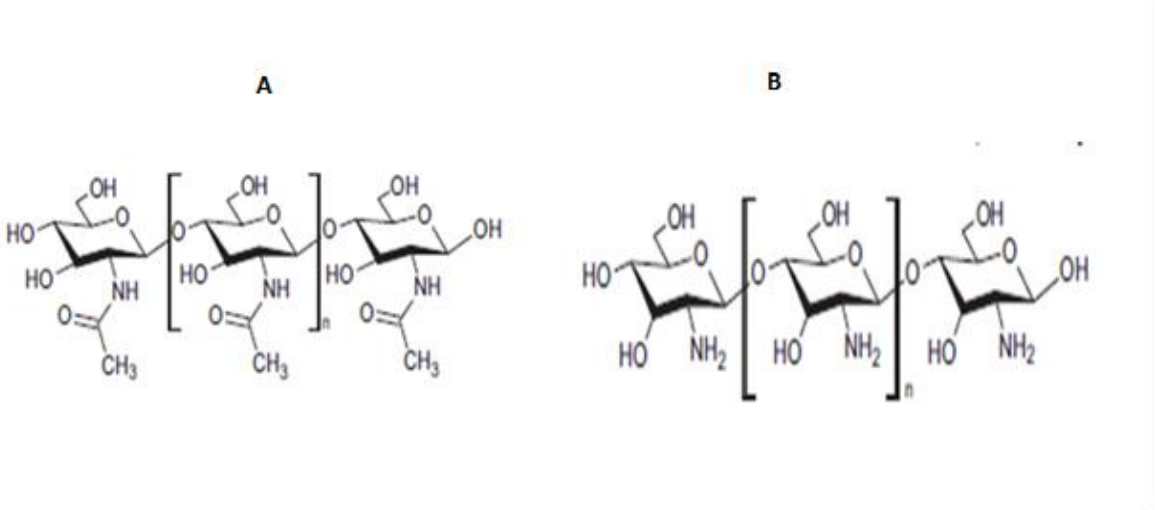


Figure 2.14: Structure of (a) Chitin and (b) Chitosan (Shukla et al., 2013, used with permission from Elsevier)

Recently, the use of chitosan has been receiving great attention in the development of novel functional composite materials, which are produced either by chemical modification or physical modification. Physical modification is the easiest way and is mostly done by physically mixing (Shukla et al., 2013). Although chitosan has lived up to some of its expectation of being a promising renewable polymeric material, some significant barriers to its

broader usage exist. Chitosan is characterized by its easy dissolution in many dilute mineral acids and thus improving the chemical stability using modifying agents for better treatment of acidic solutions containing heavy metals is essential (Anirudhan and Rijith, 2012). The study conducted by Juan and Shiau (1999) reported on the use of water-soluble chitosan membrane for the removal of divalent metal ions including Cu (II), Co (II), Ni (II), and Zn (II) from aqueous solutions by membrane filtration. High removal efficiency was observed with increasing chitosan concentration to metal ions due to high number of available binding sites on the chitosan structure. However, further increasing chitosan concentration triggered decline in membrane flux due to increased viscosity which enhanced concentration polarization and formation of a cake near the membrane surface.

Xie et al. (2013) studied chitosan modified zeolite as an adsorbent for the removal of different wastewater pollutants. The authors synthesized the zeolite from coal fly ash and modified it with chitosan. Results obtained showed that chitosan modified zeolite enhanced adsorption efficiency compared to the unmodified zeolite material during wastewater treatment. Ngah et al. (1998) also reported on high copper ions removal from solution using chitosan-zeolite composite as an adsorbent. . Popuri et al. (2008) demonstrated the possible removal of metal ions (Cu and Ni) from aqueous medium through biosorption on to chitosan coated PVC beads in column experiments. The chitosan coated PVC beads FTIR spectrum indicated the presence of original functional groups such as NH_2, OH which were still intact and available for interaction with metal ions after coating. The surface area (120.24 $m^2\ g^{-1}$), porosity (52.78%), pore volume (0.167 $cm^3\ g^{-1}$), cation exchange capacity (CEC) (4.6 eq g^{-1}) and surface charge density (SCD) (0.0034 m eq m^2) evaluated to the influence of surface properties on the extent of adsorption showed improved superior properties. Characteristic adsorption of platinum and palladium from aqueous medium using ethylenediamine-modified magnetic chitosan nanoparticles (EMCN) was demonstrated (Zhou et al, 2010). The study revealed several single

or mixed mechanisms including (i) Coordination on amino groups in a suspended manner or in combination with adjacent hydroxyl groups (ii) Electrostatic attraction in acidic media (iii) Ion exchange with protonated amino groups through proton or anion exchange, the counter ion being exchanged with the metal ion. Also, electrostatic attraction of anionic metal complexes was induced by the protonation of the amine groups on the EMCN and it increased available binding sites for the precious metal ion uptake.

Chethan and Vishalakshi (2013) achieved selective modification of chitosan through incorporation of ethylene-1, 2-diamine molecule for removal of divalent ions. The study employed chitosan derivative ethylene-1, 2-diamine-6-deoxy-chitosan (CtsEn) and its pthaloylated precursor ethylene-1, 2-diamine-6-diamine-N-pthaloylchitosan (PtCtsEn) for the removal of divalent ions (Copper, Zinc and Lead) from solution. The prepared chitosan derivatives showed to have higher metal ion adsorption capacity compared to the parent chitosan due to introduction of additional $–NH_2$ groups. Desorption studies also revealed possible successful regeneration of the adsorbents. The desorption tests carried out with an aqueous salt solution of pH 1,2 showed 92% of Cu and 97% of Zn desorbing from the loaded PtCtsEn while 83% of Cu and 85% of Zn desorbed from the CtsEn samples. This indicate possible regeneration at a pH of 1.2, because at this pH the nitrogen of the amine groups gets protonated and lose its affinity for metal ions releasing the latter from the binding sites. High hydrophilicity, charge density, mechanical and chemical stabilities, forms part of suitable features of using chitosan as a membrane modifier. Polyvinyl alcohol PVA/chitosan magnetic composite membrane was examined for the removal Co^{2+} from radioactive wastewater (Zhu et al., 2014b). In comparison with other adsorbents, the PVA/chitosan magnetic composite membrane prepared by Zhu et al. (2014b) reported high metal ion removal. In another study, Wang et al. (2011b) reported maximum adsorption capacity of 8.85 mg/g for applying magnetic multi-walled carbon nanotube/iron oxide composites for removing cobalt from solution.

Reiad et al. (2012) prepared microporous chitosan/polyethylene glycol mixed matrix membrane for the adsorptive removal of iron and manganese from aqueous solution. The polymeric blend of chitosan (CS) and polyethylene glycol (PEG) solutions was thoroughly stirred with 2% solution of glutaraldehyde as a cross linking agent between the two polymers. A cross-linked chitosan-PEG blend membrane was formed on a Teflon covered glass plate and was neutralized with NaOH solution. Three different membranes were prepared (CS: PEG 1:1, 2:1 and 4:1). The XRD patterns indicated a higher crystallinity for the blend membrane than that of chitosan and this confirmed its stability. The authors also concluded that the blend membrane is reusable after successfully desorbing iron and manganese ions adsorbed during the treatment using batch adsorptive.

Boricha and Murthy (2009) synthesised new blend membranes with different chitosan (CHS) and acrylonitrile butadiene styrene (ABS) composition coated onto Polyethersulphone (PES) as a backbone. The polymer blend was prepared by mixing various proportions of CHS and ABS polymer solutions in continuous agitation to obtain a homogenous polymer blend solution. A cross-linking agent glutaraldehyde was also added during agitation to provide intermediate link between the two polymers. FTIR-ATR characterization results confirmed the coating of CHS and ABS polymer blend on the PES membrane substrate. The XRD spectra of the four-polymer blend showed sharp peaks attributing to the semi-crystalline nature of the polymer blends. An increased in CHS content showed variation in intensity indicating the amorphous nature of the membranes. Permeate flux is directly related to amorphous nature of membranes, therefore it was clear that CHS was more amorphous than ABS. The TGA analysis indicated that all the membranes coated with various polymer blends were stable up to +140 ^{o}C and no membrane material was lost but beyond this temperature a slight material loss was observed. After +330 ^{o}C there was rapid loss of membrane material indicating optimum thermal stability of the membranes.

The study conducted by Gherasim et al. (2013) reported the rejection efficiency of polyamide NF membrane (AFC 80) using lead solution. The AFC 80 thin-film composite membrane was characterised by an aromatic polyamide skin-layer coated on a polysulphone substrate was supplied to carry out the study. During the structural characterization of the membrane to determine the membrane's effective pore size and effective thickness to porosity, uncharged 500 mg/L glucose (MW = 180 g/mol, rs = 0.355 nm) was employed. l, 100% rejection was observed due to smaller pores of the membrane. Since the membrane pore sizes were to small, rejection tests with glycerol were then carried out. The findings revealed that the AFC 80 had very small effective pore sizes. The dissociation of functional groups of the membrane material and adsorption of different charged or polarizable solutes from the solution forms part of the most important processes of membrane charge formation. The Isoelectric point (IEP) of the AFC 80 membrane was reported to be at pH of 3.6, which pH≥ IEP becomes negatively charged and at pH ≤ IEP it becomes positively charged. Partial hydrolysis of polyamide leads to formation of ammonium ($-NH_3^+$) and carboxyl (-COOH) groups in which below the IEP the carboxyl groups remain dissociated while the amine groups are protonated and the cause the membrane to become positively charged. In contrast, above the IEP the carboxyl groups are dissociated, and the membrane becomes negatively charged. It was observed that the AFC 80 membrane was positively charged in Pb $(NO_3)_2$ solutions with pH≤ 6. This indicated that the AFC 80 membrane can carry out NF tests for removal of lead from solution at a near neutral pH. Introducing additional amine groups through modification with chitosan which is more hydrophilic than polyamide material will lead to improved membrane flux and rejection

Uranium removal from solution by polyethersulphone and polyamide nanofiltration membranes was studied and compared by Torkabad et al. (2017) under various operating conditions (feed pH, uranium feed concentration and transmembrane pressure). It was found that charge properties of both membranes and uranium constituents changed with pH. The

rejection and permeate flux results showed better performance for the polyamide membrane than the polyethersulphone membrane. However, the authors concluded that both nanofiltration membranes could effectively be used for uranium removal from wastewaters. Table 2.2 presented some PES and PA membranes modified with chitosan studies reported in literature

Table 2.2: Comparison of PES and PA membranes modified with chitosan.

Membrane	Target contaminate	Outcomes	Reference
PES Membrane	Fe^{2+}, Na^{+}, Mn^{2+}, Mg^{2+}, SO_4^{2-}, Cl^{-}	• Cation rejection more than anions • Divalent ions more than monovalent ions • Flux was very poor	Mthethwa, 2014
PES/PA Membrane	BSA	• 2wt% PA content had 10 times permeability • No metal ion removal	Shokckravi et al., 2017
PA Membrane	Glucose aqueous solution	• CAIP membrane had 4 times more water flux with no loss in salt rejection • CAIP gives control over thickness and effective pore sizes • 2wt% Acetone	Kong et al., 2011

PA/PEI membrane	NaCl salt Foulants (Lysozyme and cationic surfactant: DTAC &TAC)	• Increased flux after grafting with PEI • Poor salt rejection • Anti-fouling properties improved with addition of amines	Xu et al., 2015
PA/CHITOSAN Membrane	NaCl, Na_2SO_4,$CaCl_2$	• Increased flux • Reduced surface roughness • Improve anti-fouling • High salt rejection	Akbari at al., 2015

Shockravi et al. (2017) fabricated asymmetric high-performance membrane by directly blending already synthesised polyamide (PA-6) as a hydrophilic polymer with PES membrane. Filtration performance of the synthesised membranes was carried out in a Dead-end filtration set-up by permeating a solution of bovine serum albumin (BSA). The results showed improved permeability and antifouling property of the membrane by optimized polyamide content. It was also reported that the permeability of the polyamide modified membrane was 10 times more than that of pure PES membrane. When polyamide was introduced, a downward trend was observed in contact angle from 75.6 to 65.2. The interaction of the amide sites of the polyamide structure with the water molecules reinforced the transport of water through the membrane. This shows the influence of polyamide as an effective hydrophilic agent which improved the hydrophilicity of the membrane. However, the study did not demonstrate retention of metal ions by the membranes.

Akbari et al. (2015) studied the influence of coating chitosan onto polyamide nanofiltration membrane and evaluated its effect on separation performance, morphology and antifouling properties (Figure 2.15). The membrane was fabricated by first preparing a polyacrylonitrile (PAN) support by uniformly hand-casting 16% (w/w) PAN in DMF solution onto a glass substrate. Secondly, a conventional interfacial polymerization method was utilized to prepare polyamide (PA) membrane active skin layer on the microporous PAN support. Lastly, the polyamide membrane surface onto PAN support was then modified with chitosan by immersing in chitosan solution with different concentrations (0.1, 0.2, 0.3% w/w). Interfacial polymerization was confirmed to have occurred in the organic phase and amine monomers diffused through the PA layer already formed and reacted with the acylchloride in the organic side of the interface region (Kim et al., 2005). It was observed from the feasibility results of coating PA NF membrane with chitosan that increasing the PA top layer thickness leads to reduced amine monomers diffusion rate which in turn leads to fewer amine groups and more un-reacted acylchloride groups on the organic phase side. Then, when exposed to water the un-reacted acylchloride groups get hydrolysed into carboxylic acid. However, hydrolysis reaction of acylchloride is a relatively slower reaction compared to reaction of acylchloride with chitosan (amine and hydroxyl groups). As a result, it makes it possible to modify the PA surface layer by reacting the un-reacted acylchloride with the amine and hydroxyl groups of chitosan. The study investigated the effect of chitosan concentration up to 0.3 wt%, which reported the highest permeate flux of 63.6 $l/m^2.hr$ compared to 40.8 $l/m^2.hr$ of unmodified membrane. Additionally, chitosan has been proven to be more hydrophilic than polyamide hence high flux is reported with increasing chitosan content. The charge property of the membrane surface was investigated by changing pH of the feed solution (3, 7 and 11) using hydrochloric acid and sodium hydroxide. It was observed that under basic conditions, it led to formation of carboxylate anion which caused the membrane to become negatively charged. In acidic

medium, the amine groups on the chitosan structure attracted protons which converted them into quaternary amines and caused the membrane charge to be positive.

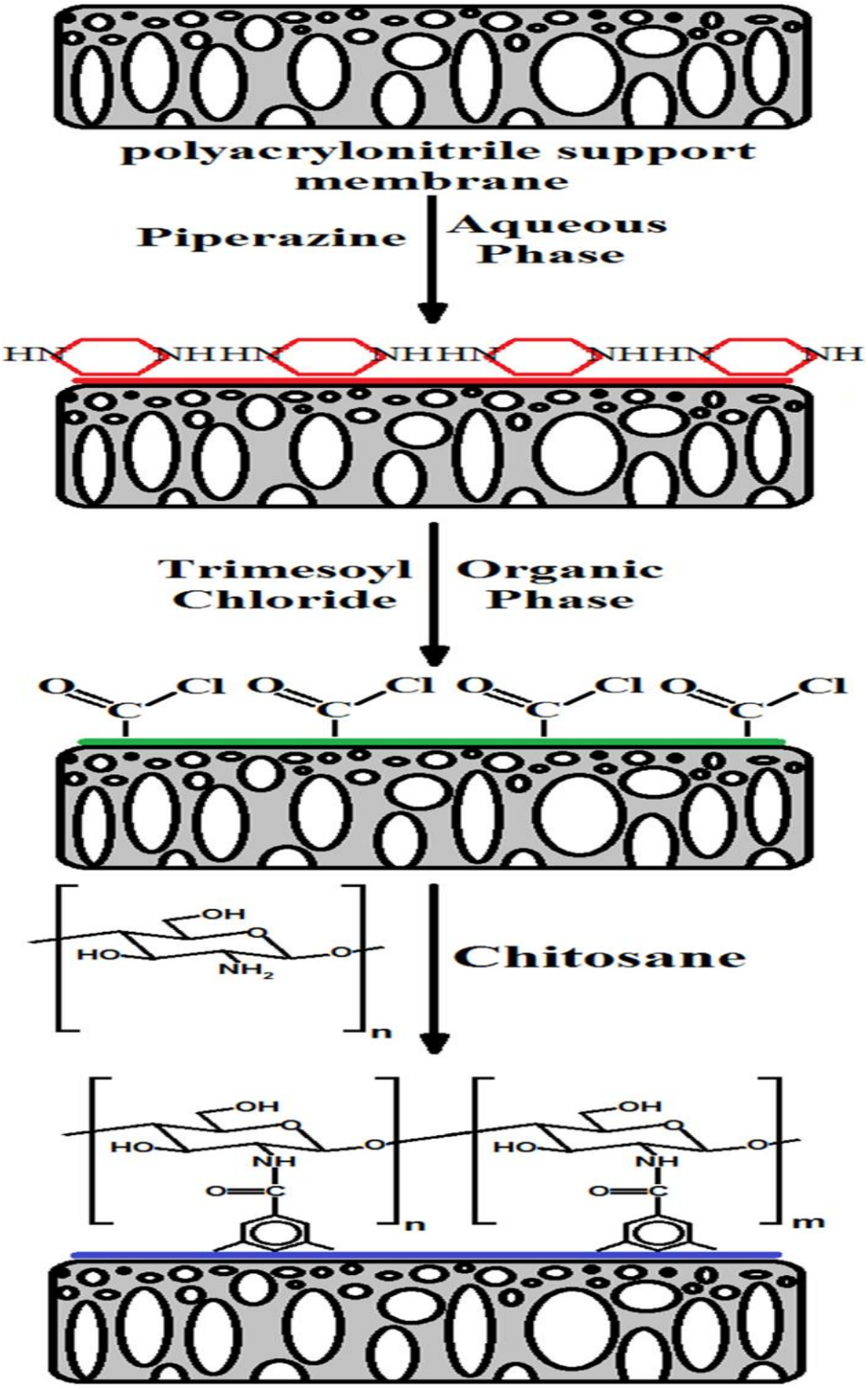


Figure 2.15: Conventional Interfacial polymerization and modification with chitosan (Akbari et al., 2015, used with permission from Elsevier).

According to a study by Kong et al. (2011) which fabricated high performance polyamide membrane from a novel polymerization procedure referred to as co-solvent assisted interfacial polymerization procedure (CAIP) (Figure 2.16), the current interfacial polymerization methods provide little control over the size interstitial voids and nanopores and the thickness of the polymer dense layer and in turn that limits permeability. In this study, it was possible to develop a novel polymerization procedure which will effectively have control on the thickness of the polyamide dense layer and nanopores sizes. This was done through a method they referred to as co-solvent assisted interfacial polymerization by adding a co-solvent (acetone) to a nonpolar organic (hexane) phase. The TEM and FE-SEM characterization results revealed a much thinner dense layer (less than 8nm) which is much thinner than the dense layer of membranes produced by conventional IP (more than 15nm). Thin dense layer will result in much higher water permeability because of less permeation resistance. Co-solvent acetone concentration within the 2.5 -5 wt% with the organic phase, increases the miscibility zone which in turn leads to lose reaction zone and a membrane with large pore sizes will results. The advantage of this technique is that a thin miscible zone will be formed in the water/hexane and acetone system once the acetone content is controlled. Immiscible binary system of water and hexane will form and a wide liquid to liquid region for the ternary mixture will remain giving control of the interfacial polymerization process. The membrane prepared via CAIP with 2 wt% acetone had 4 times higher water flux than those prepared by conventional interfacial polymerization.

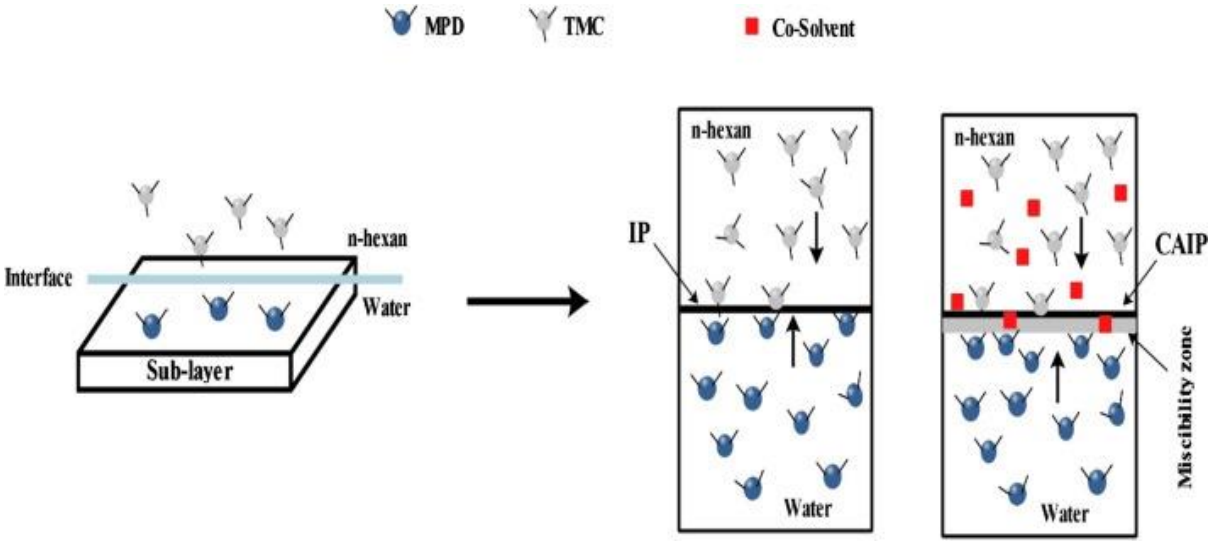


Figure 2.16: Schematic representation of conventional IP and CAIP using acetone (Kong et al., 2011, used with permission from Elsevier).

2.9 Hermia's models adapted to crossflow filtration

It's very important to predict membrane fouling during the design stage and as well as for monitoring during plant operation. Colloidal and soluble materials are considered to be responsible for membrane blockage while suspended solids account mainly for the cake layer formation (Judd, 2010).

Herman and Bredée (1936) studied the blocking filtration law during membrane filtration operation. Hermia (1966) first developed empirical intermediate blocking model and later revised and formulated four blocking laws in a common frame of power-law non-Newtonian fluids (Hermia, 1982). These four simplified fouling models by Hermia (1982) have been used for evaluating the membrane fouling mechanisms by various types of wastewater with complex compositions (Huang et al., 2007). Figure 2.17 depicts the membrane fouling

mechanisms of the respective blocking models

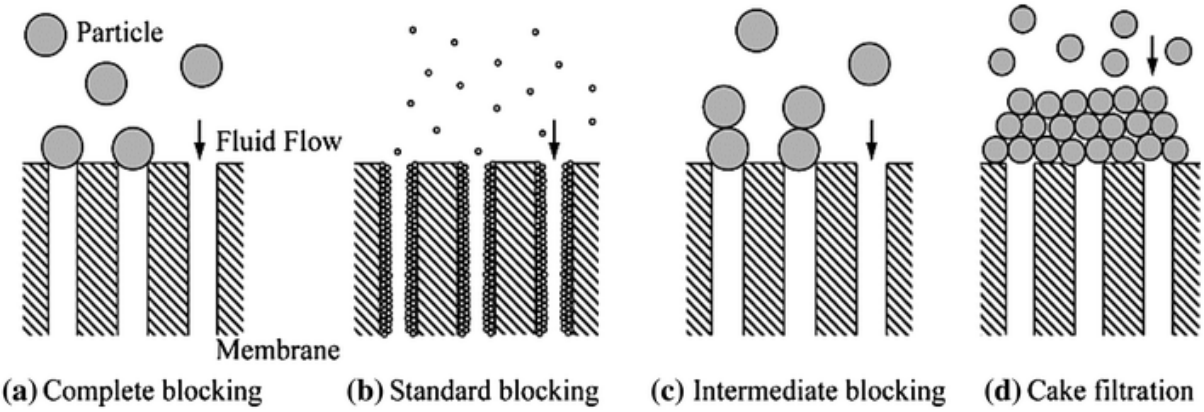


Figure 2.17: Schematic of membrane fouling mechanisms of the filtration laws (Amosa, 2017).

Four empirical models to describe fouling mechanisms for cross flow based on constant pressure filtration laws were developed by Hermia (Vela et al., 2009; Corbatón-Báguena et al., 2016). Hermia's model limitation is the assumption that some process parameters such as bulk concentration, temperature and TMP. Although, it's possible to control and maintain TMP and temperature of the system, bulk concentration of feed solution such as AMD containing more than solute concentration were filtrates are continuously rejected for further analysis becomes uncontrollable and accuracy might be significantly reduced (Jepsen et al., 2018). The four basic types of fouling are (i) complete blocking (ii) intermediate blocking (iii) standard blocking and cake layer formation models. The general equation is as follows (Eq (2.1)):

$$\frac{d^2t}{dV^2} = K_{DF}.\left(\frac{dt}{dV}\right)^n \qquad (2.1)$$

where *V* refers to the permeate volume while *t* is the filtration time is the filtration time. K_{DF} is a coefficient, K_{DF} is a phenomenological coefficient for dead-end filtration and n is the characteristic model constant. The classical filtration models were modified by Field et al (1995) to account for fouling removal mechanism occurring in crossflow filtration and the modification resulted in the following general differential equation ((Eq (2.2)):

$$-\frac{dJ_P}{dt} = K_{CF}.(J_P - J_{PSS}).J_P^{2-n} \tag{2.2}$$

where J_P and J_{PSS} represent the permeate flux at a specified time and flux when steady state is achieved, respectively. K_{CF} is a phenomenological coefficient for crossflow filtration and its units depend on the fouling mechanism which could either be complete blocking (n = 2), intermediate blocking (n = 1), standard blocking (n = 3/2) or cake layer formation (n = 0).

Complete blocking model for crossflow filtration (n= 2)

This model assumes that each solute molecule at the membrane surface contribute to blocking due to pore sealing. Additionally, each molecule settles on the membrane surface solely and never settles over other molecules that have previously settled and thus the permeate flux through the unblocked pores of the membrane is not affected. However, the fractional decline in flux is equal to the fractional decline in membrane surface area relative to the, thus the fractional reduction in permeate flux is equal to the fractional reduction in the membrane surface area corresponding to unblocked pores. The fouling mechanism which occurs during complete blocking takes place when the size of the membrane pores is less than that of the solute molecules. Hence it is assumed that pore blocking takes place over the membrane surface

and not inside the membrane pores (Hwang and Lin, 2002) . Complete blocking model can be adapted from the Hermia model: Equation (2.3)):

$$J_P = J_{PSS} + (J_0 - J_{PSS})e^{-K_c J_0 t} \quad (2.3)$$

$$K_c = \frac{3}{4}\frac{\rho_m \times X_m}{\rho_s a_P \varphi} \quad (2.4)$$

Where J_P and $J_0$are the permeate and initial fluxes (L/m^2.hr), respectively. J_{PSS} represents the steady state flux L/m^2.hr. K_c (Equation 2.4) is a constant that corresponds to the complete blocking model for crossflow filtration (m^{-1}). T is the filtration time (s). ρ_m andρ_s is the density of the feed solution and solute density over the membrane surface (kg/m^3). X_m = Solute mass fraction over the membrane surface (dimensionless). a_P= Is the radius of the solute molecule. φ = is the solute form fraction which is related to the ration of the major to minor dimension of the molecule.

Intermediate blocking model for crossflow filtration (n =1)

This type of a model contemplates that one membrane pore is not essentially blocked by one solute molecule. Thus, the probability of solute molecules landing on top of molecules already on the membrane surface is taken into consideration (Field, 1995). As such, intermediate blocking model is presumed to be less restrictive since some molecules might settle over others which are already on the membrane surface. Over time, the number of non-blocked membrane pores reduces with time, that is the probability of solute molecule blocking the membrane pores diminishes with time must be considered (Kołtuniewicz and Field, 1996). The physical model leads to Equation (2.5)):

$$J_P = \frac{J_0 J_{PSS} e^{K_i J_{PSS} t}}{J_{PSS} + J_0 (e^{K_i J_{PSS} t} - 1)} \quad (2.5)$$

The parameter K_i is the same as to the parameter K_c in Eq. (2.4). K_i represents the membrane surface blocked pores per unit of total volume passed through the membrane and unit of initial membrane surface porosity.

Standard blocking model for cross flow filtration (n = 3/2)

Standard blocking model considers that solute molecules enter the membrane pores and localize over the pore walls due to the irregularity of pore passages. This results in reduction of membrane pore volume. Some of the solute molecules are adsorbed over the pore walls and are not simply deposited over the internal surface of the membrane pores. Fouling during standard blocking is caused by molecules smaller than the membrane pore size and pore blocking occurs inside the membrane pores (Mohammadi et al., 2003). Consequently, the volume of membrane pores decreases proportionally to the filtered permeates volume. The decrease in the volume of membrane pores with time is equal to the decrease in their cross section. Besides, as fouling is caused by internal pore blocking, fouling becomes independent of the crossflow velocity and no limiting value for the permeate flux is attained, i.e. steady state permeate flux is zero for long time scales. Equation (2.6)) describes this model.

$$J_p = \frac{J_0}{\left(J_0 + J_0^{1/2} K_s\right)^2} \quad (2.6)$$

The parameter K_s represents the volume of solid retained per unit of filtrate volume, membrane thickness and inverse membrane surface porosity.

$$K_s = 2\frac{K_B}{A_0}AJ_0^{1/2} \tag{2.7}$$

K_B refers to the decrease in the cross-sectional area of membrane pores (due to adsorption on the pore walls) per unit of total volume permeated through the membrane. A_0 is the membrane porous surface while A is the membrane area.

Cake layer formation model for crossflow filtration (n = 0)

During cake layer formation model, it assumed fouling takes place due to solute molecules forming a layer or cake over the membrane surface (De Barros et al., 2003). Solute molecules do not enter the membrane pores. Therefore, pore blocking phenomenon is not considered although solute molecules in both pore blocking and cake layer formation models are greater than the membrane pores and do not enter them. The resulting equation is (Eq 2.8)):

$$t = \frac{1}{K_{gl}J_{PSS}}\ln\left[\left(\frac{J_P}{J_0}\frac{J_0-J_{PSS}}{J_P-J_{PSS}}\right) - J_{PSS}\left(\frac{1}{J_P}-\frac{1}{J_0}\right)\right] \tag{2.8}$$

The parameter K_{gl} is given by Eq (2.9). This parameter represents a ratio between the characteristics of the gel layer and those of the un-fouled membrane.

$$K_{gl} = \frac{aK_G}{J_0 R_m} \tag{2.9}$$

a and K_G represent the specific resistance of the gel layer and the gel layer mass per unit of total volume permeated through the membrane, respectively. R_m refers to the intrinsic membrane resistance determined using pure water as feed. The parameter K_G is related to the mass ration of wet to dry gel, the membrane area, filtrate density and the mass fraction of solutes in slurry. The specific resistance of the gel layer, a, represents the ratio of gel layer resistance and the accumulated solute mass per unit area of the membrane surface and it depends on solute density, solute radius and gel layer porosity.

It is worth noting that all the four models mentioned considers for the effect of temperature since they are all dependent on the initial flux, J_0, which depends on permeate viscosity and is highly influenced by the operating temperature. Additionally, all model constants are highly dependent on the density of the feed solution which is also influenced by temperature (Sommer and Melin, 2005). The adsorption of solute molecules on the membrane is also influenced by temperature. Therefore, depending on the measured temperature, the nature of this adsorption can be exothermic (Sen and Sarzali, 2008) (adsorption decreases with an increase in temperature) or endothermic (adsorption increases with an increase in temperature) (Bhatnagar et al., 2008). Adsorption of foulants onto the membrane surface occurs by diffusion of foulants to membrane surface followed by their interaction. Therefore, it is slightly influenced by tangential shear (Choi et al., 2005). The effect of adsorption may be higher in the case of the standard blocking model since, adsorption may occur inside the pores, which represent a higher area than that of the membrane surface (Blanpain-Avet et al., 1999).

2.10 Summary

This Chapter encapsulated a detailed and concise literature review related to this study. Membrane technology has emerged as a promising alternative for the treatment of acid mine drainage since most conventional treatment technologies have disadvantages of producing large volume of toxic sludge could pose secondary pollution, require frequent maintenance and achieve partial treatment. Performance of membranes is highly influenced by the construction material. Polymeric membranes attracted significant attention to be used as membrane material due to their non-toxic and biodegradable properties. The major disadvantage with most polymeric membranes is their high degree of hydrophobicity which limits their full utilization and reduces their lifespan due to fouling.

PES and PSf gained significant progress in acid mine drainage (AMD) treatment because of high chemical and thermal resistance, mechanical stability in hot and wet conditions and high permeability. PES and PES-based membranes have shown to have excellent thermal, oxidative and hydrolytic stability as well as good mechanical property, hence the choice to use PES as membrane support in the study.

Membrane modification becomes useful to improve the antifouling properties of the membrane. Blending and coating polymeric membranes with hydrophilic copolymers improves the membranes hydrophilicity without compromising selectivity. Introducing chitosan and polyamide polymers as hydrophilic copolymers will improve the membrane's hydrophilic nature, antifouling property and selectivity. The advantage of blending PES with chitosan is that modification does not only take place on the membrane surface but also inside the pores. The large number of amino ($-NH_2$) and hydroxyl (-OH) groups which can act as contaminate binding sites and additional features such as high hydrophilicity, mechanical and chemical stability makes it attractive as membrane material and modifier.

Polyamide offers numerous active functional groups such as amines, free carboxylic acid and unreacted acylchloride groups which are prone to modification and can act as binding sites. This study seeks to blend chitosan polymer within PES membrane matrix and coat polyamide layer on top to synthesise a novel membrane with enhanced hydrophilic, antifouling property and enhanced rejection during acid mine drainage treatment.

Chapter 3 Experimental Procedure and Materials

This Chapter gives an overview of the experimental methodology, which was followed, materials and equipment used in the study.

3.1 Introduction

In this study, pristine polyethersulphone (PES), polyethersulphone membrane infused with chitosan (PES/chitosan membrane) were synthesised using phase inversion method and PES/chitosan membrane was coated with polyamide (PES/chitosan/PA membrane) using co-solvent interfacial polymerization (CAIP). Chitosan used was synthesised from chitin found in crab and shrimp shells through the deacetylation process under strong alkaline solution of sodium hydroxide. Chitosan contains large number of hydroxyl and amine functional groups which can act as potential binding sites for contaminants. Polyethersulphone was infused with chitosan by blending PES suspension with chitosan particles to enhance its hydrophilicity and improve perm-selectivity of PES/chitosan membrane. Polyamide layer was formed on the PES/chitosan membrane through co-solvent assisted interfacial polymerization (CAIP) to produce PES/chitosan/PA membrane. Physicochemical properties of the synthesised chitosan and membranes were evaluated using TGA, FTIR, SEM, contact angle analyser and Tensile strength. Dead-end filtration and cross flow setup were used to evaluate the performance of the synthesised membranes during acid mine drainage treatment. Metal ion and sulphates of the feed and filtrates were analysed using AAS and Uv-Vis respectively. Standard solutions were used to calibrate the AAS equipment to produce a calibration curve. Different solutions of Na_2SO_4 concentrations were used to prepare SO_4^- ion for the calibration of the Uv-Vis equipment.

3.2 Material and Chemicals

Chitosan used in this study was synthesized from chitin which was obtained by processing seashells collected from Durban South Beach, Rutherford in KwaZulu Natal, South Africa and waste shrimp shells obtained from Jimmy's Killer Prawns in Fordsburg, Johannesburg, South Africa. Chemicals such as solvent dimethyl sulfoxide (DMSO), polyethersulphone (PES) granules (3mm), piperazine (PIP), triethylamine(TEA), trimesoyl chloride(TMC), acetone (C_3H_6O), sodium hydroxide (NaOH), hexane (C_6H_{14}), ethanol (C_2H_6O), sulphuric (H_2SO_4) and hydrochloric (HCl) acids and metal sulphates salts were purchased from Sigma-Aldrich (Pty) Johannesburg, South Africa. The chemicals were analytical grade, therefore, were used without purification. Deionized water was prepared in-house by-passing tap water through Ion exchange polymer resins. The water had pH of 6.89 and conductivity of 0.19 mS/cm.

3.3 Apparatus

The pH was measured using Metler Toledo dual meter (Sevenduo pH /conductivity meter with a Metler Toledo inLab Pro ISM pH electrode and inLab 738 ISM conductivity probe). Atomic Absorption Spectrometer (Thermo scientific ICE 3000 series) was used for analysis of metal ions. Uv-Vis was used to determine the sulphate content. Particle size distribution of the synthesised chitosan was analysed using laser diffraction technique (Malvern Mastersizer 2000 instrument). Surface morphology and cross-sectional image of the membranes were observed with Scanning Electron Microscopy (SEM), (TESCAN Vega 3xmu) equipped with EDS (OXFORD Xmas). TA. XT plus texture analyser was used to evaluate mechanical property of the membranes at room temperature. The membrane's hydrophobicity/hydrophilicity was investigated using Dataphysics Optical contact angle analyser (OCA 15 EC GOP). The contact angles of de-ionized water were measured using the sessile drop method on a dried surface of the membranes. Ten measurements were taken and averaged on different locations of the membranes. The characteristic functional peaks of the produced chitosan particles and surface

chemical structure of the membranes was analysed using Fourier Transform Infrared Spectroscopy (FTIR). The infrared spectra were recorded at room temperature in the wavenumber range of 4000 to 650 cm^{-1} using Perkin Elmer Spectrum. Thermal stability of the synthesised membranes was checked with Thermogravimetric Analyser (TGA).

3.4 Experimental methodology summary

Chitosan used in this study was synthesised from chitin by subjecting it to strong alkaline solution at high temperature through deacetylation process. The strength of the alkaline solution, time and temperature are the major variables affecting chitosan's degree of deacetylation (DD). FTIR was used to verify and confirm success in synthesising chitosan from chitin and was used to determine its degree of deacetylation. The effect of chitosan loading and its DD on the performance of the produced membranes was investigated. The synthesised chitosan particles were blended with PES suspension in dimethyl sulfoxide (DMSO) to produce PES/chitosan membrane casted using phase inversion method. Polyamide layer was coated onto the PES/chitosan membrane via co-solvent interfacial polymerization with acetone as a co-solvent to hexane. Properties of the produced membranes were characterized using TGA, SEM, FTIR, contact angle analysis and mechanical property. The permselectivity of the membranes was evaluated using a dead-end and crossflow filtration during the treatment of acid mine drainage. AAS and Uv-Vis were used to determine the metal and sulphate ions content respectively. The overall experimental procedure is given in the form of flow diagram in Figure 3.1.

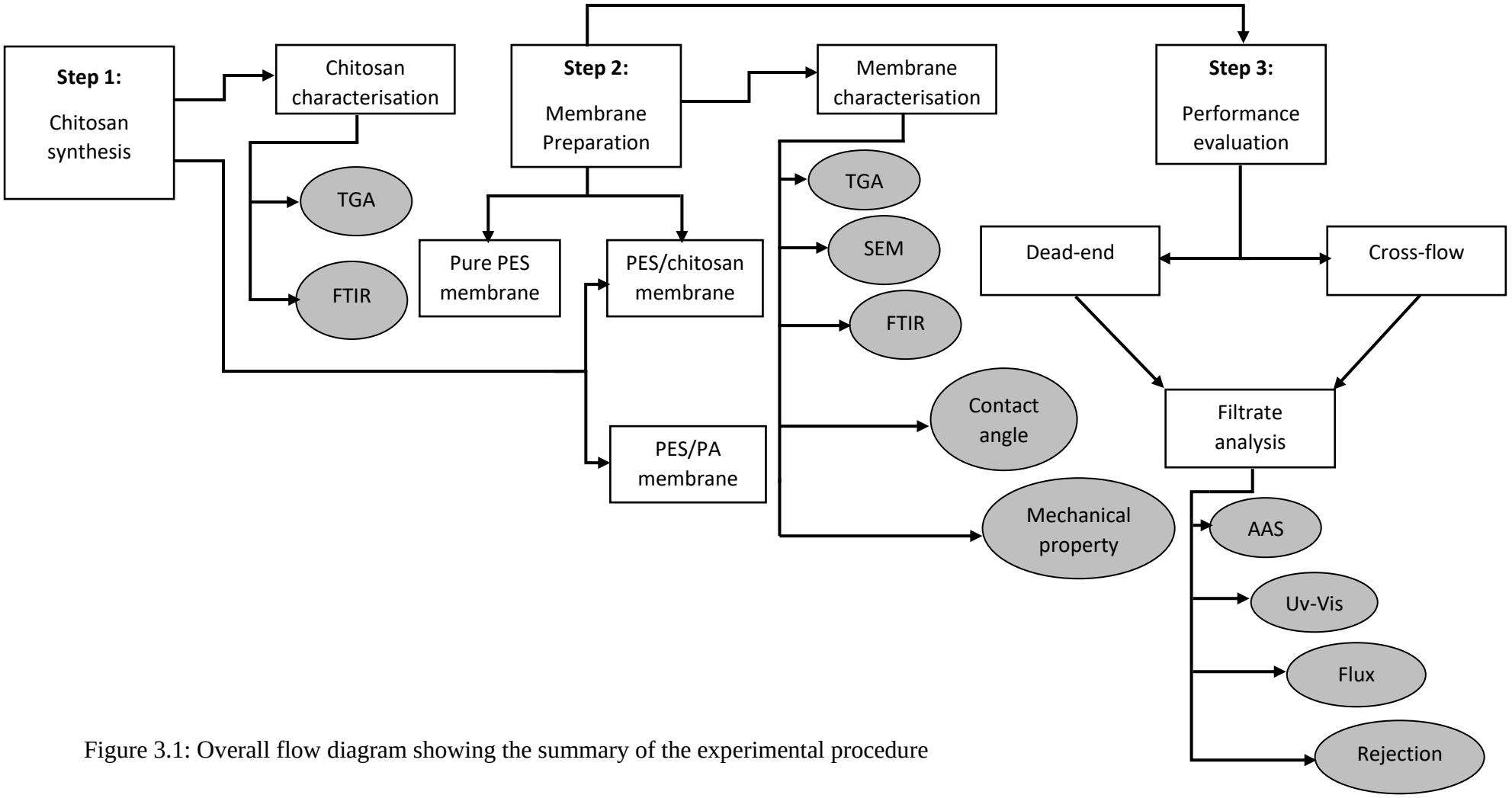


Figure 3.1: Overall flow diagram showing the summary of the experimental procedure

3.5 Chitosan production from chitin

Firstly, seashells were washed with water, and shrimp shells were boiled (94 ± 5 ^{o}C) in deionized water for 2 hours and dried in an oven at 120 ^{o}C for 1 hour in order to remove any impurities before crushing and milled with milling rods into fine powder (chitin). Crushed chitin was sieved to less than 100 µm before synthesising chitosan. The following steps were carried out in chronological order to synthesise chitosan from the milled chitin:

(i) Deproteinization: Chitin was treated with 6% NaOH solution at 60 ^{o}C in a 500 mL Erlenmeyer flask. The mixture was kept under constant stirring for 2 hours on a heating plate equipped with a magnetic stirrer. After 2 hours, the mixture was kept undisturbed under ambient conditions to settle the chitin particles and the supernatant alkaline solution was decanted. The residual was washed with deionized water until neutral pH.

(ii) Demineralization: The deproteinized chitin was subjected to a 6% HCl solution for 2 hours at 60 ^{o}C in a 500 mL Erlenmeyer flask. The mixture was kept under constant stirring for 2 hours on a heating plate equipped with a magnetic stirrer. After 2 hours, the mixture was kept undisturbed under ambient conditions to settle the chitin particles and the supernatant acidic solution was decanted. The residual was washed with deionized water until neutral pH.

(iii) Deacetylation: The deproteinized and demineralized chitin underwent treatment with various NaOH concentration and temperature to manipulate the DD of chitosan. Nine chitosan samples were synthesised and stored inside air tight containers. The solid to liquid ratio for all processes was set at 1:20.

It is postulated in literature that the NaOH concentration and temperature have the most significant effect on the DD of the synthesised chitosan (Habiba et al., 2017). Chitosan samples used to investigate the effect of chitosan loading were deacetylated with 40 wt% NaOH

solution, at 120 ºC for 6 hours. When optimum chitosan loading was determined, the DD of chitosan samples was optimized by investigating the synthesis process conditions to obtain chitosan with various DD. Table 3.1 shows synthesis process conditions. Those chitosan samples with various degree of deacetylation where then used to modify the membranes and determine their quality and performance during AMD treatment. It is against this background that temperature (80, 100 and 120 ºC) and NaOH (20, 40 and 60 wt%) concentration were varied, and reaction time was kept constant at 6 hours. The samples were prepared in duplicates to increase accuracy of the results obtained

Table 3.1: Chitosan synthesis process conditions from chitin

Chitosan Sample No	Synthesis Process	conditions
	Temperature(ºC)	**NaOH Conc (wt%)**
1	80	20
2	80	40
3	80	60
4	100	20
5	100	40
6	100	60
7	120	20
8	120	40
9	120	60

3.6 Membrane synthesis

The membranes were prepared by phase inversion method. Firstly, pure polyethersulphone membrane was prepared as a reference to the modified membranes. Secondly, the effect of chitosan loading and its DD on the quality and performance of the produced membrane (PES/chitosan membrane) was investigated. Lastly, the effect of coating polyamide layer on the PES and PES/chitosan membrane was also investigated.

3.6.1 Synthesis of Pure PES

Figure 3.2 depict steps followed to synthesise pure PES membrane. Firstly, 0.4g of PES granules were added to 3.6g of DMSO solvent (total mixture 4g) and agitated on a magnetic stirrer for 24 hours under room temperature which was measured as 26.8 ^{o}C at the time. Post 24 hours, the casting gel was left at ambient condition to liberate any available air bubbles. The casting gel was cast on a flat glass plate using a hand casting knife set up at 250 µm thickness. The glass plate with cast gel was immediately immersed inside a coagulation bath containing deionized water. The membrane was left inside deionized water for complete desorption of the solvent from the membrane sheet. The membranes were heated in oven to evaporate any trapped water and/or solvent from the membrane at 60 ^{o}C for 15 minutes.

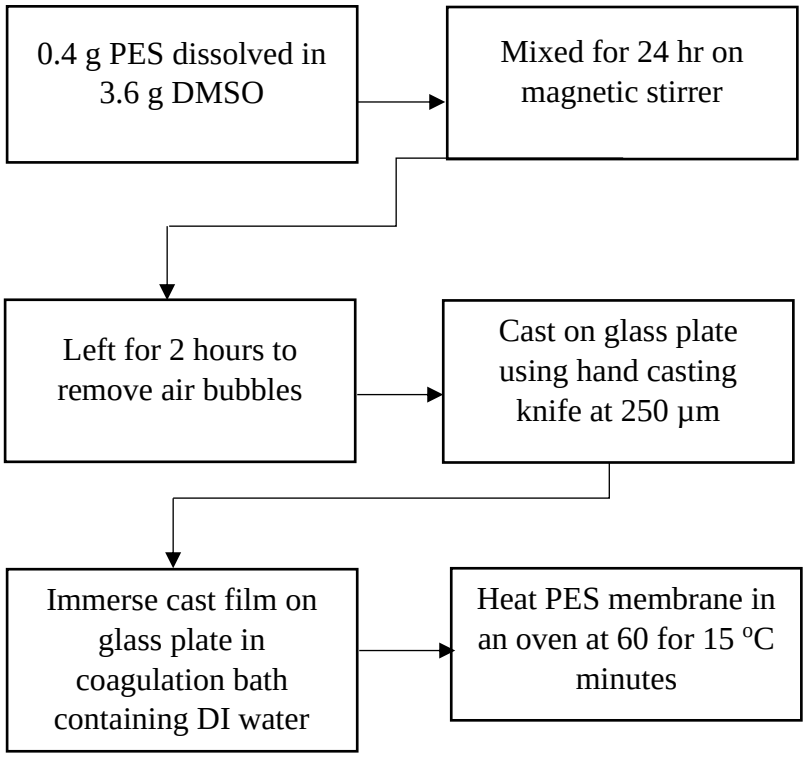


Figure 3.2: Steps followed to synthesis Pure PES membrane

3.6.2 Synthesis of PES membrane infused with chitosan (PES/chitosan membrane)

Similar phase inversion method was followed to synthesise PES/chitosan membrane. Only difference was that chitosan particles were blended with PES suspension after PES granules were dissolved with DMSO solvent. Figure 3.3 shows the steps followed and Table 3.2 shows composition of the cast mixture. PES granules were dissolved in dimethyl sulfoxide on a magnetic stirrer at room temperature measured at 26.8 °C. Once the PES granules dissolved, chitosan was added to the mix and was left for 24 hours to obtain a homogenous gel. Before casting, the casting solution was left at ambient conditions to remove any air bubbles. The gel was cast on a glass plate with a casting knife at 250 µm thickness. The membranes were heated in oven to evaporate any trapped water and/or solvent from the membrane at 60 °C for 15 minutes. First, the effect of chitosan loading was investigated and after the effect of chitosan's DD on the quality and performance of the membrane was investigated.

Table 3.2: Casting solution composition

Membrane Name	PES (wt%)	DMSO (wt%)	chitosan (wt%)
Bare PES	10	90	0
PES/0.5 wt% chitosan	10	89.5	0.5
PES/0.75 wt% chitosan	10	89.25	0.75
PES/1 wt% chitosan	10	89	1

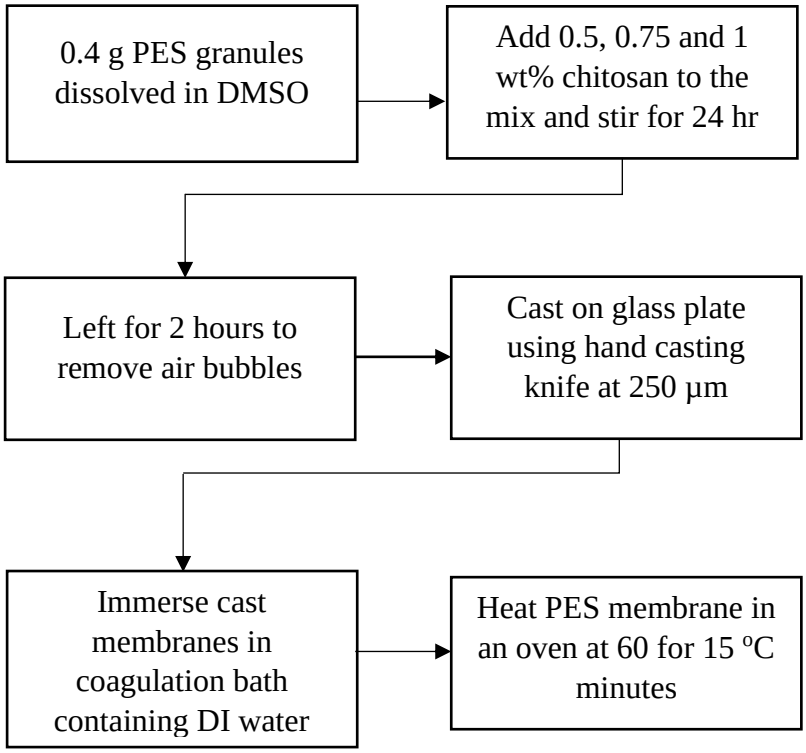


Figure 3.3: Steps followed to synthesis PES membrane infused with chitosan

3.6.3 Fabricating Polyamide layer

Co-solvent assisted interfacial polymerization (Kong et al., 2011) technique was followed to fabricate polyamide layer onto the prepared porous PES and PES/chitosan membranes. Diamine aqueous solution was prepared by mixing 2 wt% of piperazine (PIP) and 0.6 wt% of triethylamine (TEA). The already synthesised PES and PES/chitosan membranes were dipped in the diamine solution for 120s and placed between two filter papers to absorb any excess amine solution. Conventional interfacial polymerization occurred when the amine saturated PES and PES/chitosan membranes were immediately immersed in an organic phase solution containing 0.1 wt% trimesoyl chloride (TMC) and 5 wt% acetone in n-hexane for 60 seconds. The resulting membranes were cured at 60 ^{o}C for 5 minutes before washing thoroughly with deionized water. Digital Micrometer was used to measure the thickness of the membranes. The steps are schematically represented in Figure 3.4.

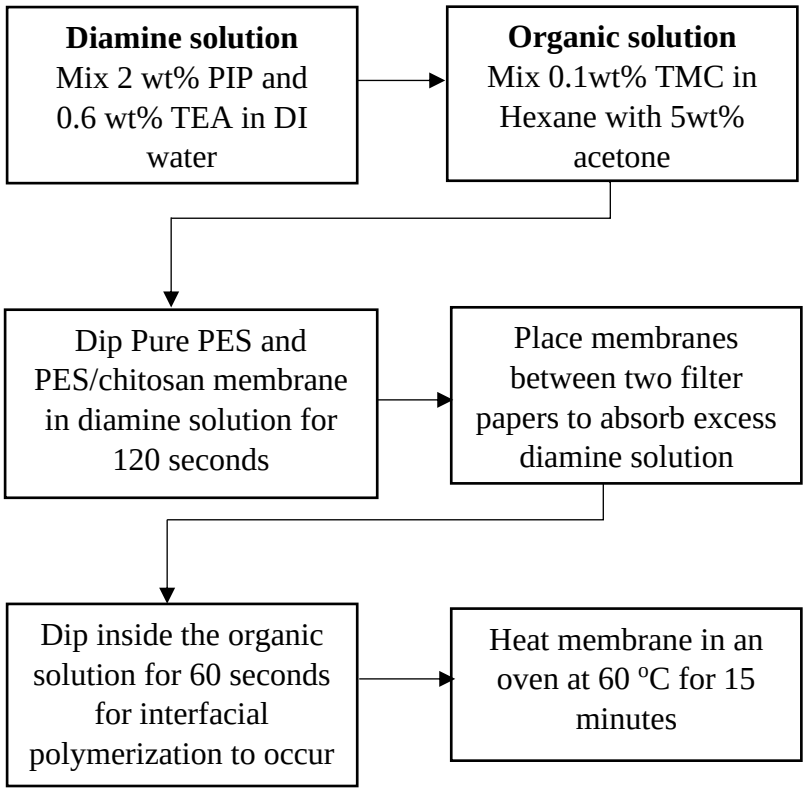


Figure 3.4: Steps followed to synthesis PES membrane infused with chitosan

3.7 Characterization of physicochemical properties of synthesized chitosan particles, pure PES, PES/chitosan and PES/chitosan/PA membranes

Chitosan was characterized using PSD and FTIR techniques. Pure PES, PES/chitosan and PES/chitosan/PA membranes were characterised using TGA, FTIR, SEM, contact angle analysis and mechanical strength techniques.

3.7.1 Thermogravimetric Analysis (TGA)

Thermogravimetric Analysis (TGA) is an analytical technique which measures the amount and rate of change in the weight of a material as a function of temperature or time in a controlled atmosphere. Measurements provide information which could be used primarily to determine the composition of materials and predict their thermal stability. The technique can characterize materials that exhibit weight loss or gain due to decomposition, oxidation, or dehydration. TGA analysis were carried out in the School of Civil and Chemical Engineering at UNISA, Florida campus, Johannesburg, South Africa.

3.7.2 Particle size distribution (PSD)

Particle size distribution (PSD) is an analytical technique which is based on the principle of laser beam scattering light through particles at angle that is directly related to the size. Smaller particles scatter light at high angles while larger particles scatter light at low angles. The measurable size ranges from 50 nm to 1000 μm. For PSD samples, the chitosan particles were sieved to obtain relatively uniform sample and was suspended in water as dispersant. The particle size distribution of chitosan was determined using laser diffraction method (Malvern Mastersizer 2000 instrument) in the School of Chemical, Metallurgical and Mining Engineering at the University of Johannesburg, Johannesburg, South Africa.

3.7.3 Fourier-Transform Infrared (FTIR) spectroscopy

Fourier- Transform Infrared (FTIR) spectroscopy is an analytical technique that measures and records infrared light absorption or emission of chemical bonds in molecules. Every bond or atom in a molecule absorb and/or vibrate at different specific wavelengths and that makes possible to identify them at those wavelengths. A beam of radiation energy passes through an aperture controlling the amount of energy delivered to the sample and ultimately to the detector. The beam then enters the interferometer where spectral coding occurs before the resulting interferogram signal exit the interferometer. The beam enters the sample compartment and depending on the required analysis, it is transmitted or reflected off the surface of the sample. This is where specific frequencies of energy are absorbed. Energy frequencies are uniquely characteristic of the sample, this makes it possible to determine and show which functional groups are present in the sample. FTIR can identify unknown materials and their quality. Chitosan was characterized using FTIR. Chitosan which is a principal derivative of chitin refers to partially or fully deacetylated chitin, which means the degree of acetylation is around or lower than 50%. Also means the degree of deacetylation is around or higher than 50%. Various methods are available in literature for chitosan characterisation, but the most discussed due to its simplicity is the infrared spectroscopy (Brugnerotto et al., 2001). It is for this reason that FTIR was employed to characterize chitosan and to determine its degree of deacetylation of the chitosan samples. Absorption band rations such as A_{1655}/ A_{3450}, $A_{1560}/ A_{897,}$ $A_{1320}/ A_{3450,}$ A_{1655}/ A_{2875} and A_{1655}/ A_{3450} have been previously used to determine the DD of chitosan samples (Tanhaei et al., 2016). However, the absorption band ration of A_{1320}/ A_{1420} have proven to shows superior agreement between the absolute and estimated DD values (Habiba et al., 2017, Abdou et al., 2008). The DD of the chitosan samples was determined using the following Equations (3.1) & (3.2) (Habiba et al., 2017, Brugnerotto et al., 2001, Abdou et al., 2008).

$$DA\% = 13.9\left(\frac{A1320}{A1420}\right) - 12.20 \quad (3.1)$$

$$DD\% = 1 - DA\% \quad (3.2)$$

Where DA% is percentage degree of acetylation and

DD% is the degree of deacetylation

Duplicate chitosan samples were prepared, and average values were taken.

An FTIR spectrum was also used to confirm functional groups present chitosan and polyamide on the PES/chitosan and PES/chitosan/PA membranes, respectively. FTIR analysis was performed in the School of Chemical, Metallurgical and Mining Engineering at the University of Johannesburg, Johannesburg, South Africa.

3.7.4 Scanning Electron Microscopy (SEM)

Surface morphology and cross-sectional images of the fabricated membrane were observed with Scanning Electron Microscopy (SEM), (TESCAN Vega 3xmu) equipped with EDS (OXFORD Xmas). SEM analysis was performed in the School of Chemical, Metallurgical and Mining Engineering at the University of Johannesburg, Johannesburg, South Africa.

3.7.5 Contact angle analysis

The wettability of the membranes was investigated using Dataphysics Optical contact angle analyser (OCA 15 EC GOP) to quantify the hydrophilic property of the membranes. Ten random measurements were taken at different places on the membrane surface and the average value was utilized. Contact angle analysis was conducted in Department of Chemical Science department at the University of Johannesburg, Johannesburg, South Africa.

3.7.6 Mechanical strength analysis

Tensile strength is referring to the maximum pulling stress a material can withstand before breaking. The breaking powers of the membranes were obtained using tensile testing machine and the thickness was obtained using digital Micrometer. The tensile strength (TS) was obtained using the following Equation (3.3):

$$TS = \frac{F}{20b} \tag{3.3}$$

Where TS(MPa) is the tensile strength, F(N) is the breaking power and b (nm) is the membrane thickness which was measured using a digital Micrometer. The tensile strength was carried out at the medical school of the University of the Witwatersrand in Parktown campus, Johannesburg, South Africa.

3.7.7 Bulk porosity

Bulk porosity of the membranes was estimated gravimetrically. Three pieces of membranes were cut and immersed in 2-propanol for 24 hours at room temperature. Then the wet membranes were taken and placed between two filter papers and weighed to achieve wet weight (W_w). Thereafter, the wet membranes were dried in oven at 50 ^oC for 2 hours and weighed to obtained dry weight (W_d). The bulk porosity was obtained using Equation (3.4):

$$Porosity\ (\%) = \frac{W_w - W_d}{A \times l \times d_b} \times 100 \tag{3.4}$$

Where A, is the membrane effective areas, l is the average thickness of the membranes measured using a digital Micrometer, d_b is 2-propanol density (0.786 g/cm^3).

3.8 Membrane performance evaluation

Performance evaluation of the synthesised PES/chitosan and PES/chitosan/PA membranes was carried out using dead-end and crossflow filtration systems during AMD treatment. Dead-end filtration system was utilized for the investigation of the effect of chitosan loading and its DD on the performance of PES/chitosan and PES/chitosan/PA membranes, respectively. Synthetic AMD was used for optimization of chitosan loading and its DD used by blending chitosan with PES suspension to produce PES/chitosan and PES/chitosan/PA membranes. The optimized membranes were then used in the crossflow system to investigate their operational stability and antifouling property during real industrial AMD treatment.

3.8.1 Dead-end filtration setup

3.8.1.1 Simulated feed solution

Synthetic feed solution was prepared as per the characterized data obtained from Tutu et al. (2008), composition of mine water collected from Randfontein (Black Reef Incline, 17 and 18 Winzes). Synthetic feed solution was used to prevent competition of desired and undesired species present in real industrial AMD. An appropriate amount of metal sulphate salts (Table 3.1) were dissolved in 1000 ml of deionized water and agitated for 30 minutes at 200 rpm to ensure complete dissolution and the pH was adjusted to 3.2 using 0.1 M sulphuric acid. The AMD solution was prepared and used on the same day without storage to ensure consistent quality.

Table 3.3: Synthetic Feed composition

Salt dissolved	Species	Concentration (mg/L)
$FeSO_4.7H_2O$	Fe^{2+}	933
$CaSO_4.2H_2O$	Ca^{2+}	461
$MgSO_4.7H_2O$	Mg^{2+}	345
$MnSO_4.H_2O$	Mn^{2+}	321
Na_2SO_4	SO_4^{2-}	4556

3.8.1.2 Permeation tests

The experiments were conducted on laboratory-scale dead-end filtration setup (Figure 3.5) mainly consisting of a holding cell capacity of 300 mL volume and effective filtration area of 14.6 cm^2. The desired pressure was achieved by applying nitrogen gas. After the membrane was fixed, deionized water was passed through the membrane to pre-press and compact the membrane to ensure complete immersion of water. Pure water flux (J, L/m^2 h) was determined at ambient temperature by permeating deionized water through the membrane. This was necessary to determine the initial flux of the membrane before evaluating with AMD. Pure water flux (J, L/m^2 h) was determined by direct measurement of membrane permeate volume using the following Equation (3.5):

$$J = \frac{V}{At} \tag{3.5}$$

Where V (Litre) is the volume of permeated water, A (m^2) is the effective membrane area and *t* (hours) is the filtration time. To minimize errors, water flux and rejection experiments were carried out three times and average values were reported.

Synthetic feed solution was fed through the membranes pressured with nitrogen gas and the filtrates were collected and analysed for metal content with Atomic Absorption Spectroscopy with operating parameters listed in Table 3.4. Calibration standards were prepared by appropriately mixing 1000ppm standard solution with deionized water.

Table 3.4: AAS operating parameters

Metal	Lamp Current (mA)	Wavelength (nm)	Flame used
1. Fe	15	248.30	Air/Acetylene
2. Ca	18	422.67	Air/Acetylene
3. Mg	18	285.21	Air/Acetylene
4. Mn	25	279.50	Air/Acetylene

Sulphates were analysed using Uv-vis spectrophotomer by following the Environmental Protection Agency (EPA) method 3754. Filtrates for sulphates analysis were conditioned. The conditioning solution was prepared by mixing 100 ml 95% ethanol, 30 ml of HCl with 75 g NaCl in a 500 ml flask. Thereafter, glycerol was added to the mixture. Then 1 ml of the filtrates for sulphate analysis and 5 ml of the conditioning agent were transferred to another 500 ml flask and stirred on a magnetic stirrer. A spoonful $BaCl_2$ was added and continued stirring for additional 5 minutes. Immediately after stirring, the solution was placed into a cuvette to measure the turbidity of the solution for 4 minutes at 30 seconds intervals. A calibration curve was prepared by appropriate dilution of 100 ppm Na_2SO_4 bulk solution.

Rejection was determined with the following Equation (3.6):

$$R(\%) = \frac{C_{feed} - C_{permeate}}{C_{feed}} \times 100\% \quad (3.6)$$

Where R is the percentage rejection, C_{feed} and $C_{permeate}$ (mg/L) are feed and permeate concentrations respectively.

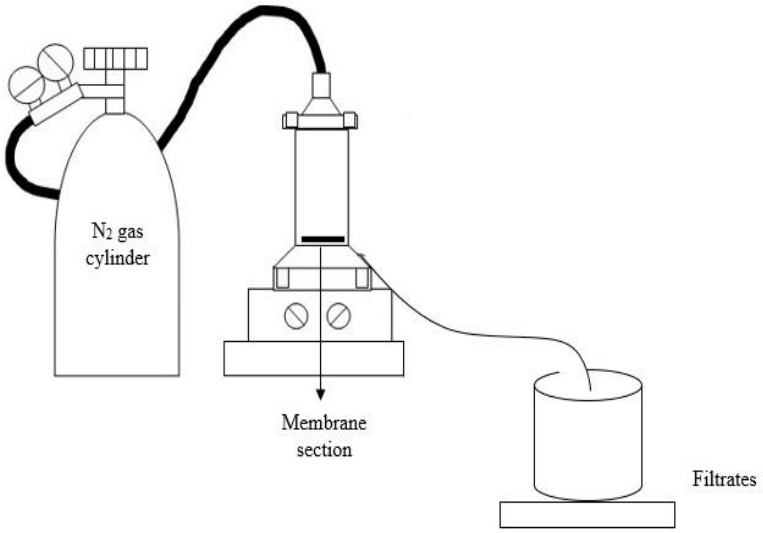


Figure 3.5: Dead-end filtration setup.

3.8.2 Crossflow filtration tests

The performance of the optimized PES/chitosan and PES/chitosan/PA membranes (optimum chitosan loading and DD) were evaluated on crossflow filtrations set up. The crossflow filtration module is composed of the feed tank, feeding pump, 3 filtration cells, and a pressure measuring device. AMD was transferred from the feed tank to the filtration cells fitted with membranes. Permeates can be recycled back to the feeding tank or directed to the measuring beakers for readings and analysis. The Pure Water Flux ((L, l/m^2 h), permeability (L/m^2 h. bar)

and Rejection were calculated using Equation (3.7), Equation (3.8) and Equation (3.10), respectively.

$$J = \frac{V}{At} \tag{3.7}$$

Where V (Liters) is the volume of permeated water, A (m^2) is the effective membrane area and t (hours) is the filtration time.

$$P = \frac{J}{TMP} \tag{3.8}$$

Where P is the permeability (L/m^2 h. bar), J is the pure water flux (L/m^2 h) and TMP (bar) is the transmembrane pressure expressed by Equation (3.9):

$$TMP = \frac{P_1+P_2}{2} \tag{3.9}$$

P1 (bar) and P2 (bar) is the measured pressure on the feeding line and atmospheric pressure during operation.

$$R(\%) = \frac{C_{feed}-C_{permeate}}{C_{feed}} \times 100\% \tag{3.10}$$

Where R is the percentage rejection, C_{feed} and $C_{permeate}$ (mg/L) are feed and permeate concentration, respectively.

3.9 Fouling and operational stability experiments

Antifouling and operational stability of the optimized membrane was investigated using real industrial AMD in the crossflow filtration module. For comparison, the Flux Recovery Ratio (FRR), the Reversible Resistance (R_r) and Irreversible Resistance (R_{ir}) of the optimized PES/chitosan/PA membrane was compared to those of pristine PES and PES/chitosan membranes. FFR, R_r and R_{ir} were determined using Equation (3.11), Equation (3.12) and Equation (3.13), respectively.

$$FRR = \left(\frac{J_{w2}}{J_{w1}}\right) \times 100 \tag{3.11}$$

$$R_r\% = \left(\frac{J_{w2} - J_{AMD}}{J_{w1}}\right) \times 100 \tag{3.12}$$

$$R_{ir}\% = \left(\frac{J_{w1} - J_{w2}}{J_{w1}}\right) \times 100 \tag{3.13}$$

Where J_{w1},the water flux (L/m^{2}h) was calculated using Equation (3.7) and after that, flux (J_{AMD})of AMD feed (foulant solution) was measured and water flux was measured again to determine if there was loss of flux to warrant backwashing (Shockravi et al., 2017). Furthermore, the membrane was cleaned with deionized water and the permeate of cleaned membrane was measured again as J_{w2} (L/m^{2}h) to confirm restoration of original flux to substantiate the effect of backwashing. Figure 3.6 depicts step by step procedure which was followed to conduct fouling experiments. Fouling was circumvented by hydraulic cleaning

(backwashing) which is a reversed filtration process whereby water is permeated in the opposite direction to expand the fouling layer and fluidises it for ease of removal of trapped contaminants. The flux measurements were taken after almost steady state is reached and replicate measurements were taken, and average values reported.

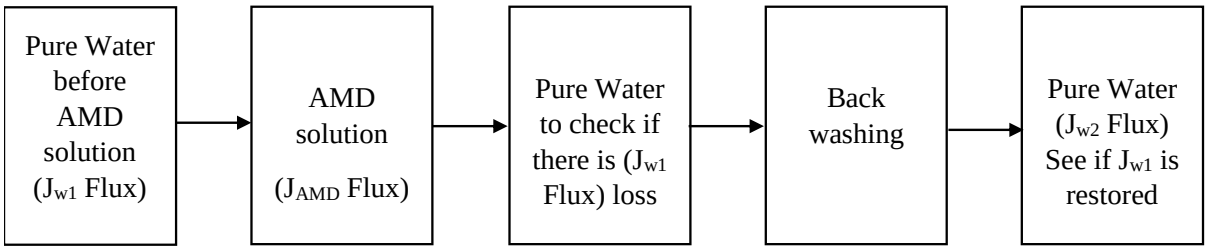


Figure 3.6: Fouling experiments procedure

Chapter 4 Effect of chitosan and polyamide layer on the quality and performance of the synthesized PES/chitosan and PES/chitosan/PA membranes

This Chapter contains results on the effect of chitosan content which was infused within PES membrane by blending PES suspension with chitosan particles to produce PES/chitosan membrane and coated polyamide layer to produce PES/chitosan/PA membrane on the quality and performance during AMD treatment.

4.1 Introduction

Amongst other polymeric membranes, polyethersulphone (PES) and polysulphone (PSf) have gained significant progress in acid mine drainage (AMD) treatment because of high chemical and thermal resistance, mechanical stability and high permeability. Although PES exhibits higher degree of hydrophilicity compared to PSf, its inherent hydrophobic character result in serious membrane fouling which could lead to deterioration in permeation flux, shortening membrane lifespan and unpredictable separation efficiency. Several interventions have been used to increase PES membrane hydrophilic nature to circumvent fouling. One approach is to modify PES membranes with hydrophilic polymers. Studies have reported on modifying PES membranes by coating the membrane surface with chitosan. However, in this study a novel approach is followed by infusing chitosan within the PES membrane matrix by blending chitosan particles with PES to influence the membrane's hydrophilicity from within. To overcome the surface hydrophilicity, polyamide layer was coated on the membrane surface by co-solvent interfacial polymerization (CAIP). The advantages of blending and coating with hydrophilic polymers such as chitosan and polyamide are that modification does not only take place on the membrane surface but also inside the membrane.

Chitosan used in the study was synthesised from chitin obtained from crab and shrimp shells through deacetylation process. This Chapter focuses firstly on chitosan production from chitin and its characteristics. Secondly, chitosan was used to modify the PES membrane and polyamide was coated on top to assess the effect of chitosan loading on the quality and performance of PES/chitosan and PES/chitosan/PA membrane during AMD treatment. TGA technique was used to determine the thermal stability of the synthesised membranes. FTIR was used to confirm success in synthesising chitosan from chitin and determine its degree of deacetylation. It was further used to determine the functional groups on the synthesised membrane surface. SEM, contact angle and texture analysis were used to observe the surface morphologies and cross-sectional image, the wettability and mechanical strength of the synthesised membranes respectively.

4.2 Chitosan production from chitin

Chitosan can be synthesised from chitin through demineralization, deproteinization, decolourization and deacetylation processes performed sequentially. Decolourisation is necessary for chitosan used in biological application such as drug manufacturing. However, chitosan used for treatment of AMD, the decolourisation step is not necessary hence the step was omitted in this study. Demineralization and deproteinization was conducted by treating chitin with 6% HCl and 6% NaOH respectively. The resulting chitin was filtered with a vacuum pump and washed with deionized water until neutral pH. Deacetylation was carried out with 40% NaOH at 120 ^{o}C for 6 hours. The deacetylated chitosan was washed with deionized water until neutral pH. The solid to liquid ratio for all processes was set at 1:20. The effect degree of deacetylation of chitosan on the performance of the synthesised membranes is reported in Chapter 5.

4.3 Characterization

4.3.1 FTIR

FTIR analytical technique is commonly used to analyse the chemical bonds and functional groups that are present. In this study, FTIR analysis was conducted on the synthesised chitosan to observe and verify functional groups present. It was also used to determine the degree of deacetylation (DD) of the synthesised chitosan as previously explained in Chapter 3. Figure 4.1 shows FTIR spectra of synthesised chitosan prepared in duplicate. The samples yielded similar FTIR spectrum indicating accuracy and repeatability of the synthesis processes. The FTIR spectrum depicts typical amine peaks at around 3388 and 1659 cm^{-1}, with COH peak at 1201 cm^{-1} and COC representative peak was identified at 1175 cm^{-1}. CN peak was identified at 2927 cm^{-1} while the vibrations at 2619 and 2473 cm^{-1} were assigned to CH

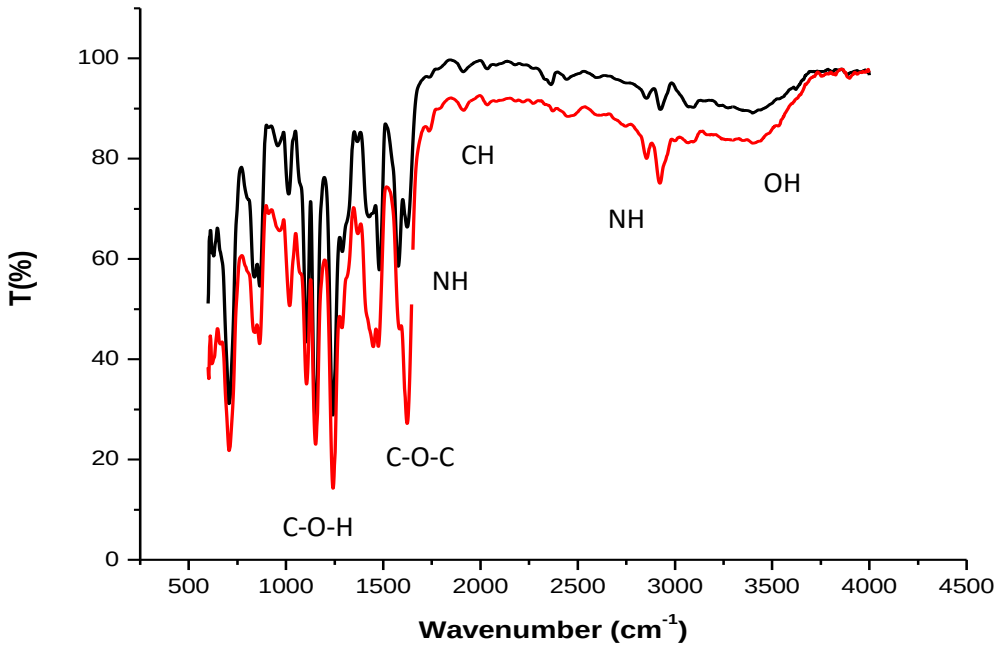


Figure 4.1: FTIR spectrum of chitosan synthesised from chitin

4.4 Effect of chitosan loading on the quality and performance of produced PES/chitosan and PES/chitosan/PA membranes during AMD treatment

The synthesised chitosan particles were blended with PES suspension to produce PES/chitosan membranes and polyamide layer was coated on top to produce PES/chitosan/PA membranes. Chitosan was loaded at various concentration (0, 0.5, 0.75, 1 wt%). The synthesised membranes were characterised and evaluated for performance during AMD treatment in a dead-end filtration cell. SEM was used to observe the surface morphology and cross-sectional view of the synthesised membranes. FTIR spectra were obtained to confirm the chemical bonds and functional groups on the surface of the synthesised membranes. The wettability of the membranes was determined using contact angle analysis. Dead-end filtration system was used to evaluate the performance of synthesised membranes using synthetic AMD as the feed.

4.4.1 Physicochemical properties of the synthesized PES/chitosan and PES/chitosan/PA membranes

4.4.1.1 Scanning electron microscopy

To examine the surface morphologies and cross-sectional view of the synthesised membranes, SEM analysis was carried out on the PES/chitosan and PES/chitosan/PA membranes. SEM has previously been used to examine the characteristic morphology and cross-sectional view of polyamide membrane modified with chitosan by Akbari et al. (2015). Samples to be analysed with SEM should be conductive or semi conductive. However, polymeric materials and membrane are nonconductive by nature hence coating is necessary (Liu et al., 2010). Samples for both surface morphology and cross section were exposed to carbon coating before mounting onto the SEM equipment specimen holder. Additionally, samples for cross section were immersed in liquid nitrogen for 10 minutes and cryogenically fractured quickly by hand before carbon coating and mounting onto the specimen holder.

SEM images of both surface and cross-section of the prepared membranes to evaluate the effect of chitosan concentration are shown in Figure 4.3 and Figure 4.4 for PES/chitosan and PES/chitosan/PA membranes, respectively. The SEM images illustrated in Figure 4.3 shed light on the surface morphology and surface porosity of the PES/chitosan membranes. The difference between surface morphology of pristine PES membrane (Figure 4.3(a)) and PES/chitosan membranes having 0.5 wt% (Figure 4.3 (c)), 0.75 wt%(Figure 4.3 (e)) and 1wt% (Figure 4.3 (g)) chitosan concentration can be observed. Surface morphology of pristine PES membrane (Figure 4(a)) illustrates a smooth and integrity surface structure with uniformly distributed pores. Comparing the images of PES/chitosan reveals diminished number of pore sizes relative to PES membrane (Mu and Zhao, 2009). This is due to the addition of hydrophilic chitosan particles which produces more compact surface structure. The dense structure of PES/chitosan is clearly seen in the SEM images which increased with chitosan content. Increasing chitosan content to 0.75 wt% and 1 wt% resulted in a high viscous casting gel which reduced the rate of phase inversion and produced a denser and compact membrane (Ghaemi et al, 2018). Boricha and Murthy. (2009) prepared membranes with different compositions of acrylonitrile butadiene styrene (ABS) and chitosan (CHS) on PES substrate support. PES substrate support was cast first and the ABS and CHS homogeneous polymer blend solution were coated on top. The SEM images revealed highly compact surface structure and decreased porosity with increased chitosan in the polymer blend. Coating the polymer blend on top of the PES support resulted in some of the pristine PES pores blocked by the rich chitosan and ABS poly blend. The novelty in this study of infusing chitosan polymer within the PES membrane matrix demonstrated to have positively influenced the membrane permeability, porosity and hydrophilicity from within without necessarily blocking the pores. This is affirmed by the porosity and contact angle and water flux results depicted in Figure 4.7 (a) and Figure 4.9 (b), respectively.

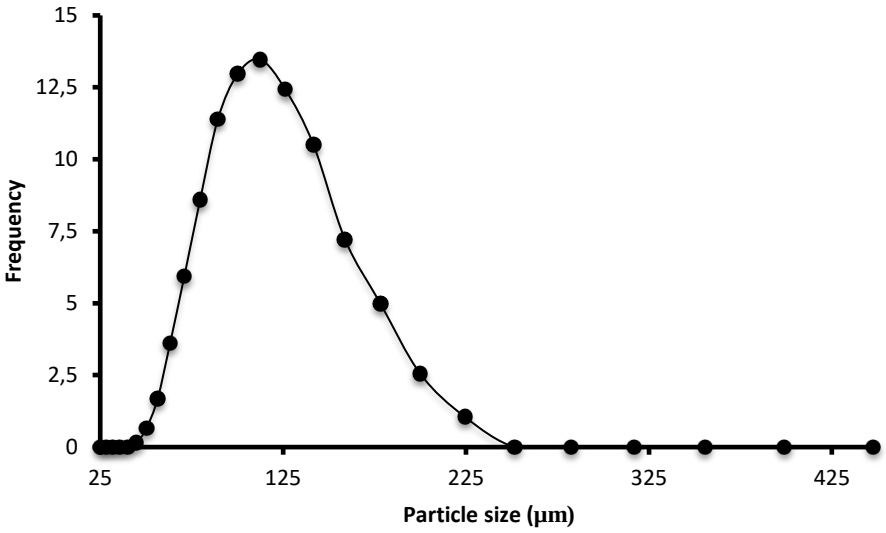


Figure 4.2: Particle size distribution of the synthesised chitosan.

During phase inversion method, the cast film is immersed in coagulation bath containing water. Therefore, hydrophilic membrane modifiers such as chitosan tend to accumulate on the membrane surface due to the high presence of hydroxyl and amino groups. Contact angle results (Figure 4.7 (a)) demonstrated the increasing hydrophilicity of the membranes with increasing chitosan content. The contact angle of PES membrane reduced from 92^{O} to 64^{O}, 60^{O} and 58^{O} for PES/0.5 wt% chitosan, PES/0.75 wt% chitosan and PES/1 wt% chitosan membranes, respectively. SEM images revealed membrane with smooth structures with no cracks even after the addition of chitosan particles. This is confirmed by the particle size distribution (Figure 4.2) results which show that the synthesized chitosan samples had acceptable dimensions to be added to the membrane without creating cracks within the membrane. The cross-section SEM images (Figure 4.3 (b)) illustrate typical asymmetric pristine PES structure with dense skin top layer and a porous sublayer with large pore wall thickness. The image is characterised by a finger like macro voids spreading from the inner and outer walls of the membrane. The cross -section images of the PES/chitosan membranes (Figure 4.3 (d, f and h)) revealed a more porous sublayer and reduced pore wall thickness

compared to pristine PES membrane. Moreover, the skin layer thickness decreased with addition of chitosan particles up to 0.75 wt%. Further addition to 1 wt% chitosan increased pore wall thickness and caused reduction in membrane porosity. Figure 4.6 showed declines in membrane porosity when chitosan content increased from 0.75 wt% to 1 wt %, showing reduction of porosity from 66 to 41%, respectively. Although unmodified PES membrane has bigger pores, its hydrophobic character is responsible for the low water flux.

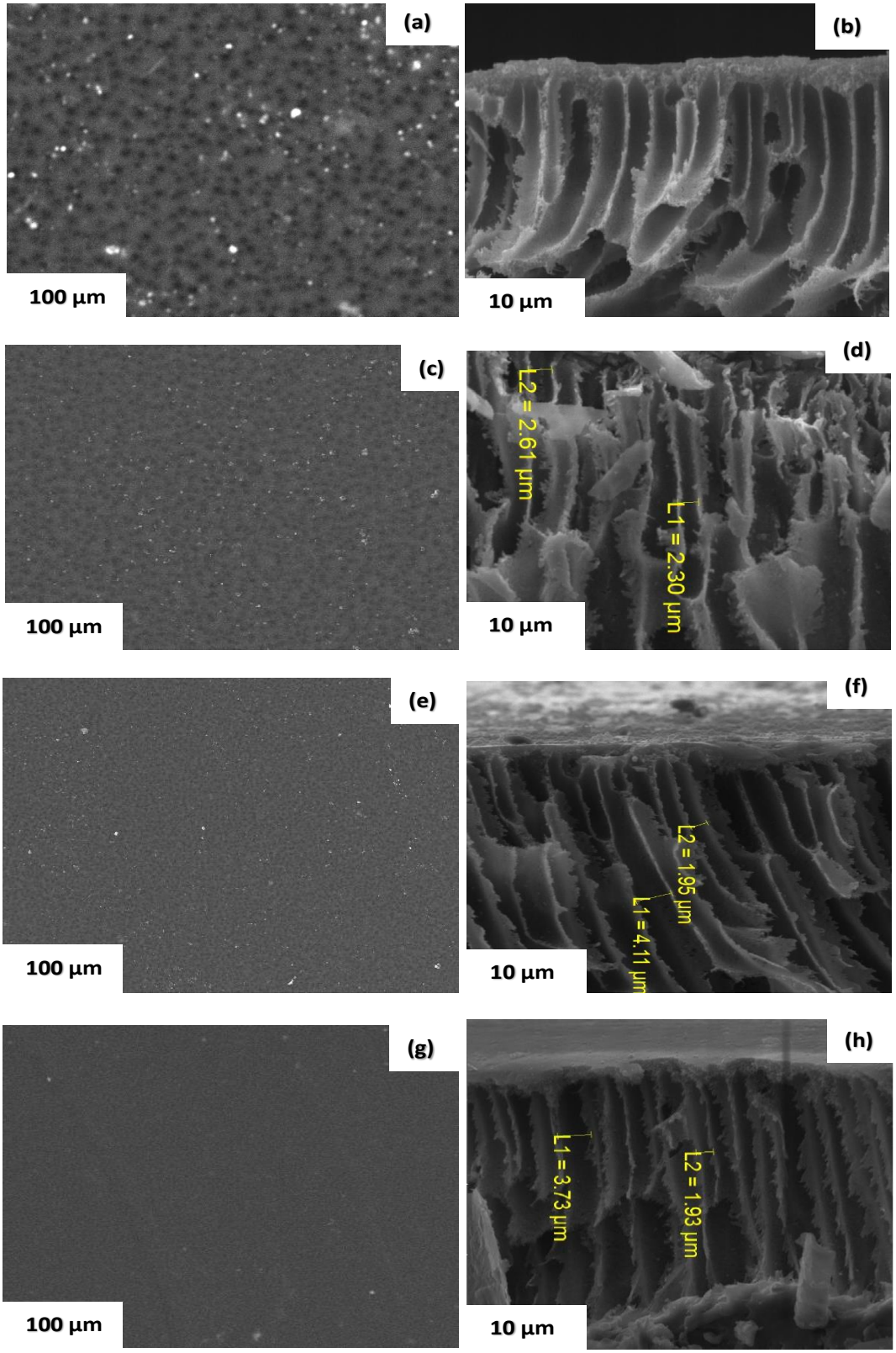


Figure 4.3: SEM images showing surface morphology and cross-section of (a and b) PES, (c and d) PES/ 0.5 wt% chitosan, (e and f) PES/0.75 wt% chitosan and (g and h) PES/1 wt% chitosan membranes

Furthermore, Figure 4.4 shows surface morphology and the corresponding cross-sectional images of PES membranes infused with chitosan and coated with polyamide layer on top to produce PES/chitosan/PA membranes. As it can be observed on Figure 4.4 (a), there are obvious differences between surface morphologies of polyamide layer formed over hydrophobic PES membrane (PES/PA) and those formed over PES membrane infused with hydrophilic chitosan as seen on Figure 4.4 (c) (PES/0.5 wt% chitosan/PA), Figure 4.4 (e) (PES/0.75 wt% chitosan/PA) and Figure 4.4 (g) (PES/1 wt% chitosan/PA). The roughness character of the PA membranes reduced with increasing chitosan concentration and this could be due to chitosan forming complexes with PA structure and filling empty spaces of the PA layer. Moreover, typical surface morphologies of polyamide membranes prepared via conventional interfacial polymerization technique using piperazine and trimesoyl chloride with hexane alone as an organic solvent without acetone, depicts a typical ridge- and – valley structure like that of commercial membranes which leads to a more roughness character (Wu et al., 2009; An et al., 2011). Polyamide layer formed over unmodified PES showed scattered fine grains as compared to smooth polyamide layer formed over PES modified with chitosan. Similar observations were made by Akbari et al. (2015) when polyamide layer formed over unmodified polyacrylonitrile depicted a very rough surface compared to the one formed on the modified support. The effect of chitosan loading on the thin film layer thickness could not be evidently observed cross-section view of the membranes. The same conclusions were made in literature even at high magnification and it was argued to be because of the extremely thin polyamide layer (Akbari et al., 2015). However, co-solvent assisted interfacial polymerization was followed in this study, with acetone as a co-solvent. Figure 4.4(a, c, e and g) shows the smooth character of polyamide membranes prepared via CAIP method. The surface morphology of PA membrane prepared by adding acetone as a co-solvent were greatly altered and the typical ridge – and – valley structure was flattered as compared to those prepared by

conventional interfacial polymerization (Akbari et al., 2015). Figure 4.4 (b) shows the cross-sectional view of the PES/PA membrane and larger macro voids in the sublayer could be observed. However, the permeability of the membranes was found to be 14, 15.5, 18.25 and 23.25 l/m^2.hr.bar for PES/PA, PES/0.5wt% chitosan/PA, PES/0.75wt% chitosan/PA and PES/1wt% chitosan/PA, respectively. Since membrane permeability is affected by both membrane porosity and hydrophilic property, the contact angle (Figure 4.7 (b)) results showed enhanced degree of hydrophilicity for PES/PA compared to others hence the permeability increased with increasing hydrophilic chitosan content.

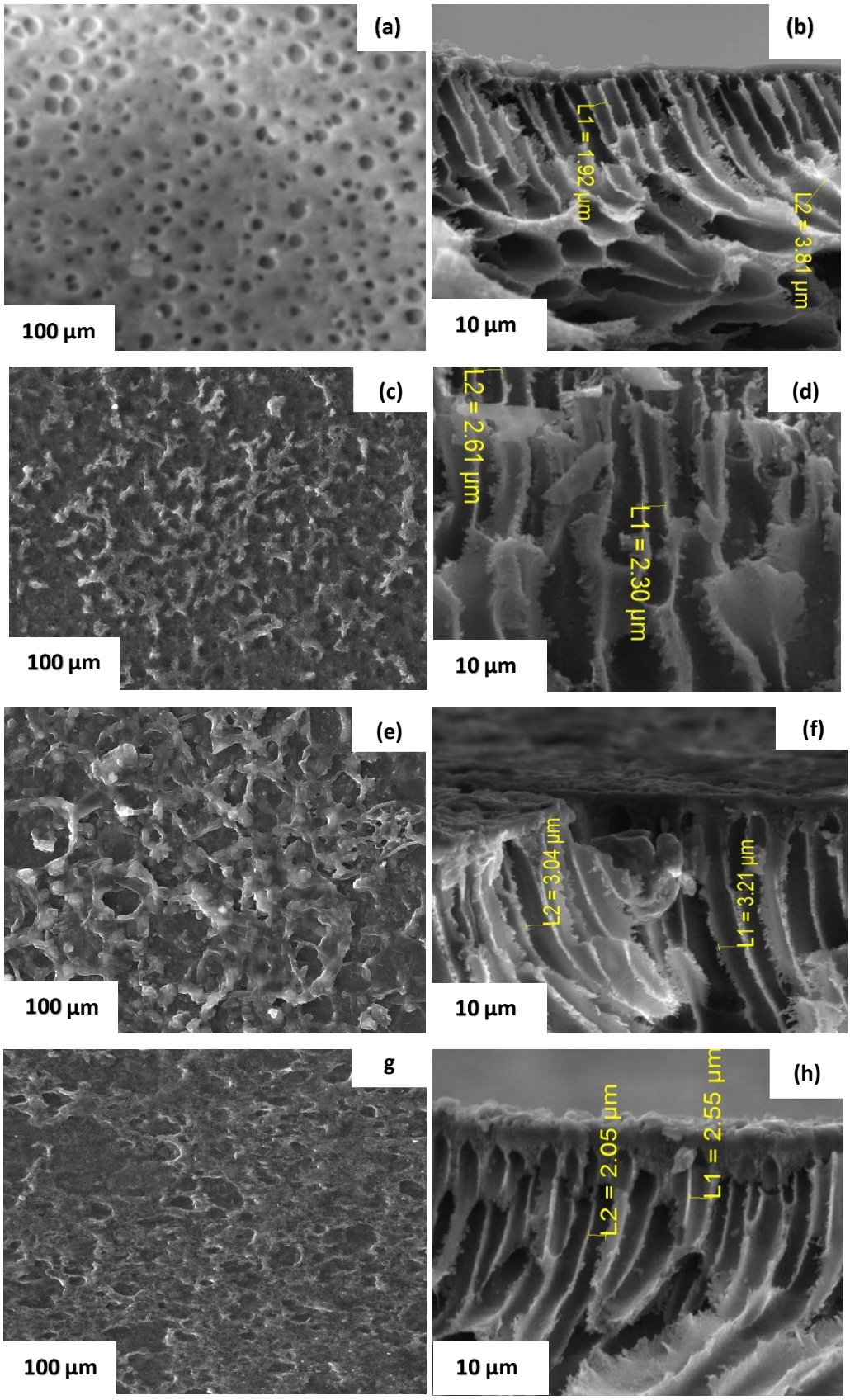


Figure 4.4: SEM images showing surface morphology and cross-section of (a and b) PES/PA, (c and d) PES/ 0.5 wt% chitosan/PA, (e and f) PES/0.75 wt% chitosan/PA and (g and h) PES/1 wt% chitosan/PA membranes

4.4.1.2 Fourier Transform Infrared

FTIR has been extensively used to characterize chemical composition on surface modification of PES modified membranes (Zhao et al., 2013). Figure 4.5 compares the IR spectra of pristine PES membrane (Figure 4.5 (d) and PES membranes infused with chitosan (Figure 4.5 (a) to (c)). Figure 4.5 (d) shows structural information of pristine PES membrane and Figure 4.4 (a), (b) and (c) verify structural information of PES membrane infused with 0.5 wt%, 0.75 wt% and 1 wt%, respectively. Looking at the IR spectra, no significant difference between PES and PES/chitosan membranes could be observed. However, flux and rejection results revealed that the PES and PES/chitosan membranes performances were different. Additionally, although pristine PES and PES/chitosan membranes had similar spectra peaks, SEM (Figure 4.3) results showed reduced surface porous structure and enlarged macro voids and pores in the sublayer region after the addition of chitosan. These spectra similarities could be attributed to the properties of PES basic structure. Spectra of PES sample was verified and is shown in Figure 4.4 (d). The identified peak at 621 cm^{-1} was attributed to the C-stretching and 880 cm^{-1} to the C=C stretching on the aromatic ring structure. The peaks at 1150 cm^{-1}, 1239 cm^{-1} and 1483 cm^{-1} attributes to the sulfonyl (O=S=O) group while the aromatic ether (C-O-C) group is represented by the peak at 1296 cm^{-1}. The sharp peak at 706 cm^{-1} attributes to the C-S stretching. PES chemical structure does not contain O-H groups, however a typical O-H stretching between 3200 and 3500 cm^{-1} was observed. The membrane was immersed in a coagulation bath containing deionized water to allow complete desorption. And heated in an oven at 60 ^{o}C to evaporate any trapped water or solvent and it seems small amount of water molecules penetrated and remained within the porous structure. Similar conclusions were made in literature (Belfer et al., 2000; Ghiggi et al., 2017).

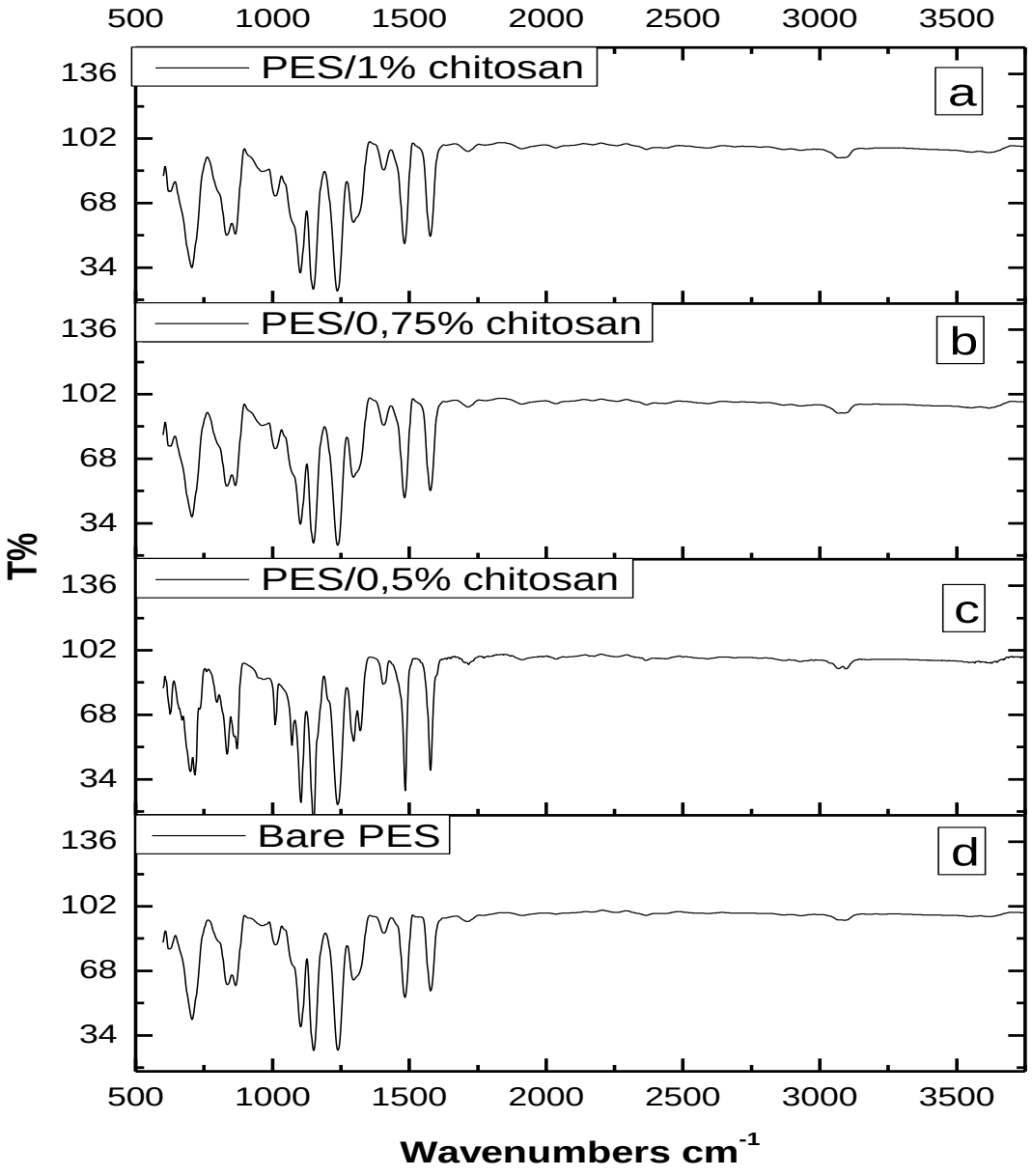


Figure 4.5: FTIR spectra of (a) PES/1wt% chitosan, (b) PES/0.75wt% chitosan, (c) PES/0.5wt% chitosan and (d) Bare PES membranes.

Figure 4.6 compares membranes synthesised by coating polyamide layer on top of a hydrophobic PES support (Figure 4.6 (d)) and those prepared on top of PES infused with hydrophilic chitosan (Figure 4.6 (a) to (c)). As expected, membranes showed typical characteristics of PES basic structure and this evidently show that polyamide layer did not cover the entire PES/chitosan surface. The identified peaks at 660.46 cm^{-1},660.16 cm^{-1}, 691.87 cm^{-1} and 662.96 cm^{-1} was attributed to the C-stretching and 866.02 cm^{-1}, 864.54 cm^{-1}, 864.96 cm^{-1} and 829.62 cm^{-1} to the C=C stretching on the aromatic ring structure for PES/PA, PES/PA 0.5, PES/PA 0.75 and PES/PA 1 membranes, respectively. The peaks at 1240.49 cm^{-1}, 1237.03 cm^{-1}, 1230.73 cm^{-1} and 1226.62 cm^{-1} attributes to the sulfonyl (O=S=O) group while the aromatic ether (C-O-C) group is represented by the peak at 1153.21 cm^{-1}, 1151.34 cm^{-1}, 1144.34 cm^{-1} and 1149.81 cm^{-1} for PES/PA, PES/PA 0.5, PES/PA 0.75 and PES/PA 1 membranes, respectively. The strong band at 1712.23 cm^{-1}, 1711.72 cm^{-1}, 1752.98 cm^{-1} and 1700.01 cm^{-1} was associated with the stretching vibration of the C=O group of PES/PA, PES/PA 0.5, PES/PA 0.75 and PES/PA 1 membranes, respectively. The polyamide layer was coated onto the membrane using co-solvent assisted interfacial polymerization method instead of typical interfacial polymerization method. The broad band at around 3369 cm^{-1} was attributed to the N-H stretching frequency. In addition, the peak at 3380.91 cm^{-1}, 3379.42 cm^{-1}, 3072.30 cm^{-1} and 3075.46 cm^{-1} corresponded to the combined N-H stretching and C-N stretching vibrations for PES/PA, PES/PA 0.5, PES/PA 0.75 and PES/PA 1 membranes. The decreased intensity of C=O, N-H and combined N-H and C-N groups polyamide is reflective of the thin layer of polyamide produced via co-solvent assisted interfacial polymerization. Similar observations were reported in literature, whereby no significant differences were made between polyethersulphone and polyamide membranes, both modified with chitosan (Torkabad et al., 2017; Singh et al., 2006)

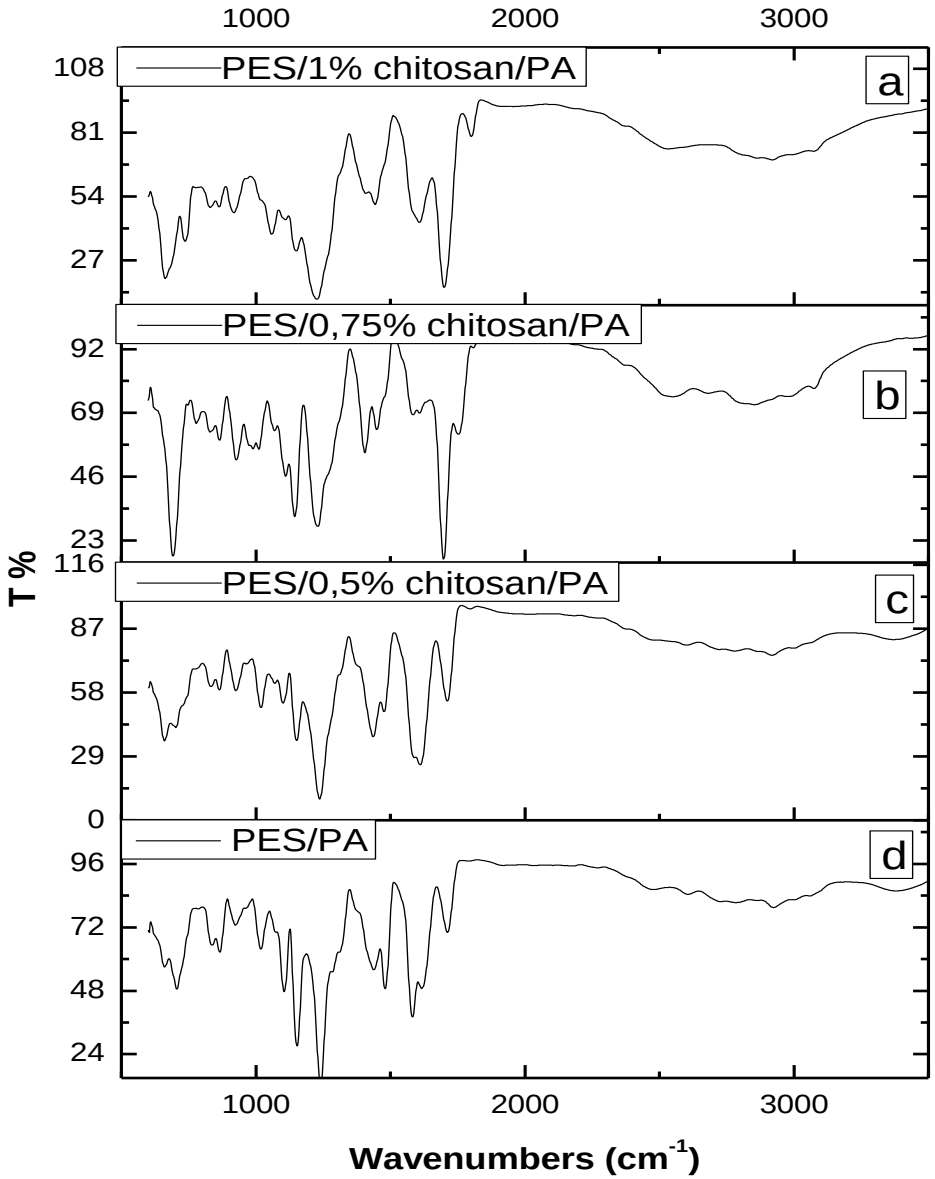


Figure 4.6: FTIR spectra of PES/1wt% chitosan/PA (a), PES/0.75wt% chitosan/PA (b), PES/0.5wt% chitosan (c) and PES (d) membranes.

4.4.1.3 Contact angle analysis

It is a known fact that membrane hydrophilicity is an important character because it does not only influence the membrane's water permeate flux, but it also reduces its fouling potential from various pollutants (Xu et al., 2015). Contact angle measurements reveal information about the hydrophilicity and/or hydrophobicity of the membranes. Relatively low contact angle is an indication of the enhanced hydrophilic property of the membranes whereas high contact angle indicates hydrophobic character. It has been extensively reported that membrane water contact angle kept changing with time after dropped on the membrane surface. This was attributed to evaporative effect. Therefore, as recommended by Bolong et al (2009), to avoid this evaporative effect, measurements in this study were conducted as quickly as possible (less than 10 seconds).

Figure 4.7 (a) shows contact angle measurements and porosity of pristine PES and PES membranes infused with varying chitosan content. Blending hydrophilic chitosan with PES membrane had significant influence on the hydrophilicity of the membrane. Introduction of hydrophilic component inside PES membrane induces a remarkable reduction in water contact angle of the membrane. Looking at Figure 4.7 (a), its evidently clear that introduction of hydrophilic chitosan triggered a downward trend in contact angle of the membranes. Addition of 0.5 wt% chitosan reduced the contact angle of PES membrane from 92^{O} to 63.6^{O}. Further addition of chitosan to 0.75 wt% and 1 wt% reduced the contact angle to 60.8^{O} and 58^{O}, respectively. This reduction in contact angle could be explained by the enhancement of water transport through the membranes as a result of water molecules interaction with amide of the hydrophilic chitosan through hydrogen bonding. This decrease in contact angle with increasing chitosan content affirms the influence of chitosan as an agent to enhance the membrane surface hydrophilicity. Although the membranes hydrophilicity increased after adding chitosan from 0 to 1 wt%, water flux results (Figure 4.9 (b)) revealed that water flux of PES membranes having

1 wt% (97 L/m^2.hr) chitosan content was lower than that at 0.75 wt% (121 L/m^2.hr). Expectedly, membrane wettability is ought to positively influence membrane water flux, however, a contrast behaviour was observed. This could be justified by the fact that membrane permeability is considerably affected by membrane porosity, hydrophilicity and surface roughness. The chitosan content increase from 0.75 to 1 wt% resulted in the decrease of the membrane‘s effective pore sizes (as seen in SEM cross section view in Figure 4.3) which reduced the membrane porosity from 66 to 41.3%, respectively. Therefore, membrane permeability was dominated by porosity more than it was by hydrophilicity.

Figure 4.7 (b) exhibits overall porosity and contact angle of the prepared membranes infused with chitosan and coated with polyamide layer. All the membranes infused with chitosan (PES/0.5wt% chitosan/PA, PES/0.75wt% chitosan/PA and PES/1wt% chitosan/PA) showed an enhanced surface porosity and improved degree of hydrophilicity. Addition of chitosan particles influenced the wettability of the membranes (PES/0.5wt% chitosan/PA, PES/0.75wt% chitosan/PA and PES/1wt% chitosan/PA) in comparison with unmodified PES/PA membrane. The contact angle was reduced by 39, 18 and 9% for PES/1wt% chitosan/PA, PES/0.75wt% chitosan/PA and PES/0.5wt% chitosan/PA, respectively. The results presented in Figure 4.10 (b) favours promotion of membrane permeability hence the water flux of the membrane increased with increasing chitosan content. Both membrane hydrophilicity and porosity had a positive influence on the membrane permeability. Introducing chitosan as an additional hydrophilic agent improved the degree of hydrophilicity of the membranes compared to membranes prepared in the study conducted by Shockravi et al. (2017). Introduction of chitosan improved the degree of hydrophilicity of the membrane by 58%. This is due to the addition of hydrophilic amide sites introduced by coating with polyamide layer which resulted in enhancing water molecules transportation through the membrane.

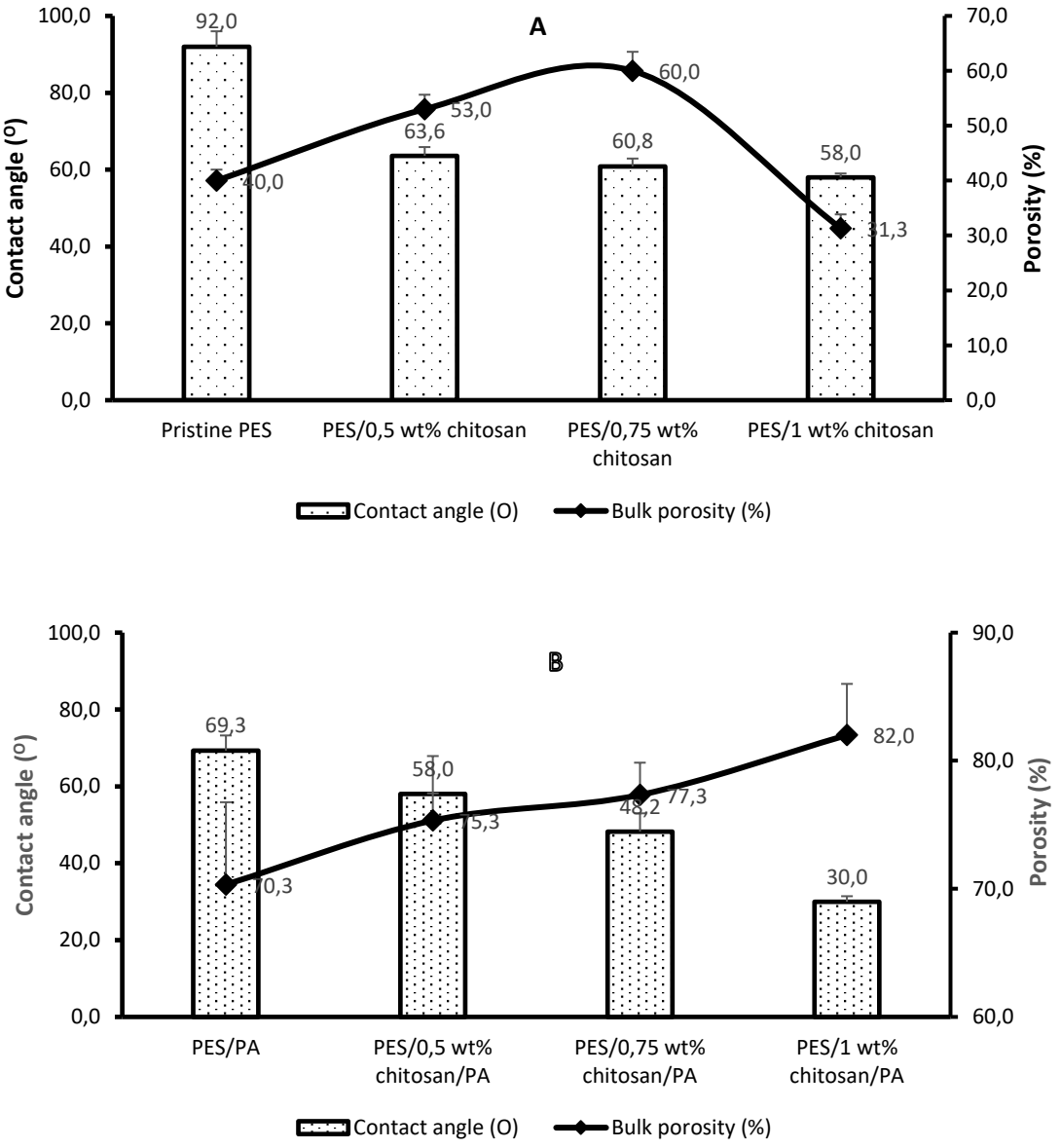


Figure 4.7: Static water contact angle and bulk porosity of the (a) PES/chitosan and (b) PES/chitosan/PA membranes

4.4.1.4 Tensile strength of the membranes

During membrane operation, adequate thermal and mechanical stabilities are required to ensure efficient application during wastewater treatment. Tensile strength of the membranes was obtained and is presented in Figure 4.8. As expected, the addition of chitosan particles and coating polyamide layer enhanced the tensile strength of the membranes. The pristine PES membrane showed tensile strength of 2.52 MPa. In comparison with chitosan modified membranes, addition of 0.5, 075 and 1 wt% in the blend raises the tensile strength to 6.82, 8.36 and 10.25 MPa, respectively. This could be attributed to the fact that when external forces are applied to the composite membrane, those stresses are transferred efficiently to the chitosan polymer which allows them to take significant share of the load (Gumbi et al., 2018). Additionally, the uniform distribution of chitosan particles within the membrane matrix as observed with SEM images assisted in the improvement of the tensile strength. Coating polyamide layer onto the pristine PES membrane and PES/chitosan membranes induced reduction in tensile strength. This phenomenon is better explained by Bai et a. (2018). The researchers argued that the formation of polyamide molecules would exert plasticizing effect on the membrane surface and loosen the compact packing of the membrane matrix backbones due to the interaction of the chitosan's amine groups and unreacted acylchloride groups of the polyamide. Thus, making the membrane to be more flexible and loses its strength.

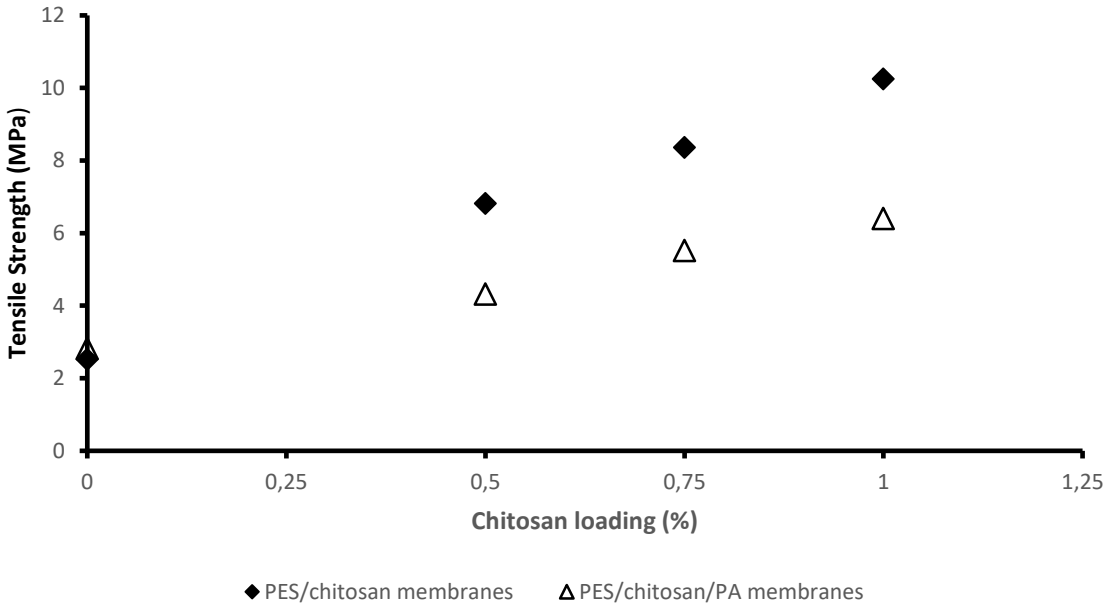


Figure 4.8: Effect of chitosan loading on the Tensile Strength of PES/chitosan and PES/chitosan/PA membranes

4.4.2 Membrane Performance Investigation

4.4.2.1 Initial membrane flux

Permeability of most porous membranes is reflected by water flux measurement and as such, pure water was permeated through the membranes over a certain period to determine the original flux of the membranes on a dead-end filtration setup. The membranes were pre-pressed with deionized water for 4 hours to obtain a steady flux before commencing with actual flux determination. Deionized water was passed through the membrane pressurised by N_2 gas to ensure complete swelling and/or immersion of water molecules and to avoid inconsistent results. Figure 4.9 (a) and Figure 4.10 (a) demonstrates initial flux of PES/chitosan membranes against pressure (1 to 4 bar). The operating pressure was increased at an interval of 1 bar to determine maximum pressure which the membranes can operate at without disintegrating. When the pressure was increased from 4 to 5 bars, most of the membranes got ripped apart. This is because, increasing the applied pressure across the membrane is associated with large

shear stress forces which pushes water molecules through the membrane wall surface to a point where the strength of the membrane cannot withstand the applied pressure. Under high pressure, more pollutants will be transported and retained on the membrane surface in a short period. Conversely, low applied pressure will result in reduced pressure which may lead to accumulation of particles on membrane surface wall necessitated by laminar flow (Chen and Lin, 2004). It would be expected that high pressures will force retained materials on the membrane surface to permeate through the membrane and reduce rejection. However, studies proved that increased transmembrane pressure in nanofiltration and reverse osmosis membrane application promote sorption of water molecules than solutes (Zhong et al., 2007). It is against this background that the membrane tests in this study were conducted at 4 bars and the pure water and AMD fluxes presented are those conducted at 4 bars.

Figure 4.9 (a) presents pure water flux of PES/chitosan membranes having various chitosan content against pressure. The pure water flux increased with increasing pressure. Addition of 0.5 wt% of chitosan polymer induced an increment of permeates flux from 102 L/m^2.hr to 107 L/m^2.hr when the pressure was 4 bars. When chitosan concentration was increased to 0.75 wt%, the permeate flux reached its highest value of 133 L/m^2.hr, which is 20% more than the unmodified PES membrane. This behaviour is affirmed by the fact that introduction of chitosan introduced number of functional groups which influenced the wettability of the membrane which favoured sorption of water molecules. However, increasing the chitosan amount in the blend to 1 wt% caused the flux to decline to 116 L/m^2.hr, but it was still higher than that of unmodified PES membrane (97 L/m^2.hr) . This could be attributed to the fact that increasing chitosan beyond 0.75 wt% amount reduced effective pore sizes of the membrane as observed in the SEM cross section view (Figure 4.3) and porosity results (Figure 4.7(a)) where the porosity of PES/0.75wt% chitosan and PES/1wt% chitosan membranes were reported as 66 and 41.3%, respectively. Chitosan is more hydrophilic than PES membrane due to its numerous

functional groups which favours sorption of water molecules on the membrane surface hence increased water flux was realised with increasing chitosan concentration until its porosity was compromised. As previously mentioned, that membrane porosity and hydrophilicity play a vital role in membrane permeability, the results show that membrane permeability was influenced positively by hydrophilic nature of the membrane when chitosan content was at 0.75 wt%. Further addition to 1 wt% showed that porosity dominated and influenced permeability hence the flux declined. Although chitosan is a hydrophilic filler and its addition should improve membrane permeability, the reduced water flux at 1 wt% chitosan content indicate that addition of chitosan at more than optimum compromises membrane permeability.

After pure water flux were obtained, AMD was filtered through the dead-end filtration system and Figure 4.9 (b) present the permeate flux of the AMD solution. The AMD flux was conducted at a pressure of 4 bar and the filtrates was kept for metal and sulphate analysis. AMD permeate flux reported slightly reduced flux as compared to that of pure water flux. This was attributed to the fact that the retained ions on the membrane surface created a layer which obstructed solvent movement through the membrane as a result of concentration polarisation phenomenon. AMD flux results could be correlated with the rejection data reported in Figure 4.11. AMD flux increased with increasing rejection up to 0.75 wt% and beyond that rejection was reduced. This behaviour was attributed to the fact that although chitosan content improves the membrane rejection, more chitosan particles blocked solvent molecules and functional groups required for contaminants attachment. AMD was fed at a pH of 3.2, thus the membrane was positively charged due to the protonation of the amine's groups on the chitosan structure. The cations were pushed back by the positively charged membrane and the sulphate ions were drawn towards the membrane surface and retained.

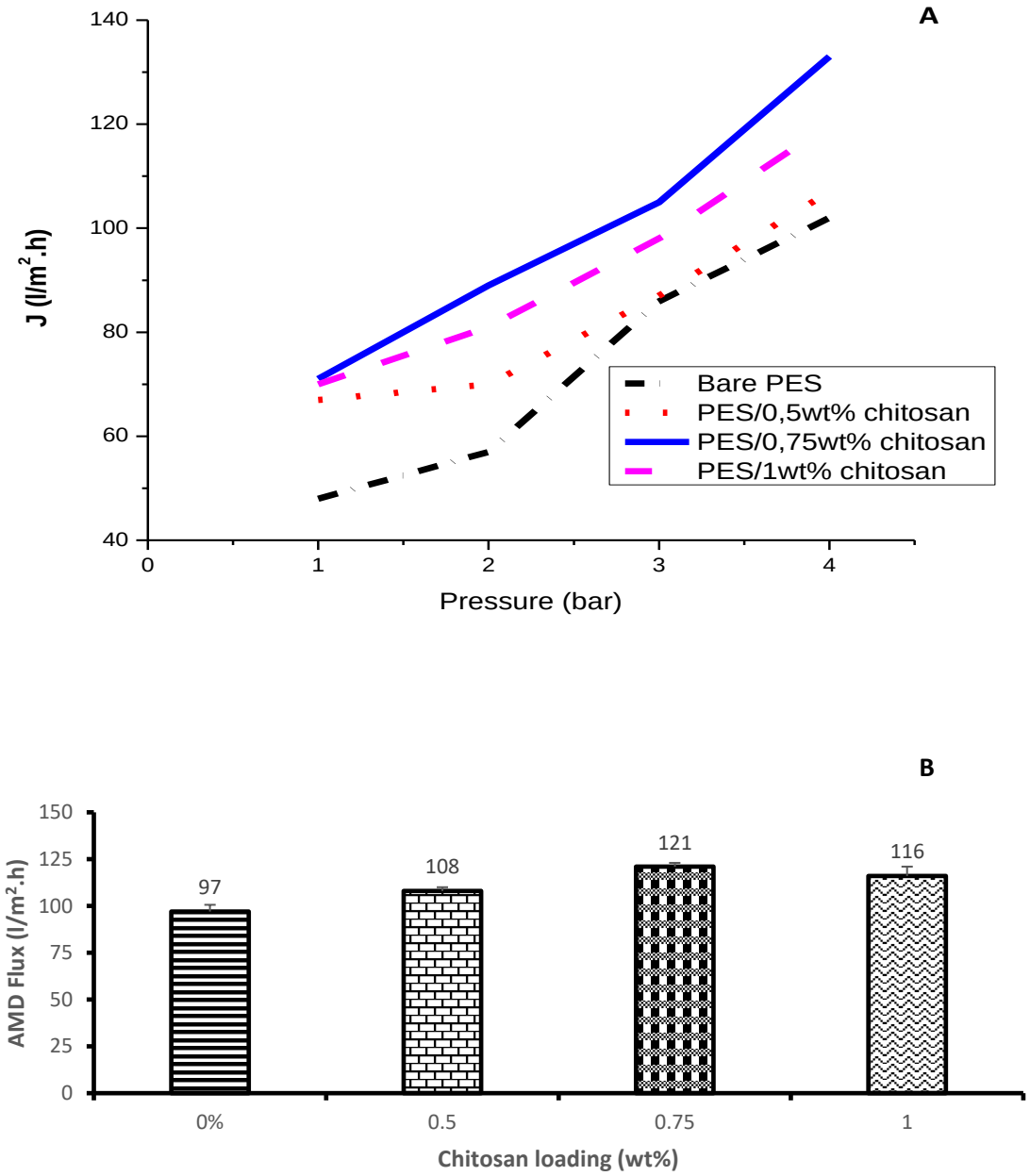


Figure 4.9: Membrane (a) pure water flux and (b) AMD flux of PES/chitosan membranes

Figure 4.10 (a) illustrate the pure water flux of PES/chitosan membranes coated with polyamide layer (PES/0.5wt% chitosan/PA, PES/0.75wt% chitosan/PA and PES/1wt% chitosan/PA). All four membranes had a linear volumetric water flux increase with increasing pressure from 1 to 4 bars. Polyamide materials are usually used to construct reverse osmosis membranes, which have smaller surface pore sizes, compared to other membranes hence the observed reduced water flux. Effective membrane thickness and pore sizes also influence solute/solvent permeability through the membrane (Shockravi et al., 2017). Although the PA layer contributed to the reduced water permeability, increasing chitosan content improved the water flux from 56 L/m^2.hr to 62, 73 and 93 L/m^2.hr for PES/0.5wt% chitosan/PA, PES/0.75wt% chitosan/PA and PES/1wt% chitosan/PA, respectively. This could be attributed to the fact that, the interaction of chitosan's amine group and PA active layer's unreacted acylchloride group created a thin layer on the membrane surface. Additional chitosan's amine groups which could not interact with unreacted acylchloride groups favoured sorption of water molecules by the membrane (Xu et al., 2015). Moreover, further chitosan addition resulted in molecular aggregation which leads to weak and thick chitosan layer having weak pore wall and big pore sizes. This phenomenon leads to improved permeate flux of 93 L/m^2.hr for PES/1wt% chitosan/PA compared to 73 L/m^2.hr of PES/0.75wt%. Similar observations were made by Akbari et al. (2015). The permeability of the membranes was found to be 14, 15.5, 18.25 and 23.25 L/m^2.hr.bar for PES/PA, PES/0.5wt% chitosan/PA, PES/0.75wt% chitosan/PA and PES/1wt% chitosan/PA, respectively.

Similarly, AMD solution was filtered through, permeate fluxes were measured and the results are presented in Figure 4.10 (b). The AMD flux reduced by 8, 10, 15 and 18 L/m^2.hr for PES/PA, PES/0.5wt% chitosan/PA, PES/0.75wt% chitosan/PA and PES/1wt% chitosan/PA compared to the pure water fluxes. The permeate flux reduction seemed to increase with

increasing chitosan content. Figure 4.7(b) shows improving porosity and reduction in contact angle with increasing chitosan content, signifying enhanced hydrophilicity. Therefore, the increasing loss of flux with increasing chitosan content could be attributed to the high rejection percentage shown in Figure 4.12. PES/chitosan membranes results presented in Figure 4.9 (a) and 4.9 (b) had flux loss of 5 (pristine membrane), 1 (PES/0.5 wt% chitosan), 12 (PES/0.75 wt% chitosan) and 4 L/m^2.hr (PES/1 wt% chitosan) between pure water and AMD fluxes. It's clear that the loss of flux of PES/chitosan/PA membranes was higher than those of PES/chitosan membranes. This was attributed to more functional groups afford by both chitosan and polyamide co-polymers as compared to only by chitosan in the PES/chitosan membranes. Increasing chitosan content provide large number of functional groups which participating during contaminate rejection. AMD was fed at 3.2 pH, the amine and amide groups on the chitosan and polyamide polymer get protonated under acidic condition and cause the membrane to become positively charged. The electrostatic repulsive or attraction forces of PES/chitosan/PA membranes were stronger than those of PES/chitosan membranes hence rejection of the former was better that of the latter.

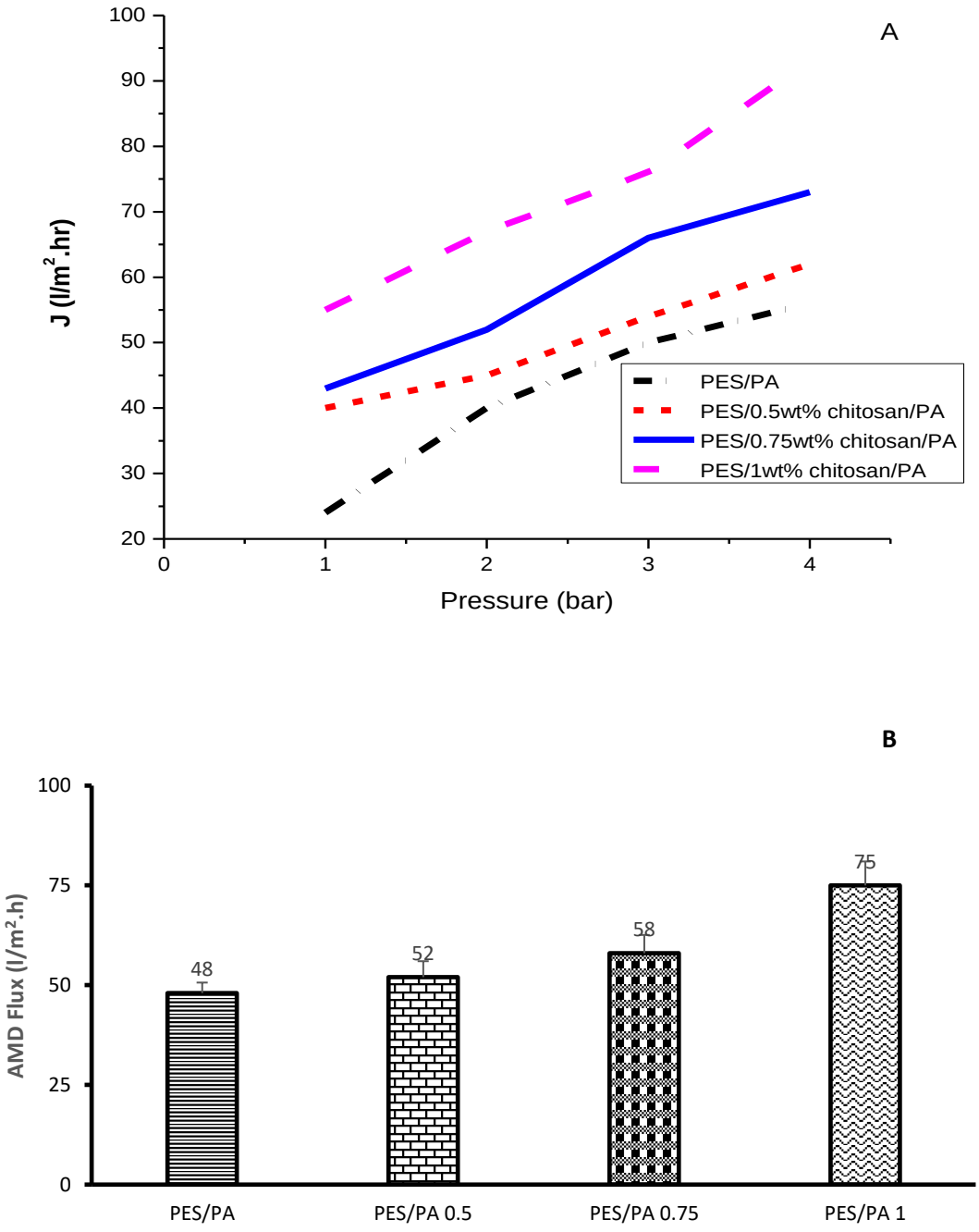


Figure 4.10: Membrane (a) pure water flux and (b) AMD flux of PES/chitosan/PA membranes

4.4.2.2 Membrane rejection during treatment of AMD

Figure 4.11 illustrate the rejection performance of selected individual constituents in the synthetic AMD. The feed and permeate temperatures did not differ significantly, therefore, the effect of temperature on membrane performance was neglected. The amount of chitosan loading was one of the most significant parameters that strongly affected membrane performance. As such, the dependence of membrane rejection on chitosan loading was studied by varying chitosan content (0, 0.5, 0.75 and 1 wt%) while fixing other parameters such as feed solution pH, concentration and operating pressure. The observed general trend showed that, addition of chitosan into the PES membrane matrix improved contaminants rejection. Additionally, the rejection of cations (Fe^{2+}, Mn^{2+}, Mg^{2+} and Ca^{2+}) was higher than that of the anion (SO_4^{2-}). In membrane separation process, not only filtration mechanism exhibits rejection process, but membrane surface charge also plays a vital role. It is generally known that PES membranes exhibit negatively charged surface (Ghaemi et al., 2011), therefore, rejection of anions was due to repulsion forces between anions and negatively charged membrane and sieving effect through Donnan exclusion mechanism (Crespo et al., 2014). Addition of chitosan in the PES membrane matrix improved sulphate ions removal ability. Amine groups on chitosan structure remains uncharged at neutral pH and addition of chitosan into PES membrane matrix cannot affect surface charge of PES membrane. Under neutral filtration tests, addition of chitosan inside PES membrane would not be as significant since the membrane charge would not be affected. However, filtration tests in this study were conducted at pH of 3.2, which resulted in the protonation of the amine groups on the chitosan structure and caused the membrane to be positively charged (Liu et al., 2013). It could be observed that sulphate ion rejection improved from 53% for pristine PES membrane to 62, 73 and 72% for PES/0.5 wt%, PES/0.75 wt% and PES/1 wt%, respectively. This improvement in the rejection of sulphate

ions by modified PES membrane was due to adsorption of sulphate ions by the positively charged sites on the chitosan structure created under acidic conditions.

In addition to membrane sieving mechanism, the high cation removal behaviour was also due to strong dominant electrostatic repulsive forces generated between positively charged membrane surface and the cations. Cation metals selectivity by the pristine PES membranes was 50 % (Ca^{2+}), 52 % (Fe^{2+}), 63 % (Mn^{2+}) and 65 % (Mg^{2+}). Addition of 0.5 wt% chitosan to the PES blend improved membrane rejection to 55%, 56 %, 74 % and 76 % for Ca^{2+}, Fe^{2+}, Mn^{2+} and Mg^{2+}, respectively. The general observed trend for the ions were that, rejection increased with increasing chitosan content from 0 up to 0.75 wt%. This was due to introduction of more amine functional groups which when protonated repel cations or attract anions. Literature argues that metal ions tends to form metal complexes with OH^- groups at higher pH and membrane rejection favour metal complexes than metal ions (Al-Zoubi et al., 2010). As recorded earlier, pH of the feed solution was acidic, therefore it can be argued that the cations were removed as metal ions. Furthermore, introducing more chitosan particles to 1 wt% reduced membrane flux and rejection. This could attribute to the molecular entanglement and aggregation which forms thick layer of chitosan and create weaker pore wall with reduced pore sizes. The reduced rejection could be attributed to the agglomeration of chitosan particles which leads to low utilization of binding sites on the membrane surface and within the porous matrix (Sivakami et al., 2013). Figure 4.12 was plotted in order to select a membrane with acceptable flux and metal ion removal. The results showed improving flux and metal ion rejection with increased amount of chitosan content from 0, 0.5 and 0.75 wt%. Further chitosan addition to 1wt% induced a decline in membrane flux and metal ion rejection. Reduced membrane flux signified low volume of AMD containing the solute ions was transported towards the membrane surface hence reduced rejection was recorded compared to when chitosan was 0.75 wt%.

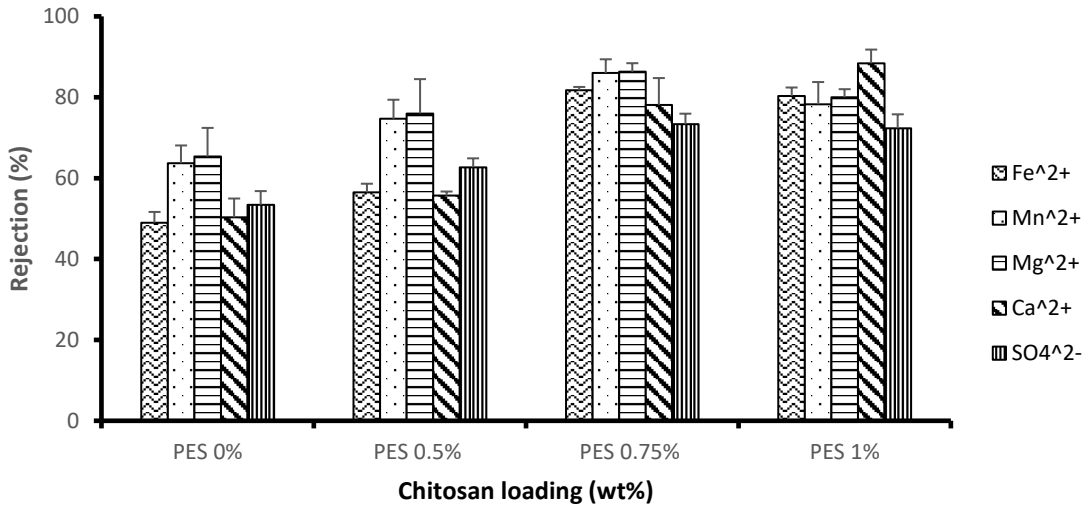
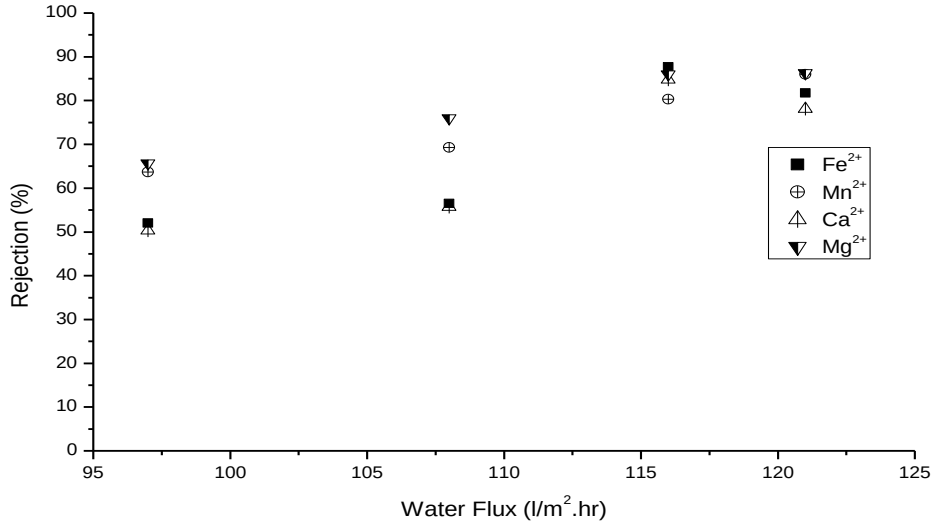


Figure 4.11: Rejection (%) of metal and sulphates ions using PES/chitosan membranes having various chitosan loading.



Chitosan loading	0 wt%	0,5 wt%	1 wt%	0,75 wt%

Figure 4.12: Metal ion rejection against flux of the prepared PES/chitosan membranes

Figure 4.13 presents rejection of selected metal and sulphates ions by PES/PA membrane and PES/PA infused with chitosan. PES membrane was coated with polyamide layer to produce PES/PA membrane and PES was infused with chitosan and coated with polyamide layer to produce PES/0.5 wt% chitosan/PA, PES/0.75 wt% chitosan/PA and PES/1 wt% chitosan/PA membranes. Although the addition of chitosan in the PES/PA blend had increasing linear effect on the membrane permeability, such could not be reported on metal and sulphate ion rejection. All membranes had increased rejection for all selected contaminants until when chitosan content was 0.75 wt% (PES/0.75wt% chitosan/PA membrane) with Fe^{2+}, Mn^{2+}, Mg^{2+}, Ca^{2+} and SO_4^{2-} reporting highest rejection of 88, 90, 89, 76% and 56%, respectively. Further chitosan addition to 1 wt% (PES/1 wt% chitosan/PA membrane) either had no significant effect on rejection or induced a decline. As reported in Figure 4.6 (b) and 4.7 (b), the porosity and water flux of the membranes was enhanced by chitosan addition due to the improved hydrophilic nature of the membranes. The declining contaminant rejection could be attributed to the fact that at high fluxes, trapped metal and sulphates ions trapped on the membrane surface were pushed through the membranes into the permeate stream. Rejection of Fe^{2+}, Mn^{2+}, Mg^{2+}, Ca^{2+} and SO_4^{2-} was recorded as 67, 71, 63, 62 and 36% for PES/PA membrane without chitosan, respectively. The study conducted by Mthethwa (2014) which used PES membrane to treat AMD without modification reported low metal rejection and flux and recommended modification with hydrophilic materials. Under acidic conditions, the amine and amide functional groups of chitosan particles and polyamide layer, get positively charged (Liu et al., 2013). This tends to make the membrane to be positively charged. Rejection of anions takes advantage of appositional charges between the positive charged membranes and anions through electrostatic attraction forces; however, the low anion removal shows that repulsion forces were stronger than attraction forces. Table 4.1 provide comparison of outcomes in this research and

those in literature. The membranes synthesised in the study proved to have better flux as compared to those in literature.

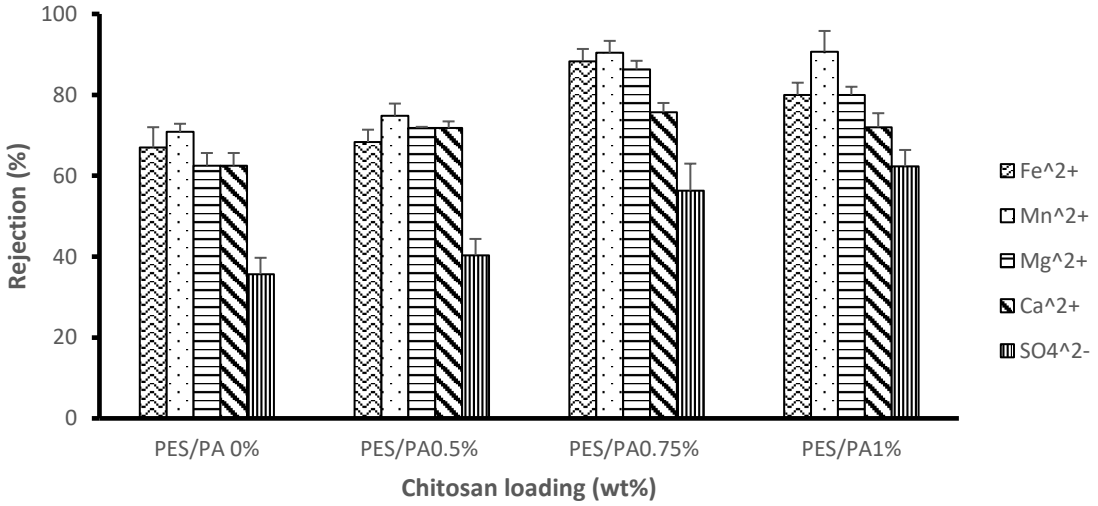


Figure 4.13: Rejection (%) of metal and sulphates ions using PES/chitosan membranes coated with polyamide layer having various chitosan loading.

Table 4.5: Performance comparison of this research with other studies in literature

Membrane	Target contaminate	Outcomes	Reference
Commercial CPA2, ESPA1 Polyamide membranes	Stainless steel wastewater (Cr, Ni, Fe, Mn, Cu, Zn, NO_3-N, NO_2 but the target was NO_3-N)	1. ESPA1 had a flux of ± 39 L/m^2.hr and CPA2 had ± 18 L/m^2.hr 2. Rejection of polyamide membranes was between 90 to 99% for 1000 to 60 mg/L of NO_3-N	Kim et al., 2007
PES/PA membrane	BSA	1. Unblended PES had 7.5 L/m^2.hr and PES blended with 2wt% PA had 80.4 L/m^2.hr	Shockravi et al., 2017
Commercial AFC NF polyamide membrane	$Pb(NO_3)_2$	1. Flux of ± 30 L/m^2.hr 2. Reported rejection of 99.4% for 50 mg/L of $Pb(NO_3)_2$ at pH of 5.7	Gherasim et al., 2013
PA/chitosan membrane	NaCl, $CaCl_2$ and Na_2SO_4	1. Flux was between 32.9 to 59.6 L/m^2.hr 2. Rejection of ±38 % for NaCl, $CaCl_2$ at 93.8% and 97.3% for Na_2SO_4	Akbari et al., 2015
PES/chitosan/PA membrane	Ca^{2+}, Fe^{2+}, Mn^{2+}, Mg^{2+}, and SO_4^{2-}	1. Maximum flux of 93 and 133 L/m^2.hr for PES/chitosan and PES/chitosan/PA respectively 2. Cation rejection (86% Mn^{2+},81% Fe^{2+}, 86.% Mg^{2+} and 88% Ca^{2+}) and 73% for SO_4^{2-} for PES/chitosan membranes 3. Cation rejection (91% Mn^{2+},88 Fe^{2+}, 86%, % Mg^{2+} and 76% Ca^{2+}) and 62% for SO_4^{2-} for PES/chitosan/PA membranes.	This study

4.5 Summary

Membrane modification with chitosan and polyamide as hydrophilic copolymers enhanced PES membrane antifouling and hydrophilic properties. Additionally, they present more functional groups which acts as contaminant binding sites during the treatment of acid mine drainage. PES membrane was infused with chitosan to produce PES/chitosan membrane and polyamide layer was coated on top to produce PES/chitosan/PA membrane. The chitosan content was varied (0, 0.5, 0.75 and 1 wt%) and 4 PES/chitosan membranes and 4 PES/chitosan/PA membranes were synthesised

The synthesised membranes were characterised with FTIR which gave an indication of the chemical and functional groups present on the membrane surface. It was also used to verify functional groups on the chitosan samples to confirm success in synthesizing chitosan from chitin. SEM was used to observe the surface morphology and cross-sectional view of the membrane to determine the effect of chitosan loading and coating polyamide layer on top. Contact angle analysis confirmed the influence of chitosan addition and coating polyamide layer on the hydrophilicity of the membranes. Tensile strength evaluated the effect of chitosan and polyamide modification on the mechanical properties of the synthesised membranes. The membranes were tested in Dead-End filtration set up to evaluate the influence of chitosan content and coating polyamide layer on membrane flux and rejection during the treatment of acid mine drainage.

The FTIR spectra of PES/chitosan membranes showed no presence of chitosan on the membrane surface since the chitosan was infused within the PES membrane. The PES/chitosan membranes assumed the properties of basic PES structure only due to chitosan which was infused within the PES membrane matrix. Similar conclusions were made in literature by Belfer et al. (2000) and Ghiggi et al. (2017). The FTIR spectra of PES/chitosan/PA membranes showed the basic structure of PES and polyamide layer.

A contact angle measurement which characterises membrane's wettability showed that introduction of hydrophilic chitosan and polyamide co-polymers inside and on the surface of PES membrane induced a remarkable reduction in water contact angle of the membrane. It was evidently clear that introduction of hydrophilic chitosan and polyamide layer triggered a downward trend in contact angle of the membranes. This decrease in contact angle with increasing chitosan content affirms the influence of chitosan as an agent to enhance the membrane surface hydrophilicity.

Mechanical property of the membranes was evaluated by checking the effect of chitosan content and coating polyamide layer on the tensile strength of the membranes. Addition of chitosan had a positive effect on the mechanical property of pristine PES membrane as tensile strength was increasing with increasing chitosan content. Coating polyamide layer onto the pristine PES membrane and PES/chitosan membranes induced reduction in tensile strength due to the formation of polyamide molecules exerting plasticizing effect on the membrane surface and making it to be more flexible and cause it to lose its strength.

SEM images revealed uniformly distributed pores on the pristine PES membrane. Addition of chitosan co polymer and coating polyamide layer on top resulted in a more compact and denser surface with reduced effective pore sizes. The intensity of the compact and dense structure increased with increasing chitosan content. However, the cross -sectional images of the PES/chitosan and PES/chitosan/PA membranes revealed a more porous sublayer and reduced pore wall thickness compared to pristine PES membrane. Moreover, the skin layer thickness decreased with addition of chitosan particles up to 0.75 wt%. Further addition to 1 wt% chitosan increased pore wall thickness and caused reduction in membrane porosity. Similar observations were made by Ghaemi et al. (2018) and Boricha and Murthy (2009). Polyamide membranes are characterized by rough surface which enhance fouling potential. However, co-solvent assisted interfacial polymerization was followed in this study, with acetone as a co-

solvent and the SEM images showed smooth character compared to those prepared using the conventional interfacial polymerization (Akbari et al., 2015).

Considering the results of the membrane performance evaluation, the pure water flux of the PES/chitosan membrane increased from 102 L/m^2.hr to 107 L/m^2.hr after the addition of 0.5 wt% chitosan. It was further increased to peak flux of 133 L/m^2.hr with the addition of 0.75 wt%, which is 20% more than the pristine PES membrane. However, increasing the chitosan amount in the blend to 1 wt% caused the flux to decline to 120 L/m^2.hr, but it was still higher than that of unmodified PES membrane. This was attributed to the fact that increasing chitosan amount caused blockage of effective pore sizes of the membrane. Coating the polyamide layer on top had adverse effect on the pure water flux. Pure water flux of polyamide materials of 56 L/m^2.hr to 62, 73 and 93 L/m^2.hr when polyamide was coated onto the PES/0.5 wt% chitosan, PES/0.75 wt% chitosan and PES/1 wt% chitosan membranes, respectively. This is because polyamide materials are usually used to construct reverse osmosis membranes, which are characterised by smaller pore sizes compared to other membranes.

The amount of chitosan loading was one of the most significant parameters that strongly affected the membrane performance. As such, the dependence of membrane rejection on chitosan loading was studied by varying chitosan content (0, 0.5, 0.75 and 1 wt%) while fixing other parameters such as feed solution pH and concentration and operating pressure. The observed general trend showed that, addition of chitosan content from 0 to 0.75 wt% into the PES membrane matrix improved contaminants rejection. Additionally, the rejection of cations (Fe^{2+}, Mn^{2+}, Mg^{2+} and Ca^{2+}) was higher than that of the anion (SO_4^{2-}). Further chitosan addition to 1wt% induced a declined in ions rejection. 0.75 wt% chitosan addition reported satisfactory results in this Chapter, as such; chitosan addition will be fixed as 0.75 wt% for further investigation.

Chapter 5: Effect of chitosan's degree of deacetylation on the performance of the synthesized PES/chitosan and PES/chitosan/PA membranes

This Chapter reports on the results of synthesis and characterisation of chitosan samples from chitin by treatment with strong alkaline solution. It presents on the effect of synthesis process variables (NaOH concentration and temperature) on the degree of deacetylation of the chitosan samples. It further reports on the effect of chitosan's degree of deacetylation on the quality and performance of PES membranes infused with chitosan and PES membranes infused with chitosan (PES/chitosan membranes) and coated with polyamide (PES/chitosan/PA) layer during AMD treatment. Lastly, the effect of feed pH, initial concentration and pressure on water flux and rejection performance is reported.

5.1 Introduction

Chitosan with different chemical structures can be synthesised by manipulating reaction time, synthesis temperature and strength of the alkaline solution utilized during the deacetylation process. Degree of deacetylation influences the chemical, biological and mechanical properties of the synthesised chitosan and should be determined to confirm the success of the synthesis process. The properties include acid base and electrostatics characteristics, sorption properties, biodegradability and the ability to chelate metal ions. Degree of deacetylation gives an indication of available free amino groups in the polysaccharide which could act as potential binding sites for contaminants. When chitosan is used to modify polymeric membranes for metal ion removal from solution, it's expected that high number of available amino groups on the chitosan structure should translate into more effective sorption capacity. However, the influence of chitosan's degree of deacetylation on the effectiveness of metal ion binding during AMD treatment is non-existent and this Chapter seeks to demonstrate that.

This Chapter focuses firstly on several techniques which were used to evaluate properties of the synthesized chitosan to determine the effect of degree of deacetylation on the quality of the synthesised chitosan. Secondly, it reports on the effect of synthesis process variables on the degree of deacetylation of the chitosan samples. FTIR was used to confirm success in synthesising chitosan from chitin and determine its degree of deacetylation. Higher degree of deacetylation indicates more amine groups exposed and available as metal ion binding sites. Therefore, it further reports on the effect of chitosan's degree of deacetylation on the performance of PES membranes and PES membranes infused with chitosan (PES/chitosan) and coated with polyamide layer (PES/chitosan/PA) during AMD treatment. The performance of the membranes was tested using a dead-end filtration setup as previously outlined in Chapter 3.

5.2 Synthesis of chitosan with different degree of deacetylation

As previously outlined in Chapter 4, chitosan samples were synthesised from chitin by chronologically conducting these steps (i) Demineralization, (ii) Deproteinization and (iii) Deacetylation. Nine chitosan samples having different degree of deacetylation were synthesised by varying synthesis process variables. The demineralization and deproteinization steps conducted previously in Chapter 4 were repeated in this section. The deacetylation temperature and strength of the alkaline solution were varied to obtained nine chitosan samples having different degree of deacetylation. The samples were prepared in duplicate to improve accuracy of the results.

5.3 Characterization

5.3.1 Yield (%)

Percentage yield was determined to understand the efficiency of the synthesis process and conditions in terms of chitosan quantity which was obtained. Equation 5.1 was used to

determine the percentage yield. Table 5.1 presents overall yield for all nine chitosan samples. The calculation for percentage yield for all nine samples is contained in Appendix A1.

$$\%Yield = \frac{total\ grams\ of\ products(chitin)}{total\ grams\ of\ reactants(chitosan)} \times 100\% \quad (5.1)$$

Table 5.1: Chitosan yield

Chitosan Sample No	%Yield	Std deviation
1	28.8	5.4
2	25.3	1.9
3	18.2	2.6
4	23.8	4.0
5	19.8	3.5
6	14.2	1.6
7	13.7	4.2
8	12.7	0.9
9	10.8	1.6

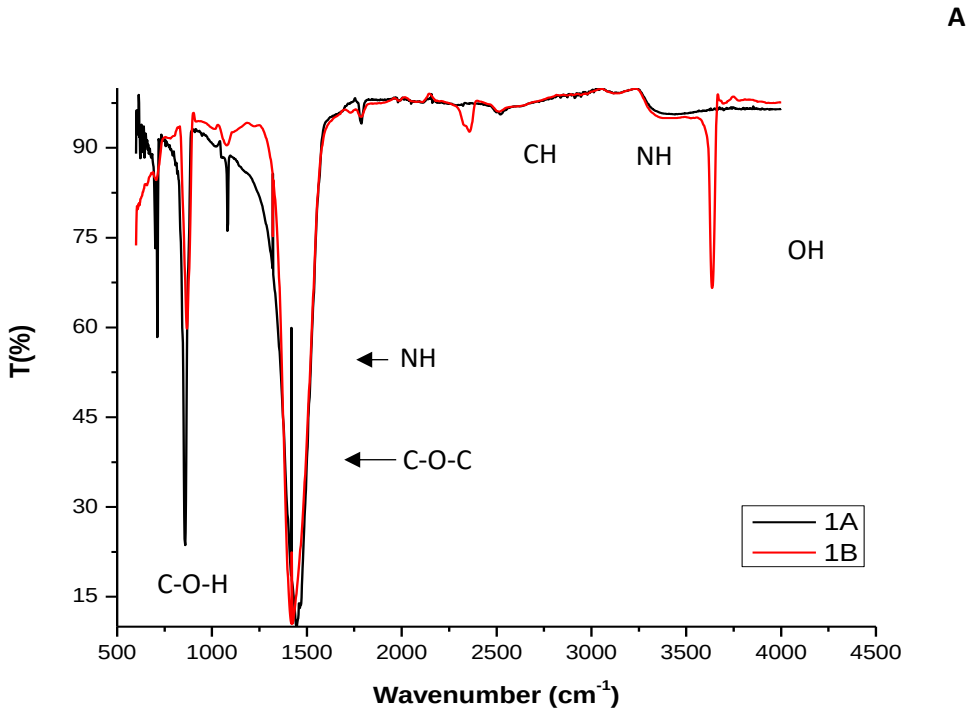
Crushed and milled chitin was in flakes structure and the intensity of the dark brown colour shifted from light to dark brown after the demineralization, deproteinization and deacetylation process. The percentage yield was low for all nine samples and this was attributed to the nature

of the synthesis process. Removal of minerals and proteins from chitin via demineralization and deproteinization accounted for this huge percentage mass loss. Percentage yield of chitosan from chitin decreased as the concentration of NaOH and temperature increased, respectively. Higher temperature and NaOH concentration showed to have high capabilities to remove proteins from the chitin structure. Similar observations were made by Soon et al. (2018) and Srinivasan et al. (2018). Srinivasan et al. (2018) reported yield of 35% using 50% NaOH concentration at 90 ^{o}C for 50 min as deacetylation conditions. Chitosan yield in the range of 4.77% - 5.43% was realised by Soon et al. (2018) using deacetylation conditions of 50% NaOH at 90 ^{o}C for 30 hours. These conditions are closely similar to deacetylation conditions used to synthesise sample 2 and 5 in this study, respectively. Sample 2 and Sample 5 displayed yields of 25.3 and 19.8%, respectively. The higher yield reported by Srinivasan et al. (2018) as comparable to sample 2 and sample 5 could be attributed to low synthesis time of 50 min as compared to 6 hours used in this study. Sample 6, 7, 8 and 9 had even lower yields and this was attributed to either increased synthesis temperature and/or NaOH concentration.

5.3.2 FTIR analysis

Figure 5.1 shows FTIR spectra of the selected chitosan samples (Samples 1, 5 and 9), the rest of the samples are contained in Appendix A2. Duplicates were prepared to confirm accuracy and repeatability of the synthesis process. Chitosan samples having different degree of deacetylation showed no obvious differences (Chen et al., 2002). The FTIR spectra of the chitosan samples exhibited characteristic amino peaks at around 3300 cm^{-1} to 3500 cm^{-1} overlapping with the N-H stretching with a minimum intensity of the amine functional group of chitosan units in polymer. The observed bending vibration at around 1450 cm^{-1} to 1480 cm^{-1} was assigned to the N-H bending vibration of the R-NH_2 functional group which indicate an increased degree of deacetylation. The typical alcohol peaks (OH and COH) are observed to occur at around 3500 cm^{-1} and just before 1000 cm^{-1}. According to the study conducted by

Marei et al. (2016), the absorption peaks observed at around 1080 cm^{-1} is due to the C-O-C stretching. The peaks observed between 2400 cm^{-1} and 2800 cm^{-1} indicate the alkaline C-H vibration of CH_2 (Srinivasan et al., 2017). Studies in literature revealed FTIR spectroscopies of chitosan samples having similar characteristic peaks obtained in this study (Kumari et al., 2017). This indicates successful chitosan synthesis from chitin. The large presence of various functional groups available on the chitosan structure formed basis of why chitosan was selected to modify the PES membrane. The protonation of available NH and NH_2 functional groups under acidic medium favours electrostatic repulsion and attraction of cations and anions, respectively.



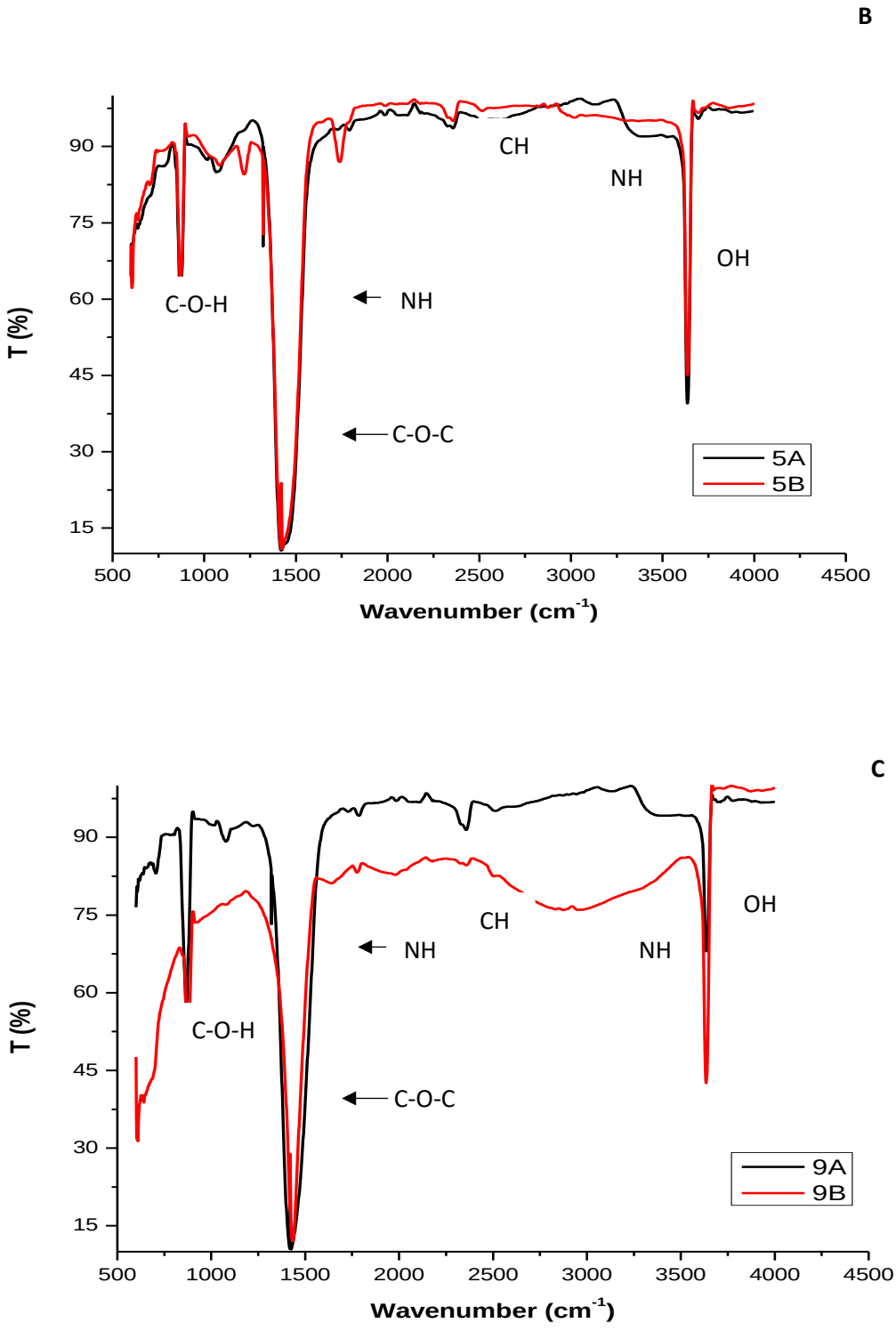
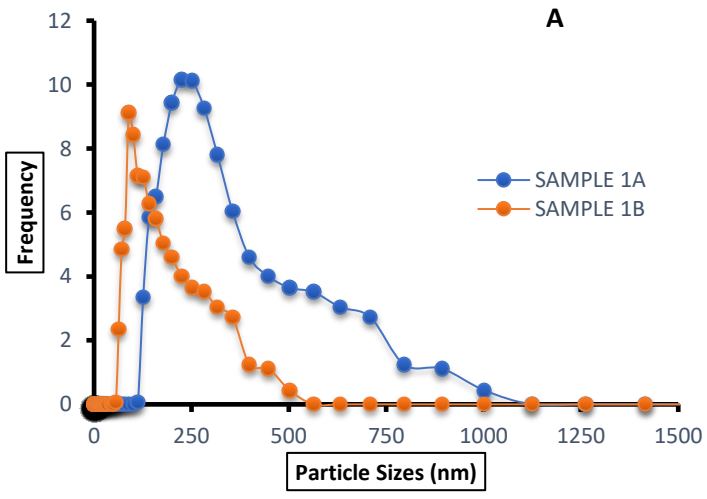


Figure 5.1: FTIR spectra of selected chitosan (a) Samples 1A and 1B, (b) Samples 5A and 5B, (c) Samples 9A and 9B

5.3.3 PSD of chitosan samples

The particle size distribution of chitosan samples was determined using laser diffraction method (Malvern Mastersizer 2000 instrument). Figure 5.2 (a), (b) and (c) presents PSD results of only samples 1, 6 and 9, respectively. The rest are contained in Appendix A3.The samples were prepared in duplicate. Figure 5.2 indicate particle size distribution of chitosan particles which were synthesised from chitin and a mean size of less than 1500 nm was observed, generally. Limitation of this laser method appear to be for small particle sizes (≤ 1µm), material with low refractive index with respect to dispersive medium and for non-spherical particles. The analysis was conducted under ambient conditions, therefore, the conditions which the measurement were conducted could not affect results. The flat sheet membranes were cast using a 250 µm thickness blade. This particle size distribution results shows that the synthesized chitosan had acceptable dimensions to be added to the membrane without creating cracks within the membrane. Additionally, another observation was that a decrease in maximum particle size was observed with increasing NaOH concentration at constant temperature. On the other hand, no clear significant effect of temperature on the particle sizes could be observed.



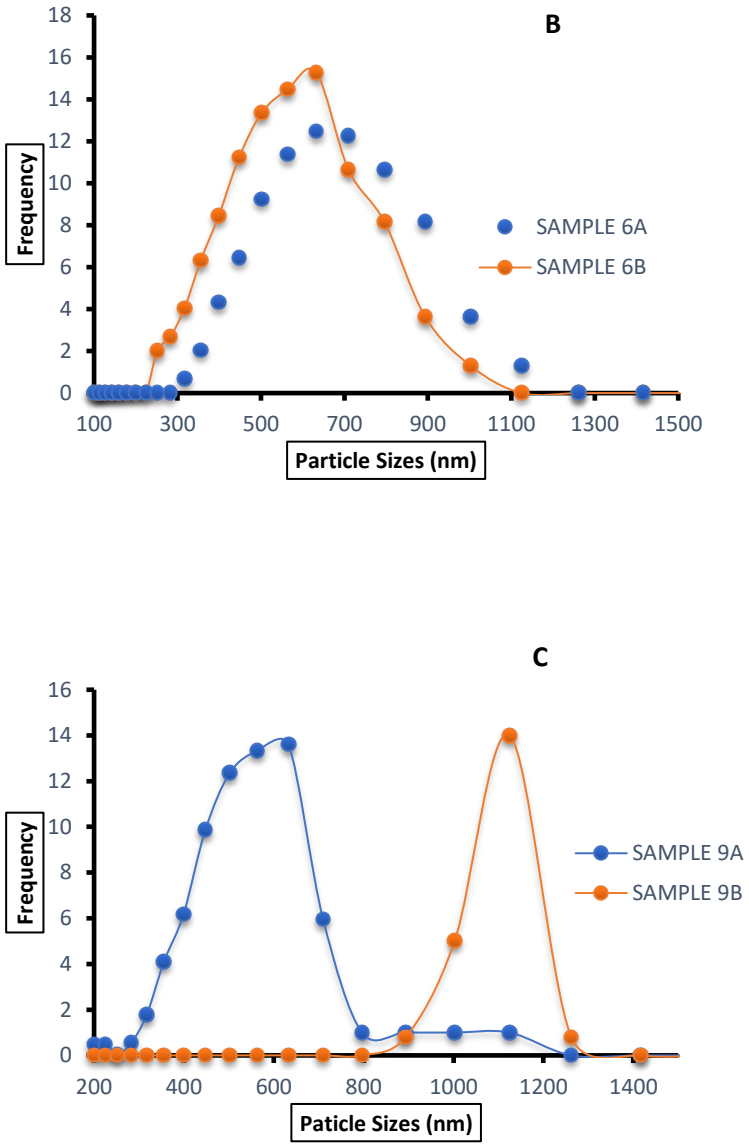


Figure 5.2: Particle size distribution of synthesised chitosan of (a) Sample 1A and 1B (b), Samples 6A and 6B and (c) Samples 9A and 9B

5.4 Effect of chitosan synthesis process on the degree of deacetylation (DD)

The degree of deacetylation (DD) of chitosan determines the amount of acetyl groups which have been removed from the chitosan structure leaving behind free amino groups on the polysaccharide. The greater the DD, the more available amine groups are exposed as potential binding sites for contaminants. Studies have concluded that temperature, reaction time and

NaOH concentration have a significant effect on the DD of the synthesised chitosan. Deacetylation process is achieved by treating chitin with concentrated NaOH or KOH (40 to 50%) usually at around 100 ^{o}C for several hours (Rinaudo, 1999). Palpandi et al.(2009) synthesised chitosan by treating chitin with 40% NaOH solution at 110 ^{o}C for 6 hours, Kumari et al.(2017) synthesised chitosan from fish scales, shrimp and crab shells using 40% KOH at various temperatures for 6 hours and Hussain et al.(2013) synthesised chitosan by treating chitin with 40% NaOH at 80 ^{o}C for 4 and 8 hours. In the present case, the reaction time was kept constant at 6 hours and temperature (80 ^{o}C, 100 ^{o}C and 120 ^{o}C) and NaOH (20%, 40% and 60%) concentration was varied to synthesise chitosan having different DD as explained in Chapter 3.

Table 5.2 shows the determined DD of chitosan samples synthesised under different deacetylation conditions. The general trend observed was that DD increased from 34%, to 73% when the NaOH concentration was increased from 20% to 40% and the synthesis temperature was kept constant at 80 ^{o}C, respectively. Similar observations were made when synthesis temperature was increased to 100 ^{o}C and 120 ^{o}C for the same NaOH concentration (from 20% to 40%, respectively). This is due to the higher strength of the NaOH solution which promotes the degradation of the acetyl group and formation or exposure of more amine groups, thus increasing the DD of the sample. Increasing NaOH concentration to more than 40% induced reduction in DD of the chitosan. DD was reported as 73% when the NaOH was 40% at 80 ^{o}C but increasing NaOH concentration to 60% at the same temperature reduced the DD to 61%. This indicated that NaOH concentration of greater than 40 % encourages the degradation of the chitosan sample as a whole (Hongpattarakere and Riyaphan, 2008). Similar observations were made in the case of temperature in isolation. The DD increased from 73% to 96%when the temperature was increased from 80 ^{o}C to 100 ^{o}C and NaOH concentration was kept constant at 40%, respectively. This is attributed to the greater kinetic energy induced by higher

temperatures which causes degradation of the acetyl groups as more reactions occur. When more acetyl groups are degraded, more amine groups are exposed, thus increasing the DD of the chitosan. Increasing the temperature to 120 ^{o}C caused a decline in DD of the chitosan sample. Based on this behaviour, it can be argued that at above 100 ^{o}C, chitosan sample started to degrade and destroying the already formed or exposed amine groups, thus reducing the DD of the chitosan sample (Barbosa et al., 2019 and Gámiz-González et al., 2017)

Table 5.2: Degree of deacetylation of chitosan under different synthesis conditions

Sample No	Experimental Conditions		DD%	Std Deviation
	Temperature(^{o}C)	NaOH Conc (wt%)		
1	80	20	33.93	1.41
2	80	40	73.05	5.20
3	80	60	60.82	1.67
4	100	20	61.94	0.10
5	100	40	95.97	1.49
6	100	60	82.92	2.65
7	120	20	79.92	3.59
8	120	40	90.17	0.82
9	120	60	85.55	5.11

Kumari et al.(2017) reported DD of 70%, 75% and 78% by extracting chitosan from fish, crab and shrimp shells using 40% NaOH concentration at for 6 hours at 90 ^{o}C. The deacetylation conditions used by Kumari et al. (2017) are similar to deacetylation conditions used to synthesis sample 2, 6 and 8 with a slight difference in temperature. The obtained DD in this study were different from the DD obtained by Kumari et al. (2017). The DD obtained at 80 ^{o}C, 100 ^{o}C and

120 ^{o}C was reported as 73%, 96% and 90%, respectively. For both NaOH concentration and temperature in isolation, the DD increased up to a certain point and then decreased when the other is kept constant. At a temperature of 120 ^{o}C and NaOH concentration of 60 % the DDA is 86 %, if the temperature is decreased by a ratio of 1.5 to 80 ^{o}C the DD decreases to 61 %. In contrast, when NaOH concentration is decreased by a ratio of 1.5 from 60% to 40% at the same synthesis temperature, the DD increased to 90%. Thus, there is a decrease in the DD when the temperature is reduced and an increase in the DD when NaOH concentration is decreased by the same ratio. Thus, temperature is more significant than NaOH concentration. A higher DD of 96 % was achieved with a temperature of 100 ^{o}C and NaOH concentration of 40 %.

5.5 Effect of chitosan degree of deacetylation (DD) on the quality and performance of PES/chitosan and PES/chitosan/PA membranes

The nine synthesised chitosan samples having different degree of deacetylation were used to modify PES membranes to produce nine PES/chitosan membranes. Another set of nine PES/chitosan membranes using chitosan with different degree of deacetylation was synthesised and a polyamide layer was coated on top to produce PES/chitosan/PA membranes. Based on the optimized chitosan loading, which was reported in Chapter 4, 0.7 wt% loading was fixed. Dead-end filtration system was used to evaluate the performance of synthesised membranes during synthetic AMD treatment.

5.5.1 Characterization of the synthesized membranes

The synthesised membranes infused with chitosan having various DD (PES/chitosan membranes) and then coated with polyamide layer (PES/chitosan/PA membranes) were examined with contact angle to determine the hydrophobicity/hydrophilicity, FTIR to identify functional groups and TGA to confirm thermal stability of the synthesised membranes. In order to distinguish the membranes used, Table 5.3 shows coded names assigned to the synthesised membranes for easy identification with PES referring to PES membranes modified with

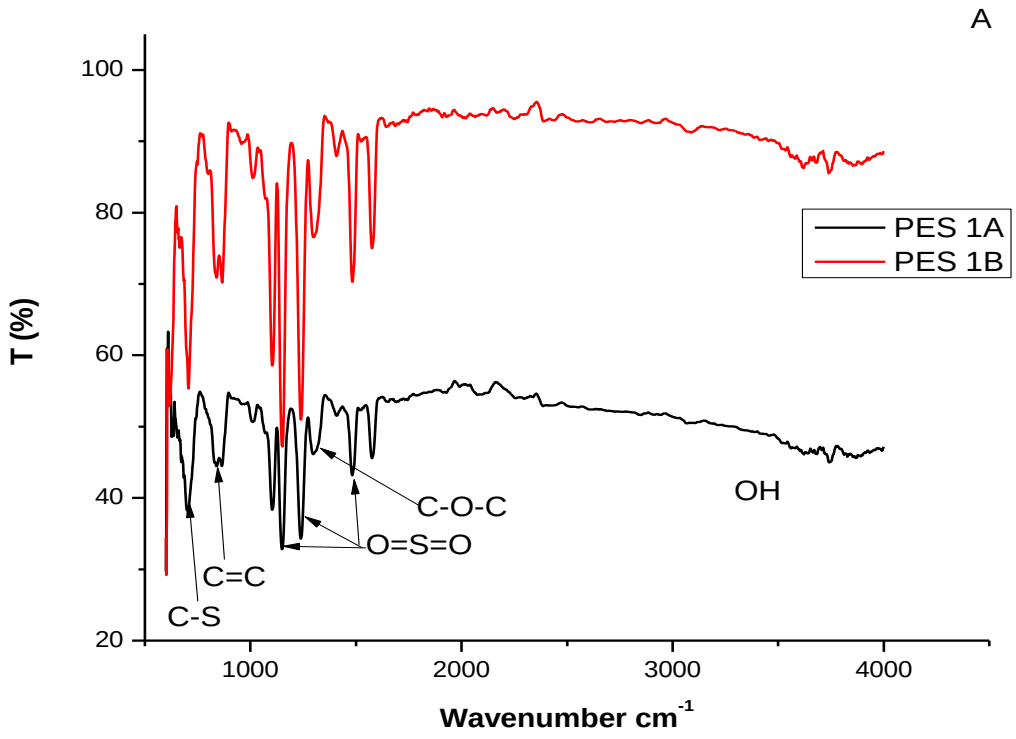
chitosan and PA membranes to PES membranes infused with chitosan and coated with polyamide layer. Table 5.3 presents chitosan samples (samples numbers) with corresponding degree of deacetylations, as such; the synthesised membranes were assigned according to that format. That is, chitosan sample 2, was used to synthesis PES/chitosan membrane PES 2 and PES/chitosan/PA membrane PA 2 for example.

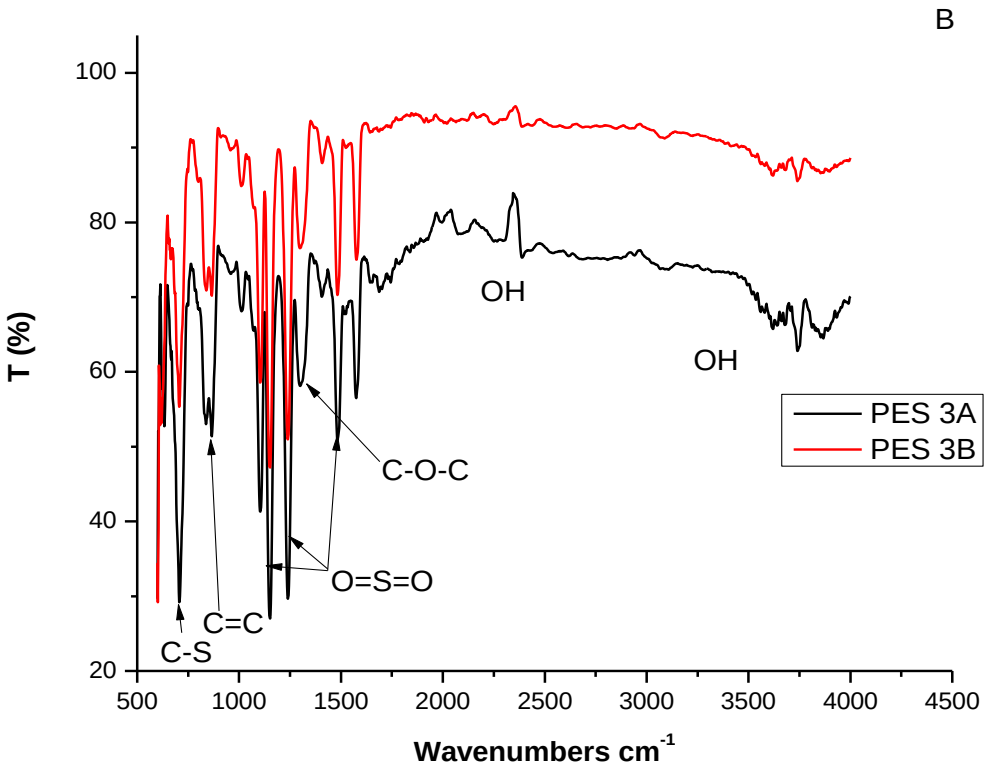
Table 5.3: Coded names of the synthesised membranes

Sample No	%DD	PES/chitosan Membranes coded names	PES/chitosan/PA Membranes coded names
1	33.93	PES 1	PA 1
2	73.05	PES 2	PA 2
3	60.82	PES 3	PA 3
4	61.94	PES 4	PA 4
5	95.97	PES 5	PA 5
6	82.92	PES 6	PA 6
7	79.92	PES 7	PA 7
8	90.17	PES 8	PA 8
9	85.55	PES 9	PA 9

5.5.1.1 FTIR analysis

Figure 5.3 (a and b) depicts FTIR spectra of both PES/chitosan (PES 1 and PES 3) and Figure (c and d) shows that of PES/chitosan/PA (PA 1 and PA 3), respectively. Appendix B1 and B2 shows FTIR for the rest of the PES/chitosan and PES/chitosan/PA membranes, respectively. Chitosan samples had different degree of deacetylation. Looking at the FITR spectra, the effect of chitosan's degree of deacetylation could not be verified. As already mentioned in Chapter 4 (section 4.4.1.3), IR spectra of the membranes was attributed to the properties of basic PES structure as no significant different between PES and PES/chitosan membranes could be observed. FTIR spectra of the synthesised chitosan samples did not show significant difference. Similar observations were made by Chen et al. (2012). Additionally, Boricha and Murthy (2009) also observed no structural differences on the surface of PES membranes modified with different chitosan concentrations. In this study, the FTIR spectra of membranes modified with 0.75 wt% chitosan reported in Chapter 4 had similar characteristics with those prepared having chitosan with various degree of deacetylations. The C-stretching and C=C stretching on the aromatic rings were identified with the peaks at 620 and 880 cm^{-1}, respectively. The PES characteristic sulfonyl group was confirmed with peaks at 1150 cm^{-1}, 1239 cm^{-1} and 1483 cm^{-1} The aromatic ether (C-O-C) group was assigned to the peak at 1244 cm^{-1}. Moreover, FTIR spectra of PES membranes infused with chitosan and coated with polyamide layer reported in Chapter 4, are similar to the FTIR spectra of the membranes reported here even though the chitosan samples used in this Chapter had different degree of deacetylation. This confirms that chitosan's degree of deacetylation does not have significant impact on the surface structure of the membranes.


A
T (%)
100
80
60
40
20
1000
2000
3000
4000
Wavenumber cm-1
PES 1A
PES 1B
C-S
C=C
O=S=O
C-O-C
OH


B
T (%)
100
80
60
40
20
500
1000
1500
2000
2500
3000
3500
4000
4500
Wavenumbers cm-1
PES 3A
PES 3B
C-S
C=C
O=S=O
C-O-C
OH
OH

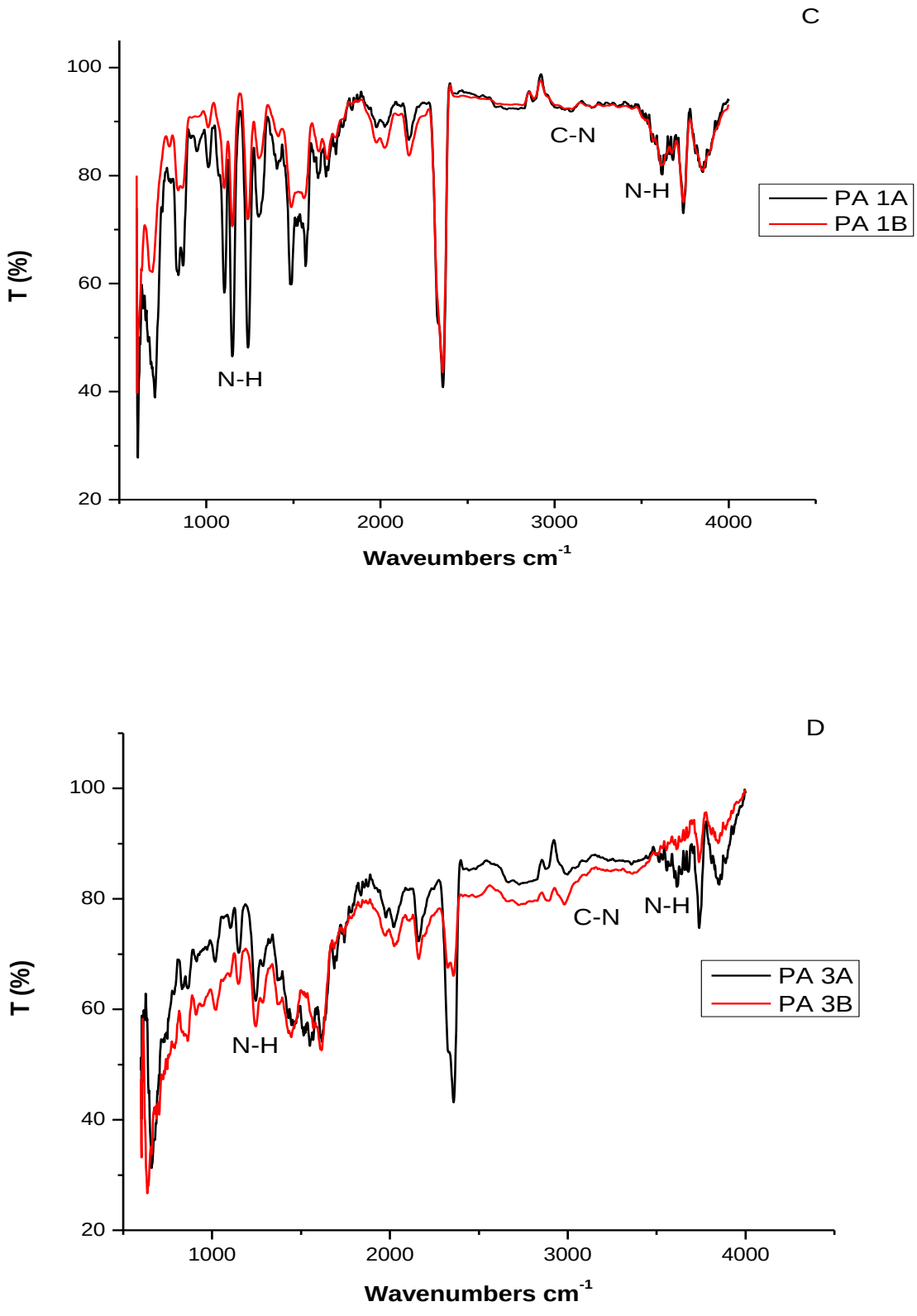
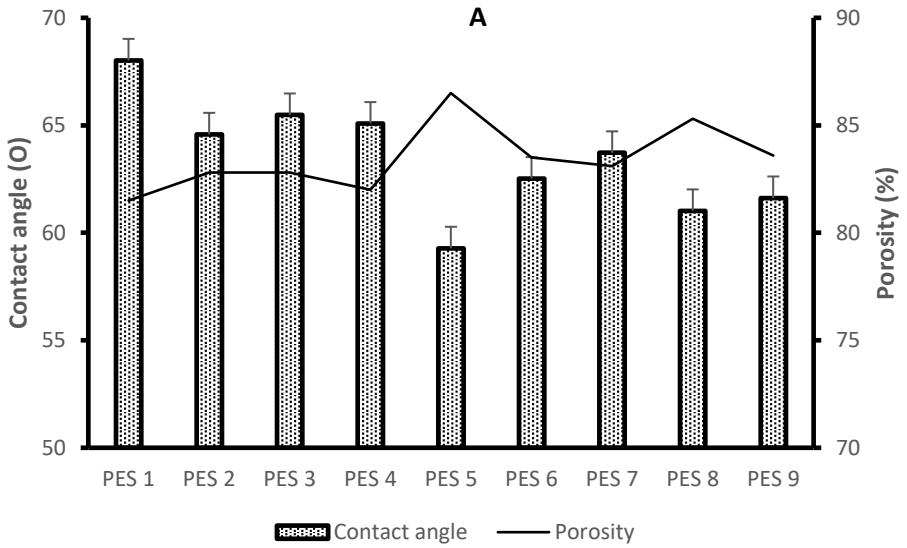


Figure 5.3: FTIR spectra of (a) PES 1A and 1B, (b) PES 3A and 3B, (c) PA 1A and 1B and (d) PA 3A and 3B

5.5.1.2 Contact angle and porosity analysis

Similar procedure as detailed in Chapter 4 was followed in conducting contact angle measurements of the membranes. The contact angle and porosity results are depicted in Figure 5.4 (a) and (b) for PES/chitosan membranes and PES/chitosan/PA membranes, respectively. As previously stated in Chapter 4, a relatively low contact angle indicates a hydrophilic nature of the membrane. It has been deduced previously that blending hydrophilic chitosan inside the PES membrane matrix will enhance the hydrophilic nature of the membrane. Figure 5.4 (a) and (b) reveals information about the influence of chitosan's degree of deacetylation on the hydrophilic nature and porosity of the membranes. The PES/chitosan and PES/chitosan/PA membranes synthesised in Chapter 4 with chitosan addition of 0.75 wt% had a contact angle of 61 and 48^{O}, respectively. Membranes synthesised in this Chapter had 0.75 wt% chitosan content. The deacetylation conditions used to synthesis chitosan in Chapter 4 are similar to those used to synthesise sample 8 in this Chapter and they both had comparable degree of deacetylation of 90 ± 5.2%. PES 8 and PA 8 in this Chapter had a contact angle of 61^{O} and 47^{O} and is comparable to the contact angle obtained in Chapter 4. The difference in the average contact angle was 0.4^{O} and 1.5^{O} for PES/chitosan and PES/chitosan/PA membranes, which is not very significant. It is known that there is water transport through the membranes as a result of water molecules interaction with amide of the hydrophilic chitosan through hydrogen bonding. Therefore, it is expected that high degree of deacetylation which means more amine groups available on the chitosan molecule will enhance water transport through the membrane. PES 5 and PA 5 where infused with chitosan having the highest degree of deacetylation and both reported the lowest contact angle values of $59^{O}$and 43^{O}, respectively. Same membranes had the highest porosities as they were more hydrophilic comparably with other membranes. Membranes coated with polyamide layer showed to be even more hydrophilic and this was attributed to the additional functional groups added after coating with the polyamide layer.

Although, polyamide membranes are characterised with small effective pore sizes, it would be expected that they are less porous. Figure 5.4 (b) reported significantly high porosity values and this was attributed to the available amine and amide functional groups of both chitosan and polyamide polymers which aided water transportation within the membrane matrix and on the membrane surface. This is affirmed by the SEM cross-sectional (Figure 4.4) which shows expanded pore sizes which could be caused by the reaction stretch between amine groups on the chitosan structure and unreacted acylchloride on the polyamide structure (Akari et al., 2015). PES 1 and PA 8 were modified with chitosan having the lowest degree of deacetylation of 34% and they both reported relative high contact angle values of 68^{O} and 63^{O}, respectively. This was due to the limited number of functional groups available to facilitate water movement on the membrane surface and within. Based on the results depicted in Figure 5.4 (a) and (b), the general trend is that high degree of deacetylation of chitosan enhanced the degree of hydrophilicity and porosity of the membranes.



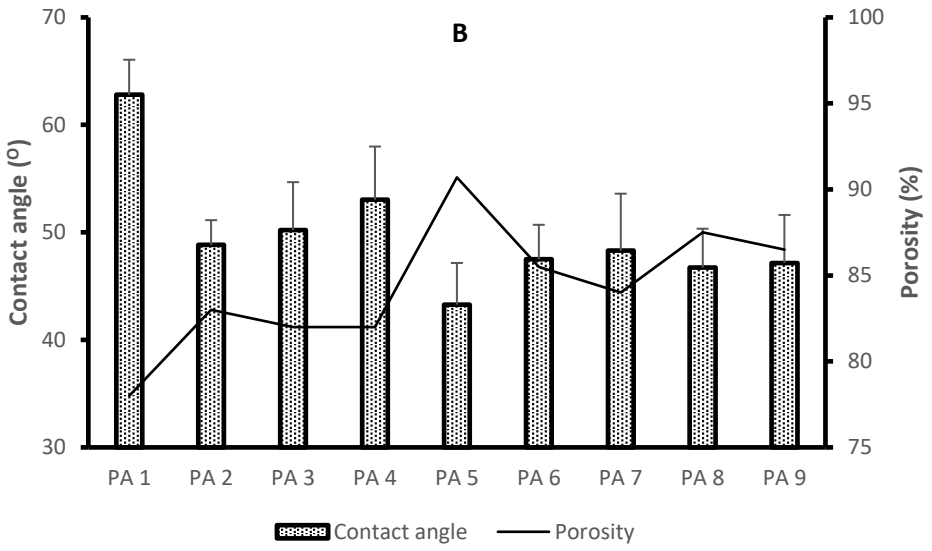


Figure 5.4: Contact angle and porosity results of (a) PES/chitosan and (b) PES/chitosan/PA membranes

5.5.1.3 TGA analysis

The thermal degradation and stability of the synthesised membranes infused with chitosan having various degree of deacetylation was evaluated and determined using thermogravimetric analyser. The results are depicted in Figure 5.5 (a) and (b) for PES/chitosan and PES/chitosan/PA membranes, respectively. Raw data is contained in Appendix B3 and B4 for PES/chitosan and PES/chitosan/PA membranes, respectively. The TGA determination reveals the maximum temperature at which the synthesised membranes can operate at before degradation.

(i) PES/chitosan membranes

Thermal behaviour of the synthesised PES/chitosan membranes is depicted in Figure 5.5 (a). The general trend observed was that, thermal stability plot showed loss of mass of the membranes with increasing temperature. Three step weight loss processes were observed

which were at 65 ^{o}C, 302 ^{o}C and 350 ^{o}C. The rapid thermal event or decrease in weight percent from 0 to 100 ^{o}C was due to the evaporation of moisture and other gases present (First thermal event). Although PES membranes do not contain water molecules, FTIR spectra showed OH functional group which was attributed to some water molecules still trapped inside the membranes matrix even after drying. Addition of chitosan polymer inside the membranes matrix also contributed to the mass loss due to hydroxyl group evaporation present on the chitosan molecule. The second and third weight degradation steps could be attributed to the destruction of the D-glucosamine and N-glucosamine on the chitosan structure respectively. As it can be observed in Figure 5.5 (a), addition of chitosan inside the membrane's matrix improved the thermal stability of the membranes as the graph shifted to the right showing high temperature tolerance. For example, the weight loss of pristine PES membrane after 5 minutes was around 89% and all membranes modified with chitosan were greater than 90%. This could be attributed to the fact that the weight loss in pristine PES membrane was accounted for by the evaporation of water which might have been still trapped inside after casting. For membranes modified with chitosan it was due to evaporation of water molecules inside the membrane matrix plus the loss of hydroxyl group on the chitosan molecule hence higher weight losses. High degree of deacetylation signifies high presence of D-glucosamine and N-glucosamine than acetyl groups. The weight loss and corresponding temperature difference for the samples is attributed to the difference in degree of deacetylation of the chitosan samples used. PES 5, PES 8 and PES 9 showed to be more thermally stable than the other membranes and this could be attributed to the fact that the chitosan used to modify the membranes had higher degree of deacetylation of 96%, 90% and 86%, respectively. More heat was required to destroy the formed D-glucosamine and N-glucosamine. Figure 5.5 (a) indicate that all the membranes were thermally stable up to 302 ^{o}C, whereby a rapid membrane loss was observed. Another membrane loss was observed beyond 380 until up to ±585 ^{o}C. The high thermal

stability could also be attributed to the long molecular chain and high molecular weight as well as the benzene rings connected by the sulfonyl group on the PES structure (Wang et al., 2011a).

(ii) PES/chitosan/PA membranes

Figure 5.5 (b) represents thermal stability of the PES/chitosan/PA membranes, these are PES membranes infused with chitosan and coated with polyamide layer. The chitosan used had various degree of deacetylation. Huge membrane loss was observed between 600 and 700 ^{o}C for all membrane, whereby the graphs were observed to have shifted towards the left when chitosan's degree of deacetylation was increasing. Membranes infused with chitosan having high degree of deacetylation showed to be less thermally stable than those with low degree of deacetylation. Unlike with PES, whereby no chemical interaction of chitosan's functional group and PES structure took place, the amine groups on the chitosan molecule interacted with unreacted acylchloride group of the PA active layer's unreacted to form thin layer on the membrane surface. In the case of PES/chitosan membranes, more heat was needed when chitosan's degree of deacetylation was high in order to decompose the expose D-glucosamine and N-glucosamine. However, when polyamide layer was coated (PES/chitosan/PA membranes), the D-glucosamine and N-glucosamine reacted with the acylchloride. Hence membranes modified with chitosan having low degree of deacetylation appeared to be more thermally stable. Feng et al. (2016) reported polyamide-based membrane loss before 330 and 450 ^{o}C. Thermally stability of PES support and the interaction of chitosan's D-glucosamine and N-glucosamine with the acylchloride of the polyamide layer showed to have improve the thermal stability of the membranes in this study.

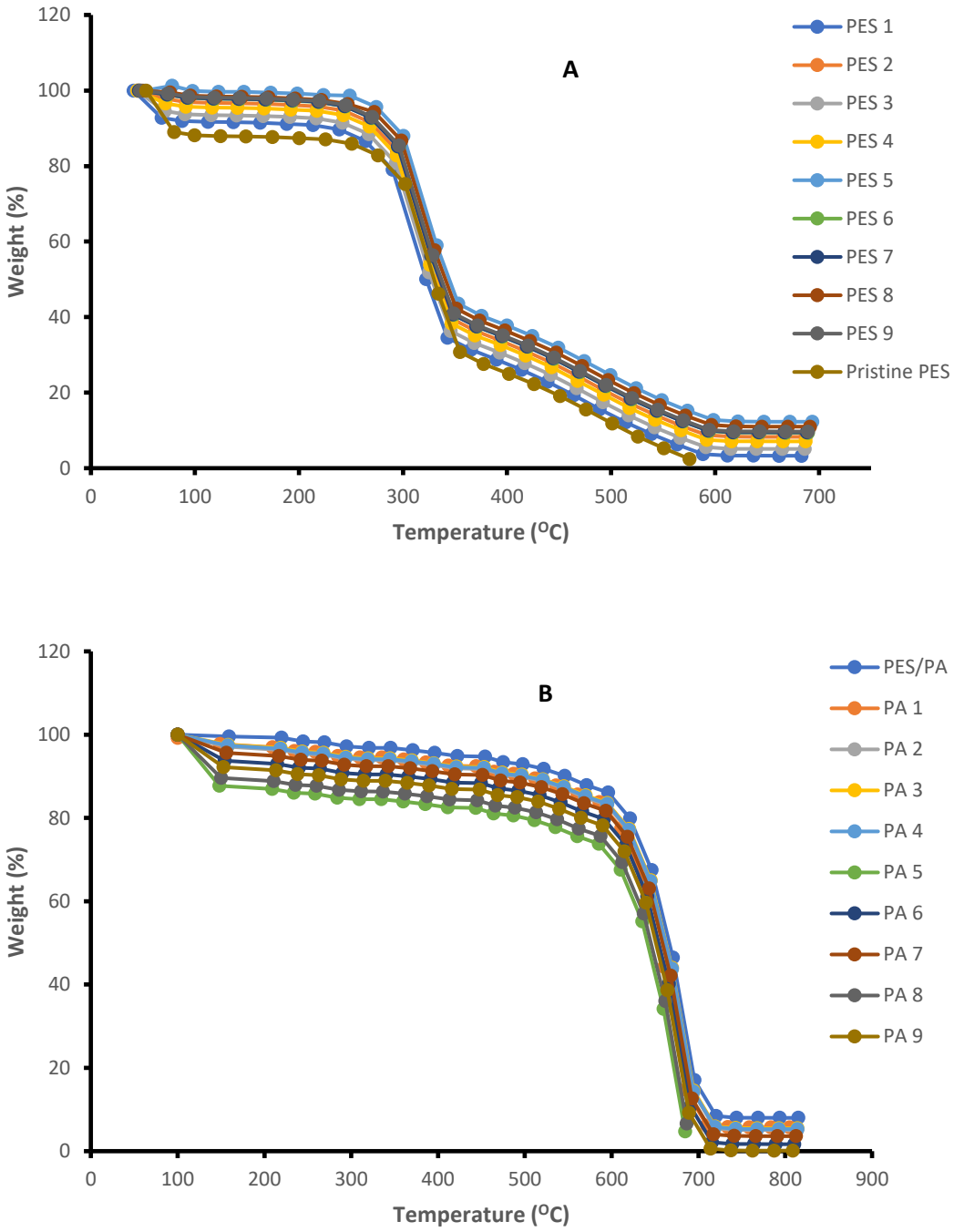


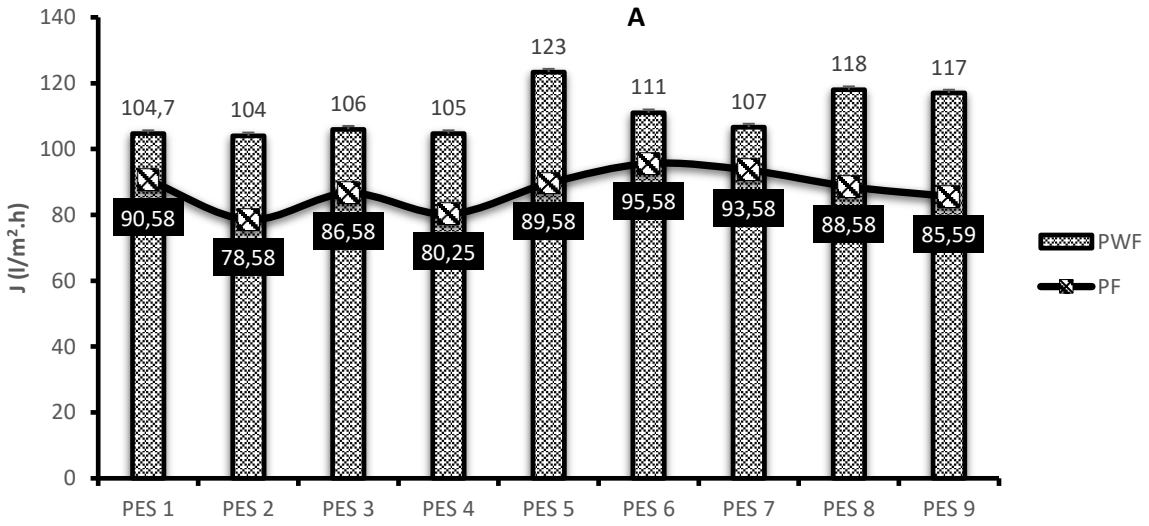
Figure 5.5: Thermal stability of the synthesised (a) PES/chitosan and (b) PES/chitosan/PA membranes

4.5.2 Evaluation of membrane performance

5.5.2.1 Membrane flux

Membrane performance evaluation was conducted as described in Chapter 3. Figure 5.6 (a) and (b) presents original water flux or pure water flux (PWF) and flux of permeate AMD (PF) solutions for the synthesised nine PES/chitosan membranes and nine PES/chitosan/PA membranes, respectively. The membranes were pre-pressed with deionized water for 4 hours to obtain a steady flux before commencing with actual flux determination. This was necessary to ensure complete immersion of water in the membranes before analyses. The highest PWF of PES/chitosan and PES/chitosan/PA membranes was measured as 123 L/m^2.hr (PES 5) and 66 L/m^2.hr (PA 5), respectively. The lowest was measured as 104 L/m^2.hr (PES 1) and 36 (PA 1) L/m^2.hr for PES/chitosan and PES/chitosan/PA membranes, respectively. Observing the FTIR spectra of the membranes reported on Figure 5.3, they all had similar surface chemistry, however, the PWF results varies. This variation could be attributed to the difference in degree of deacetylation of chitosan samples (Table 5.2) used in the blend to synthesis the membranes. The membranes synthesised in this Chapter where infused with 0.75 wt% chitosan having different degree of deacetylation. Membranes synthesised in Chapter 4 were infused with chitosan produced with the same conditions as sample 8 in this Chapter (Table 5.2). The membranes in Chapter 4 measured PWF of 105 and 66 L/m^2.hr for PES/chitosan and PES/chitosan/PA membranes, respectively. PES 8 and PA 8 in this Chapter which had similar chitosan content and degree of deacetylation had PWF reported as 118 and 59 L/m^2.hr. Membranes infused with chitosan having the highest degree of deacetylation reported high PWF and those with low degree of deacetylation reported low PWF. High degree of deacetylation implies large number of amines groups exposed after the deacetylation process. Th high PWF with high degree of deacetylation was attributed to the number of amines groups

which favoured sorption of water molecules inside the membrane matrix in the case of PES/chitosan membranes. In the case of PES/chitosan/PA membranes it was due to the interaction of chitosan's amine group and PA active layer's unreacted acylchloride group which created a thin layer on the membrane surface. Additional chitosan's amine groups which could not interact with unreacted acylchloride groups favoured sorption of water molecules by the membrane (Xu et al., 2015). Moreover, contact angle and porosity results presented in Figure 5.4 corroborated that hydrophilic nature of the membranes and porosity had a positive impact on the membranes PWF. Membranes with high degree of hydrophilicity and porosity reported high PWF.



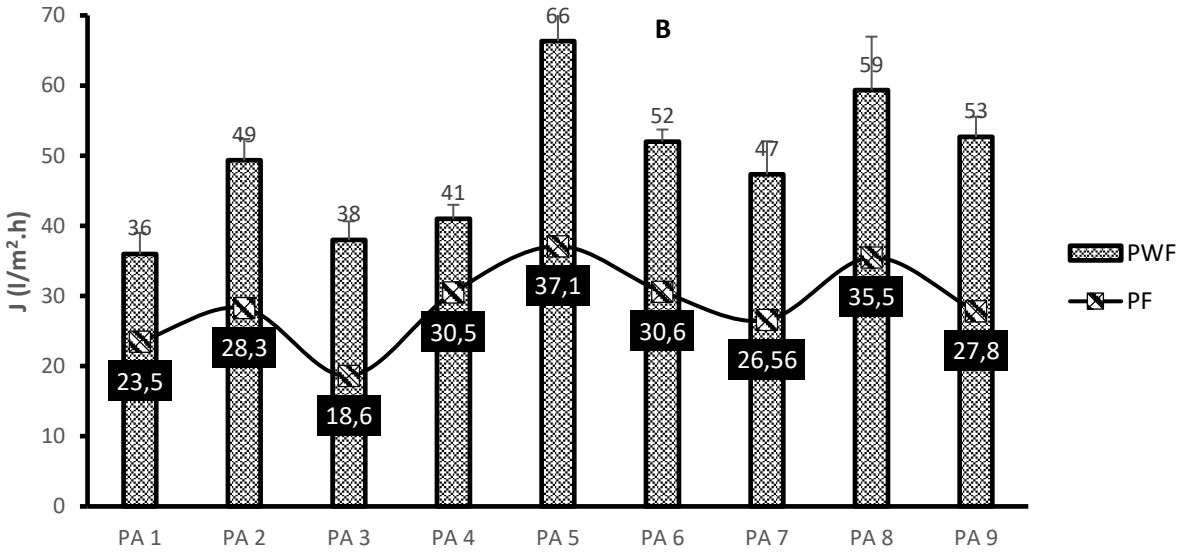


Figure 5.6: Membrane flux of (a) PES/chitosan membranes and (b) PES/chitosan/PA membranes

5.5.2.2 Membrane rejection during AMD treatment

Figure 5.7 and 5.8 illustrate the rejection of ions by the synthesised PES/chitosan and PES/chitosan/PA membranes using dead-end filtration setup described in Chapter 3. Three runs were conducted, and the rejection was averaged. Rejection of each run is contained in Appendix C1 and C2 for PES/chitosan and PES/chitosan/PA membranes, respectively. The pH of the AMD was fixed at 3.2 using 0.1 M sulphuric acid. All the membranes had similar chitosan content loading of 0.75wt%, however, the chitosan samples had different degree of deacetylation which were obtained using different synthesis conditions (Table 3.1). High degree of deacetylation signifies large number of amine group exposed during the deacetylation process. It is expected that membrane rejection will increase with increasing chitosan's degree of deacetylation due to the high number of amine groups playing important role during rejection. The general observed trend for all the contaminants was that, there is an increase in rejection with increasing degree of deacetylation. This observation is consistent with literature because increasing number of functional groups enhances membrane rejection capacity

(Akbari et al., 2015). This was affirmed by PES 1 and PA 1 which were infused with chitosan having the lowest degree of deacetylation reporting low rejection for all metal and sulphate ions. Additionally, PES 5 and PA 5 with the highest degree of deacetylation of 96% had the highest rejections. Membranes infused with chitosan and coated with polyamide layer showed even more enhanced rejection as compared to the uncoated membranes. This was attributed to combination of the electrostatic repulsion and/or attraction of the positively charged membranes generated by the protonation of the amine and amino groups in acidic medium and the Donnan exclusion phenomenon (Gonzalez et al., 2008). Polyamide membranes are characterised with small effective pore sizes and this contributed to the sieving affinity of the membrane (Ji et al., 2019).

Without measuring the surface charge of the membranes, studies have shown that polymeric membranes are usually positively and negatively charged at lower and higher pH solutions respectively (Tanninen et al., 2002). The pH of the feed used in this test was 3.2. Consequently, the higher rejection of cations (Mn^{2+}, Fe^{2+}, Mg^{2+} and Ca^{2+}) as compared to anions (SO_4^{2-}) could be attributed to the strong repulsive forces dominance between the positively charged membranes and the metal ions. High degree of deacetylation signifies more amine groups exposed during the deacetylation process which becomes potential binding sites. As the amine groups gets protonated, the repulsion and attraction forces will be stronger compared to the membranes having chitosan with low degree of deacetylation. PES 5 with chitosan having the highest degree of deacetylation (96%) reported maximum rejection of 98, 97, 96, 95 and 80% for Mn^{2+}, Fe^{2+}, Mg^{2+} and Ca^{2+} and SO_4^{2-}, respectively. PES 1 with chitosan having the lowest degree of deacetylation had poor rejection for Mn^{2+}, Fe^{2+}, Mg^{2+} and Ca^{2+} and SO_4^{2-}at 70, 64, 60, 57 and 46%, respectively. Comparably, PA 5 reported maximum rejection of 98, 90, 88, 87 and 84% for Mn^{2+}, Fe^{2+}, Mg^{2+} and Ca^{2+} and SO_4^{2-}, respectively. While PA 1 had 76, 62, 61, 57 and 50% rejection for Mn^{2+}, Fe^{2+}, Mg^{2+}, Ca^{2+} and SO_4^{2-}, respectively. The slight difference

in rejection between the PES and PA membrane could be affirmed by the high flux of PES membrane reported in Figure 5.6 which would push ions retained on the membrane surface. The general observed rejection percentage trend is Mn^{2+} > Fe^{2+} > Mg^{2+} > Ca^{2+} >SO_4^{2-}, respectively. The higher rejection of Fe^{2+} in comparison to Mg^{2+} could be argued by what Mthethwa (2014) had observed. This could be attributed to the fact that Fe^{2+}tend to form stable chitosan-metal complex compared to Mg^{2+} and Mn^{2+}

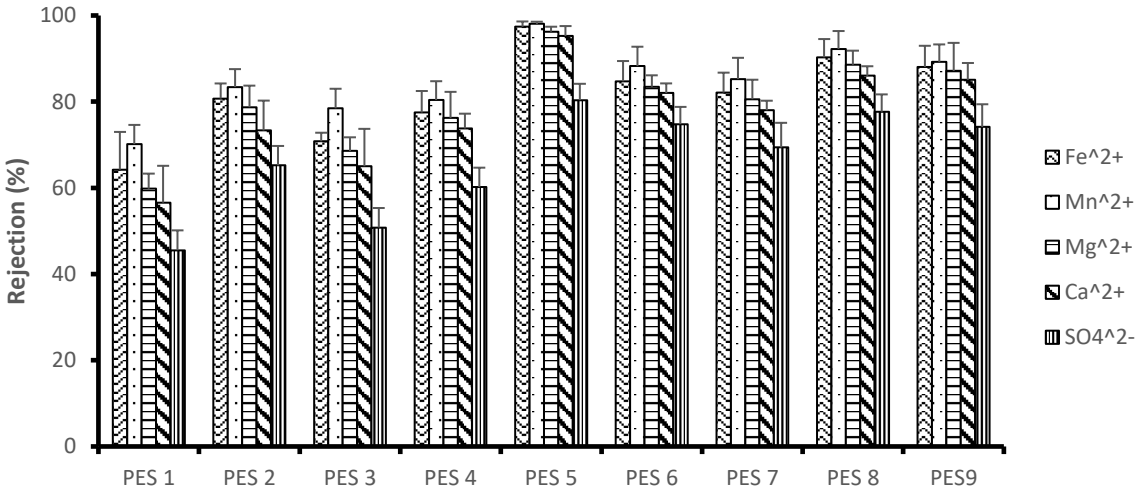


Figure 5.7: Rejection (%) of metal and sulphates ions using PES/chitosan membranes

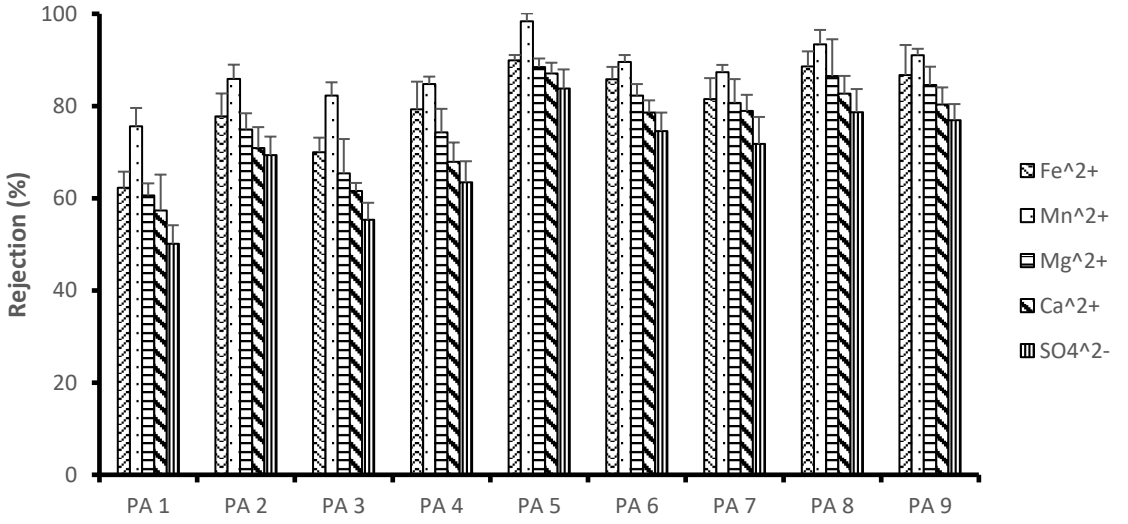


Figure 5.8: Rejection (%) of metal and sulphates ions using PES/chitosan membranes coated with polyamide layer (PES/chitosan/PA membranes)

5.5.2.3 Effect of feed pH on membrane rejection

The previous membrane performance evaluation showed that membranes infused with sample 5 chitosan, which had the highest degree of deacetylation of 96% was suitable as it produced satisfactory results. Feed pH is very important during membrane operation because it influences membrane charge and solution chemistry. Membranes to evaluate the effect of pH were synthesised with chitosan having degree of deacetylation of 96%. Chitosan was loaded at 0.75 wt% to synthesis PES/chitosan membrane and polyamide layer was coated on top to produce PES/chitosan/PA membrane, respectively. AMD feed solution containing Fe^{2+} (933 mg/L), Ca^{2+} (461 mg/L), Mg^{2+} (345 mg/L), Mn^{2+}(321 mg/L) and SO_4^{2-} (4556 mg/L) was prepared at various pH (2.4, 3.5, 4.7, 5.5, 6.8 and 8.6) using Sulphuric acid and Sodium hydroxide. The AMD was filtered through a dead-end filtration setup and the permeate was analysed for metal and sulphate ions content and rejection was calculated using Equation 3.6. Three runs were conducted, and the rejection of each run is presented in Appendix C3 and C4 for PES/chitosan and PES/chitosan/PA membranes, respectively. Figure 4.9 (a) and (b) illustrate the effect of pH on the performance of the PES/chitosan and PES/chitosan/PA membranes, respectively. Figure 5.9 illustrate the effect of feed pH on the rejection of Mn^{2+}, Fe^{2+}, Mg^{2+}, Ca^{2+} and SO_4^{2-}.

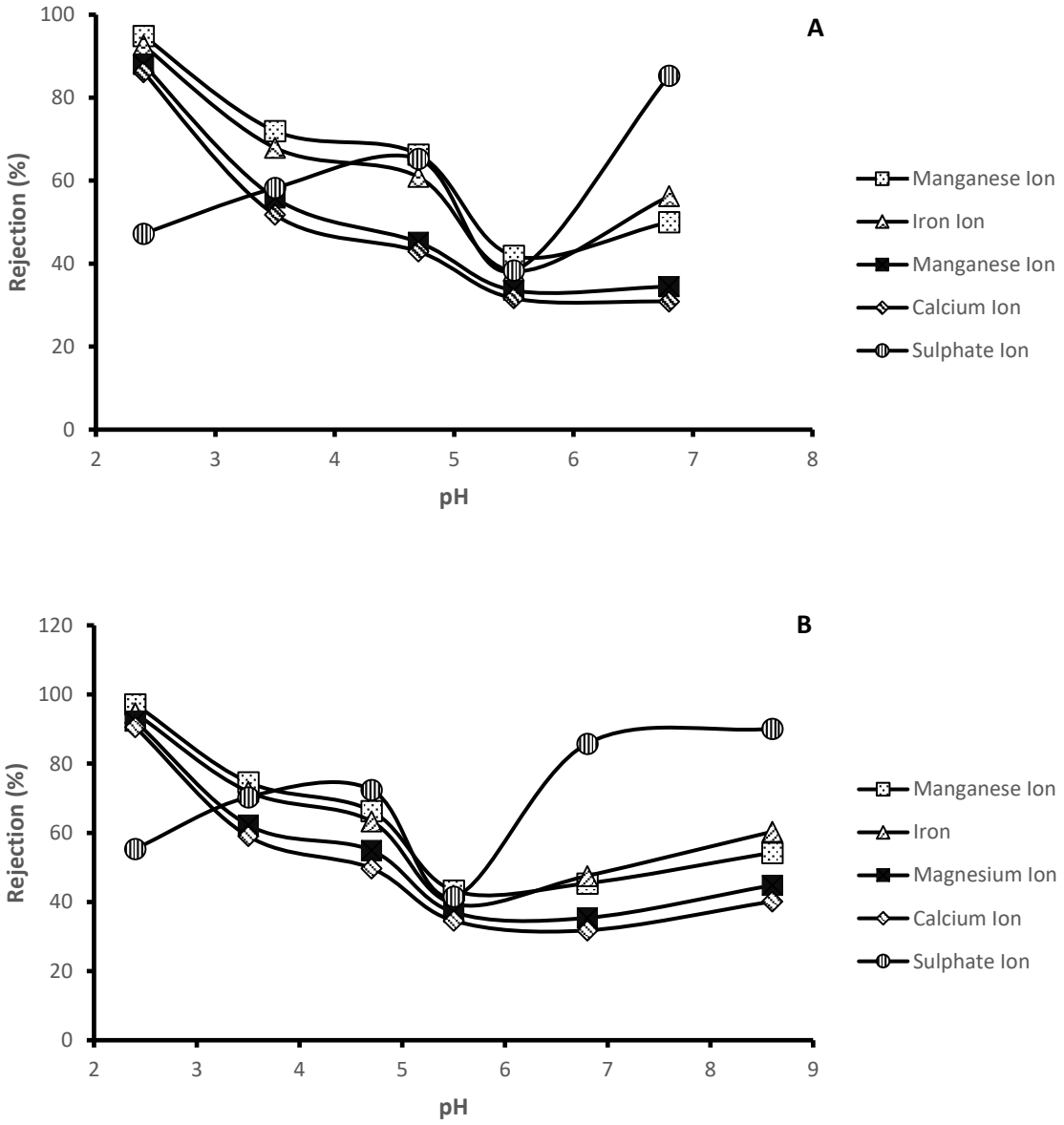


Figure 5.9: Effect feed pH on rejection efficiency of (a) PES/chitosan and (b) PES/chitosan/PA membranes

The rejection of the ions decreases to its lowest at pH values of around 5.7 and picks up again when pH increases. This behaviour could be attributed to the isoelectric point (IEP) or zero potential charge effect within a certain pH range of the membrane. Charge density of a membrane depends on various functional groups on its surface, chemical structure of the membrane due to dissociation of the functional groups and migration of charged solutes from solution on to the membrane surface (Akbari et al., 2015; Gherasim et al., 2013). Literature has

shown that pH values corresponding to a peak in flux reporting the lowest rejection of ions by a membrane indicates the IEP or zero potential charge of the membrane (Mthethwa et al., 2014). Lowest rejection and peak in flux for both PES/chitosan and PES/chitosan/PA membranes are reported at pH values between 5 and 6. In comparison with literature, Mthethwa (2014) reported IEP of PES membrane to be around pH value of 5.04 during the treatment of acid mine drainage. Gherasim et al. (2013) observed an IEP of an AFC 80 Nanofiltration membrane to be a pH of about 5.7 when exposed to $Pb(NO_3)_2$ solution. AFC 80 is a thin-film composite membrane consisting of a polyamide skin-layer on top of polysulphone support supplied by PCI membrane systems. FTIR spectra of PES/chitosan membranes reported that the PES membranes infused with chitosan attributed to the properties of PES basic structure (Chapter 4, section 4.4.13 and Chapter 5, section 5.5.1.1). It can be concluded that the IEP of PES/chitosan and PES/chitosan membranes is around pH of 5.5. It can further be concluded that the surface charge of both PES/chitosan and PES/chitosan/PA membranes becomes positive at pH lower than 5.5 and at pH above 5.5 have negative charge.

Maximum rejection of the cations (Mn^{2+}, Fe^{2+}, Mg^{2+} and Ca^{2+}) by PES/chitosan membrane (Figure 4.9 (a)) was experience at the pH of 2.4 reporting rejection of 95, 93, 88 and 86%, respectively. The cation removal mechanism could be attributed to the strong repulsive forces formed between the positively charged membrane due to the protonation of the chitosan amine groups and the cations. In acidic solutions, the amine groups on the chitosan structure attract protons to form quaternary amine groups which turn the membrane to be more positive. Raising the pH to 3.5 and 4.7 induced a slight decline in cation rejection. This could be attributed to the fact that raising the pH triggers a decline in amine protonation due to limited number of H^+ and thus reduces strength of repulsion forces. Cations rejection is high when pH < IEP compared to when lower. This behaviour can be explained by the fact that metal ions tends to form complexes with OH^- and/or exist as metal oxides and precipitates at high pH and be

removed through sieving. The point of zero charge was assumed to be around pH of 5.5, meaning the membrane is neither positive nor negative. As such, rejection mode at this point was due to sieving potential of the membrane hence it reported the lowest rejection of the ions regardless of their charge.

In the case of anions, high rejection of sulphate ions was observed at pH > IEP. This could be attributed to the repulsive forces between the negatively charged membrane and the anions. Maximum rejection of the sulphates was reported as 85% at pH 6.8. At high pH, the number of protonated $-NH_2$ groups diminishes and more OH^- is formed and tends to compete with anions. Raising the pH from 6.8 to 8.6 induced anions rejection decline and this was due to the excess OH^- competing with anions and increased strength of repulsive forces created by the negatively charged membrane. Sulphate ions rejection was poor when pH< IEP compared to when pH >IEP. This could be explained by the fact that according to Donnan exclusion and electrostatic repulsive theories, when a membrane is positively charged, some SO_4^{2-} are retained on the membrane surface and form a layer and the rest will pass through easily. This causes low sulphate rejection and low flux (Ji et al., 2019).

The rejection of ions by PES/chitosan/PA membrane is illustrated in Figure 5.9(b). Coating polyamide layer onto the PES/chitosan membrane to produce PES/chitosan/PA membrane provided amide, amines, carboxylic and alcoholic functional groups onto the membrane surface. Chitosan infused within PES membrane will provide amine groups inside the membrane matrix. During membrane rejection process, partial hydrolysis of polyamide leads to formation of ammonium ($-NH_3^+$) and carboxyl (-COOH) groups. Thus at , pH > IEP the carboxyl groups are dissociated, and the membrane become negatively charged. No protonation of the amine groups takes place. At pH > IEP, cation removal will be due to the ionic interaction of the metal ions and the negatively charged membrane, whereas, sulphates will be repelled. In contrast, at pH < IEP, carboxyl groups are un-dissociated, and the amine groups are protonated,

and the membrane becomes positively charged (Gherasim et al., 2013). Rejection of ions by PES/chitosan/PA membrane was slightly higher than that of PES/chitosan membrane and this could be attributed to increased number of available functional groups after coating PES/chitosan with polyamide layer.

Comparing the rejection of the cations (Mn^{2+}, Fe^{2+}, Mg^{2+} and Ca^{2+}), it is important to mention that the metals were treated simultaneously, not separately. Therefore, the interaction amongst the metals can influence the rejection efficiency. Hydroxides of Mn^{2+}, Fe^{2+}, Mg^{2+} and Ca^{2+}) are reported in literal data to precipitates at 9.0 to 9.5, 5.5 to 8.5, >9 and >10 (Balintova and Petrilakova, 2011; Stratful et al., 2001). When the pH was greater than the IEP, Fe^{2+} reported high rejection compared to other metal complexes. This is affirmed by the view that it started to form hydroxides at lower pH of 5.5. It was followed by Mn^{2+} due to the fact that Mn^{2+} will simultaneously precipitate with Fe^{2+} at pH of 8, provided the concentration of Fe^{2+} is much greater than that of Mn^{2+} (Balintova and Petrilakova,2011). The feed solution used in these tests had Fe^{2+} at 933 mg/L and Mn^{2+} at 321 mg/L.

5.5.2.4 Effect of feed pH on membrane flux

The effect of pH on membrane flux was investigated following similar procedure mentioned above. Similarly, the membranes used to evaluate the effect of feed pH on permeate flux were synthesised with chitosan having degree of deacetylation of 96%. Chitosan was loaded at 0.75 wt% to synthesis PES/chitosan membrane and polyamide layer was coated on top to produce PES/chitosan/PA membrane, respectively. Figure 5.10 illustrate the effect of feed pH on membrane flux. Flux was carried 3 times and the fluxes of each run are presented in Appendix C5 and C6 for PES/chitosan and PES/chitosan/PA membranes, respectively. It is worth

mentioning that after the membrane was fixed, it was pre-pressed with deionized water to obtain steady original flux before filtering AMD through.

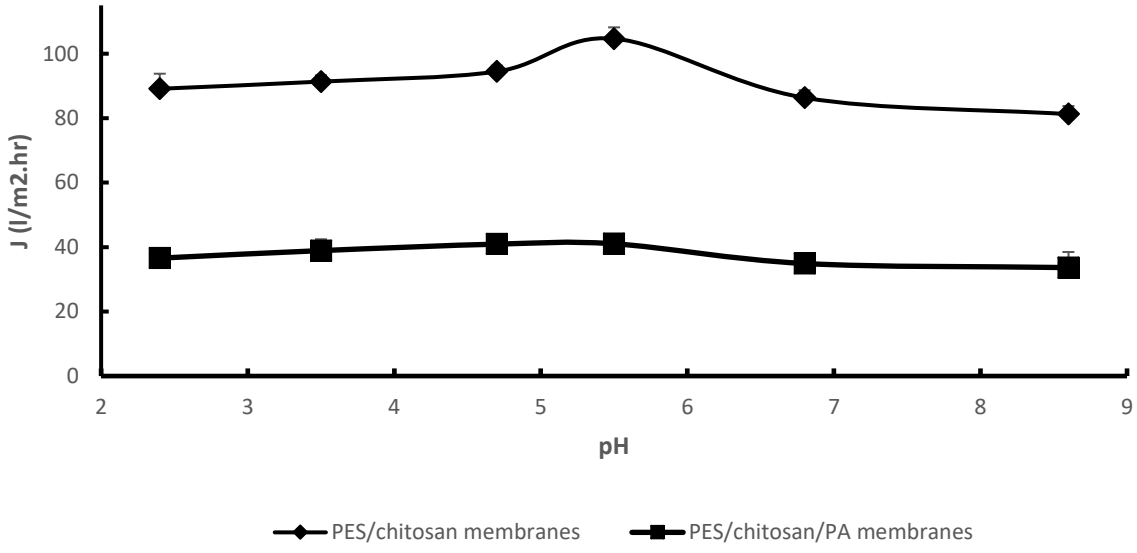


Figure 5.10: Effect feed pH on AMD permeate flux of PES/chitosan and PES/chitosan membrane.

It can be observed from Figure 5.10 that the permeate flux is affected by the feed pH for both PES/chitosan and PES/chitosan/PA membranes. The permeate flux increases slightly with increasing pH from 2.4, 3.5 and 4.7. The highest flux was recorded as 104.5 and 41 L/m^2.hr for PES/chitosan and PES/chitosan/PA membranes when the pH is raised to 5.5. This behaviour could be attributed and aggregated with the observations made in Figure 5.9. Figure 5.9 showed the lowest rejection of ions was at pH 5.5. As reported in literature, high permeate flux rates are associated with strong forces on the membrane surface wall which prevents accumulation of ions and formation of gel layer on the membrane surface (Cheng and Lin, 2004). This behaviour is best described by Childress et al. (2000). The authors argued, it can be determined by several mechanisms such as membrane size modification, osmotic pressure gradient and electro-viscous effect. When membrane is charged, the charged groups found on the membrane material assume an extended configuration due to electrostatic repulsive forces between them

(like charges repel each other). Thus, causes the membrane pore sizes to diminish and subsequently decreases permeate flux and increase rejection (Gherasim et al., 2013). It's already alluded that PES/chitosan and PES/chitosan/PA membranes are uncharged at pH 5.5 (IEP) and their positive charge increase with decreasing pH for pH > IEP and becomes negative for pH < IEP. When pH < IEP, the electrostatic repulsion of the protonated amino groups gradually increases with decreasing pH and causes reduction in permeate flux and increased rejection. Hence, as it can be observed from Figure 5.9 and 5.10 permeate flux was decreasing and rejection was increasing with declining pH. The electrostatic viscous effect is observed when an electrolyte passes through a charged surface pore. At pH< IEP>pH, the pore sizes reduce due to electrostatic repulsion and attractive forces and the permeate solution will exhibit reduced viscosity and therefore, will have high flux as compared to uncharged pores when the membrane is at isoelectric point. Lastly, osmotic pressure near the membrane surface increases at low pH due to retention of ions on the membranes surface. Increase in osmotic pressure will determine a decrease in net driving pressure and thus leads to reduce permeate flux at low pH.

5.5.2.4 Effect of feed pressure and feed concentration

Investigating the effect of initial feed concentration and pressure is very essential in order to assess the applicability range and determine optimum conditions for an efficient membrane separation operation. In order to study the influence of these variables, rejection tests were conducted on a dead-end setup using synthetic AMD. Feed solutions with various concentrations at were filtered through the dead-end setup at different feed pressures. The feed pH was fixed at 5.5 for all the tests using sulphuric acid and sodium hydroxide. Table 5.4 presents the feed composition. The pressure was increased from 1 to 4 bars. Figure 5.11 illustrate the permeated fluxes of solutions with different metals concentrations. Three tests

were conducted, and the results of each run are contained in Appendix C7 and C8. For easy of identification, the name of the run number will be used to refer to the sample containing corresponding feed composition as depicted in Table 5.4.

Table: 5.4: Feed composition to investigate effect of feed pressure and initial concentration

Runs	**Feed composition**				
	SO_4^{2-} (mg/L)	Fe^{2+} (mg/L)	Ca^{2+} (mg/L)	Mg^{2+} (mg/L)	Mn^{2+} (mg/L)
Run 1	4556	933	461	345	321
Run 2	1139	233	115	86	80
Run 3	1518	311	154	115	107
Run 4	2278	467	231	173	161

The measured permeated flux for solutions with different concentrations against feed pressure is presented in Figure 5.11 (a) and (b) for PES/chitosan and PES/chitosan/PA membranes, respectively. The permeated flux with different concentrations had huge differences at low pressure of 1 bar with Run 1 (75 L/m^2.hr) and Run 4 (44 L/m^2.hr) having significant variation of 31.23 L/m^2.hr for PES/chitosan/PA membrane. As the pressure increases to the highest pressure of 4 bar, the gap between the permeated fluxes of different concentration narrows with Run 1 and Run 4 having 14 L/m^2.hr gap apart. In the case of PES/chitosan/PA membranes at 1 bar, Run 1 had flux of 33 L/m^2.hr and Run 4 was 21 L/m^2.hr. When the pressure was raised at 4 bars, then Run 1 reached flux of 49 L/m^2.hr and 41 L/m^2.hr for Run, respectively. The general trend observed was that, the flux increases with increasing pressure. This is attributed to the increase forces which forces water molecules through the membrane as the pressure increases. Moreover, solutions with low concentration reported high permeated flux due to low number

of ions being trapped on the membrane surface and subsequently blocking the pores and forming a layer obstructing flow. At high concentrations, more ions are trapped on the membrane surface and within the pores, thereby forming a layer which leads to concentration polarisation. Maximum permeated fluxes were observed at high pressure of 4 bar for both PES/chitosan and PES/chitosan/PA membranes, respectively.

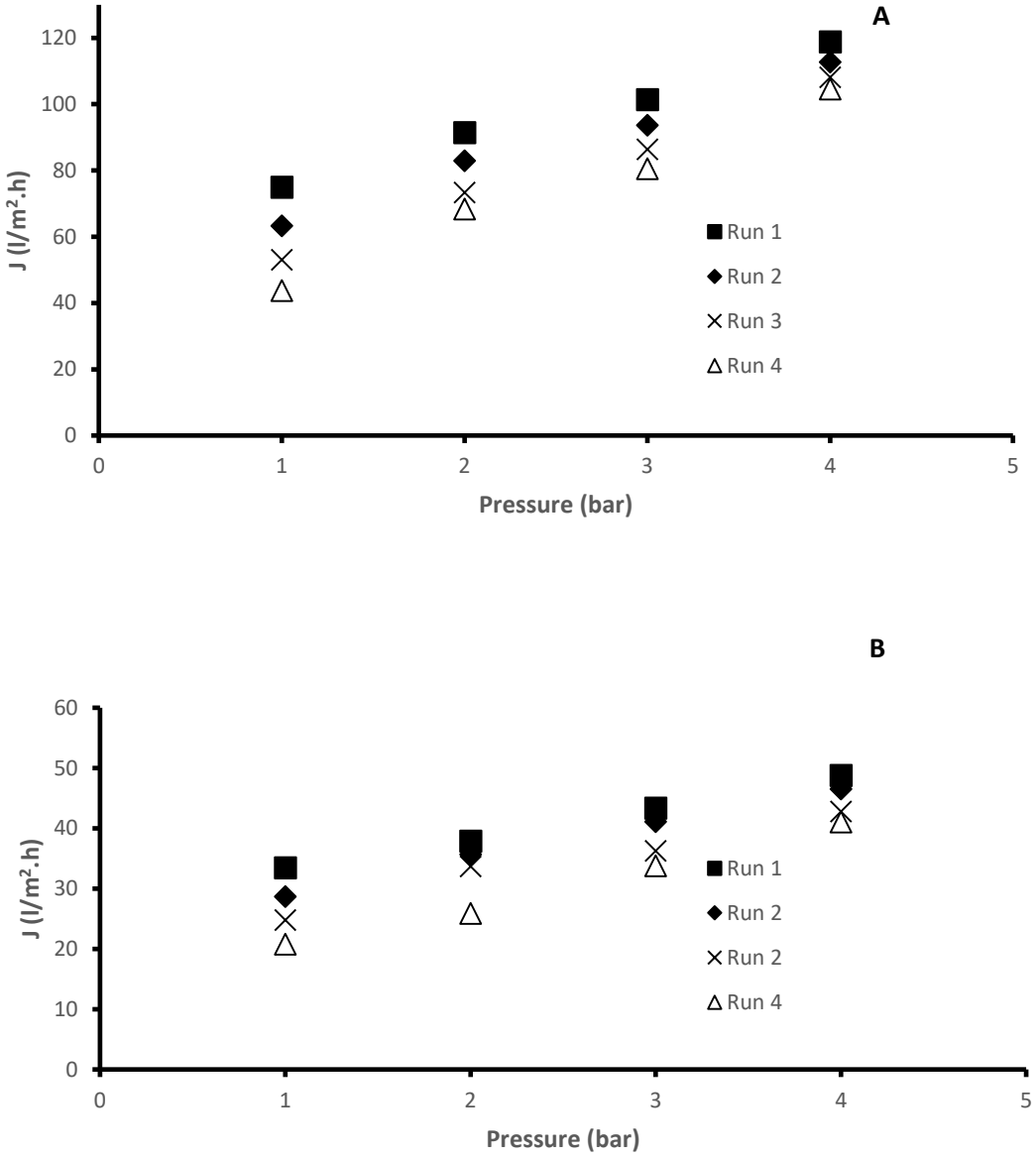
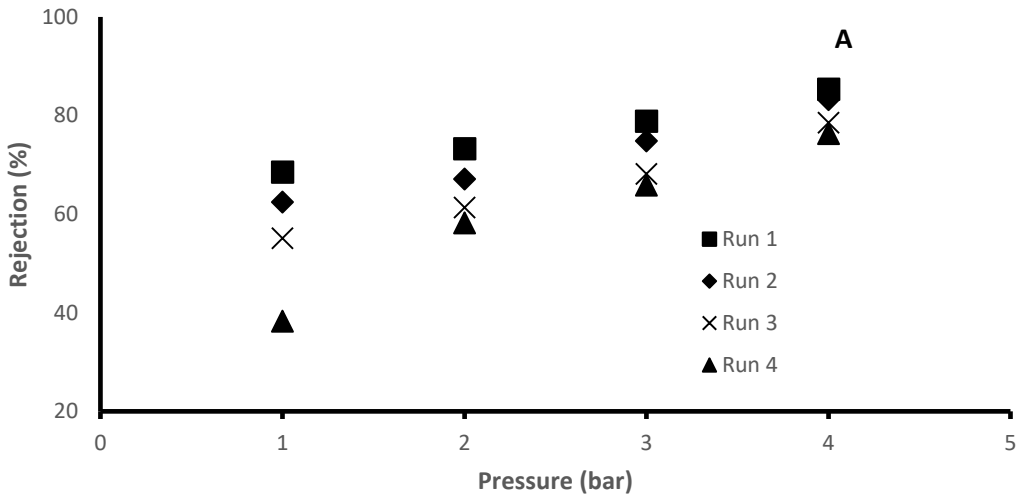


Figure 5.11: Fluxes versus feed pressure for solutions with various concentrations for (a) PES/chitosan and (b) PES/chitosan/PA membranes.

Figure 5.12 and Figure 5.13 illustrate the influence of feed pressure on the rejection of Fe^{2+} and SO_4^{2-} solutions by PES/chitosan and PES/chitosan/PA membranes, respectively. The rest of the feed constituencies are contained in the Appendix C7 and C8 for PES/chitosan and PES/chitosan/PA membranes, respectively. The general observed trend is that rejection by both PES/chitosan and PES/chitosan/PA membrane is increasing with increasing pressure for both Fe^{2+} and SO_4^{2-} solutions. Additionally, rejection significantly reduces with increasing initial ions concentrations. Gherasim et al. (2015) and Gherasim et al. (2013) describe the two competitive phenomena governing the pressure effect during membranes separation for a charged membrane. Firstly, the authors argue that increasing pressure of the feed solution will result in transportation of more solute ions towards the membrane surface, which will consequently result in increased concentration polarisation. Thus, cause a decline in permeated flux and rejection as the solute transfer through the membrane will increase. Hence its observed that with increasing initial concentration, the rejection efficiency reduces.

Secondly, increasing feed pressure leads to increased solvent flux but hindered ions transportation due to steric hindrance effect between the ions (negative or positive) and the uncharged membrane. Charged membranes would lead to a different behaviour as a result of electrostatic repulsion and attraction forces. The concurrent occurrence of these two phenomena will determine rejection behaviour under different feed pressures. As previously alluded, tests to investigate the effect of feed pressure on the membrane rejection were conducted with pH of 5.5, which has proven to be a point of zero charge for both PES/chitosan and PES/chitosan/PA membranes. Therefore, rejection of ions could be attributed to steric hindrance effect. Gherasim et al. (2013) investigated the effect of pressure on the rejection of $Pb(NO_3)_2$ having different concentration by polyamide NF membrane (AFC 80). The effect of pressure tests was conducted at an isoelectric point (pH 5.7) and it was found that the Pb^{2+} rejection increased with increasing feed pressure but reduced when the initial concentration

was increasing. The increase in feed pressure resulted in increased permeated flux. However, the Pb^{2+} was sterically retained (not electrically because the membrane was uncharged) and therefore results in higher rejection. Figure 5.12 and 5.13 reported similar observations were large solvent was permeated through the membrane at high pressure, but the ions were sterically retained leading to higher rejections. Gherasim et al. (2015) investigated the effect of polyamide NF membrane (AFC 40) rejection of Co^{2+} rejection using a negatively charged membrane at pH 5. The AFC 40 had isoelectric point at pH 4.1. Contrary behaviour was observed, whereby, Co^{2+} rejection and permeated flux increased with increasing initial metal concentration. The reduced rejection at high pressure was due to the concentration polarisation which contributed to decreasing the charge effect of the membrane.



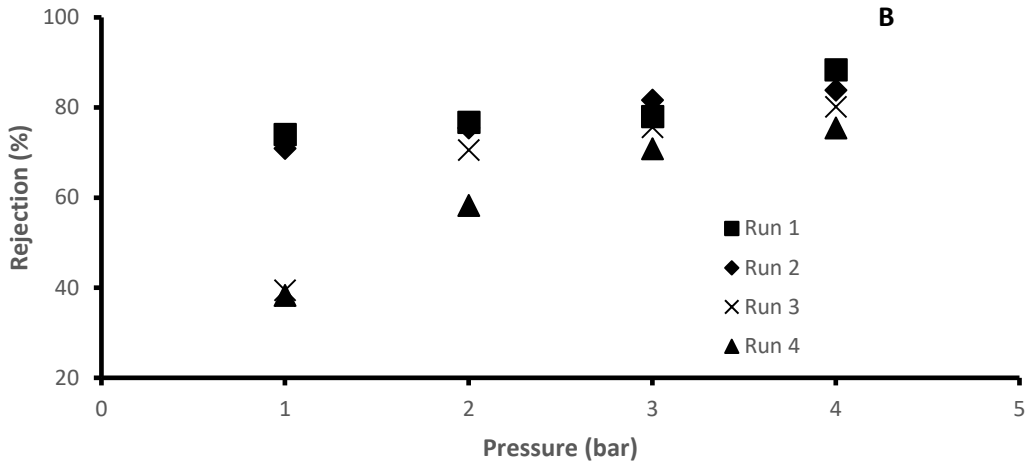


Figure 5.12: The effect of feed pressure on the rejection of iron (Fe^{2+}) solution on (a) PES/chitosan and (b) PES/chitosan/PA membranes.

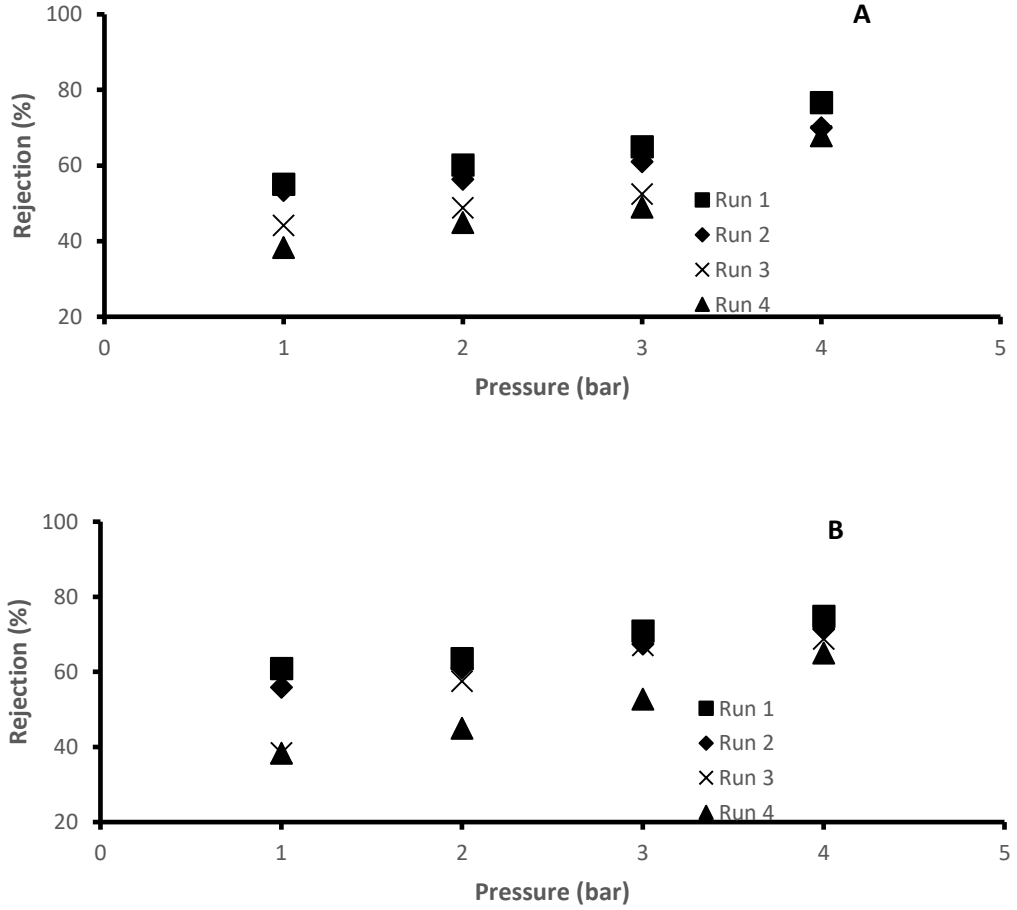


Figure 5.13: The effect of feed pressure on the rejection of sulphates (SO_4^{2+}) solution on (a) PES/chitosan and (b) PES/chitosan/PA membranes.

5.6 Summary

When chitosan is used to modify polymeric membranes for metal ion removal from solution, it's expected that high number of available amino groups on the chitosan structure should translate into more effective sorption capacity. Chitosan's degree of deacetylation gives an indication of available free amino groups in the polysaccharide which could act as potential binding sites for contaminants. However, the influence of chitosan's degree of deacetylation on the effectiveness of metal ion binding during AMD treatment is non-existent in literature. This Chapter provides information on using chitosan with various degree of deacetylation to modify PES and PES/PA membrane and evaluated for AMD treatment.

Nine chitosan samples were synthesised by manipulating NaOH concentration and synthesis temperature and fixing the reaction time to 6 hours. It was observed that DD increased when the strength of NaOH concentration was increased from 20% to 40%. However, when it was further raised to 60 % it triggered reduction in DD of chitosan. The DD increased when the temperature was increased from 80 to 100 ^{o}C and increasing temperature to 120 ^{o}C caused a decline in DD. Based on this behaviour, it can be argued that at above 100 ^{o}C, chitosan sample started to degrade and destroying the already formed or exposed amine groups, thus reducing the DD of the chitosan sample. The chitosan with the highest degree of deacetylation of 96% was reported with 40% NaOH concentration and temperature of 100 ^{o}C.

The synthesised chitosan samples were characterised with FTIR, to confirm success in synthesis of chitosan from chitin and to determine the degree of deacetylation. FTIR spectra of the nine samples indicated success in synthesis chitosan from chitin. Studies in literature revealed FTIR spectroscopies of chitosan samples having similar characteristic peaks obtained in this study. (Yong Soon et al., 2017; Teil and Sheikh, 2012; Kumari et al., 2017).

Percentage yield was determined to understand the efficiency of the synthesis process and conditions in terms of chitosan quantity which was obtained. The percentage yield was low for all nine samples and the removal of minerals and proteins from chitin via demineralization and deproteinization accounted for this huge percentage mass loss. Percentage yield of chitosan from chitin decreased as the concentration of NaOH and temperature increased, respectively. Higher temperature and NaOH concentration showed to have high capabilities to remove proteins from the chitin structure, thus the low yield was expected. Similar observations were made by Soon et al. (2018) and Srinivasan et al. (2018).

The effect of chitosan's degree of deacetylation on the quality and performance of PES membranes infused with chitosan (PES/chitosan) and coated with polyamide (PES/chitosan/PA) layer during AMD treatment was investigated. Additionally, the effect of feed pH, initial concentration and operating pressure on water flux and rejection performance is also reported. The synthesised membranes infused with chitosan having various DD (PES/chitosan membranes) and then coated with polyamide layer (PES/chitosan/PA membranes) were examined with contact angle to determine the hydrophobicity/hydrophilicity, FTIR to identify functional groups and TGA to confirm thermal stability of the synthesised membranes. FTIR spectra observed were like those in Chapter 4 (section 4.4.1.3). PES 5 and PA 5 where infused with chitosan having the highest degree of deacetylation and both reported the lowest contact angle values of 59^{O} and 44^{O}, respectively. The thermal degradation and stability of the synthesised membranes were checked, and PES/chitosan membranes showed a three-step degradation process observed at 65 ^{o}C, 302 ^{o}C and 350 ^{o}C. In the case of PES/chitosan/PA membranes, significant membrane loss was observed between 600 and 700 ^{o}C for all membrane, whereby the graphs were observed to have shifted towards the left when chitosan's degree of deacetylation was increasing.

The performance evaluation of the membranes was conducted on Dead-End filtration set up by filtering synthetic AMD through. The pure water flux of the membranes showed to be enhanced with increasing degree of deacetylation. Membranes PES and PA were infused with chitosan having the highest degree of deacetylation and both reported high pure water fluxes of 123 L/m^2.hr and 66 L/m^2.hr, respectively. Moreover, PES 1 and PA were infused with chitosan with the lowest degree of deacetylation and both had the least pure water flux of 104 L/m^2.hr and 36 L/m^2.hr, respectively. Similar behaviour was observed for rejection investigations of the membranes. PES 5 and PA 5 reported high rejection and PES 1 and PA 1 the least rejection. PES 5 with chitosan having the highest degree of deacetylation (95.97%) reported maximum rejection of 98, 97, 96, 95 and 80% for Mn^{2+}, Fe^{2+}, Mg^{2+} and Ca^{2+} and SO_4^{2-}, respectively. Comparably, PA 5 reported maximum rejection of 98, 90, 88, 87 and 84% for Mn^{2+}, Fe^{2+}, Mg^{2+} and Ca^{2+} and SO_4^{2-}, respectively.

Feed pH is very important during membrane operation because it influences membrane charge and solution chemistry. Chitosan sample used to synthesis PES 5 and PA 5 membranes had the highest degree of deacetylation and both membranes revealed satisfactory performance compared to others. As such, membranes to evaluate the effect of pH were synthesised with chitosan having degree of deacetylation of 96% loaded at 0.75 wt% to synthesis PES/chitosan membrane and polyamide layer was coated on top to produce PES/chitosan/PA membrane, respectively. Lowest rejection and peak in flux for both PES/chitosan and PES/chitosan/PA membranes were reported at pH values between 5 and 6. It was deduced that the IEP of PES/chitosan and PES/chitosan membranes is around pH of 5.5.

Investigating the effect of initial feed concentration and pressure is very essential in order to assess the applicability range and determine optimum conditions for an efficient membrane separation operation. The general trend observed was that, the flux increases with increasing pressure. This was attributed to the increase forces which forces water molecules through the

membrane as the pressure increases. Moreover, solutions with low concentration reported high permeated flux due to low number of ions being trapped on the membrane surface and subsequently blocking the pores and forming a layer obstructing flow. At high concentrations, more ions are trapped on the membrane surface and within the pores, thereby forming a layer which leads to concentration polarisation.

Chapter 6: Operational stability and antifouling property of the membranes

This Chapter contains the results pertaining to the operational stability and fouling behaviour of the PES/chitosan and PES/chitosan/PA membranes during the treatment of real industrial AMD.

6.1 Introduction

The preliminary investigations on the synthesis, characterization and performance evaluation of PES/chitosan and PES/chitosan/PA membranes provided optimized results which was used to synthesis membranes used in this Chapter. The previous tests used synthetic feed AMD filtered through a dead-end filtration setup. The investigation reported in this Chapter used real industrial AMD as the feed and was filtered through a crossflow filtration system. The reason for using real AMD in this Chapter is because the objective was to understand the operational stability and fouling behaviour of the membranes for AMD in real life situation.

6.2 Membrane synthesis

Firstly, chitosan sample was synthesised from chitin following previously discussed procedures. Then followed by deproteinization step with 6% NaOH solution at 60 ^{o}C ; and demineralization using 6% HCl 60 ^{o}C, both for 2 hours in a 500 mL Erlenmeyer flask. The residual was washed with deionized water until neutral pH. The deproteinized and demineralized chitin was subjected 40% NaOH concentration at 100 ^{o}C for 6 hours. The resultant chitosan sample was washed with deionized water until neutral pH and was dried in an oven.

0.75 wt% chitosan sample was infused with 10 wt% PES suspension in DMSO solvent for 24 hours on a magnetic stirrer to produce a cast gel. The gel was left at ambient conditions to get rid of any air bubbles trapped inside the gel. The gel was cast on a flat glass plate using a hand

casting knife set up at 250 µm thickness. After immersing in deionized water in coagulation the membranes were dried in oven to evaporate any trapped water and/or solvent from the membrane at 60 ^{o}C for 15 minutes. Polyamide layer was fabricated on top following the procedure as discussed in in Chapter 3 (section 3.6.3) to produce PES/chitosan/PA membrane.

6.3 AMD sampling and characterization

Real industrial AMD sample was collected in Randfontein sites in the Western basin of the Witwatersrand region using 5 (5 Liters) polypropylene bottles. At first the sampling bottles were rinsed with the site AMD to ensure consistency between the sampling bottles and the sampling environment. The AMD was transported as it is without preservation because the distance between the sampling point and the laboratory were analysis were carried out was around 40 km reach. Therefore, no oxidation or interference which would change the quality of the AMD was expected. Upon arrival in the laboratory, the AMD samples were filtered using 0.45µm filter paper before analysis were carried out (Figure 6.1).This was necessary to remove any suspended solids. It is worth mentioning that although real AMD contains concoction of both biological and chemicals species, only metal and anions analysis were carried.



Figure 6.1: AMD filtering with 0.45 µm filter paper

6.3.1 Metal analysis

Atomic Absorption Spectrometer (Thermo scientific ICE 3000 series) was used to analyse the metal ions. pH of the AMD was measured on site using Metler Toledo dual meter (Sevenduo pH /conductivity meter with a Metler Toledo inLab Pro ISM pH electrode and inLab 738 ISM conductivity probe). Table 6.1 presents operating conditions of the AAS for the targeted metals. Calibration standard solutions were prepared in volumetric flasks. Appropriate amount of 1000 ppm standard solution was added, and deionized water was topped up to prepare various calibration standard solutions. Equation 6.1 and 6.2 was used to determine how much volume (V_1) of the 1000 ppm (C_1) standard solution was needed to prepare C_2 concentrations (ppm) in the 100 mL (V_2) flask.

$$C_1V_1 = C_2V_2 \tag{6.1}$$

$$V_1 = \frac{C_2 \times V_2}{C_1} \tag{6.2}$$

Table 6.1: AAS operating parameters

Metal	Lamp Current (mA)	Wavelength (nm)	Flame used
Al	10	309.27	Air/Acetylene/N_2O
Ca	18	422.67	Air/Acetylene
Co	10	240.73	Air/Acetylene
Cu	4	324.75	Air/Acetylene
Fe	15	248.30	Air/Acetylene
Mg	18	285.21	Air/Acetylene
Mn	25	279.50	Air/Acetylene
Na	5	589.00	Air/Acetylene
Ni	5	232.00	Air/Acetylene

- The instrument mode used was flame.
- The Spectrometer used absorbance measurement mode with a bandpass of 0.5nm and it was resampled 3 times
- The fuel flow was at 4.2 L/min and the burner height was 11 mm. The nebuliser update was 4 seconds

6.3.2 Sulphate analysis

The sulphate content inside the AMD was conducted using Uv-Vis spectrophotometer by following the EPA 3754 method. First, a conditioning agent was prepared by adding 300 mL deionized water, 30 mL HCL, 100 mL of 95% ethanol and 75 grams of NaCl in a 250 mL beaker. 50 mL of glycerol was then added to the mixture. 100 mL of diluted AMD (1 ml sample of AMD diluted to a 100 mL flask) added to was added to a 250 mL Erlenmeyer flask. 5 mL

of the already prepared conditioning solution was added to the 250 mL Erlenmeyer flask containing diluted AMD and was stirred. $BaCl_2$ was then added to the mixture while stirring. After few minutes, the stirring was stopped, and the solution was discarded into a cuvette and turbidity was measure for 4 minutes in at interval of 30 seconds. A calibration curve was produced by appropriate dilution of 100 mg/L stock solution of Na_2SO_4.

6.2.3 AMD characteristics from site

The AMD composition from the analysis is presented in Table 6.2.Triplicate analysis was done to ensure consistency. The pH from the field measurement was measured as 2.7.

Table 6.2: AMD composition

Constituencies	**Al^{2+}**	**Ca^{2+}**	**Co^{2+}**	**Cu^{2+}**	**Fe^{2+}**	**Mg^{2+}**	**Mn^{2+}**	**Na^{+}**	**Ni^{2+}**	**SO_4^{2-}**
(mg/L)	0.00	483	0.00	0.00	895	308	195	153	2.8	3680
Std Dev	0.00	2.65	0.00	0.00	4.52	3.95	4.89	1.38	2.57	3.28

6.2.3 Performance evaluation of the synthesised membranes

The crossflow system was first flushed with soapy water to get rid of any dirt trapped inside which could interfere with accuracy and consistency of the system. Thereafter, deionized water was used to thoroughly rinse the system before assembling the membranes in the cells having 125×75mm dimensions (Area = 93.75 cm^2). The module had 3 filtration cells (Figure 6.4) which could be used during operation. Pressure regulating valve having maximum value of 1000 psi is fitted downstream the feeding pump and was used to control pressure. The pressure controlling valve was used to set the desired pressure by throttling the pump discharge. The membranes were compacted at 7 bars for 4 hours using deionized water. Firstly, pure water flux and permeability (using equation 3.7 and 3.8) was determined by varying the pressure

from 0.7 to 6.9 bars, to establish the original properties of the membrane. Then, AMD solution was filtered through to examine the rejection efficiency of the membranes through the crossflow system at different pressures. Flux of the AMD solution was also determined and compared to that of pure water flux. Rejection of the membranes was determined using Equation (3.10). The system was operated at room temperature measured as 26 ^{o}C on the day.



Figure 6.2: An image showing the crossflow system used

6.2.1 Membrane flux and permeability

Figure 6.3 (a) and (b) illustrate the flux of pure water and that of AMD solution collected in the permeate section over a period for PES/chitosan and PES/chitosan/PA membranes, respectively. The flux of the membrane for both pure water and AMD solution was established by noting down the time taken to collect 250 mL of the permeate volume. Both pure water and AMD flux had an increasing relationship with increasing pressure from 0.69 to 6.9 bars for

both PES/chitosan and PES/chitosan/PA membranes, respectively. PES/chitosan membrane and PES/chitosan/PA membrane reported high pure water flux of 146 and 110 L/m^2.hr when the pressure was 6.9 bars. The flux of AMD solution in the permeate at the same pressure reported 104 and 62 L/m^2.hr for PES/chitosan and PES/chitosan/PA membrane, respectively. The reduced flux could be attributed to the reduced water passage created by retaining of contaminants on the membrane surface which leads to concentration polarisation.

Both PWF and AMD flux for PES/chitosan membrane started flattening after pressure of 4.1 bar signifying permeate flux which is stabilising. In comparison to PES/chitosan/PA membrane, the flux of both pure water and AMD solution kept increasing significantly even beyond pressure of 4.1 bars. This behaviour could be attributed to the polyamide layer which added large number of hydrophilic functional groups which facilitates transportation of water molecules through the membrane. PES/chitosan membranes reported higher fluxes than PES/chitosan/PA membrane; this was attributed to the reduced effective pore sizes on the membrane surface after coating polyamide layer which is characterized by small pores. Increasing applied pressure enhances the driving force for permeation which resulted in large volume of water through the membrane. The increased pure water flux for polymeric membranes was attributed to the presence of hydrophilic chitosan and coated polyamide layer.

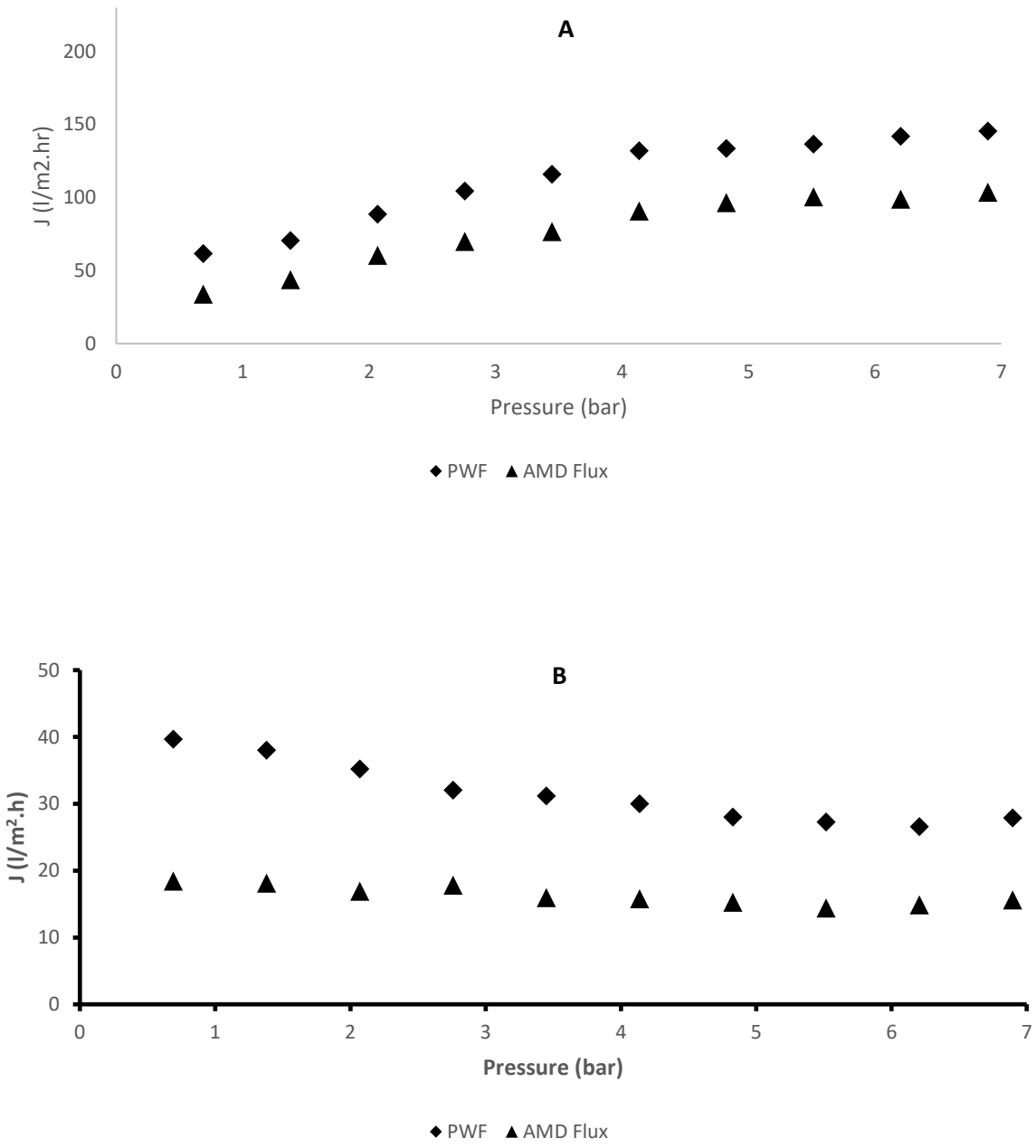
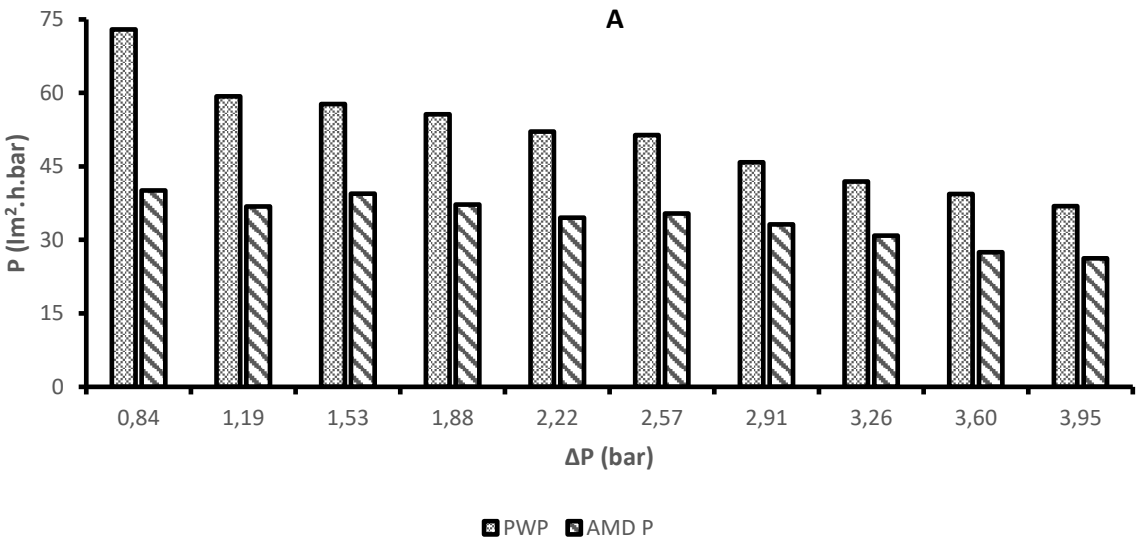


Figure 6.3: Pure water and AMD flux for both (a) PES/chitosan membranes and (b) PES/chitosan/PA membranes

Membrane permeability forms part of the requirements for a good membrane. As such, Figure 6.4 (a) and (b) illustrate permeability of pure water (PWP) and AMD (AMD P) solution which is defined as the ration of the flux and TMP for PES/chitosan and PES/chitosan/PA membranes, respectively. Permeability of 73 and 40 L/m^2.hr. bar was reported at the lowest TMP of 0.84 bar and at maximum TMP of 3.95 bars was 37 and 26 L/m^2.hr.bar for PES/chitosan and PES/chitosan/PA respectively. Permeability of AMD solution was observed as 40 and 26 L/m^2.hr.bar at TMP of 0.84 bar and 18.42 and 15.60 L/m^2.hr.bar for TMP of 3.95 bars. They are two phenomena which eventuate when the transmembrane pressure is increased, that is firstly, increasing the pressure results in more solutes forced towards the membrane surface which causes concentration polarisation and then subsequently reduced rejection. Secondly, with increased pressure, more solvent volume is passed through the membrane surface but solute transport across the membrane is hindered by steric and electric effects which lead to increased rejection. The reduced permeability at high pressure is due to the strong driving force pushing solvent molecules through the membrane as opposed to low pressure.



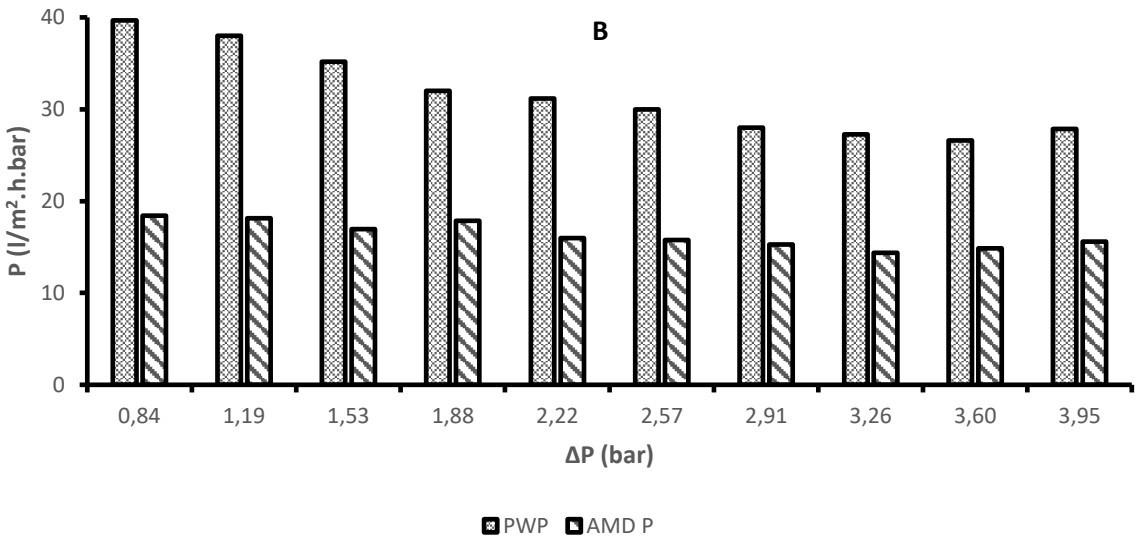


Figure 6.4: Pure water and AMD permeability for (a) PES/chitosan membranes and (b) PES/chitosan/PA membranes

6.2.3.2 Membrane rejection

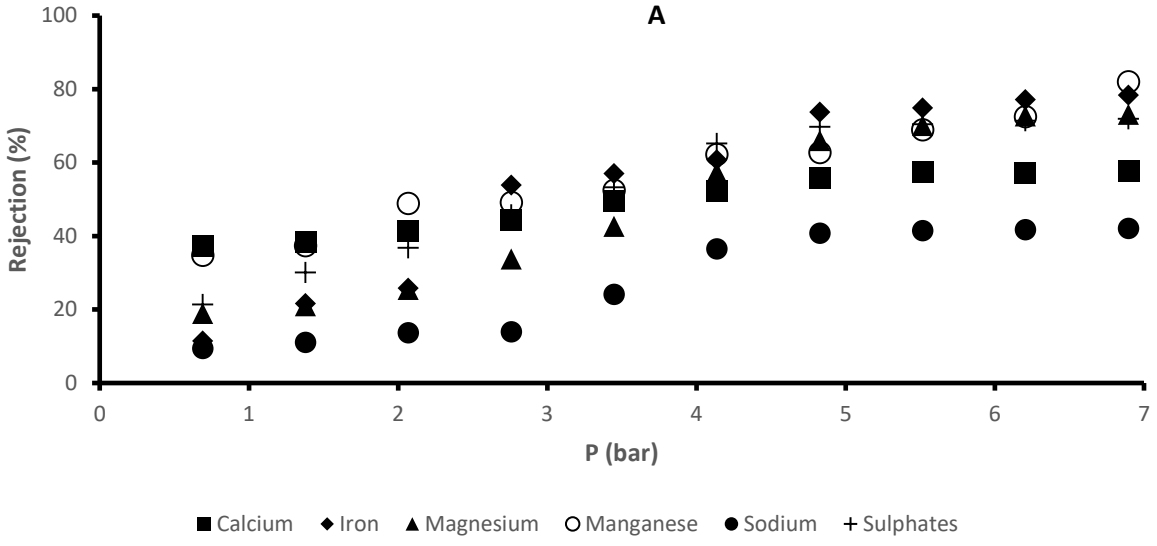
Rejection of metal and sulphate ions was conducted out using crossflow filtration module and AMD permeability was determined from TMP of 0.84 to 3.95 bar and is presented in Figure 6.5. The feed composition of the AMD is presented in Table 6.2. AMD was filtered through the membranes and permeate were collected for analysis. Metal ion contents was analysed using AAS and sulphates were determined using Uv-Vis, respectively. Figure 6.5 (a) and (b) presents the rejection percentage of the AMD constituencies by both PES/chitosan and PES/chitosan/PA membranes. The tests were conducted twice to ensure accuracy and consistency of the results obtained and each results of the two tests were averaged to get a final figure.

2.1 mg/L of Ni^{2+} was characterised in the AMD, and no nickel could be detected in the permeate streams for both membranes in all pressures. This could be attributed to the very low concentration contained in the AMD. Rejection of ions improved with increased pressure,

reaching maximum of 58, 78, 73, 82, 42 and 72% for Ca^{2+}, Fe^{2+}, Mg^{2+}, Mn^{2+}, Na^{+} and SO_4^{2-}, respectively by PES/chitosan membrane. Coating polyamide layer on the PES/chitosan membrane improved rejection of Ca^{2+}, Fe^{2+}, Mg^{2+}, Mg^{2+}, Na^{+} and SO_4^{2-} by few percentages to 60, 81, 76, 88, 43 and 79%, respectively. Rejection of Na^{+} was poor for both PES/chitosan and PES/chitosan/PA membranes. This was attributed to the particle size exclusion theory, that is, membranes remove divalent ions more than monovalent (Maryam et al., 2011). As previously mentioned in 6.2.3, pH of the AMD was measured to be 2.7. Therefore, since it was assumed that the IEP of membranes is around 5.5, the membrane was positively charged due to the protonation of the amine groups. Therefore, in addition to sieving potential, rejection was also attributed to electrostatic repulsion and attraction between the membrane and cations and anions , respectively. The slight increase in rejection after coating with polyamide layer is due to the available hydrophilic functional groups exhibiting stronger coordination with the ions which made it easy for their removal.

The observed general trend for both PES/chitosan and PES/chitosan/PA membrane for all AMD constituencies was that there is an increase in rejection with increased pressure. The effect of initial pH investigations in Chapter 5 (section 5.2.2.3) revealed that the synthesised PES/chitosan and PES/chitosan/PA membranes in this study have an isoelectric point (IEP) around pH of 5.04. pH of the permeate solution was monitored during the crossflow filtration study and the results are presented in Figure 6.7. PES/chitosan membrane reached its IEP when the pressure was around 4.83 bar and 4.1 bar for PES/chitosan membrane. The membranes were negatively charged when the pH > IEP and positively charged at pH < IEP. That is PES/chitosan membrane was negatively charged when the pressure was above 4.83 bars and positively charged when it was below. Comparatively, the PES/chitosan/PA membranes were positively charged at pressure below 4.1 bars and negatively charged when the pressure was below 4.1 bars.

Cations rejection by PES/chitosan and PES/chitosan/PA membranes when pH > IEP is attributed to the electrostatic attraction generated between the negatively charged membrane and cations. Sulphate rejection was due to repulsive forces between the negatively charged membrane and the sulphate ions. Moreover, sulphate ion and cation rejection when pH < IEP was attributed to the attraction and repulsive generated by the positively charged membrane. (Tanninen et al., 2002). Generally, sulphate ions reported low rejection compared to the cation for both PES/chitosan and PES/chitosan/PA membranes, respectively. This is because at higher pH, the number of protonated $-NH_2$ groups diminishes and more OH^- are formed and tend to compete with anions. Additionally, when a membrane is positively charged, some SO_4^{2-} is retained on the membrane surface and forms a layer and the rest will pass through easily. This causes low sulphate rejection and low flux.



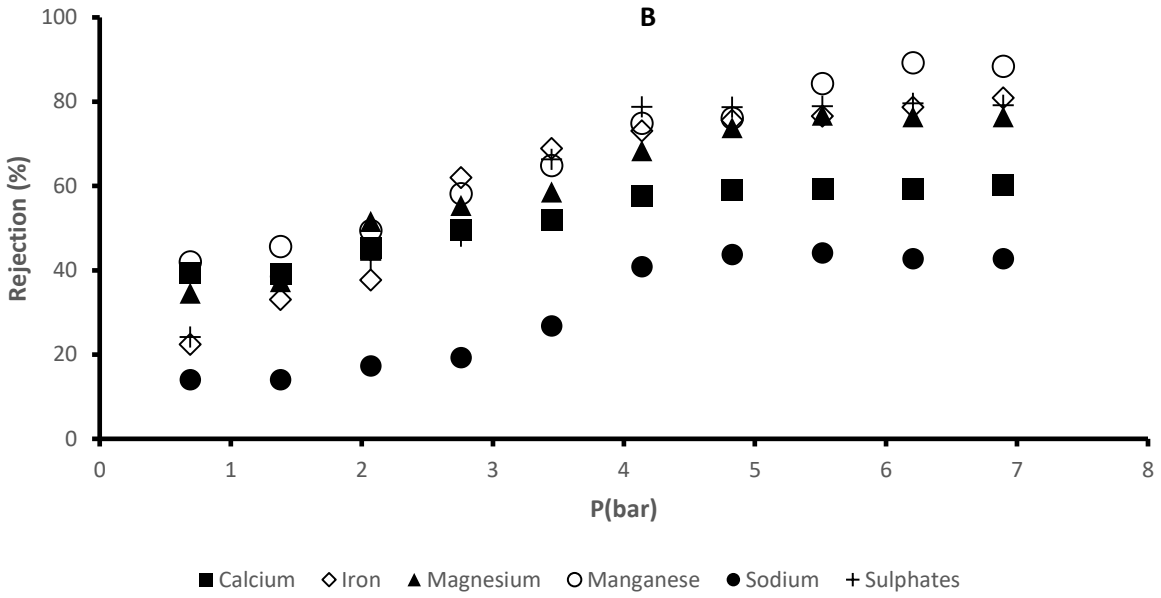


Figure 6.5: Rejection of selected AMD constituencies by (a)PES/chitosan membranes and (b) PES/chitosan/PA membranes

General observed trend as presented in Figure 6.6 is that the pH of the permeate was increasing with increasing pressure. This behaviour could be attributed to two phenomena. Firstly, Sorption of water molecules from acid solution through polymeric membranes triggers slight pH shift towards neutrality. Secondly, removal of sulphate ions, which when interacting with H^+ ions shifted the pH towards neutrality (Mthethwa, 2014). PES/chitosan membrane had higher pH of 6 when the operating pressure was 6.21 and 6.89 bar. Comparatively, highest pH of 6.2 was reported at the same operating pressures for PES/chitosan/PA membrane. This is affirmed by the maximum rejection of sulphate ions. High rejection of sulphate ions by the membranes was high at 6.21 and 6.89 bars. Over 50% rejection for most of the cations could be observed when the operating pressure was above 5 bars in Figure 6.8, and the pH was above 5 at the same pressure.

Hydroxides of Mn^{2+}, Fe^{2+}, Mg^{2+}, Na^+ and Ca^{2+} are reported in literal data to precipitates at 9.0 to 9.5, 5.5 to 8.5, >9 , 6.8 to 8.6 and >10 (Balintova and Petrilakova, 2011; Stratful et al., 2001).

Fe^{2+} and Mn^{2+} reported high rejection compared to other metal complexes. This is attributed by the fact that Mn^{2+} simultaneously precipitate with Fe^{2+} at pH of 8, provided the concentration of Fe^{2+} is much greater than that of Mn^{2+} (Balintova and Petrilakova,2011). The feed solution used in these tests had Fe^{2+} concentration which is 4.5 times more than Mn^{2+} a7 195 mg/L. Although most of the cations precipitates at much higher pH, when the pH was above 5, improved rejection could be observed. No scientific explanation could be found to corroborate this behaviour. However, general explanation could be that since rejection tests were conducted simultaneously instead of individual. Interference during rejection could have influenced the rejection behaviour of some of the metals.

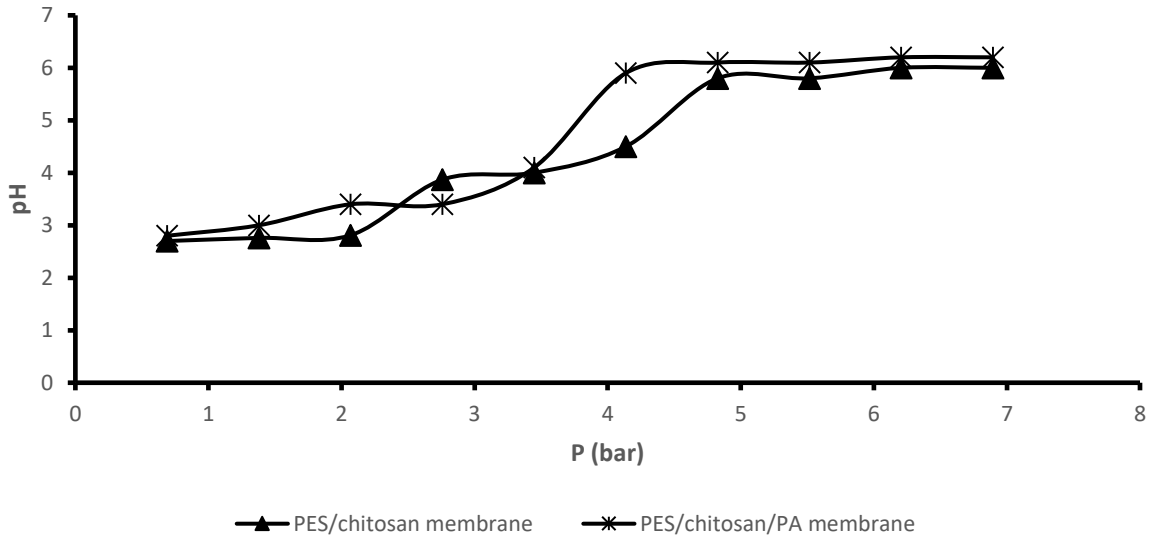


Figure 6.6: pH values of the permeate AMD solution against pressure

6.4 Fouling experiments

6.3.1 Effect of time on flux

To investigate the antifouling properties and operational stability of the membranes, pure water and AMD solution were rapidly added to the feed tank and filtered through the membranes. The filtrates were collected for analysis (flux and rejection measurements) and the retentate was continuously returned to the feed tank. First pure water flux was measured every 30 minutes for 6 hours at 6.7 bar based on the permeate volume collected. The pure water flux after 6 hours was measure as J_{w1} Thereafter, AMD solution was filtered, and similar exercise was conducted to establish AMD flux (J_{AMD}) after 6 hours. After AMD was permeated through and measure every 30 minutes for 6 hours, pure water was filtered through the membrane again for 6 hours at 6.9 bars to establish any flux (J_{w1}) loss. Backwashing was conducted and new pure water flux (J_{w2}) was measured again for 6 hours at 6.9 bars. Figure 6.7 and 6.8 presents the observed flux stability and fouling experiments, respectively.

Figure 6.7 (a) and (b) shows more or less constant pure water flux for PES/chitosan and PES/chitosan/PA membranes, respectively. The insignificant flux differences could be attributed to the privation of organic matter and dissolved ions in the water. There was fairly accentuated decrease of flux in the first hour of 3 and 10 L/m^2.hr for PES/chitosan and PES/chitosan/PA membranes, respectively. As time increases, there is clear stabilisation of pure water flux. Looking at the AMD flux, significant decrease of flux with a sharp decrease in flux could be observed in the first 30 minutes and it continued until about 3 hours whereby flux continues to decrease but not as pronounced as in the first 3 hours. This loss in flux is attributed to the concentration polarisation which forms a layer on the membrane surface and obstructs solvent movement through the membrane (Wang et al., 2012).

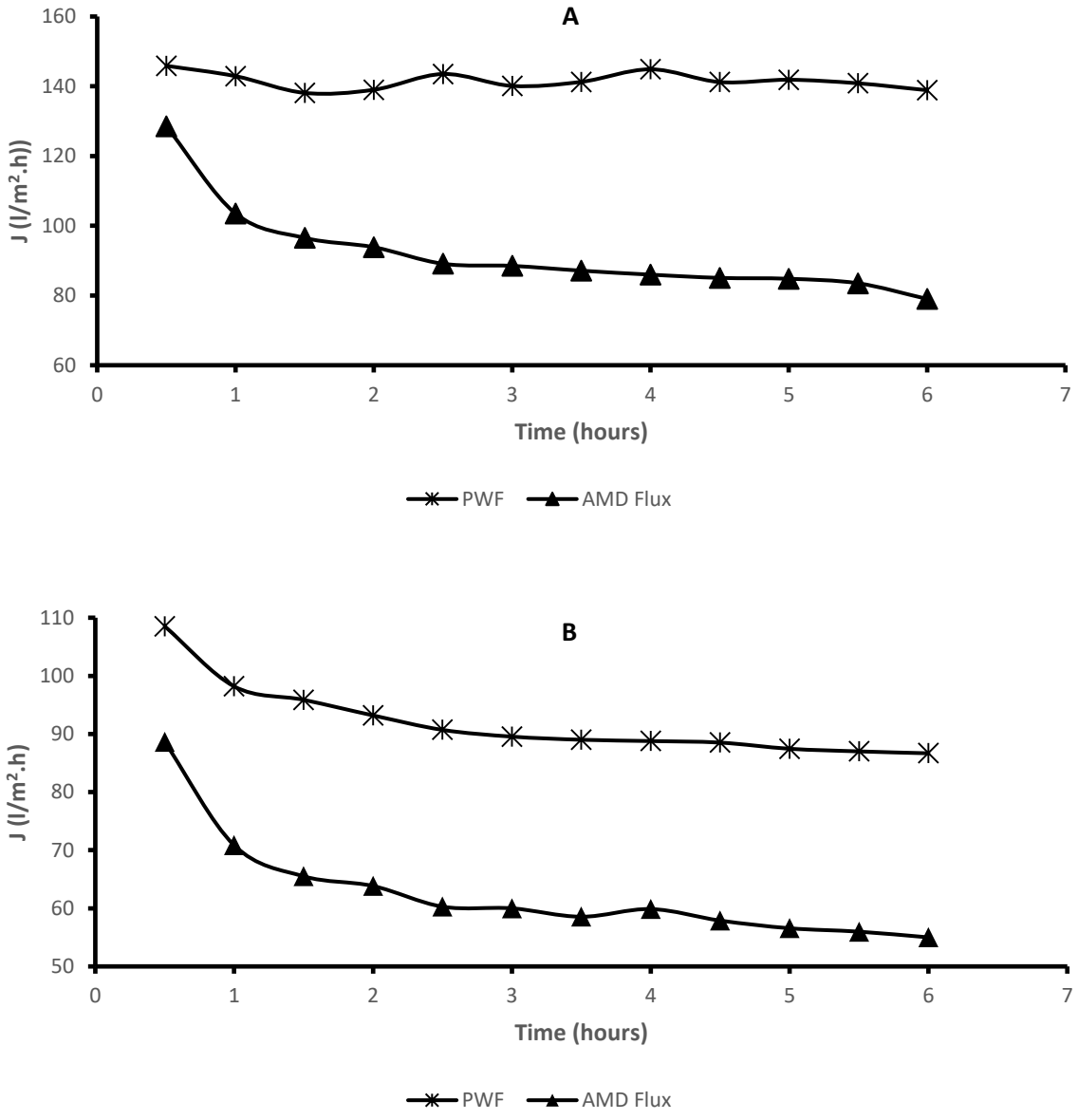


Figure 6.7: Permeate flux of pure water and AMD as a function of time for (a)PES/chitosan membranes and (b) PES/chitosan/PA membranes

6.3.2 Fouling experiments

To substantiate the effects of fouling and backwashing, after 6 hours of AMD permeation through the membranes at 6.9 bar, pure water was passed through the membrane to establish if there was any loss in membrane flux before any backwashing could be conducted. That is the original flux did not reduce. Backwashing was performed and pure water was filtered through again to check if the original flux was restored.

Figure 6.8 (a) and (b) shows the results of initial PWF ((J_{w1}), AMD flux ((J_{AMD}), which acted as a foulant, PWF before backwashing ($(PWF\ BBW)$ and PWF after backwashing ($PWF\ ABW$) of PES/chitosan and PES/chitosan/PA membranes. Equation (3.12) was used to determine the reversible resistance and it was established that about 37 and 44% of reversible resistance was observed by permeation of AMD solution through PES/chitosan and PES/chitosan/PA membranes after 6 hours at 6.9 bars. Clear difference between loss of flux for membranes presented in this Chapter and those in Chapter 5 (19.5 and 6.6% for PES/chitosan and PES/chitosan/PA membranes, respectively) is significant. This is attributed to the fact that synthetic AMD was utilized in other Chapters as compared to real AMD which was used in this Chapter. Real industrial AMD contains concoction of organic and inorganic constituencies which could accelerate concentration polarisation and subsequently fouling. After AMD permeation, pure water flux was measured as 119.58 L/m^2.hr, which was 14% loss of the initial flux for PES/chitosan membrane. PES/chitosan/PA membrane pure water flux was measured as 63 L/m^2.hr, which was 27% loss of the original flux. Back washing was performed, and PES/chitosan and PES/chitosan/PA membranes measured pure water fluxes of 137 and 85 L/m^2.hr. It is evidently clear on Figure 6.11 that the initial flux of the membranes was almost restored as it was only 1.7 and 2% less as compared to the original fluxes of PES/chitosan and PES/chitosan/PA membranes, respectively. The small irreversible resistance determined using Equation (3.13) clearly shows that the membranes have strong antifouling properties. As Kadis (2004) alluded, the small discrepancy could also be ascribed to parallax error when collecting permeates volume. The flux recovery ratio (FRR) was determined using Equation (3.11) and was found to be 98 and 98% for PES/chitosan and PES/chitosan/PA membranes, respectively. The higher percentage of reversible resistance (sometimes referred to as cake resistance) is pertaining to the concentration polarisation. The fouling experimental data confirmed superior characteristics of PES/chitosan and PES/chitosan/PA membranes

against fouling. The antifouling properties of the PES/chitosan/PA membranes synthesised in this study had better FRR results compared to the PES membrane synthesised by Shockravi et al. (2017) with polyamide as hydrophilic additive. The polyamide layer in this study was coated onto a hydrophilic PES/chitosan membrane, hence improved anti-fouling property.

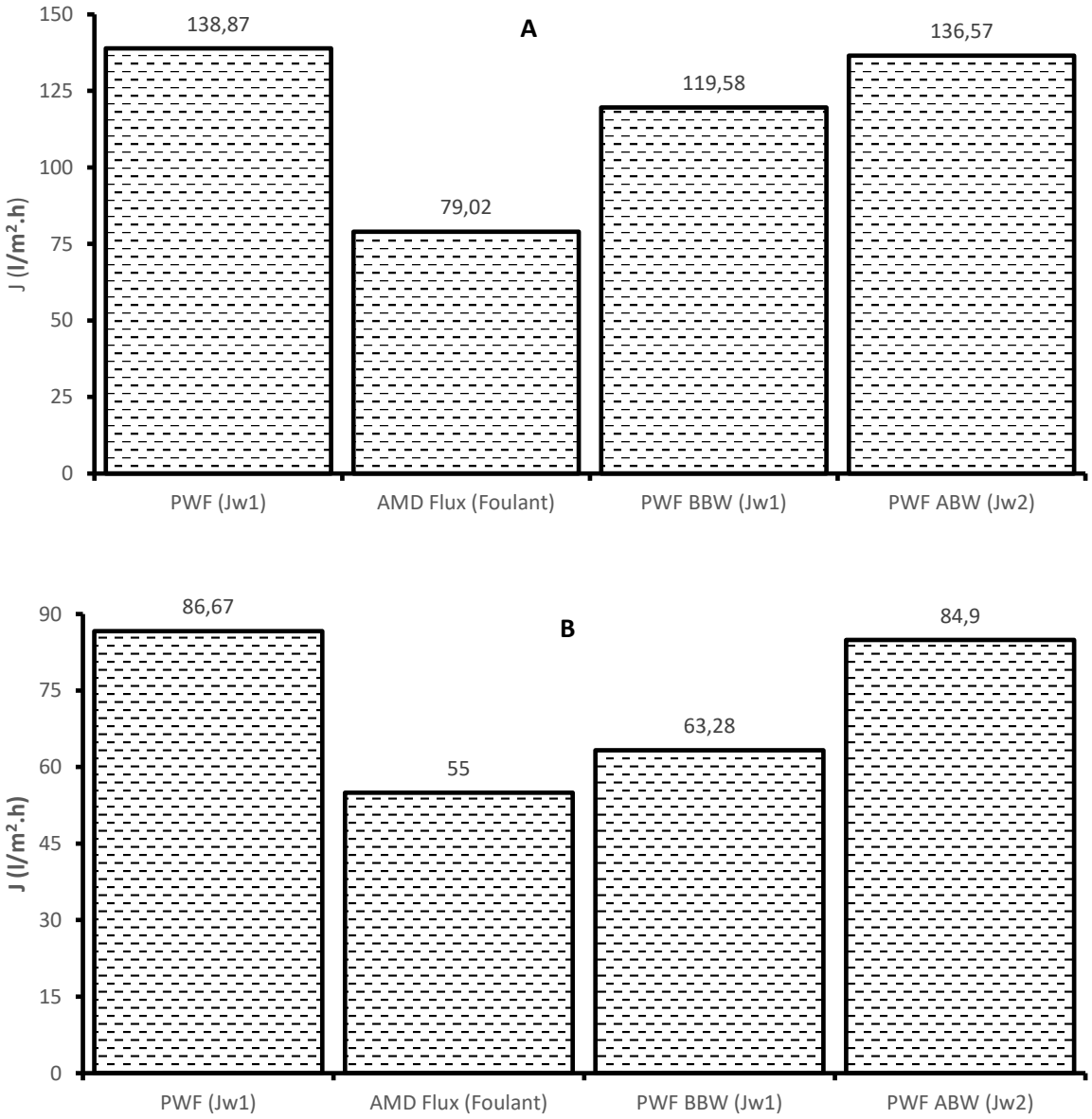


Figure 6.8: Fouling experimental results for (a) PES/chitosan membranes and (b) PES/chitosan/PA membranes.

6.3.3 Blocking filtration models

AMD (Table 6.2) was employed as feed water with metals as foulants throughout the filtration process and the results were used in plotting the flux-time correlation to evaluate the fouling tendencies of the feed water. Flux reduction with time is a general phenomenon expected to describe membrane fouling during membrane operation. The revised blocking models by Hermia were used in this study to arrive at the plots of the filtration mechanisms of complete blocking, standard blocking, intermediate blocking and cake layer formation.

In the standard initial flux experiment of the non-fouling membrane, the original flux of pure water against increasing TMP was observed to range from 61 to 145 L/ m^2.hr with a linear fit of R^2= 0.9255. Figures 6.9 to 6.1 show the fitting of the experimental data fitted to Hermia's models. The measurement of the fit, as per the R^2, is shown in Tables 6.3 and 6.4. The values of obtained R^2 obtained with the same model are compared for different foulant found in the feed (see tables 6.3 &6.4 and figures 6.9 to 6.12). Higher values of R^2correspond to a better fit of the model (Gu, 2007). Generally, it was observed that the permeation flux (J_P) gradually declined with time signifying blockage/reduction of effective of membrane pores due to accumulation of some constituents on the membrane surface. Similar flux-time trends were reported in other studies (Rashid et al., 2013).

Figure 6.9 (a and b) shows the fitting of the experimental results to complete blocking model for all the individual foulant in the feed AMD solution for PES/PA and PES/chitosan/PA membranes. General expected trend of declining flux with time was observed for all foulants. It is worth mentioning that it is adequate to compare the square regression coefficients of same foulant for different models but inadequate to compare values of R^2 for different foulants in the same model. Table 6.3 and 6.4 shows that the square regression coefficient is greater for Fe^{2+}, Mn^{2+} and SO_4^{2-} experimental results signifying best predictions and poor predictions were

obtained for Ca^{2+}, Mn^{2+} and Na^{+} which had low square regression coefficient. This behaviour could be attributed to the fact AMD feed solution contained 895 and 3680 mg/L of Fe^{2+} and $SO_4^{2-,}$ respectively, that is more solute molecules of both foulant was transported in large quantities to the membrane surface which resulted in membrane pores blocked.

Figure 6.10 and figure 6.12 shows fitting of the experimental permeate flux to the intermediate and standard blocking models for all the foulants and Table 6.3 and 6.4 depicts the square regression coefficients for PES/chitosan and PES/chitosan/PA membranes. The expectation of an intermediate blocking model is that not all solute molecules or foulants will block all the pores. That is some will attach to other solute molecules already retained on the membrane surface. On the other hand, the standard blocking model assumes that small particles will attach to the membrane wall rather blocking the pores completely and that will result in reduction of pore sizes. Poor square regression coefficients were reported for both standard and intermediate blocking models for both PES/chitosan and PES/chitosan/PA membranes, respectively. This could be attributed to the fact that all the foulant molecules were of similar radius. Figure 6.10 illustrate the fitting of the experimental data to the cake layer formation model. As it was the case with complete blocking model, Fe^{2+}, Mn^{2+} and SO_4^{2-} foulant reported best fit with. This could be attributed to the fact that all those solute molecules retained by the membrane created a cake or gel layer which obstructs flow. For all the models studied in this section, the precision in the fitted results is high when the permeate flux declined moderately with time. From the observations of Figures 6.9 to 6.12 and Tables 6.3 and 6.4 it can be concluded the best fit to the experimental data correspond to the complete and cake or gel formation layer blocking models. This implies the dominant fouling mechanisms taking place during filtration of AMD through PES/chitosan and PES/chitosan/PA membranes is complete and cake or gel layer formation blocking models

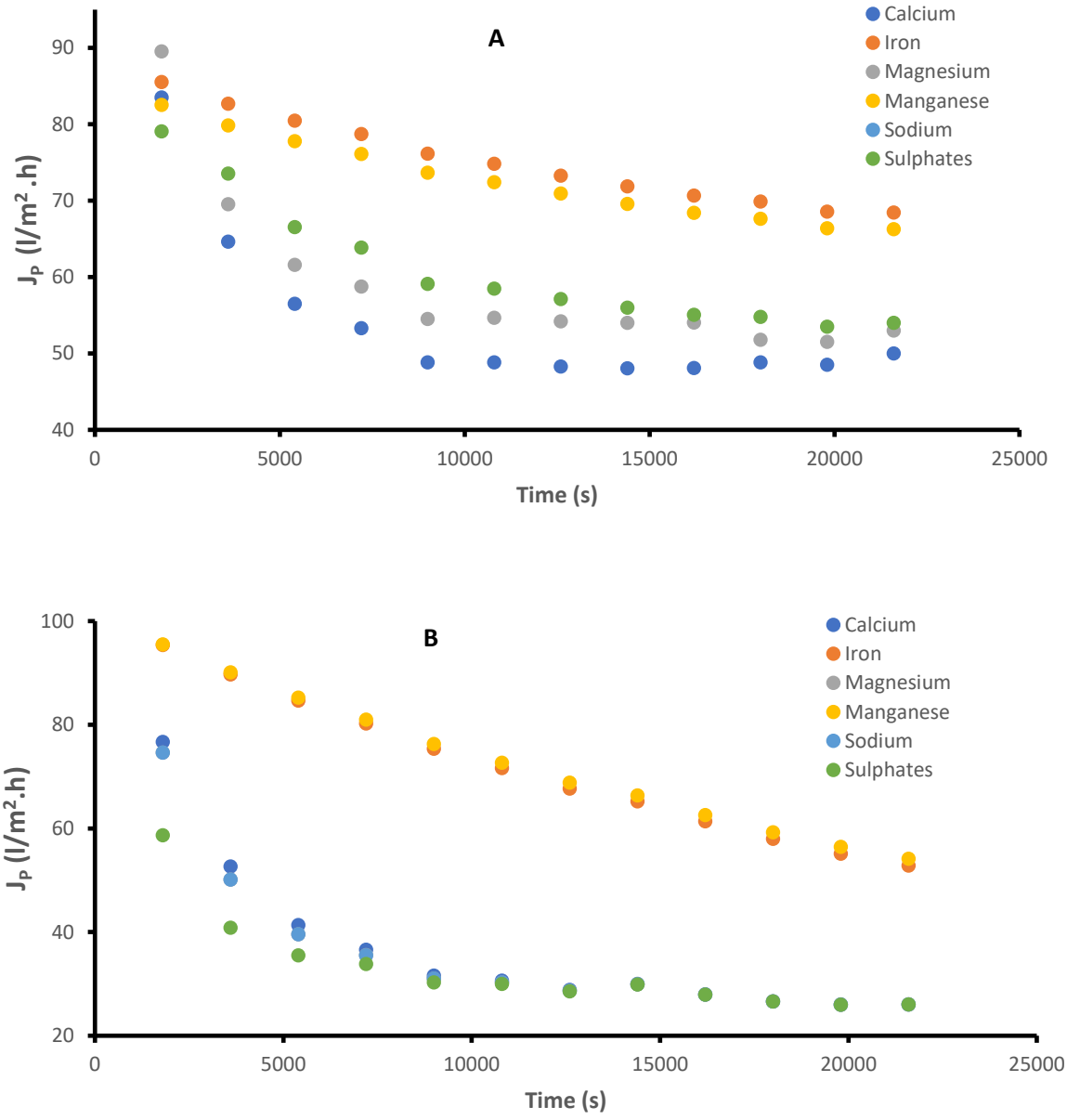


Figure 6.9: Complete blocking model for cross flow predications for (a)PES/chitosan membranes and (b) PES/chitosan/PA membranes for individual foulant in the AMD feed solution

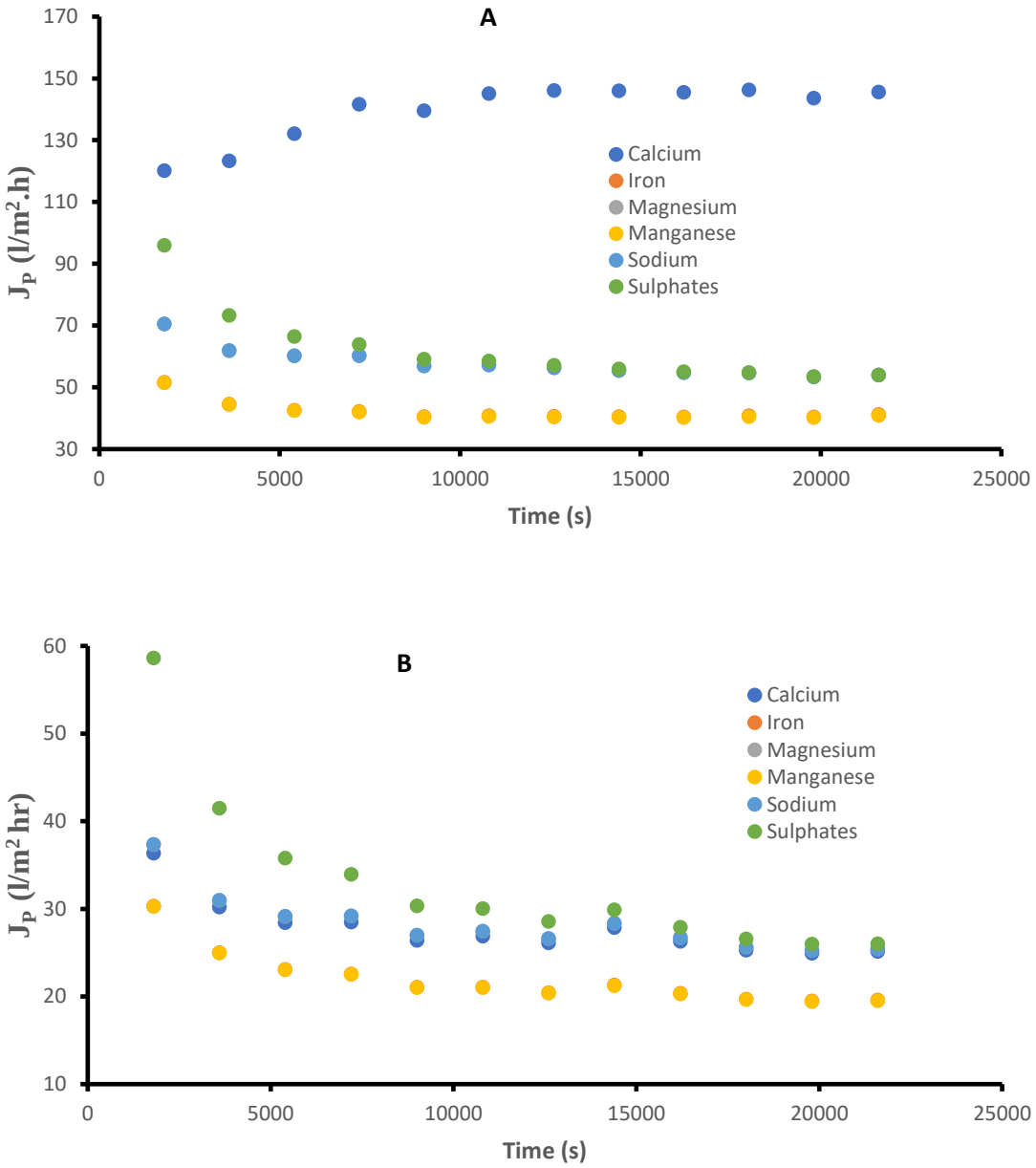


Figure 6.10: Intermediate blocking model for cross flow predicitons for (a)PES/chitosan membranes and (b) PES/chitosan/PA membranes for individual foulant in the AMD feed solution

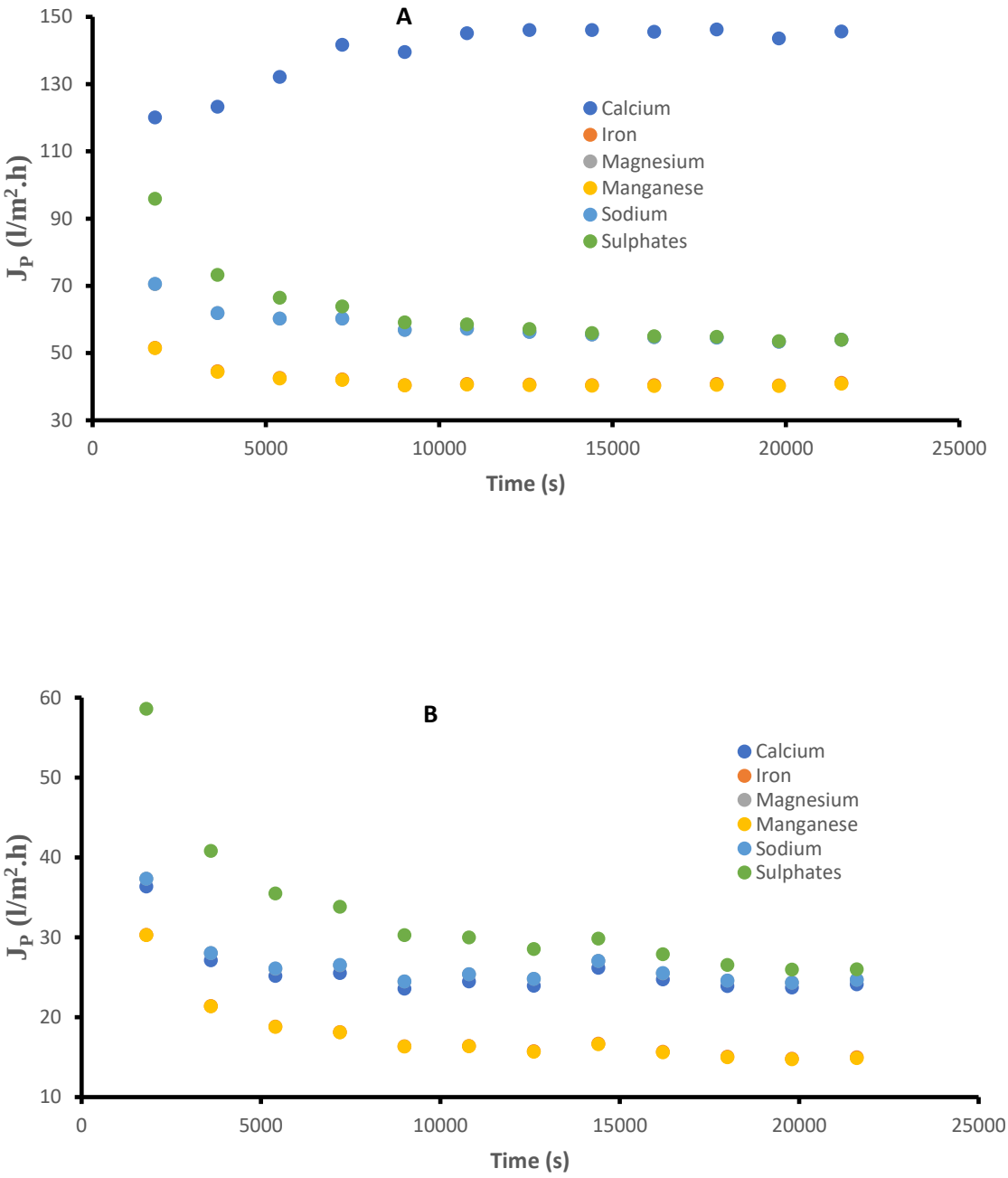


Figure 6.11: Standard blocking model for cross flow predicitons for (a)PES/chitosan membranes and (b) PES/chitosan/PA membranes for individual foulant in the AMD feed solution.

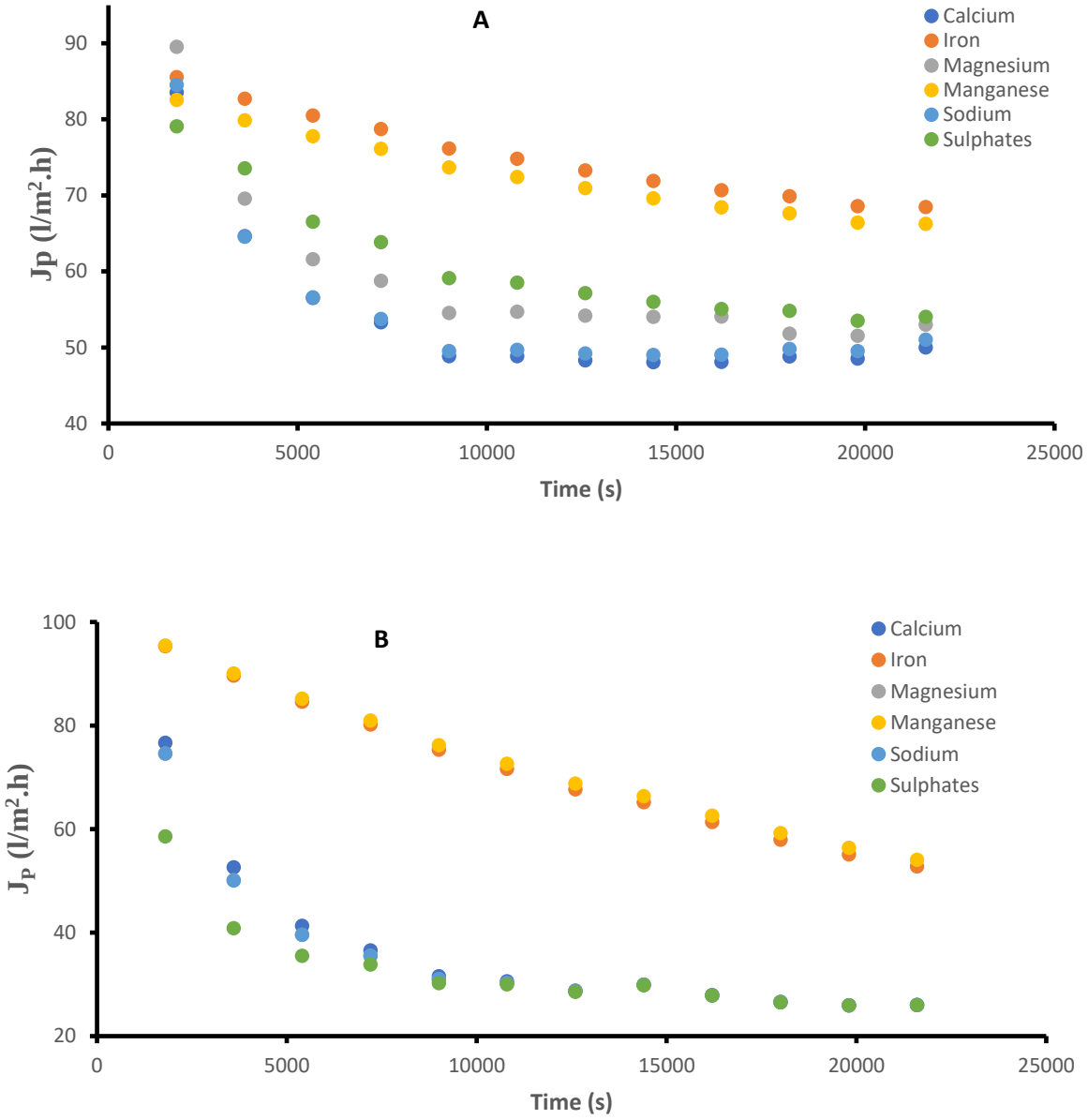


Figure 6.12: Gel layer formation blocking model for cross flow predicitons for (a)PES/chitosan membranes and (b) PES/chitosan/PA membranes for individual foulant in the AMD feed solution

Table 6.3: Measures of fit, as per the R^2s, of Hermia's models for PES/chitosan membranes.

	Measures of fit (R^2s)			
Foulant	Complete Blocking	Intermediate blocking	Standard blocking	Gel layer formation
Ca^{2+}	0.5097	0.6659	0.6658	0.5097
Fe^{2+}	0.9642	0.4635	0.4635	0.9642
Mg^{2+}	0.5799	0.7580	0.7591	0.5799
Mn^{2+}	0.9662	0.4754	0.4754	0.9662
Na^{+}	0.4838	0.7582	0.7583	0.4838
SO_4^{2-}	0.8178	0.6502	0.6502	0.8178

Table 6.4: Measures of fit, as per the R^2s, of Hermia's models for PES/chitosan/PA membranes.

	Measures of fit (R^2s)			
Foulant	Complete Blocking	Intermediate blocking	Standard blocking	Gel layer formation
Ca^{2+}	0.6641	0.6409	0.3753	0.6441
Fe^{2+}	0.9875	0.6855	0.5939	0.9875
Mg^{2+}	0.6224	0.6666	0.4059	0.6224
Mn^{2+}	0.9887	0.6875	0.5964	0.9887
Na^{+}	0.6222	0.6668	0.4062	0.6222
SO_4^{2-}	0.6446	0.6549	0.6446	0.6446

6.4 Summary

Subsequent to optimizing the chitosan loading and its degree of deacetylation for synthesising PES/chitosan and PES/chitosan/PA membranes for the treatment of AMD, its important to understand the operational stability of the membranes evaluate their fouling potential. As such, this Chapter provided information pertaining to the operational stability and antifouling property of the synthesised membranes using real industrial AMD.

Real industrial AMD was collected in Randfontein sites in the Western basin of the Witwatersrand region which is the same area in which the composition of the synthetic AMD used in previous Chapters was collected. The composition of the collected real AMD was not similar to that used to prepare the synthetic AMD used in previous Chapters; however, it contained satisfactory composition to use for the fouling experiments. The investigations were carried out in a crossflow filtration system comprised of three cells having 125×75mm dimensions (Area = 93.75 cm^2). The tests were conducted by varying the operating pressure from 0.7 to 6.9 bars.

Firstly, pure water flux and permeability of the membranes were determined by varying the pressure from 0.7 to 6.9 bars, to establish the original properties of the membrane. Then, flux of the AMD solution was established when the rejection efficiency of the membranes through the crossflow system at different pressure was examined. Flux of the AMD solution was also determined and compared to that of pure water flux. It was observed that the pure water and AMD fluxes differed significantly. This difference was due to the water passage reduction which was created by retaining of contaminants on the membrane surface which leads to concentration polarisation.

Membrane permeability of pure water (PWP) and AMD (AMD P) solution which is defined as the ration of the flux and TMP was determined. The general observed trend was that, the

permeability of the membranes was decreasing with increasing feed pressure. Additionally, the permeability of pure water was much higher than that of AMD solution. This behaviour was attributed to the fact that when the transmembrane pressure is increased, more solutes are transported towards the membrane surface and cause concentration polarisation and thus reduce permeability. Moreover, high transmembrane pressure result in large solvent volume is passed through the membrane surface. The reduced permeability at high pressure is due to the strong driving force pushing solvent molecules through the membrane as opposed to low pressure.

Permeate of the AMD solution was collected and analysed for metal and sulphate ions using AAS and Uv-Vis, respectively. Rejection of the membranes was increased with increasing operating pressure. Maximum rejection for most of the contaminants was reported at the highest pressure of 6.9 bar. PES/chitosan membrane had maximum rejection of 58, 78, 73, 82, 42 and 72% for Ca^{2+}, Fe^{2+}, Mg^{2+}, Mg^{2+}, Na^{+} and SO_4^{2-}, respectively. Coating polyamide layer on the PES/chitosan membrane improved rejection of Ca^{2+}, Fe^{2+}, Mg^{2+}, Mg^{2+}, Na^{+} and SO_4^{2-} by few percentages to 60, 81, 76, 88, 43 and 79, respectively. The slight increase in rejection after coating with polyamide layer is due to the available hydrophilic functional groups exhibiting stronger coordination with the ions which made it easy for their removal. Rejection of Na^{+} was poor for both PES/chitosan and PES/chitosan /PA membranes. This was attributed to the particle size exclusion theory, that is, membranes remove divalent ions more than monovalent (Maryam et al., 2011).

Lastly, the operational stability and fouling potential of the membranes was investigated. Firstly, pure water flux was measured every 30 minutes for 6 hours at 6.9 bar based on the permeate volume collected. The pure water flux after 6 hours was measured. Thereafter, real industrial AMD solution was filtered, and similar exercise was conducted to establish AMD flux after 6 hours. This exercise was necessary to understand the operational stability of the

membrane with time. The pure water and AMD fluxes reported fairly constant flux behaviour until 6 hours. However, AMD fluxed reported an accentuated flux loss in the first hour and this rapid loss of flux in the first hour could be attributed to the organic and inorganic materials migrating from the liquid phase to the membrane surface.

To evaluate the fouling potential of the membranes, flux of pure water was measured after 6 hours at 6.9 bar. The AMD was permeated through under the same conditions. Pure water was filtered through the membrane again for 6 hours at 6.9 bar to establish any flux loss. The backwashing was conducted, and new pure water flux was measured again for 6 hours at 6.9 bar. The reported results revealed that about 37 and 44% of reversible resistance was suffered by PES/chitosan and PES/chitosan/PA membranes after permeation of AMD solution. This was the consequential results of organic and inorganic concoction of contaminants contained in the real industrial AMD which could accelerate concentration polarisation and subsequently fouling. When pure water was filtered through after AMD permeation, the new pure water flux reported 14 and 27% loss of the initial flux for PES/chitosan and PES/chitosan/PA membrane, respectively. After backwashing, it was evidently clear that the initial flux of the membranes was almost restored with only 1.7 and 2% loss of flux compared to the original fluxes of PES/chitosan and PES/chitosan/PA membranes, respectively. The flux recovery ratio (FRR) was determined and was found to be 98.34 and 97.96% for PES/chitosan and PES/chitosan/PA membranes, respectively. The fouling experimental data confirmed superior characteristics of PES/chitosan and PES/chitosan/PA membranes against fouling. Hermia's filtration models fitted with the experimental deduced that the dominating fouling mechanisms taking place during filtration of AMD through PES/chitosan and PES/chitosan/PA membranes are complete and cake or gel layer formation blocking models.

Chapter 7: General conclusions and recommendations

7.1 Conclusions

Acid mine drainage is a significant challenge not only facing the mining industry but threatens supply of drinking water and pose environmental challenges that could have devastating repercussions if left alone without remediation. Most areas find it impossible to prevent the formation of AMD due to its complicated and self-propelling chemistry once it is formed. Most conventional active and passive treatment technologies have challenges of producing large volume of toxic sludge that could create secondary pollution if not properly disposed of, they require frequent maintenance and achieve only partial treatment. The need for efficient technology and environmental concerns warranted the need for a new technology and membrane technology has emerged as the most eminent technology.

Although membrane technology is a promising technology for the treatment of AMD, it has its drawbacks of concentration polarisation and membrane fouling which if not handled correctly could compromise its performance and reduce lifespan. Polymeric membranes attracted enormous attention to fabricate membranes for water and wastewater treatment due to their biodegradability and non-toxicity. Polyethersulphone (PES) membrane has gained significant progress in treatment of AMD of high chemical and thermal resistance, mechanical stability in hot and wet conditions and high permeability. Significant challenges limiting full utilization of PES is its inherent hydrophobicity which is directly related to membrane fouling.

It is against this background that this work aimed at developing PES membrane with enhanced antifouling and permselective properties during the treatment of AMD. This work modified PES membrane by blending with chitosan and coating with polyamide as hydrophilic copolymers. Initially, chitosan was successfully synthesised from chitin and infused within PES membrane matrix and then coated with polyamide layer on top. The effect of chitosan

loading and its degree of deacetylation on the quality and performance of the synthesised membranes was evaluated during AMD treatment.

To achieve this, the following research questions were defined and expected to be addressed during the research

(i) What is the effect of blending chitosan and chitosan having various ’s degree of deacetylation on the performance of PES membrane during AMD treatment?

(ii) What is the effect of coating polyamide layer on PES membrane infused with chitosan on the performance during AMD treatment?

(iii) What will be the effect of operating variables such as pH, feed pressure and feed composition on the separation performance of the membranes?

(iv) What will be the fouling behaviour and the operational stability of the membrane during AMD treatment?

Moreover, the following objectives were formulated to address the research questions

(i) To synthesize polyethersulphone membrane infused with chitosan and coated with polyamide layer for the treatment of AMD

(ii) Investigate the influence of chitosan content and chitosan’s degree of deacetylation of on the quality and separation performance of the modified membrane coated with polyamide top active layer during AMD treatment

(iii) Investigate to understand the effect of operating variables such pH, feed pressure and feed composition on the separation performance of the optimized membrane from (ii)

(iv) To investigate fouling behaviour and operational stability of the membrane towards enhancing the membrane integrity during AMD treatment.

The outcomes pertaining to this study are presented below:

1. Chitosan was successfully synthesised from chitin and Information on the influence of synthesis variables on chitosan's degree of deacetylation from chitin

Chitosan was successfully synthesised from chitin which was obtained from crab and shrimp shells through deacetylation process by treating chitin with strong alkaline solution at high temperatures (± 100^{O}C). Chitosan synthesis conditions tests showed 40% NaOH concentration and reaction temperature of 100 ^{o}C to be optimal conditions as they produced chitosan with the highest degree of deacetylation of 96%. The success in chitosan synthesis from chitin was confirmed by FTIR which showed typical chitosan characteristic functional groups.

2. The effect of chitosan content and chitosan's degree of deacetylation on the quality and performance of PES membrane infused with chitosan and coated with polyamide layer for the treatment of AMD

Hydrophilic chitosan and polyamide copolymers successfully and positively influenced the hydrophilic and permselectivity of the PES membrane. This was affirmed by the contact angle results which showed downward trend with increasing chitosan content and after coating with polyamide layer. The hydrophilic copolymers enhanced the synthesised membranes porosity. The flux and rejection of the PES/chitosan membranes reported high values when chitosan content was 0.75 wt%. Further addition induced reduction showing 0.75 wt% as better chitosan loading. Although, in the case of chitosan loading of 1wt% (in the case of PES/chitosan/PA membranes), the rejection performance was satisfactory with 0.75 wt% content. The effect of chitosan's degree of deacetylation on the performance of the synthesised membranes infused with chitosan showed increasing performance with increasing chitosan's degree of

deacetylation. This was because high degree of deacetylation signified large number of amino group on the chitosan structure which could act as contaminants binding sites.

3. The effect of operational conditions (feed pH, pressure and composition) on the performance of optimized membrane in (iii) during AMD treatment

The effect of feed pH on the performance of the synthesised membrane with optimized chitosan and chitosan's degree of chitosan showed the PES/chitosan and PES/chitosan/PA membranes to have an isoelectric point (IEP) at around pH 5.04. The membrane assumed a positive charge at pH values below IEP and rejection of cations and anions was due to electrostatic repulsion and attraction, respectively. Similarly, the membranes were negatively charged at pH values higher than IEP and rejection was due to repulsive and attraction forces for anions and cations, respectively. Rejection of cations was poor at pH values higher than the IEP and good at pH values below. This showed the membranes to have stronger repulsive forces than attraction ones. Rejection of cations was poor at pH values higher than the IEP and good at pH values below. This affirmed by the poor rejection of anions at pH values below IEP and good at pH higher than IEP. All in all, the results showed the membranes to have improved performance over wide pH range

Investigating the effect of initial feed concentration and pressure is essential in order to assess the applicability range and determine optimum conditions for an efficient membrane separation operation. The permeate flux of the membranes increased with increasing pressure. This behaviour was attributed to the increased forces which transport large water molecules through the membrane as the pressure increases. Moreover, solutions with low concentration reported high permeated flux due to low number of ions being trapped on the membrane surface and subsequently blocking the pores and forming a layer obstructing flow. At high concentrations,

more ions are trapped on the membrane surface and within the pores, thereby forming a layer which leads to concentration polarisation.

4. The antifouling behaviour and operational stability of the optimized membrane

The operational stability and fouling potential of the membranes was investigated. The pure water and AMD fluxes reported constant flux behaviour until 6 hours. AMD flux reported an accentuated flux loss in the first hour and after start started stabilising.

The fouling experiments results showed about 37 and 44% of reversible resistance was suffered by PES/chitosan and PES/chitosan/PA membranes after permeation of AMD solution. Immediately after AMD experiments, pure water was filtered through and the new pure water flux reported 13.89 and 27% loss of the initial flux for PES/chitosan and PES/chitosan/PA membrane, respectively. Backwashing was conducted and a new pure flux evidently affirming the membranes to have strong antifouling property. The initial flux of the membranes was almost restored with only 1.7 and 2% loss of flux compared to the original fluxes of PES/chitosan and PES/chitosan/PA membranes, respectively. The flux recovery ratio (FRR) was determined and was found to be 98 and 98% for PES/chitosan and PES/chitosan/PA membranes, respectively. Hermia's filtration models were used to predict and determine the dominant fouling mechanisms. Based on the square regression coefficient, it was concluded that complete and cake or gel layer formation blocking models best described the fouling mechanisms which took place when AMD was filtered through PES/chitosan and PES/chitosan/PA membranes.

The above observations are evident enough to conclude that the aim and objectives of the study have been met.

7.2 Recommendations

The chitosan synthesised in this study was produced from chitin coming from shrimp and crab shells. The two were mixed on a 50/50 composition; however, further research could be conducted to investigate different composition between these two sources. Additionally, other sources of chitin could be explored. Only NaOH concentration and reaction temperature were investigated in this study at ration of 1:20 (solid: liquid). Other synthesis conditions such as reaction time and other solid: liquid ratio to understand their impact on degree of deacetylation. Specifically, to obtain chitosan that would be used to blend PES and PA membranes.

10 wt% PES granules were dissolved in DMSO solvent to obtain PES support structure. Based on the effect of pressure on the pure water flux data obtained in Chapter 4, whereby the membranes could withstand pressure than 4 bar in the dead-End filtration cell, it is recommended that the PES granules could be increased to improve the strength of the membranes and so it can be able to operate at higher pressures.

When fabricating the polyamide layer onto the PES/chitosan membranes: 2 wt% piperazine (PIP) and 0.6 wt% triethylamine was used to prepare the diamine solution and 0.1 wt% trimesoyl chloride (TMC) in 5wt% acetone in *n*-hexane for organic solution. It is recommended that the TMC percentage and acetone in the organic phase be optimized because literal data showed that higher TMC concentration could lead to a thicker polyamide layer. Moreover, the acetone content in the organic phase be optimized to achieve a much thinner polyamide layer by controlling the immiscible zone created which will lead to too lose reaction zone and produce membrane with large pore sizes. Additionally, AFM studies are recommendation for proper qualitative reflection on the membrane surfaces on the effect of polyamide layer formed over unmodified and modified PES support.

It was concluded in the study that the IEP of the membranes was found to be around pH of 5.04. This was based on the literature argument which assumes that pH values corresponding to a peak in flux reporting the lowest rejection of ions by a membrane indicates the IEP or zero potential charge of the membrane. It is recommended that characterisation of the surface of membrane using streaming potential be conducted to accurately understand membrane surface charge. Lastly, it is recommended that the fate of the retained solutes and/or concentrated pollutants/sludge on the membrane surface be investigated to make this technology environmentally friendly and cost effective.

References

Abdou, E.S., Nagy, K.S. and Elsabee, M.Z., 2008. Extraction and characterization of chitin and chitosan from local sources. *Bioresource Technology*, *99*(5), pp.1359-1367.

Agenson, K.O. and Urase, T., 2007. Change in membrane performance due to organic fouling in nanofiltration (NF)/reverse osmosis (RO) applications. *Separation and Purification Technology*, *55*(2), pp.147-156.

Aguiar, A.O., Andrade, L.H., Ricci, B.C., Pires, W.L., Miranda, G.A. and Amaral, M.C., 2016. Gold acid mine drainage treatment by membrane separation processes: An evaluation of the main operational conditions. *Separation and Purification Technology*, *170*, pp.360-369.

Ahmad, A.L., Abdulkarim, A.A., Ooi, B.S. and Ismail, S., 2013. Recent development in additives modifications of polyethersulfone membrane for flux enhancement. *Chemical Engineering Journal*, *223*, pp.246-267.

Akbari, A., Derikvandi, Z. and Rostami, S.M.M., 2015. Influence of chitosan coating on the separation performance, morphology and anti-fouling properties of the polyamide nanofiltration membranes. *Journal of Industrial and Engineering Chemistry*, *28*, pp.268-276.

Akcil, A. and Koldas, S. (2006). Acid Mine Drainage (AMD): causes, treatment and case studies. *Journal of Cleaner Production, 14*, 1139-1145

Ali, N., Mohammad, A.W., Jusoh, A., Hasan, M.R., Ghazali, N., Kamaruzaman, K. 2005. Treatment of aquaculture wastewater using ultra low pressure asymmetric polyethersulfone (PES) membrane. *Desalination*. 185: 317-326.).

Al-Zoubi, H., Rieger, A., Steinberger, P., Pelz, W., Haseneder, R. and Härtel, G., 2010. Optimization study for treatment of acid mine drainage using membrane technology. *Separation Science and Technology*, *45*(14), pp.2004-2016.

Amosa, M.K., 2017. Towards sustainable membrane filtration of palm oil mill effluent: analysis of fouling phenomena from a hybrid PAC-UF process. *Applied Water Science*, *7*(6), pp.3365-3375.

An, Q., Li, F., Ji, Y. and Chen, H., 2011. Influence of polyvinyl alcohol on the surface morphology, separation and anti-fouling performance of the composite polyamide nanofiltration membranes. *Journal of Membrane Science*, *367*(1), pp.158-165

Anirudhan, T. S., Rijith, S., 2012. Synthesis and characterization of carboxyl terminated Poly (methacrylic acid) grafted chitosan/bentonite composite and its application for the recovery of uranium (VI) from aqueous media. Journal of Environmental Radioactivity, 106: 8-19.

Anirudhan, T.S. and Rijith, S., 2012. Synthesis and characterization of carboxyl terminated poly (methacrylic acid) grafted chitosan/bentonite composite and its application for the recovery of uranium (VI) from aqueous media. *Journal of Environmental Radioactivity*, *106*, pp.8-19.

Arkhangelsky, E., Kuzmenko, D. and Gitis, V., 2007. Impact of chemical cleaning on properties and functioning of polyethersulfone membranes. *Journal of Membrane Science*, *305*(1-2), pp.176-184.

Aroon, M.A., Ismail, A.F., Matsuura, T. and Montazer-Rahmati, M.M., 2010a. Performance studies of mixed matrix membranes for gas separation: a review. *Separation and purification Technology*, *75*(3), pp.229-242.

Aroon, M.A., Ismail, A.F., Montazer-Rahmati, M.M. and Matsuura, T., 2010b. Effect of chitosan as a functionalization agent on the performance and separation properties of polyimide/multi-walled carbon nanotubes mixed matrix flat sheet membranes. *Journal of membrane science*, *364*(1-2), pp.309-317.

Bai, H., Wang, H., Zhang, J., Wu, C., Zhang, J., Xiang, Y. and Lu, S., 2018. Simultaneously enhancing ionic conduction and mechanical strength of poly (ether sulfones)-poly (vinyl pyrrolidone) membrane by introducing graphitic carbon nitride nanosheets for high temperature proton exchange membrane fuel cell application. *Journal of Membrane Science*, *558*, pp.26-33.

Baker, R.W., 2004a. Membrane technology and applications. *John Wiley & Sons, Ltd*, pp.96-103.

Baker, R.W., 2004b. Overview of membrane science and technology. *Membrane Technology and Applications, Second Edition*, pp.1-14.

Balintova, M. and Petrilakova, A., 2011. Study of pH influence on selective precipitation of heavy metals from acid mine drainage. *Chemical Engineering Transactions*, *25*, pp.1-6.

Barth, C., Goncalves, M.C., Pires, A.T.N., Roeder, J. and Wolf, B.A., 2000. Asymmetric polysulphone and polyethersulphone membranes: effects of thermodynamic conditions during formation on their performance. *Journal of Membrane Science*, *169*(2), pp.287-299.

Barbosa, H.F., Francisco, D.S., Ferreira, A.P. and Cavalheiro, É.T., 2019. A new look towards the thermal decomposition of chitins and chitosans with different degrees of deacetylation by coupled TG-FTIR. *Carbohydrate polymers*, *225*, p.115232.

Belfer, S., Fainchtain, R., Purinson, Y. and Kedem, O., 2000. Surface characterization by FTIR-ATR spectroscopy of polyethersulfone membranes-unmodified, modified and protein fouled. *Journal of Membrane Science*, *172*(1), pp.113-124

Bhatnagar, A., Minocha, A.K., Pudasainee, D., Chung, H.K., Kim, S.H., Kim, H.S., Lee, G., Min, B. and Jeon, B.H., 2008. Vanadium removal from water by waste metal sludge and cement immobilization. *Chemical Engineering Journal*, *144*(2), pp.197-204.

Bi, Q., Li, Q., Tian, Y., Lin, Y. and Wang, X., 2013. Hydrophilic modification of poly (vinylidene fluoride) membrane with poly (vinyl pyrrolidone) via a cross-linking reaction. *Journal of Applied Polymer Science*, *127*(1), pp.394-401.

Blanpain-Avet, P., Fillaudeau, L. and Lalande, M., 1999. Investigation of mechanisms governing membrane fouling and protein rejection in the sterile microfiltration of beer with an organic membrane. *Food and bioproducts processing*, *77*(2), pp.75-89.

Bolong, N., Ismail, A.F., Salim, M.R., Rana, D. and Matsuura, T., 2009. Development and characterization of novel charged surface modification macromolecule to polyethersulfone hollow fiber membrane with polyvinylpyrrolidone and water. *Journal of Membrane Science*, *331*(1-2), pp.40-49.

Boricha, A.G. and Murthy, Z.V.P., 2009. Acrylonitrile butadiene styrene/chitosan blend membranes: preparation, characterization and performance for the separation of heavy metals. *Journal of Membrane Science*, *339*(1), pp.239-249.

Brown, B.E., Clarke, K.R. and Warwick, R.M. (2002). Serial patterns of biodiversity change in corals across shallow reef flats in Ko Phuket, Thailand, due to the effects of local (sedimentation) and regional (climatic) perturbations. *Marine Biology, 141*, 24-29.

Brüger, A., Fafilek, G. and Rojas-Mendoza, L., 2018. On the volatilisation and decomposition of cyanide contaminations from gold mining. *Science of The Total Environment*, *627*, pp.1167-1173.

Brugnerotto, J., Lizardi, J., Goycoolea, F.M., Argüelles-Monal, W., Desbrieres, J. and Rinaudo, M., 2001. An infrared investigation in relation with chitin and chitosan characterization. *Polymer*, *42*(8), pp.3569-3580.

Bwapwa, J.K., Jaiyeola, A.T. and Chetty, R., 2017. Bioremediation of acid mine drainage using algae strains: A review. *South African Journal of Chemical Engineering*, *24*, pp.62-70.

Carvalho, A.L., Maugeri, F., Pradanos, P., Silva, V. and Hernandez, A., 2011. Separation of potassium clavulanate and potassium chloride by nanofiltration: Transport and evaluation of membranes. *Separation and purification technology*, *83*, pp.23-30.

Cha, B.J. and Yang, J.M., 2006. Effect of high-temperature spinning and PVP additive on the properties of PVDF hollow fiber membranes for microfiltration. *Macromolecular Research*, *14*(6), pp.596-602.

Chen, T., Yan, B., Lei, C. and Xiao, X., 2014. Pollution control and metal resource recovery for acid mine drainage. *Hydrometallurgy*, *147*, pp.112-119.

Chen, X.G., Zheng, L., Wang, Z., Lee, C.Y. and Park, H.J., 2002. Molecular affinity and permeability of different molecular weight chitosan membranes. *Journal of Agricultural and Food Chemistry*, *50*(21), pp.5915-5918.

Chen, Y., Zhang, Y., Liu, J., Zhang, H. and Wang, K., 2012. Preparation and antibacterial property of polyethersulfone ultrafiltration hybrid membrane containing halloysite nanotubes loaded with copper ions. *Chemical Engineering Journal*, *210*, pp.298-308.

Chen, Y., Zhang, Y., Zhang, H., Liu, J. and Song, C., 2013. Biofouling control of halloysite nanotubes-decorated polyethersulfone ultrafiltration membrane modified with chitosan-silver nanoparticles. *Chemical Engineering Journal*,*228*, pp.12-20.

Cheng, T.W. and Lin, C.T., 2004. A study on cross-flow ultrafiltration with various membrane orientations. *Separation and Purification Technology*, *39*(1-2), pp.13-22.

Cheryan, M., 1998. *Ultrafiltration and Microfiltration Handbook*. CRC press.

Chethan, P.D. and Vishalakshi, B., 2013. Synthesis of ethylenediamine modified chitosan and evaluation for removal of divalent metal ions. *Carbohydrate Polymers*, *97*(2), pp.530-536.

Choi, H., Zhang, K., Dionysiou, D.D., Oerther, D.B. and Sorial, G.A., 2005. Effect of permeate flux and tangential flow on membrane fouling for wastewater treatment. *Separation and Purification Technology*, *45*(1), pp.68-78.

Coetzee, H., Hobbs, P. J., Burgess, J. E., Thomas, A., Keet, M., Yibas, B., van Tonder, D.,Netili, F., Rust, U., Wade, P. & Maree, J. P. 2010 Mine water management in the Witwatersrand gold fields with special emphasis on Acid Mine Drainage. Report to the Inter-ministerial Committee on Acid Mine Drainage 1–128.

Coetzee, H., Winde, F., Wade, P.W., 2006. An assessment of sources, pathways, mechanisms and risks of current and potential future pollution of water and sediments in gold-mining areas of the Wonderfonteinspruit catchment. Report No. 1214/06. Water Research Commission, Pretoria.

Corbatón-Báguena, M.J., Vincent-Vela, M.C., Gozálvez-Zafrilla, J.M., Álvarez-Blanco, S., Lora-García, J. and Catalán-Martínez, D., 2016. Comparison between artificial neural networks and Hermia's models to assess ultrafiltration performance. *Separation and Purification Technology*, *170*, pp.434-444.

Crespo, G.A., Afshar, M.G. and Bakker, E., 2014. Chronopotentiometry of pure electrolytes with anion-exchange Donnan exclusion membranes. *Journal of Electroanalytical Chemistry*, *731*, pp.100-106

Cui, Z.F., Jiang, Y. and Field, R.W., 2010. Fundamentals of pressure-driven membrane separation processes. In *Membrane Technology* (pp. 1-18).

Danielson, L., MacShame, F., 2003. Dialogue on indigenous people and the mining sector. A Report based on the work of the Mining, Minerals and Sustainable Development (MMSD)

Daraei, P., Madaeni, S.S., Ghaemi, N., Salehi, E., Khadivi, M.A., Moradian, R. and Astinchap, B., 2012. Novel polyethersulfone nanocomposite membrane prepared by PANI/Fe 3 O 4 nanoparticles with enhanced performance for Cu (II) removal from water. *Journal of Membrane Science*, *415*, pp.250-259.

Daramola, M.O., Silinda, B., Masondo, S. and Oluwasina, O.O., 2015. Polyethersulphone-sodalite (PES-SOD) mixed-matrix membranes: Prospects for acid mine drainage (AMD) treatment. *Journal of the Southern African Institute of Mining and Metallurgy*, *115*(12), pp.1221-1228.

De Barros, S.T.D., Andrade, C.M.G., Mendes, E.S. and Peres, L., 2003. Study of fouling mechanism in pineapple juice clarification by ultrafiltration. *Journal of membrane Science*, *215*(1-2), pp.213-224.

DEPARTMENT OF WATER AFFAIRS, SOUTH AFRICA, 2012. Feasibility study for a long-term solution to address the acid mine drainage associated with the East, Central and West Rand underground mining basins: DWA Report. No.: P RSA 000/00/16512/2. Resource Water Quality Objectives (RWQOs), Directorate: Water Resource Planning Systems, Chief Directorate: Integrated Water Resource Planning.

Durand, J. F., Meeuvis, J., & Fourie, M. (2010). The threat of mine effluent to the UNESCO status of the Cradle of Humankind World Heritage Site. *TD: The Journal for Transdisciplinary Research in Southern Africa*, *6*(1), 73-92

Durand, J.F., 2012. The impact of gold mining on the Witwatersrand on the rivers and karst system of Gauteng and North-West Province, South Africa. *Journal of African Earth Sciences*, *68*, pp.24-43.

DWAF (Department of Water Affairs and Forestry of the Republic of South Africa), 1996a. South African Water Quality Guidelines. Domestic Water Use, vol. 1, 2nd ed.

DWAF (Department of Water Affairs and Forestry of the Republic of South Africa), 1996b. South African Water Quality Guidelines, Agricultural Use: Irrigation, vol.4, 2nd ed.

Elimelech, M. and Phillip, W.A., 2011. The future of seawater desalination: energy, technology, and the environment. *Science*, *333*(6043), pp.712-717.

EPA, 2011. Reducing mercury pollution from gold mining. Available [Online]:. http:// www.epa.gov/oia/toxics/asgm.htm Accessed 03/07/2018

Faibish, R.S. and Cohen, Y., 2001. Fouling-resistant ceramic-supported polymer membranes for ultrafiltration of oil-in-water microemulsions. *Journal of Membrane Science*, *185*(2), pp.129-143.

Feng, Y., Xiong, T., Xu, H., Li, C. and Hou, H., 2016. Polyamide-imide reinforced polytetrafluoroethylene nanofiber membranes with enhanced mechanical properties and thermal stabilities. *Materials Letters*, *182*, pp.59-62.

Fernando, W.A.M., Ilankoon, I.M.S.K., Syed, T.H. and Yellishetty, M., 2018. Challenges and opportunities in the removal of sulphate ions in contaminated mine water: A review. *Minerals Engineering*, *117*, pp.74-90.

Field, R.W., Wu, D., Howell, J.A. and Gupta, B.B., 1995. Critical flux concept for microfiltration fouling. *Journal of membrane science*, *100*(3), pp.259-272.

Fourie, M., 2005. A rising acid tide, Johannesburg Mail and Guardian, South, Africa, 12 April 2005.

Freger, V., 2005. Kinetics of film formation by interfacial polycondensation. *Langmuir*, *21*(5), pp.1884-1894.

Gao, J., Sun, S.P., Zhu, W.P. and Chung, T.S., 2014. Chelating polymer modified P84 nanofiltration (NF) hollow fiber membranes for high efficient heavy metal removal. *Rater Research*, *63*, pp.252-261.

Gámiz-González, M.A., Correia, D.M., Lanceros-Mendez, S., Sencadas, V., Ribelles, J.G. and Vidaurre, A., 2017. Kinetic study of thermal degradation of chitosan as a function of deacetylation degree. *Carbohydrate polymers*, *167*, pp.52-58.

Garni, M., Thamboo, S., Schoenenberger, C.A. and Palivan, C.G., 2017. Biopores/membrane proteins in synthetic polymer membranes. *Biochimica et Biophysica Acta (BBA)-Biomembranes*, *1859*(4), pp.619-638.

GDARD, 2011. Feasibility Study on Reclamation of Mine Residue Areas for Development Purposes: Phase II Strategy and Implementation Plan, December 2011. Report No. 788/06/02/2011 (Final). Umvoto Africa (Chris Hartnady & Andiswa Mlisa) in association with TouchStone Resources (Anthony Turton).

Geise, G.M., Lee, H.S., Miller, D.J., Freeman, B.D., McGrath, J.E. and Paul, D.R., 2010. Water purification by membranes: the role of polymer science. *Journal of Polymer Science Part B: Polymer Physics*, *48*(15), pp.1685-1718.

Ghaemi, N., Madaeni, S.S., Daraei, P., Rajabi, H., Zinadini, S., Alizadeh, A., Heydari, R., Beygzadeh, M. and Ghouzivand, S., 2015. Polyethersulfone membrane enhanced with iron oxide nanoparticles for copper removal from water: application of new functionalized Fe3O4 nanoparticles. *Chemical Engineering Journal*, *263*, pp.101-112.

Gherasim, C.V., Cuhorka, J. and Mikulášek, P., 2013. Analysis of lead (II) retention from single salt and binary aqueous solutions by a polyamide nanofiltration membrane: experimental results and modelling. *Journal of Membrane Science*, *436*, pp.132-144.

Gherasim, C.V., Hancková, K., Palarčík, J. and Mikulášek, P., 2015. Investigation of cobalt (II) retention from aqueous solutions by a polyamide nanofiltration membrane. *Journal of Membrane Science*, *490*, pp.46-56.

Ghiggi, F.F., Pollo, L.D., Cardozo, N.S. and Tessaro, I.C., 2017. Preparation and characterization of polyethersulfone/N-phthaloyl-chitosan ultrafiltration membrane with antifouling property. *European Polymer Journal*, *92*, pp.61-70.

Gkotsis, P., Banti, D., Peleka, E., Zouboulis, A. and Samaras, P., 2014. Fouling issues in membrane bioreactors (MBRs) for wastewater treatment: major mechanisms, prevention and control strategies. *Processes*, *2*(4), pp.795-866.

Gonzalez, M.I., Alvarez, S., Riera, F.A. and Alvarez, R., 2008. Lactic acid recovery from whey ultrafiltrate fermentation broths and artificial solutions by nanofiltration. *Desalination*, *228*(1-3), pp.84-96.

Gray, N.F., (1999). Field assessment of acid mine drainage contamination in surface and ground water. *Environmental Geology*,*27*, 358e361.

Gumbi, N.N., Hu, M., Mamba, B.B., Li, J. and Nxumalo, E.N., 2018. Macrovoid-free PES/SPSf/O-MWCNT ultrafiltration membranes with improved mechanical strength, antifouling and antibacterial properties. *Journal of Membrane Science*, *566*, pp.288-300.

Guerrero-Flores, A.D., Uribe-Salas, A., Dávila-Pulido, G.I. and Flores-Álvarez, J.M., 2018. Simultaneous removal of calcium and sulfate ions from flotation water of complex sulfides. *Minerals Engineering*, *123*, pp.28-34.

Guo, X., Li, Q., Hu, W., Gao, W. and Liu, D., 2009. Ultrafiltration of dissolved organic matter in surface water by a polyvinylchloride hollow fiber membrane. *Journal of Membrane Science*, *327*(1), pp.254-263.

Gusek, J. and K. Clarke-Whistler (2005). Where Does the Recovery of Metal Resources from Passive Treatment Systems Fit in Sustainable Development Initiatives Associated with Large Mining Projects? Annual Meeting of the American Society for Mining and Reclamation, Breckenridge, USA

Hallberg, K. (2010). New perspectives in acid mine drainage microbiology.*Hydrometallurgy, 104(3)*, 448-453.

Hedin, R. S. (2003). Recovery of marketable iron oxide from mine drainage in the USA.

Hermia, J., 1982. Constant pressure blocking filtration laws-application to power-law non-Newtonian fluids. *Chem. Eng. Res. Des., 60*, pp.183-187.

Hermia, J., 1966. Etude analytique des lois de filtration à pression constante. *Rev. Univ. Mines, 2*(5).

Hilal, N., Al-Zoubi, H., Mohammad, A.W. and Darwish, N.A., 2005. Nanofiltration of highly concentrated salt solutions up to seawater salinity. *Desalination*, *184*(1-3), pp.315-326.

Hobbs, P.J., Cobbing, J.E., (2007). A hydrogeological assessment of acid mine drainage impacts in the West Rand Basin, Gauteng Province. Rep. No. CSIR/NRE/WR/ER/2007/0097/C. CSIR, Pretoria, South Africa.

Hongpattarakere, T. and Riyaphan, O., 2008. Effect of deacetylation conditions on antimicrobial activity of chitosans prepared from carapace of black tiger shrimp. *Songklanakarin Journal of Science & Technology*, *30*.

Huang, J., Xue, J., Xiang, K., Zhang, X., Cheng, C., Sun, S. and Zhao, C., 2011. Surface modification of polyethersulfone membranes by blending triblock copolymers of methoxyl poly (ethylene glycol)–polyurethane–methoxyl poly (ethylene glycol). *Colloids and Surfaces B: Biointerfaces*, *88*(1), pp.315-324.

Huang, H., Young, T.A. and Jacangelo, J.G., 2007. Unified membrane fouling index for low pressure membrane filtration of natural waters: principles and methodology. *Environmental science & technology*, *42*(3), pp.714-720.

Hughes, T., Taha, Z. 2007 Cui, Mass transfer: membrane processes, in: S.S. Sablani (Ed.), Handbook of Food and Bioprocess Modelling Techniques, CRC Press, Boca Raton, FL, pp. 145–177.

Hustwit CC, Ackman TE, Erickson PE (1992). The role of oxygen transfer in acid mine drainage treatment. Water Environ Res 64:817–823

Hussain, M.R., Iman, M. and Maji, T.K., 2013. Determination of degree of deacetylation of chitosan and their effect on the release behavior of essential oil from chitosan and chitosan-gelatin complex microcapsules. *International Journal of Advanced Engineering Applications*, *6*(4), pp.4-12.

Hwang, K.J. and Lin, T.T., 2002. Effect of morphology of polymeric membrane on the performance of crossflow microfiltration. *Journal of Membrane Science*, *199*(1-2), pp.41-52.

Hwang, S.K. and Jho, E.H., 2018. Heavy metal and sulfate removal from sulfate-rich synthetic mine drainages using sulfate reducing bacteria. *Science of the Total Environment*, *635*, pp.1308-1316.

Jarvis, A.P., Younger, P.L., 2000. Broadening the scope of mine water environmental impact assessment: a UK perspective. *Environmental Impact Assessment Review*, *20*, 85e96.

Jepsen, K.L., Bram, M.V., Pedersen, S. and Yang, Z., 2018. Membrane fouling for produced water treatment: A review study from a process control perspective. *Water*, *10*(7), p.847

Ji, J., Wu, D., Cao, Z., Deng, L. and Yun, Y., 2015. Preparation and evaluation of poly (phthalazinone ether sulfone ketone) ultrafiltration membrane with organic and inorganic nano-TiO2 additives. *Journal of Sol-gel Science and Technology*, *76*(2), pp.446-455.

Ji, Y., An, Q., Zhao, Q., Chen, H. and Gao, C., 2011. Preparation of novel positively charged copolymer membranes for nanofiltration. *Journal of Membrane Science*, *376*(1-2), pp.254-265.

Ji, Y.L., Ang, M.B.M.Y., Huang, S.H., Lu, J.Y., Tsai, S.J., De Guzman, M.R., Tsai, H.A., Hu, C.C., Lee, K.R. and Lai, J.Y., 2019. Performance evaluation of nanofiltration polyamide membranes based from 3, 3′-diaminobenzidine. *Separation and Purification Technology*, *211*, pp.170-178.

Johnson, D. B. and K. B. Hallberg (2005). Acid mine drainage remediation options: a review. Science of the total environment *338(1),* 3-14.

Johnson, D. Barrie. (1995) "Acidophilic microbial communities: candidates for bioremediation of acidic mine effluents." *International Biodeterioration & Biodegradation 35.1,* 41-58

Juang, R.S. and Shao, H.J., 2002. A simplified equilibrium model for sorption of heavy metal ions from aqueous solutions on chitosan. *Water Research*, *36*(12), pp.2999-3008.

Judd, S., 2010. *The MBR book: principles and applications of membrane bioreactors for water and wastewater treatment*. Elsevier.

Kaur, G., Couperthwaite, S.J., Hatton-Jones, B.W. and Millar, G.J., 2018. Alternative neutralisation materials for acid mine drainage treatment. *Journal of Water Process Engineering*, *22*, pp.46-58.

Kefeni, K.K., Mamba, B.B. and Msagati, T.A., 2017a. Magnetite and cobalt ferrite nanoparticles used as seeds for acid mine drainage treatment. *Journal of Hazardous Materials*, *333*, pp.308-318.

Kefeni, K.K., Msagati, T.A. and Mamba, B.B., 2017b. Acid mine drainage: prevention, treatment options, and resource recovery: a review. *Journal of Cleaner Production*, *151*, pp.475-493.

Khulbe, K.C., Feng, C. and Matsuura, T., 2010. The art of surface modification of synthetic polymeric membranes. *Journal of Applied Polymer Science*, *115*(2), pp.855-895.

Khulbe, K.C., Feng, C. and Matsuura, T., 2010. The art of surface modification of synthetic polymeric membranes. *Journal of Applied Polymer Science*, *115*(2), pp.855-895.

Kim, I.C., Jegal, J. and Lee, K.H., 2002. Effect of aqueous and organic solutions on the performance of polyamide thin-film-composite nanofiltration membranes. *Journal of Polymer Science Part B: Polymer Physics*, *40*(19), pp.2151-2163.

Kim, S.H., Kwak, S.Y. and Suzuki, T., 2005. Positron annihilation spectroscopic evidence to demonstrate the flux-enhancement mechanism in morphology-controlled thin-film-composite (TFC) membrane. *Environmental Science & Technology*, *39*(6), pp.1764-1770.

Kimura, K., Hane, Y., Watanabe, Y., Amy, G. and Ohkuma, N., 2004. Irreversible membrane fouling during ultrafiltration of surface water. *Water Research*, *38*(14), pp.3431-3441.

Knoell, T., Safarik, J., Cormack, T., Riley, R., Lin, S.W. and Ridgway, H., 1999. Biofouling potentials of microporous polysulfone membranes containing a sulfonated polyether-ethersulfone/polyethersulfone block copolymer: correlation of membrane surface properties with bacterial attachment. *Journal of Membrane Science*, *157*(1), pp.117-138.

Koĺtuniewicz, A.B. and Field, R.W., 1996. Process factors during removal of oil-in-water emulsions with cross-flow microfiltration. *Desalination*, *105*(1-2), pp.79-89.

Kołtuniewicz, A.B. (2005). The history and state of art in membrane technologies. Retrieved from: http://www.etseq.urv.es/assignatures/ops/presentacio_membranes.pdf (Accessed 19 March 2018).

Kong, C., Shintani, T., Kamada, T., Freger, V. and Tsuru, T., 2011. Co-solvent-mediated synthesis of thin polyamide membranes. *Journal of Membrane Science*, *384*(1), pp.10-16.

Koros, W.J., Ma, Y.H. and Shimidzu, T., 1996. Terminology for membranes and membrane processes. *Journal Membrane Science*, *120*(2), pp.149-159.

Koros, W.J., Ma, Y.H. and Shimidzu, T., 1996. Terminology for membranes and membrane processes (IUPAC Recommendations 1996). *Pure and Applied Chemistry*, *68*(7), pp.1479-1489.

Kumari, S., Annamareddy, S.H.K., Abanti, S. and Rath, P.K., 2017. Physicochemical properties and characterization of chitosan synthesized from fish scales, crab and shrimp shells. *International Journal of Biological Macromolecules*, *104*, pp.1697-1705.

Labbez, C., Fievet, P., Thomas, F., Szymczyk, A., Vidonne, A., Foissy, A. and Pagetti, P., 2003. Evaluation of the "DSPM" model on a titania membrane: measurements of charged and uncharged solute retention, electrokinetic charge, pore size, and water permeability. *Journal of Colloid and Interface Science*, *262*(1), pp.200-211.

Lau, W.J. and Ismail, A.F., 2011, August. Progress in interfacial polymerization technique on composite membrane preparation. In *Proceedings of the 2nd International Conference on Environmental Engineering and Applications, Shanghai, China* (pp. 19-21).

Lens, P.N.L. and Kuenen, J.G., 2001. The biological sulfur cycle: novel opportunities for environmental biotechnology. *Water Science and Technology*, *44*(8), pp.57-66.

Leštan, D., Luo, C.L. and Li, X.D., 2008. The use of chelating agents in the remediation of metal-contaminated soils: a review. *Environmental Pollution*, *153*(1), pp.3-13.

Li, H., Xia, H. and Mei, Y., 2016. Modeling organic fouling of reverse osmosis membrane: From adsorption to fouling layer formation. *Desalination*, *386*, pp.25-31.

Linde, K. and Jönsson, A.S., 1995. Nanofiltration of salt solutions and landfill leachate. *Desalination*, *103*(3), pp.223-232.

Liu, C.X., Zhang, D.R., He, Y., Zhao, X.S. and Bai, R., 2010. Modification of membrane surface for anti-biofouling performance: Effect of anti-adhesion and anti-bacteria approaches. *Journal of Membrane Science*, *346*(1), pp.121-130.

Liu, F., Hashim, N.A., Liu, Y., Abed, M.M. and Li, K., 2011. Progress in the production and modification of PVDF membranes. *Journal of membrane science*, *375*(1-2), pp.1-27.

Liu, B., Wang, D., Yu, G. and Meng, X., 2013. Adsorption of heavy metal ions, dyes and proteins by chitosan composites and derivatives—A review. *Journal of Ocean University of China*, *12*(3), pp.500-508

Luis, P. ed., 2018. *Fundamental Modeling of Membrane Systems: Membrane and Process Performance*. Elsevier.

Lottermoser, B.G., 2011. Recycling, reuse and rehabilitation of mine wastes. *Elements*, *7*(6), pp.405-410.

Louie, J.S., Pinnau, I., Ciobanu, I., Ishida, K.P., Ng, A. and Reinhard, M., 2006. Effects of polyether–polyamide block copolymer coating on performance and fouling of reverse osmosis membranes. *Journal of Membrane Science*, *280*(1-2), pp.762-770.

Lusilao-Makiese, J.G., Cukrowska, E.M., Tessier, E., Amouroux, D. and Weiersbye, I., 2013. The impact of post gold mining on mercury pollution in the West Rand region, Gauteng, South Africa. *Journal of Geochemical Exploration*, *134*, pp.111-119.

Ma, B., Yu, W., Jefferson, W.A., Liu, H. and Qu, J., 2015. Modification of ultrafiltration membrane with nanoscale zerovalent iron layers for humic acid fouling reduction. *Water research*, *71*, pp.140-149.

Malehase, T., Daso, A.P. and Okonkwo, J.O., 2016. Determination of mercury and its fractionation products in samples from legacy use of mercury amalgam in gold processing in Randfontein, South Africa. *Emerging Contaminants*, *2*(3), pp.157-165.

Manahan, S.E.,2005,Environmental chemistry,8th edition CRC Press,Boca Raton,Fla.

Maphutha, S., Moothi, K., Meyyappan, M. and Iyuke, S.E., 2013. A carbon nanotube-infused polysulphone membrane with polyvinyl alcohol layer for treating oil-containing waste water. *Scientific reports*, *3*.

Marei, N.H., El-Samie, E.A., Salah, T., Saad, G.R. and Elwahy, A.H., 2016. Isolation and characterization of chitosan from different local insects in Egypt. *International Journal of Biological Macromolecules*, *82*, pp.871-877.

Masindi, V., Gitari, M.W., Tutu, H. and DeBeer, M., 2015. Efficiency of ball milled South African bentonite clay for remediation of acid mine drainage. *Journal of Water Process Engineering*, *8*, pp.227-240.

Masukume, M.; Onyango, M. S.; Maree, J. P. (2014) Sea Shell Derived Adsorbent and Its Potential for Treating Acid Mine Drainage. Int. J. Miner. Process., 133, 52-59.

Maximous, N., Nakhla, G., Wong, K. and Wan, W., 2010. Optimization of Al 2 O 3/PES membranes for wastewater filtration. *Separation and Purification Technology*, *73*(2), pp.294-301.

McCarthy, T., Rubidge, B., 2005. The Story of Earth & Life. A Southern African Perspective on a 4.6-Billion-Year Journey. 334 pp. Cape Town: Struik Publishers/Johnnic Publishing Group).

McCarthy, T.S. and Venter, J.S., 2006. Increasing pollution levels on the Witwatersrand recorded in the peat deposits of the Klip River wetland. *South African Journal of Science*, *102*(1-2), pp.27-34.

McCarthy, T.S., 2011. The impact of acid mine drainage in South Africa. S. Afr. J. Earth Sci. 107 (5/6), 7, http://dx.doi.org/10.4102/sajs.v107i5/6.712, Art. 712.

McDonald, D.M., Webb, J.A. and Musgrave, R.J., 2006. The effect of neutralisation method and reagent on the rate of Cu and Zn release from acid rock drainage treatment sludges. *Proceedings of the 7th ICARD, St. Louis, MO, USA, March*, pp.1198-1218.

Metesh, J.J., Jarrell, T. and Oravetz, S., 1998. *Treating acid mine drainage from abandoned mines in remote areas* (Vol. 9871). Missoula, MT: USDA Forest Service, Technology and Development Program.

Misdan, N., Lau, W.J. and Ismail, A.F., 2012. Seawater Reverse Osmosis (SWRO) desalination by thin-film composite membrane—Current development, challenges and future prospects. *Desalination*, *287*, pp.228-237.

Mohammadi, T., Kazemimoghadam, M. and Saadabadi, M., 2003. Modeling of membrane fouling and flux decline in reverse osmosis during separation of oil in water emulsions. *Desalination*, *157*(1-3), pp.369-375.

Mthethwa, V., 2014, Investigation of Polyethersulphone (PES) Hollow Fiber Membrane for The Treatment of Acid Mine Drainage, Research Report Master of Science In Engineering, Faculty of Engineering And The Built Environment, University Of The Witwatersrand, Johannesburg.

Mu, L.J. and Zhao, W.Z., 2009. Hydrophilic modification of polyethersulfone porous membranes via a thermal-induced surface crosslinking approach. *Applied Surface Science*, *255*(16), pp.7273-7278.

Muir, A., Mitchell, J., Flatman, S. and Sabbagha, C., 2016. Retreatment of gold residues. In *Gold Ore Processing (Second Edition)* (pp. 709-728).

Naicker, K., Cukrowska, E. and McCarthy, T.S., 2003. Acid mine drainage arising from gold mining activity in Johannesburg, South Africa and environs. *Environmental Pollution*, *122*(1), pp.29-40.

Neculita, C.-M., G. J. Zagury, et al. (2007). Passive treatment of acid mine drainage in bioreactors using sulfate-reducing bacteria. *Journal of Environmental Quality 36(1)*, 1-16.

Nędzarek, A., Drost, A., Harasimiuk, F.B. and Tórz, A., 2015. The influence of pH and BSA on the retention of selected heavy metals in the nanofiltration process using ceramic membrane. *Desalination*, *369*, pp.62-67.

Neumann, S. and Fatula, P., 2009. Principles of Ion Exchange in Wastewater Treatment. *Asian Water*, *19*.

Ngah, W.S. and Isa, I.M., 1998. Comparison study of copper ion adsorption on chitosan, Dowex A-1, and Zerolit 225. *Journal of Applied Polymer Science*, *67*(6), pp.1067-1070.

Nhlengetwa, K. and Hein, K.A., 2015. Zama-Zama mining in the Durban Deep/Roodepoort area of Johannesburg, South Africa: An invasive or alternative livelihood?. *The Extractive Industries and Society*, *2*(1), pp.1-3.

Nhlengetwa, K. and Hein, K.A., 2015. Zama-Zama mining in the Durban Deep/Roodepoort area of Johannesburg, South Africa: An invasive or alternative livelihood?. *The Extractive Industries and Society*, *2*(1), pp.1-3.

Nhlengetwa, K. and Hein, K.A., 2015. Zama-Zama mining in the Durban Deep/Roodepoort area of Johannesburg, South Africa: An invasive or alternative livelihood?. *The Extractive Industries and Society*, *2*(1), pp.1-3.

Oberholster, P.J, B. Genthe ,B, Hobbs, P, Cheng, P.H, de Klerk, A.R, Botha, A.-M, (2013). An ecotoxicological screening tool to prioritise acid mine drainage impacted streams for future restoration. *Environmental Pollution 176,* 244-253.

Ochieng, G., E. Seanego, and O. Nkwonta, (2010). Impacts of mining on water resources in South Africa: A review. *Scientific Research and Essays* 5.22 (2010): 3351-3357.

Oelofse, S., P.Hobbs Rashcer ,J.,and Cobbing J.E. (2007) The pollution and Destruction Threat of Gold Mining Waste on the Witwatersrand: A West Rand Case Study. 10th International Symposium on Environmental Issues and Waste management in Energy and Mineral Production(SWEMP) ,Bangkok, Thailand

Othman, A., Sulaiman, A. and Sulaiman, S.K., 2017. Carbide lime in acid mine drainage treatment. *Journal of Water Process Engineering*, *15*, pp.31-36.

Palmer, Margaret A., E. S. Bernhardt, W. H. ,Schlesinger, K. N. Eshleman, E. Foufoula-Georgiou, M. S. Hendryx, A. D. Lemly, G. E. ,Likens, O. L. Loucks, M. E. Power, P. S. White, P. R. Wilcock (2010). Mountain top mining consequences. *Science, 327, 5962* (2010): 148-149.

Palpandi, C., Shanmugam, V. and Shanmugam, A., 2009. Extraction of chitin and chitosan from shell and operculum of mangrove gastropod Nerita (Dostia) crepidularia Lamarck. *International Journal of Medicine and Medical Sciences*, *1*(5), pp.198-205.

Peyravi, M., Rahimpour, A., Jahanshahi, M., Javadi, A. and Shockravi, A., 2012. Tailoring the surface properties of PES ultrafiltration membranes to reduce the fouling resistance using synthesized hydrophilic copolymer. *Microporous and Mesoporous Materials*, *160*, pp.114-125.

Peyravi, M., Rahimpour, A., Jahanshahi, M., Javadi, A. and Shockravi, A., 2012. Tailoring the surface properties of PES ultrafiltration membranes to reduce the fouling resistance using synthesized hydrophilic copolymer. *Microporous and Mesoporous Materials*, *160*, pp.114-125.

Pierre Louis, A.M., Yu, H., Shumlas, S.L., Van Aken, B., Schoonen, M.A. and Strongin, D.R., 2015. Effect of phospholipid on pyrite oxidation and microbial communities under simulated acid mine drainage (AMD) conditions. *Environmental Science & Technology*, *49*(13), pp.7701-7708.

Popuri, S. R., Vijaya, Y., Boddu, V. M., & Krishnaiah, A. (2009). Adsorptive removal of copper and nickel ions from water using chitosan coated PVC beads. *Bioresource Technology*, 100, 194–199.

Qu, X., Alvarez, P.J. and Li, Q., 2013. Applications of nanotechnology in water and wastewater treatment. *Water Research*, *47*(12), pp.3931-3946.

Rahimpour, A., Madaeni, S.S., Shockravi, A. and Ghorbani, S., 2009. Preparation and characterization of hydrophile nano-porous polyethersulphone membranes using synthesized poly (sulfoxide-amide) as additive in the casting solution. *Journal of Membrane Science*, *334*(1), pp.64-73.

Rana, D. and Matsuura, T., 2010. Surface modifications for antifouling membranes. *Chemical reviews*, *110*(4), pp.2448-2471.

Raphulu, M.C. and Scurrell, M.S., 2015. Cyanide leaching of gold catalysts. *Catalysis Communications*, *67*, pp.87-89.

Rawlings, D.E. and Kusano, T., 1994. Molecular genetics of Thiobacillus ferrooxidans. *Microbiological Reviews*, *58*(1), pp.39-55.

Razmjou, A., Mansouri, J. and Chen, V., 2011. The effects of mechanical and chemical modification of TiO 2 nanoparticles on the surface chemistry, structure and fouling performance of PES ultrafiltration membranes. *Journal of Membrane Science*, *378*(1), pp.73-84.

Reddy, A.V.R., Mohan, D.J., Bhattacharya, A., Shah, V.J. and Ghosh, P.K., 2003. Surface modification of ultrafiltration membranes by preadsorption of a negatively charged polymer: I. Permeation of water soluble polymers and inorganic salt solutions and fouling resistance properties. *Journal of Membrane Science*, *214*(2), pp.211-221.

Reiad, N.A., Salam, O.E.A., Abadir, E.F. and Harraz, F.A., 2012. Adsorptive removal of iron and manganese ions from aqueous solutions with microporous chitosan/polyethylene glycol blend membrane. *Journal of Environmental Sciences*, *24*(8), pp.1425-1432.

Ricci, B.C., Ferreira, C.D., Aguiar, A.O. and Amaral, M.C., 2015. Integration of nanofiltration and reverse osmosis for metal separation and sulfuric acid recovery from gold mining effluent. *Separation and Purification Technology*, *154*, pp.11-21.

Richards, H.L., Baker, P.G. and Iwuoha, E., 2012. Metal nanoparticle modified polysulfone membranes for use in wastewater treatment: a critical review. *Journal of Surface Engineered Materials and Advanced Technology*, *2*(03), p.183.

Rinaudo, M., 2006. Chitin and chitosan: properties and applications. *Progress in Polymer science*, *31*(7), pp.603-632.

Rinaudo, M., Pavlov, G. and Desbrieres, J., 1999. Influence of acetic acid concentration on the solubilization of chitosan. *Polymer*, *40*(25), pp.7029-7032.

Ritchie, S.M.C. and Bhattacharyya, D., 2002. Membrane-based hybrid processes for high water recovery and selective inorganic pollutant separation. *Journal of Hazardous Materials*, *92*(1), pp.21-32.

Robb, L.J., 2008. The Witwatersrand Basin – A Review of Contrasting Viewpoints. Presentation at the GSSA-SEG 2008 Conference, Gold Deposit of the African Continent, 39 Slides.

Roh, I.J., Kim, J.J. and Park, S.Y., 2002. Mechanical properties and reverse osmosis performance of interfacially polymerized polyamide thin films. *Journal of membrane Science*, *197*(1-2), pp.199-210.

Salahi, A., Mohammadi, T., Behbahani, R.M. and Hemmati, M., 2015. Asymmetric polyethersulfone ultrafiltration membranes for oily wastewater treatment: synthesis, characterization, ANFIS modeling, and performance. *Journal of Environmental Chemical Engineering*, *3*(1), pp.170-178.

Sen, T.K. and Sarzali, M.V., 2008. Removal of cadmium metal ion (Cd2+) from its aqueous solution by aluminium oxide (Al2O3): A kinetic and equilibrium study. *Chemical Engineering Journal*, *142*(3), pp.256-262.

Shen, J.N., Ruan, H.M., Wu, L.G. and Gao, C.J., 2011. Preparation and characterization of PES–SiO 2 organic–inorganic composite ultrafiltration membrane for raw water pretreatment. *Chemical Engineering Journal*, *168*(3), pp.1272-1278.

Shi, X., Tal, G., Hankins, N.P. and Gitis, V., 2014. Fouling and cleaning of ultrafiltration membranes: a review. *Journal of Water Process Engineering*, *1*, pp.121-138.

Shi, L., Huang, J., Zhu, L., Shi, Y., Yi, K. and Li, X., 2019. Role of concentration polarization in cross flow micellar enhanced ultrafiltration of cadmium with low surfactant concentration. *Chemosphere*, *237*, p.124859.

Shockravi, A., Vatanpour, V., Najjar, Z., Bahadori, S. and Javadi, A., 2017. A new high-performance polyamide as an effective additive for modification of antifouling properties and morphology of asymmetric PES blend ultrafiltration membranes. *Microporous and Mesoporous Materials*, *246*, pp.24-36

Shukla, S.K., Mishra, A.K., Arotiba, O.A. and Mamba, B.B., 2013. Chitosan-based nanomaterials: A state-of-the-art review. *International journal of biological macromolecules*, *59*, pp.46-58.

Singh, P.S., Joshi, S.V., Trivedi, J.J., Devmurari, C.V., Rao, A.P. and Ghosh, P.K., 2006. Probing the structural variations of thin film composite RO membranes obtained by coating polyamide over polysulfone membranes of different pore dimensions. *Journal of Membrane Science*, *278*(1-2), pp.19-25.

Sivakami, M.S., Gomathi, T., Venkatesan, J., Jeong, H.S., Kim, S.K. and Sudha, P.N., 2013. Preparation and characterization of nano chitosan for treatment wastewaters. *International Journal of Biological Macromolecules*, *57*, pp.204-212.

Silva, A.M., Lima, R.M. and Leão, V.A., 2012. Mine water treatment with limestone for sulfate removal. *Journal of hazardous materials*, *221*, pp.45-55.

Sommer, S. and Melin, T., 2005. Influence of operation parameters on the separation of mixtures by pervaporation and vapor permeation with inorganic membranes. Part 1: Dehydration of solvents. *Chemical Engineering Science*, *60*(16), pp.4509-4523.

Soon, C.Y., Tee, Y.B., Tan, C.H., Rosnita, A.T. and Khalina, A., 2018. Extraction and physicochemical characterization of chitin and chitosan from Zophobas morio larvae in varying sodium hydroxide concentration. *International Journal of Biological Macromolecules*, *108*, pp.135-142.

Srinivasan, H., Kanayairam, V. and Ravichandran, R., 2018. Chitin and chitosan preparation from shrimp shells Penaeus monodon and its human ovarian cancer cell line, PA-1. *International journal of Biological Macromolecules*, *107*, pp.662-667.

Stevenson, R.J., White, K.D., (1995). A comparison of natural and human determinants of phytoplankton communities in the Kentucky River Basin, USA. Hydrobiologia 297, 201e216.
Stratful, I., Scrimshaw, M.D. and Lester, J.N., 2001. Conditions influencing the precipitation of magnesium ammonium phosphate. *Water research*, *35*(17), pp.4191-4199

Tanhaei, B., Ayati, A., Bamoharram, F.F., Lahtinen, M. and Sillanpää, M., 2016. A novel magnetic Preyssler acid grafted chitosan nano adsorbent: synthesis, characterization and adsorption activity. *Journal of Chemical Technology & Biotechnology*, *91*(5), pp.1452-1460.

Tanninen, J. and Nyström, M., 2002. Separation of ions in acidic conditions using NF. *Desalination*, *147*(1-3), pp.295-299.

Tolonen, E.T., Sarpola, A., Hu, T., Rämö, J. and Lassi, U., 2014. Acid mine drainage treatment using by-products from quicklime manufacturing as neutralization chemicals. *Chemosphere*, *117*, pp.419-424.

Torkabad, M.G., Keshtkar, A.R. and Safdari, S.J., 2017. Comparison of polyethersulfone and polyamide nanofiltration membranes for uranium removal from aqueous solution. *Progress in Nuclear Energy*, *94*, pp.93-100.

Turton A (2013) Debunking Persistent Myths about AMD in the Quest for a Sustainable Solution. SAWEF Paradigm Shifter No.1. Johannesburg: South African Water, Energy and Food Forum (SAWEF).

Tutu, H., McCarthy, T.S. and Cukrowska, E., 2008. The chemical characteristics of acid mine drainage with particular reference to sources, distribution and remediation: The Witwatersrand Basin, South Africa as a case study. *Applied Geochemistry*, *23*(12), pp.3666-3684.

Van Biljon, M., 2007. Geohydrological Review of the potential impact on the Sterkfontein dolomite during increased surface water run-off, April 2006–February 2007. Report Prepared for Johan Fourie and Associates for Harmony Gold Mining Limited.

Van der Bruggen, B., 2009. Chemical modification of polyethersulphone nanofiltration membranes: a review. *Journal of Applied Polymer Science*, *114*(1), pp.630-642.

Vela, M.C.V., Blanco, S.Á., García, J.L. and Rodríguez, E.B., 2009. Analysis of membrane pore blocking models adapted to crossflow ultrafiltration in the ultrafiltration of PEG. *Chemical Engineering Journal*, *149*(1-3), pp.232-241.

Verb, R.G., Vis, M.L., 2000. Comparison of benthic diatom assemblages from streams draining abandoned and reclaimed coal mines and non-impacted sites. Journal of the North American Benthological Society 19, 274e288.

Vieira, R.S. and Beppu, M.M., 2006. Interaction of natural and crosslinked chitosan membranes with Hg (II) ions. *Colloids and Surfaces A: Physicochemical and Engineering Aspects*, *279*(1), pp.196-207.

Visser, T. J. K., Modise, S. J., Krieg, H. M, Keizer, K. 2001. The removal of acid sulphate pollution by nanofiltration. Desalination. 140: 79-86.

Wan Ngaha, W.S., Teonga, L.C., Hanafiah, M.A.K.M. 2011 “Adsorption of dyes and heavy metal ions by chitosan composites: A review” Elsevier Carbohydrate Polymers Vol.83, pp.1446–1456.

Wang, K.Y., Chung, T.S. and Amy, G., 2012. Developing thin-film-composite forward osmosis membranes on the PES/SPSf substrate through interfacial polymerization. *AIChE Journal*, *58*(3), pp.770-781.

Wang, F.J., Li, W., Xue, M.S., Yao, J.P. and Lu, J.S., 2011a. BaTiO3–polyethersulfone nanocomposites with high dielectric constant and excellent thermal stability. *Composites Part B: Engineering*, *42*(1), pp.87-91.

Wang, Q., Li, J., Chen, C., Ren, X., Hu, J. and Wang, X., 2011b. Removal of cobalt from aqueous solution by magnetic multiwalled carbon nanotube/iron oxide composites. *Chemical Engineering Journal*, *174*(1), pp.126-133.

Wei, X., Wang, Z., Fan, F., Wang, J. and Wang, S., 2010. Advanced treatment of a complex pharmaceutical wastewater by nanofiltration: membrane foulant identification and cleaning. *Desalination*, *251*(1), pp.167-175.

WHO (World Health Organization), 2011. Uranium in drinking water. <http://www.who.int/water_sanitation_health/dwq/chemicals/en/uranium.pdf> (Accessed 05 May 2016).

Winde, F. and Wade, P.W., 2006. *An Assessment of Sources, Pathways, Mechanisms and Risks of Current and Potential Future Pollution of Water and Sediments in Gold-mining Areas of the Wonderfonteinspruit Catchment: Report to the Water Research Commission*. Water Research Comission.

Wu, C., Zhang, S., Yang, D. and Jian, X., 2009. Preparation, characterization and application of a novel thermal stable composite nanofiltration membrane. *Journal of Membrane Science*, *326*(2), pp.429-434.

Wu, D., Liu, X., Yu, S., Liu, M. and Gao, C., 2010. Modification of aromatic polyamide thin-film composite reverse osmosis membranes by surface coating of thermo-responsive copolymers P (NIPAM-co-Am). I: Preparation and characterization. *Journal of Membrane Science*, *352*(1-2), pp.76-85.

Xie, J., Li, C., Chi, L. and Wu, D., 2013. Chitosan modified zeolite as a versatile adsorbent for the removal of different pollutants from water. *Fuel*, *103*, pp.480-485.

Xu, G.R., Wang, J.N. and Li, C.J., 2013. Strategies for improving the performance of the polyamide thin film composite (PA-TFC) reverse osmosis (RO) membranes: Surface modifications and nanoparticles incorporations. *Desalination*, *328*, pp.83-100.

Xu, J., Wang, Z., Wang, J. and Wang, S., 2015. Positively charged aromatic polyamide reverse osmosis membrane with high anti-fouling property prepared by polyethyleneimine grafting. *Desalination*, *365*, pp.398-406.

Xu, J., Wang, Z., Wang, J. and Wang, S., 2015. Positively charged aromatic polyamide reverse osmosis membrane with high anti-fouling property prepared by polyethyleneimine grafting. *Desalination*, *365*, pp.398-406.

Yager, T.R., 2004. The mineral industry of South Africa. *Energy*, pp.21-22.

Yang, X., Du, Y., Zhang, X., He, A. and Xu, Z.K., 2017. Nanofiltration membrane with a mussel-inspired interlayer for improved permeation performance. *Langmuir*, *33*(9), pp.2318-2324.

Zhao, C., Xue, J., Ran, F. and Sun, S., 2013. Modification of polyethersulphone membranes–a review of methods. *Progress in Materials Science*, *58*(1), pp.76-150.

Zhong, C., Xu, Z., Fang, X., Cheng, L. 2006. Treatment of Acid Mine Drainage (AMD) by Ultra- Low-Pressure Reverse Osmosis and Nanofiltration. *Environmental Engineering Science*. 24 (9): 1297-1306.

Zhong, C.M., Xu, Z.L., Fang, X.H. and Cheng, L., 2007. Treatment of acid mine drainage (AMD) by ultra-low-pressure reverse osmosis and nanofiltration. *Environmental Engineering Science*, *24*(9), pp.1297-1306.

Zhou, L., Xu, J., Liang, X. and Liu, Z., 2010. Adsorption of platinum (IV) and palladium (II) from aqueous solution by magnetic cross-linking chitosan nanoparticles modified with ethylenediamine. *Journal of Hazardous Materials*, *182*(1), pp.518-524.

Zhu, W.P., Sun, S.P., Gao, J., Fu, F.J. and Chung, T.S., 2014. Dual-layer polybenzimidazole/polyethersulfone (PBI/PES) nanofiltration (NF) hollow fiber membranes for heavy metals removal from wastewater. *Journal of Membrane Science*, *456*, pp.117-127.

Zhu, Y., Hu, J. and Wang, J., 2014. Removal of Co^{2+} from radioactive wastewater by polyvinyl alcohol (PVA)/chitosan magnetic composite. *Progress in Nuclear Energy*, *71*, pp.172-178.

Zhu, X., Bai, R., Wee, K.H., Liu, C. and Tang, S.L., 2010. Membrane surfaces immobilized with ionic or reduced silver and their anti-biofouling performances. *Journal of Membrane Science*, *363*(1), pp.278-286.

Zolnikov, T.R. and Ortiz, D.R., 2018. A systematic review on the management and treatment of mercury in artisanal gold mining. *Science of the Total Environment*, *633*, pp.816-824.

Zou, H., Jin, Y., Yang, J., Dai, H., Yu, X. and Xu, J., 2010. Synthesis and characterization of thin film composite reverse osmosis membranes via novel interfacial polymerization approach. *Separation and Purification Technology*, *72*(3), pp.256-262.

Zularisam, A.W., Ismail, A.F., Salim, M.R., Sakinah, M. and Ozaki, H., 2007. The effects of natural organic matter (NOM) fractions on fouling characteristics and flux recovery of ultrafiltration membranes. *Desalination*,*212*(1), pp.191-208.

Zvarivadza, T. and Nhleko, A.S., 2018. Resolving artisanal and small-scale mining challenges: Moving from conflict to cooperation for sustainability in mine planning. *Resources Policy*, *56*, pp.78-86.

Appendices

Appendix A: Synthesis and characterization of chitosan

A1: Calculation for chitosan percentage yield

Table A1 - 1: Calculations of chitosan percentage yield

	Mass of Reactants(g)	**Mass of Products(g)**	**Mass Loss(g)**	**%Yield**	**Average Yield**	**Std Dev**
Formula	Mass of chitin	Mass of chitin	(Reactants - Products)	(Products/Reactants) *100%	Yield A+ Yield B)/2	Standard Deviation between A and B
Sample 1A	30,0	9,8	20,2	32,7	28,8	5,4
Sample 1B	30,0	7,5	22,5	25,0		
Sample 2A	30,0	8,0	22,0	26,7	25,3	1,9
Sample 2B	30,0	7,2	22,8	24,0		
Sample 3A	30,0	6,0	24,0	20,0	18,2	2,6
Sample 3B	30,0	4,9	25,1	16,3		
Sample 4A	30,0	8,0	22,0	26,7	23,8	4,0
Sample 4B	30,0	6,3	23,7	21,0		
Sample 5A	30,0	6,7	23,3	22,3	19,8	3,5
Sample 5B	30,0	5,2	24,8	17,3		
Sample 6A	30,0	4,6	25,4	15,3	14,2	1,6
Sample 6B	30,0	3,9	26,1	13,0		
Sample 7A	30,0	5,0	25,0	16,7	13,7	4,2
Sample 7B	30,0	3,2	26,8	10,7		

Sample 8A	30,0	4,0	26,0	13,3	12,7	0,9
Sample 8B	30,0	3,6	26,4	12,0		
Sample 9A	30,0	3,6	26,4	12,0	10,8	1,6
Sample 9B	30,0	2,9	27,1	9,7		

A2: FTIR graphs of the synthesized chitosan samples

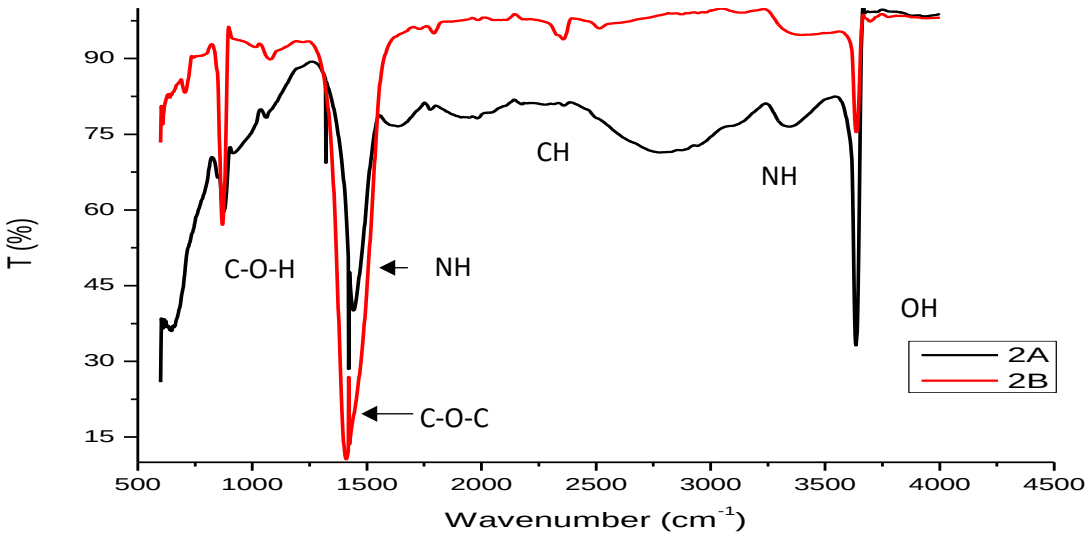


Figure A2 - 1: FTIR graph for chitosan sample 2A and 2B

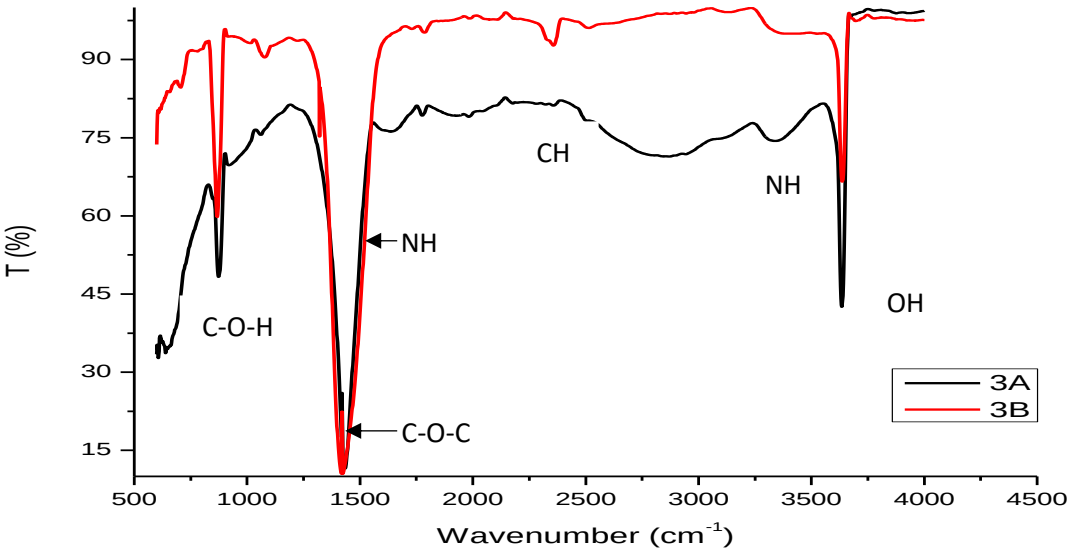


Figure A2 - 2: FTIR graph for chitosan sample 3A and 3B

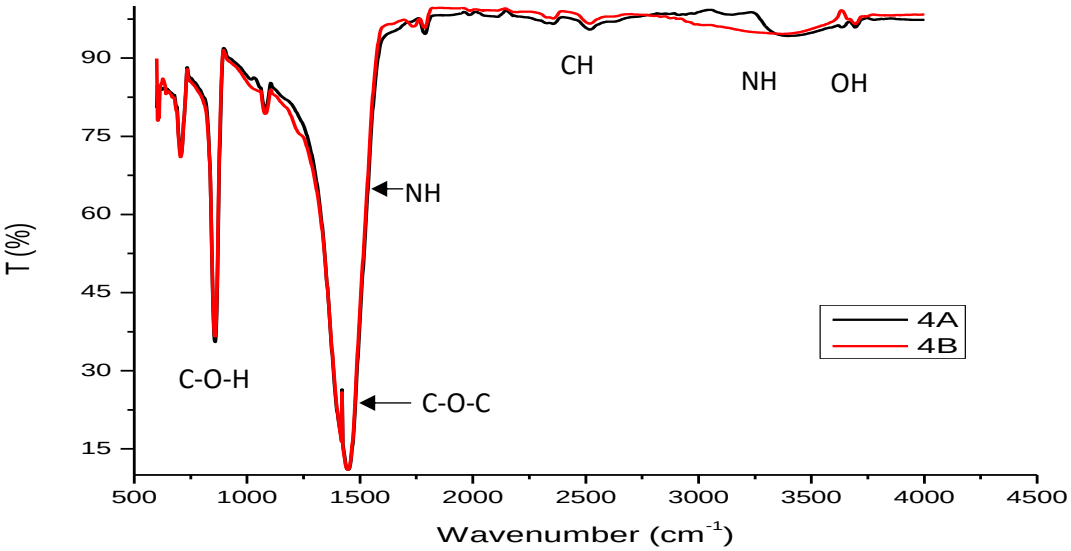


Figure A2 - 3: FTIR graph for chitosan sample 4A and 4B

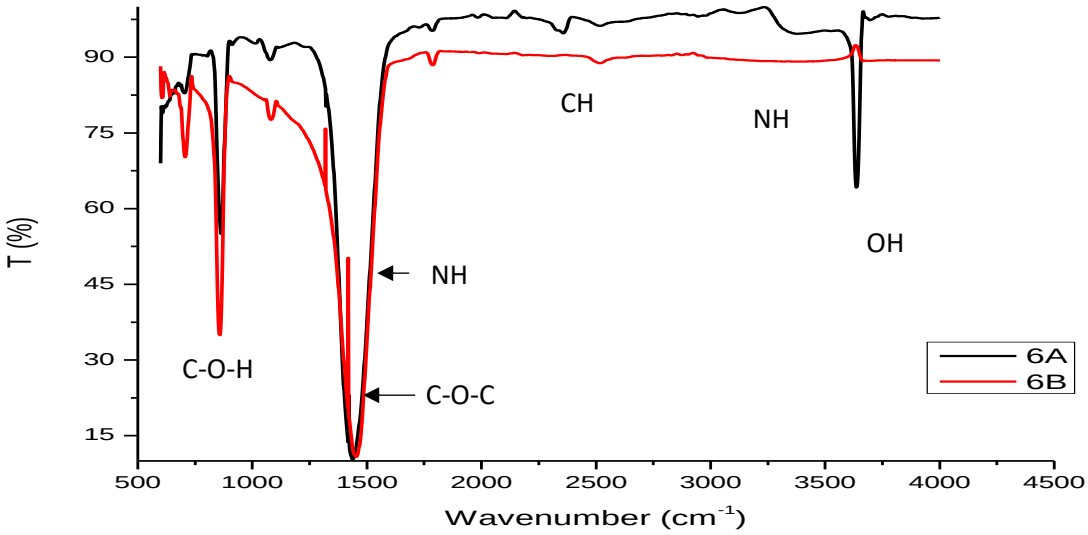


Figure A2 - 4: FTIR graph for chitosan sample 6A and 6B

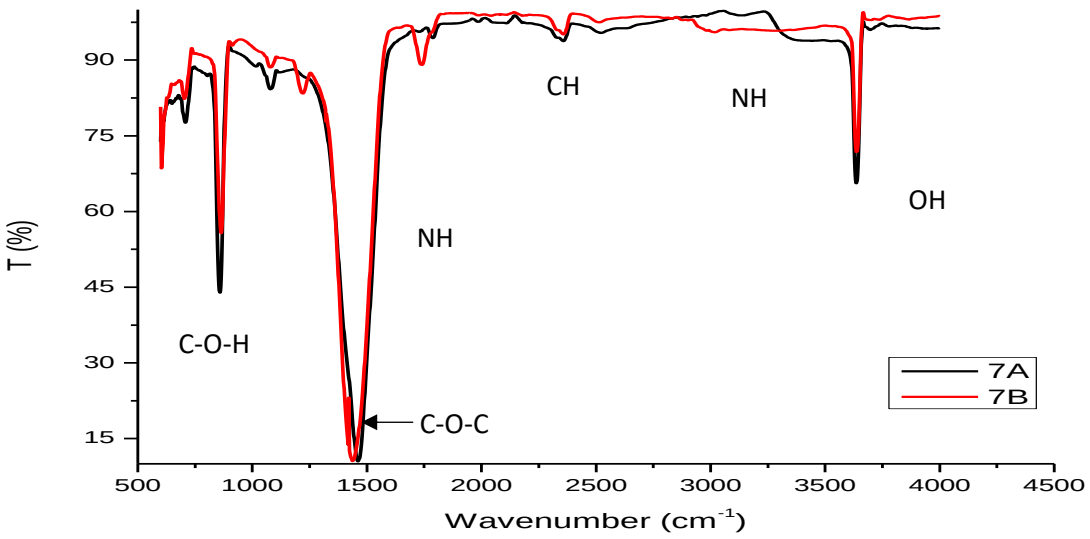


Figure A2 - 5: FTIR graph for chitosan sample 7A and 7B

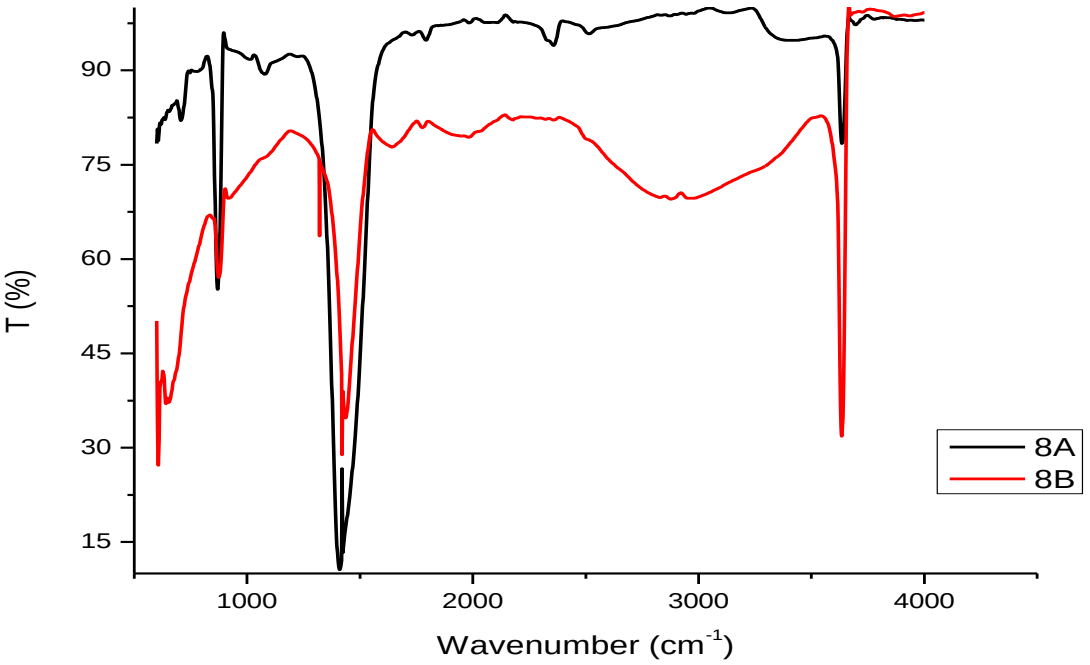


Figure A2 - 6: FTIR graph for chitosan sample 8A and 8B

A3: PSD results for the synthesized chitosan samples

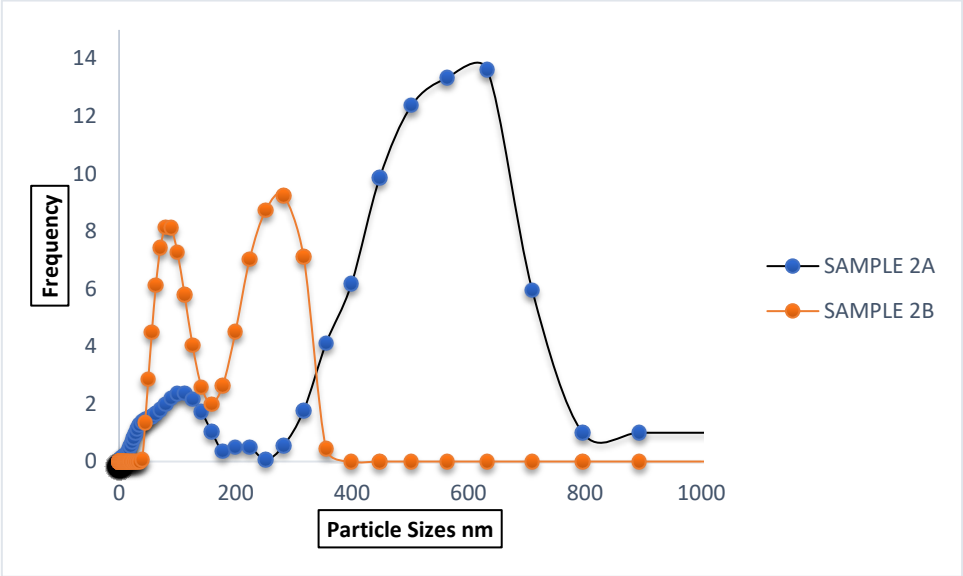


Figure A3 - 1: Particle size distribution for chitosan sample 2A and 2B

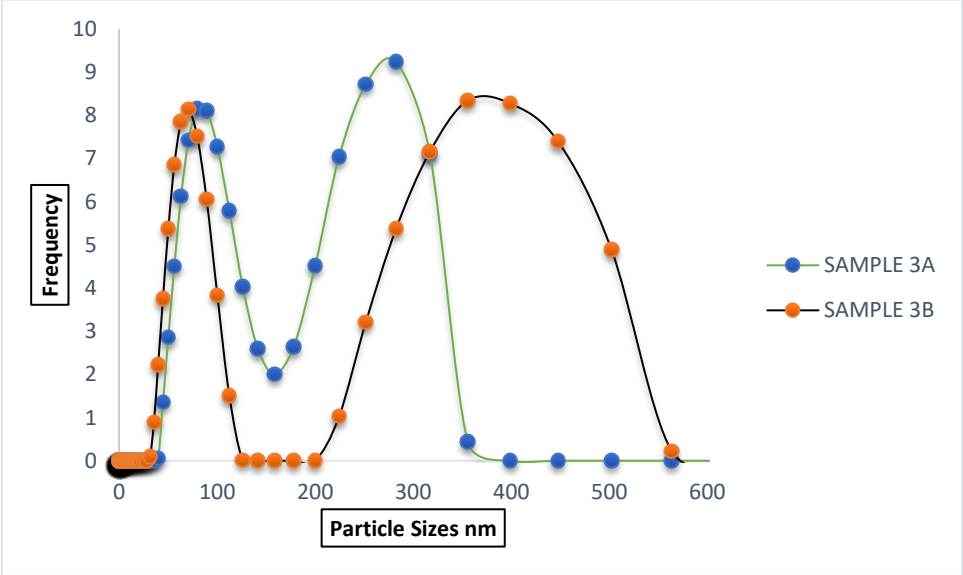


Figure A3 - 2: Particle size distribution for chitosan sample 3A and 3B

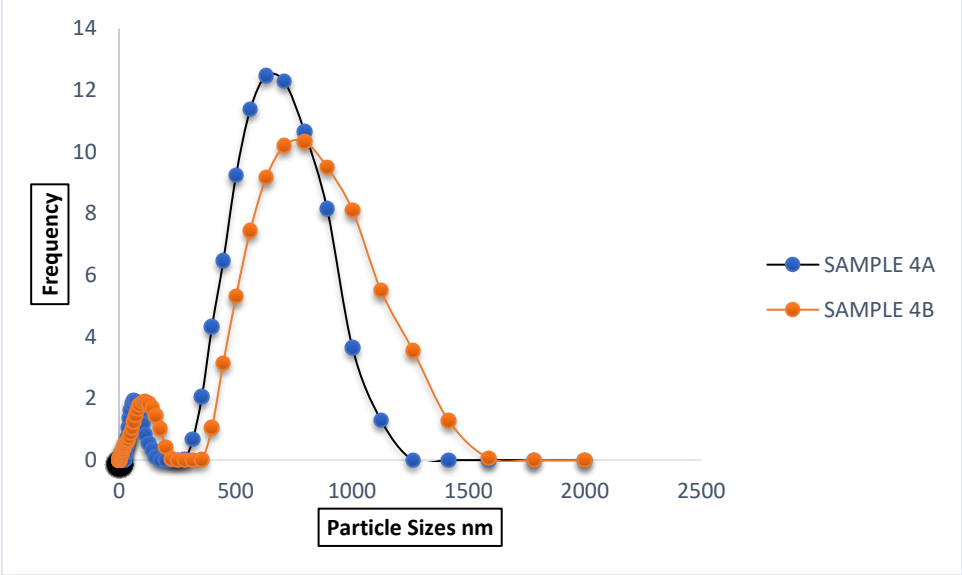


Figure A3 - 3: Particle size distribution for chitosan sample 4A and 4B

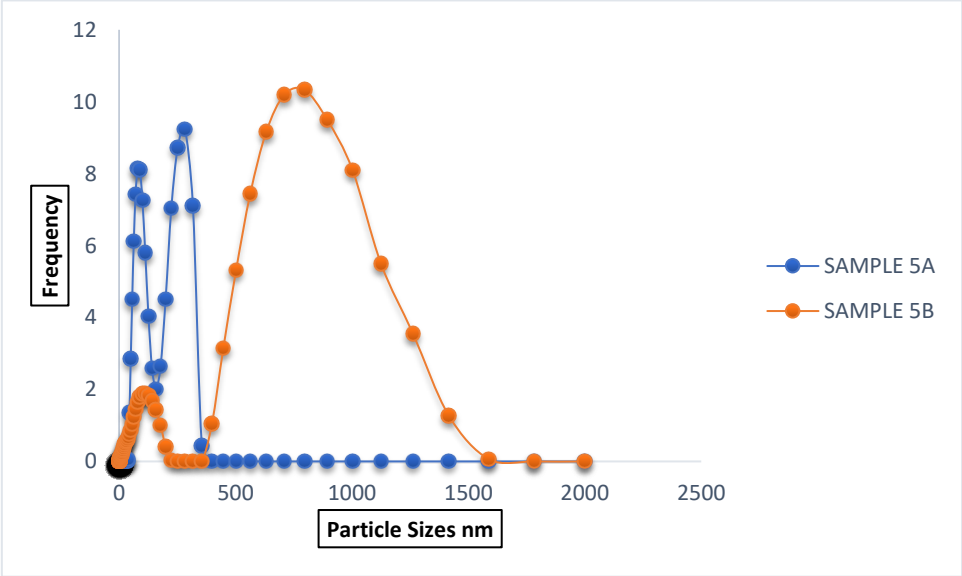


Figure A3 - 4: Particle size distribution for chitosan sample 5A and 5B

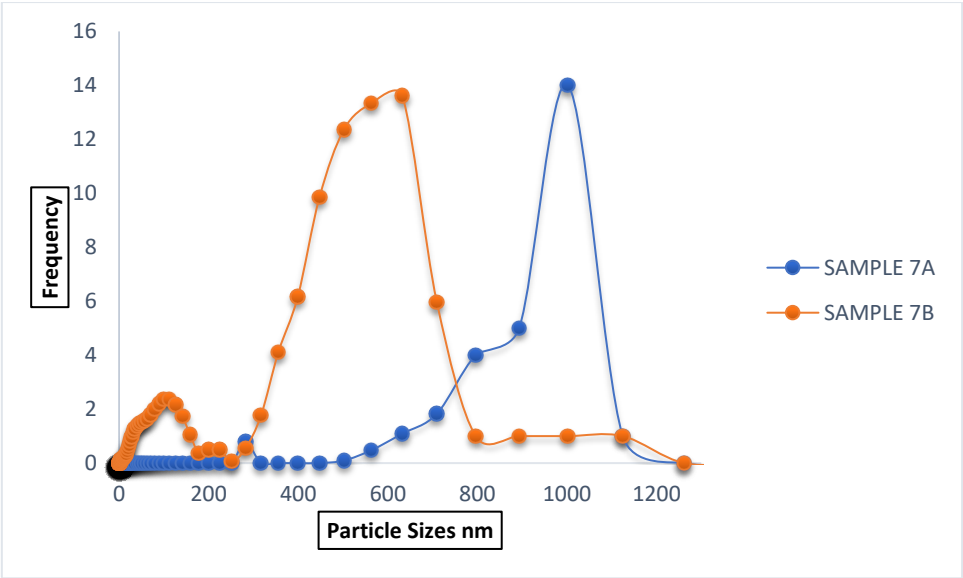


Figure A3 - 5: Particle size distribution for chitosan sample 7A and 7B

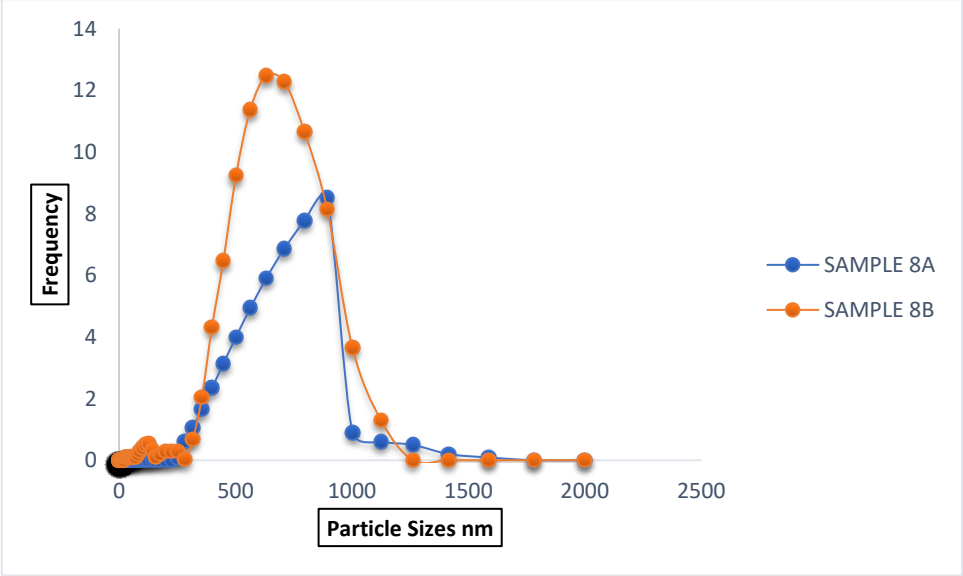


Figure A3 - 6: Particle size distribution for chitosan sample 8A and 8B

Appendix B: Membrane synthesis and characterization

B1: FTIR graphs for synthesized PES/chitosan membranes

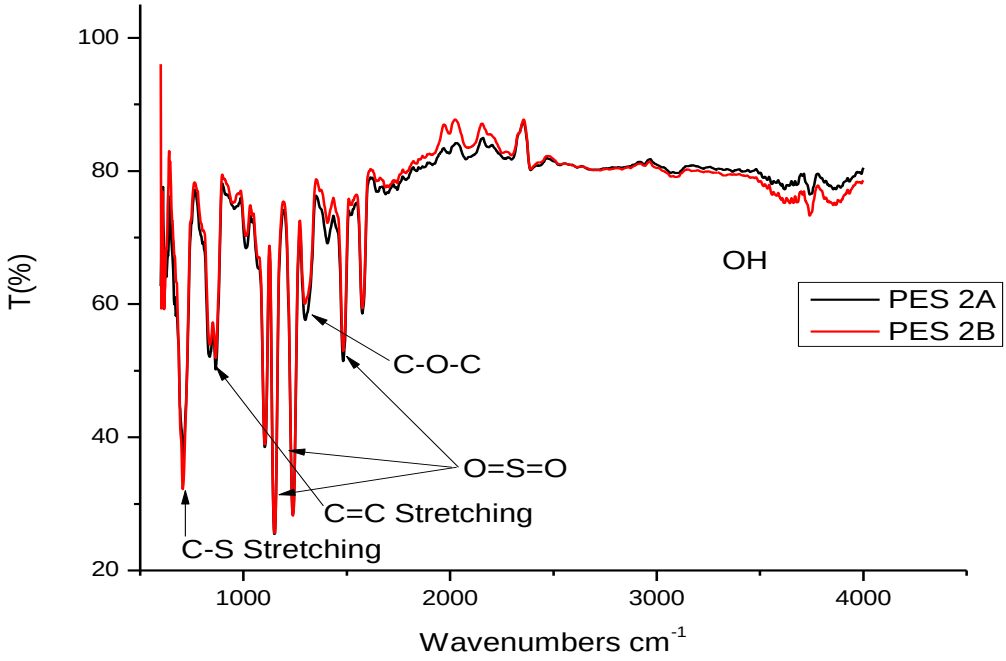


Figure B1 - 1: FTIR graph for PES/chitosan membranes 2A and 2B

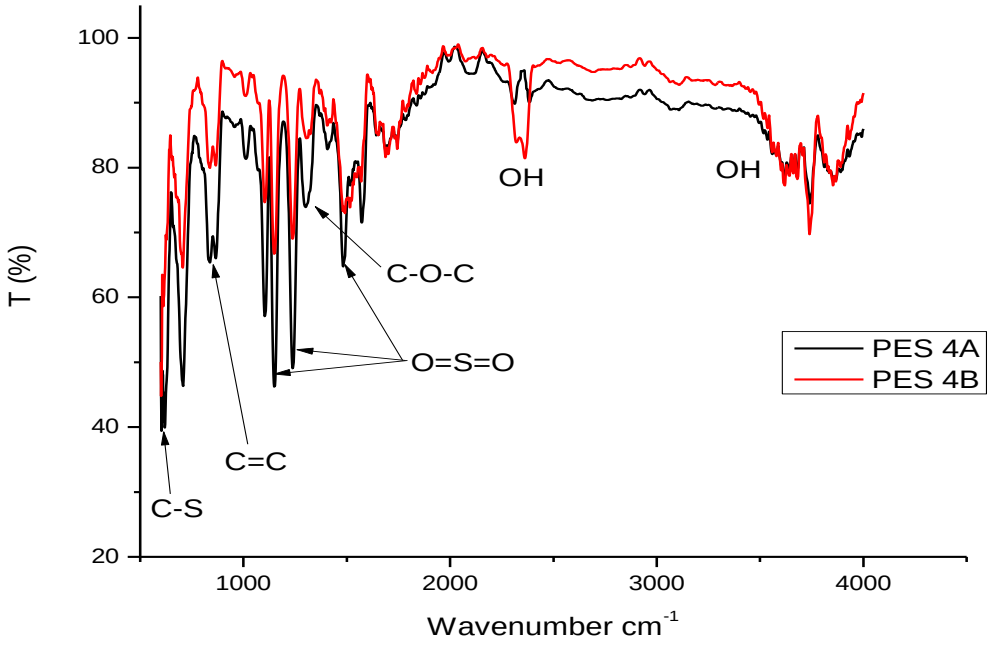


Figure B1 - 2: FTIR graph for PES/chitosan membranes 4A and 4B

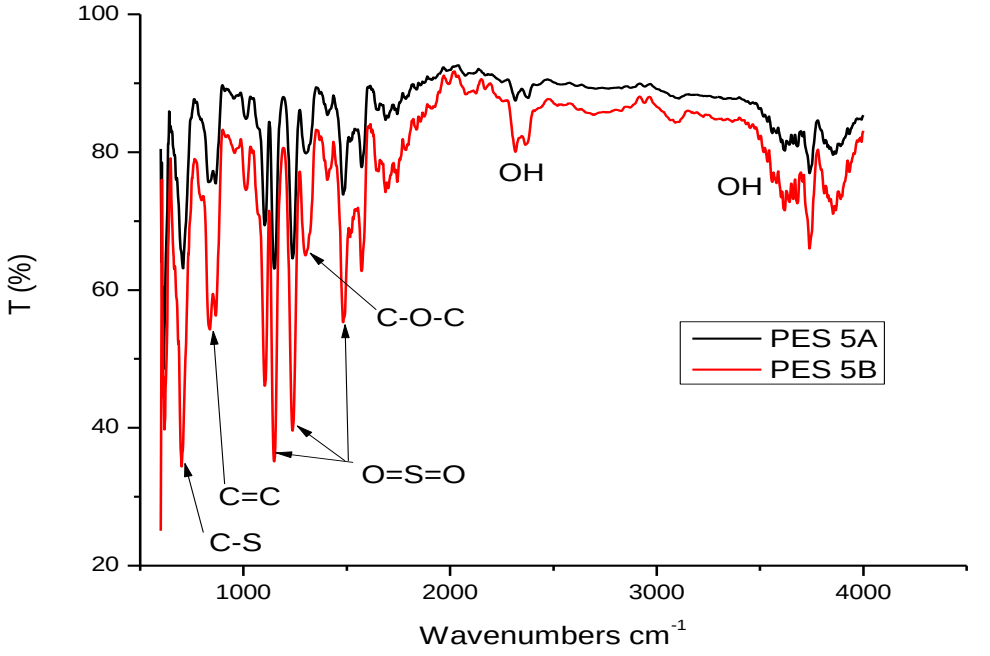


Figure B1 - 3: FTIR graph for PES/chitosan membranes 5A and 5B

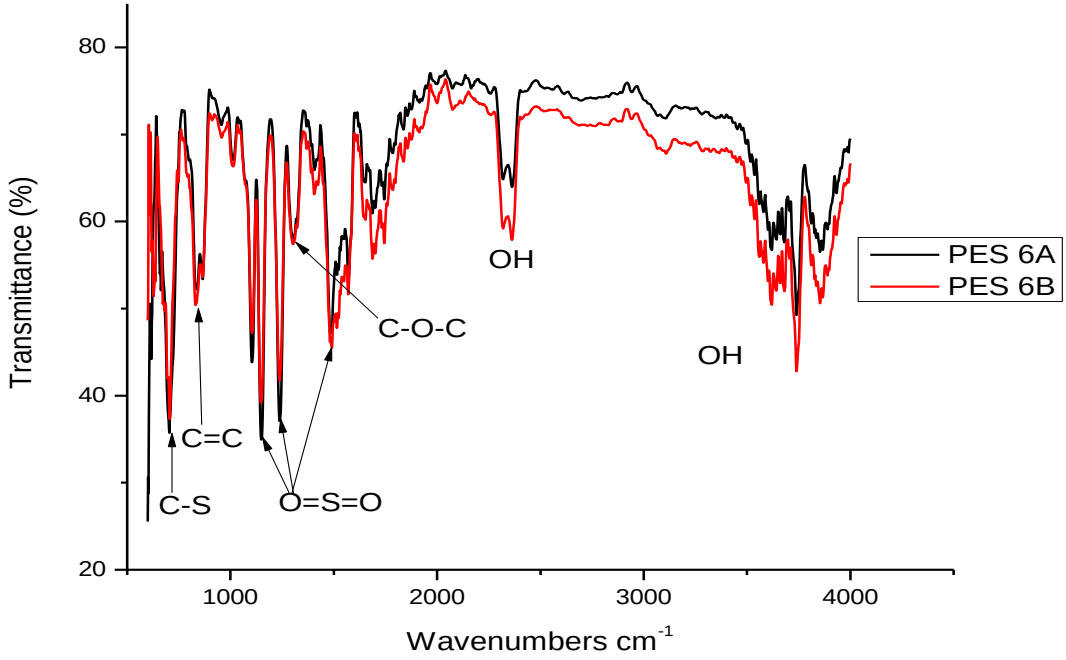


Figure B1 - 4: FTIR graph for PES/chitosan membranes 6A and 6B

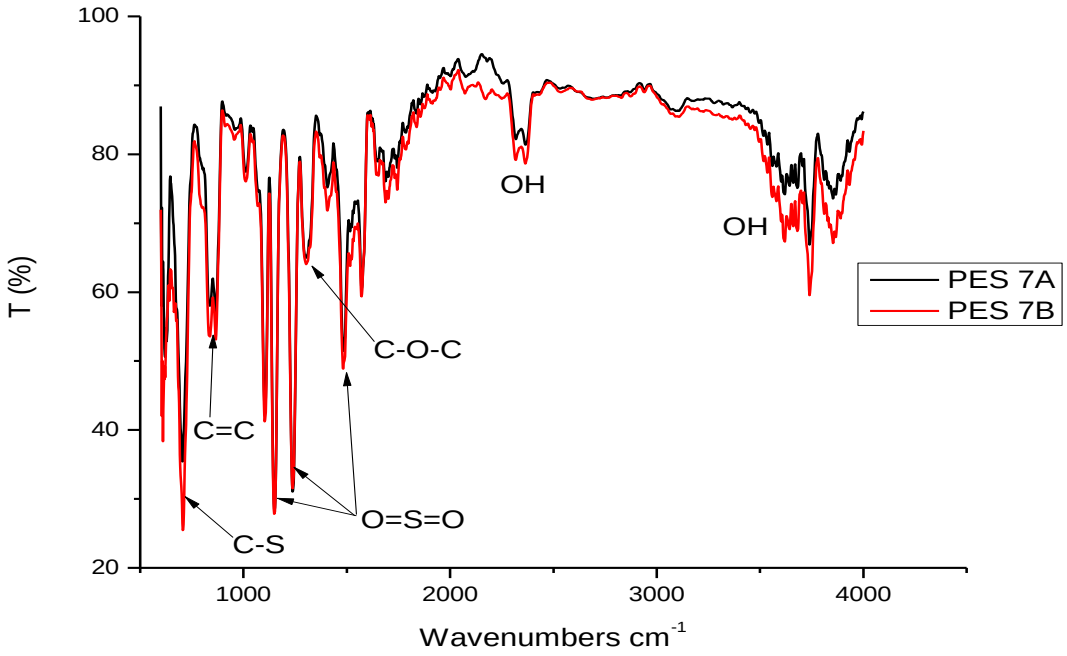


Figure B1 - 5: FTIR graph for PES/chitosan membranes 7A and 7B

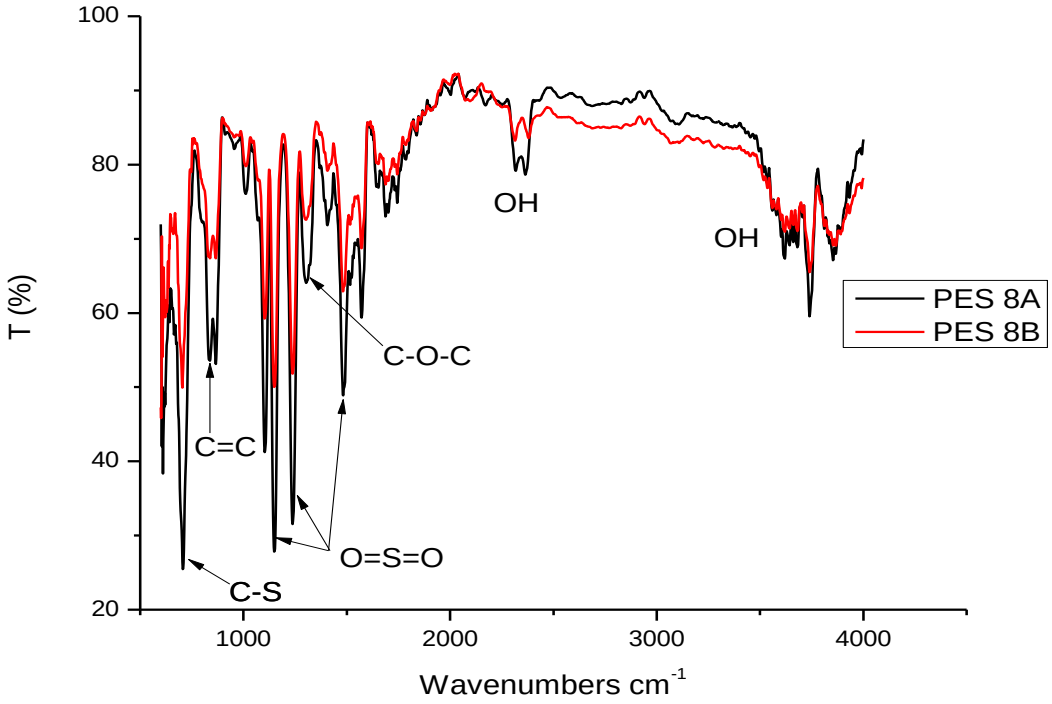


Figure B1 - 6: FTIR graph for PES/chitosan membranes 8A and 8B

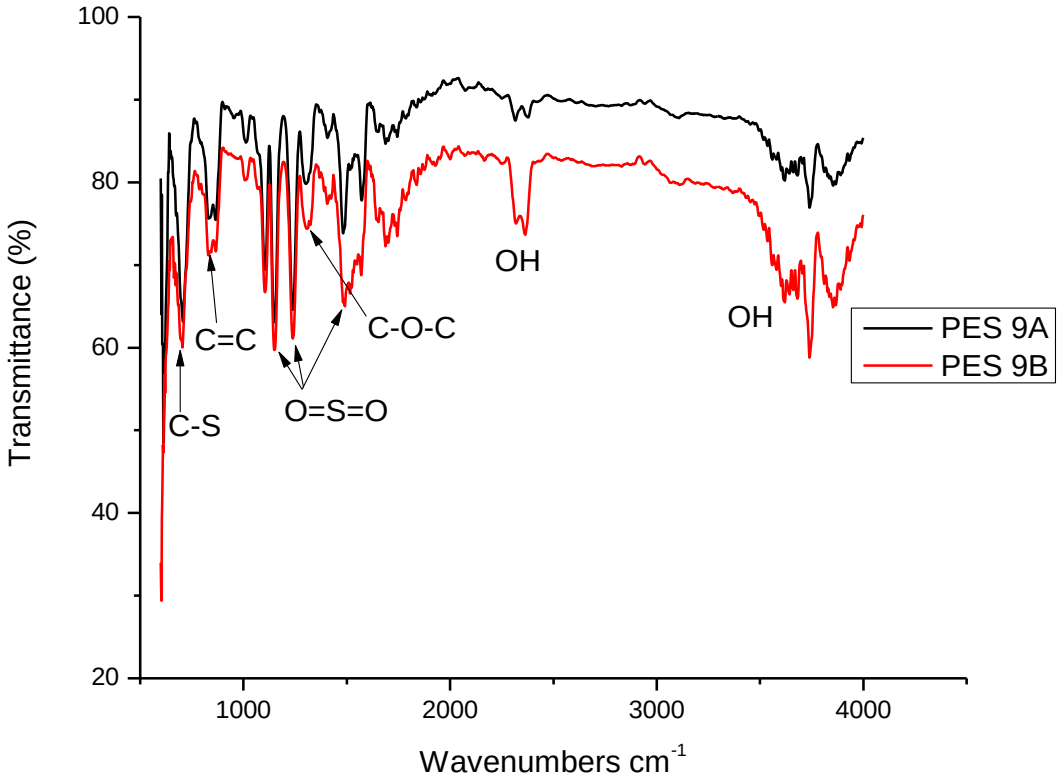


Figure B1 - 7: FTIR graph for PES/chitosan membranes 9A and 9B

B2: FTIR graphs for synthesised PES/chitosan/PA membranes

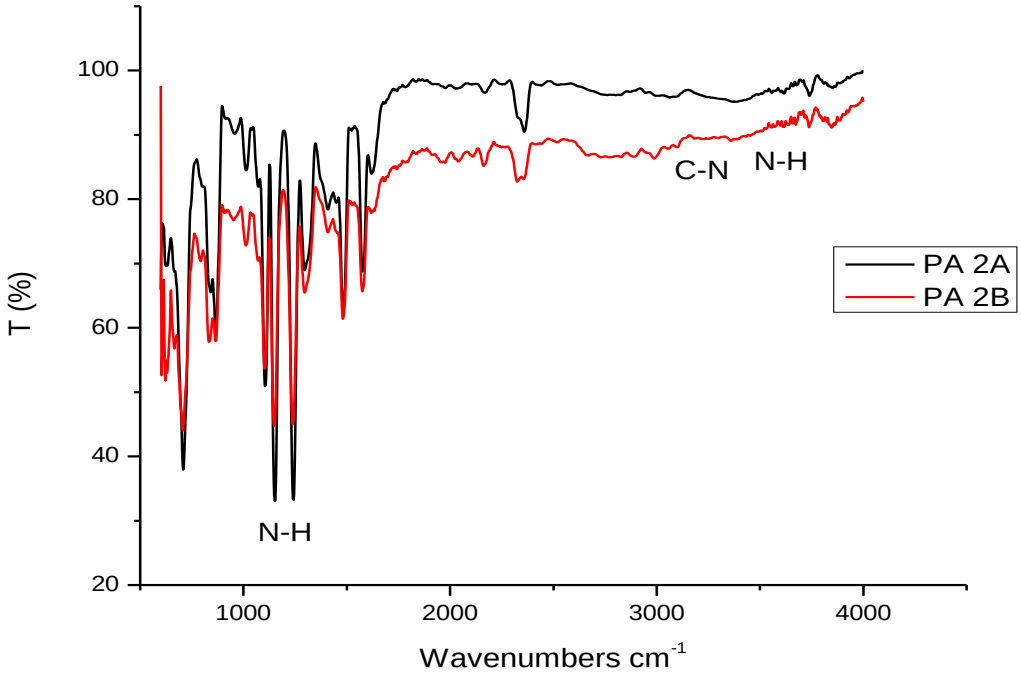


Figure B2 - 1: FTIR graph for PES/chitosan/PA membrane 2A and 2B

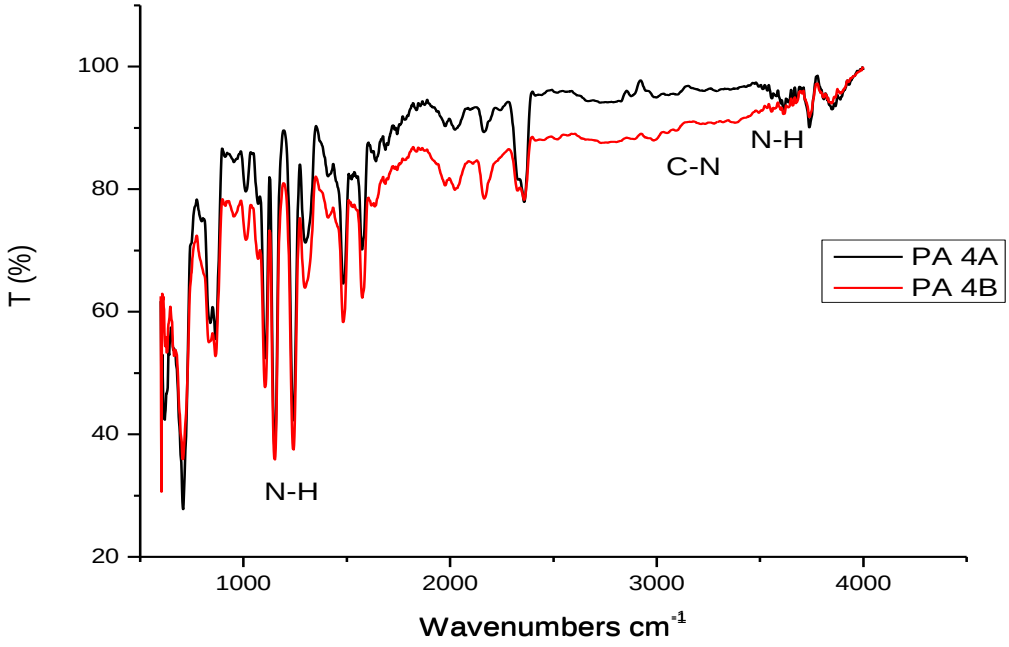


Figure B2 - 2: FTIR graph for PES/chitosan/PA membrane 4A and 4B

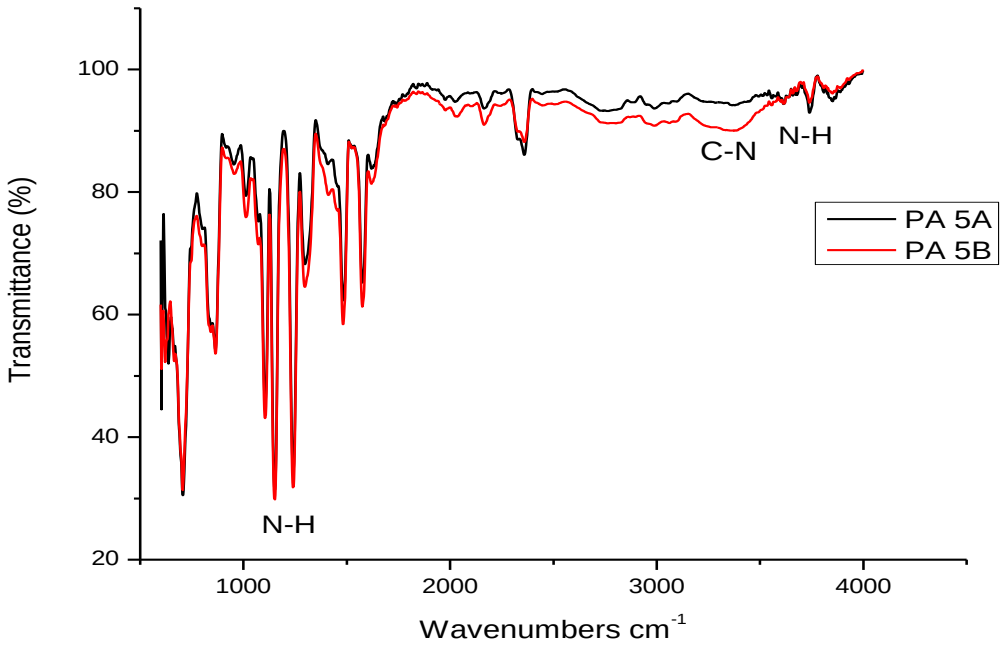


Figure B2 - 3: FTIR graph for PES/chitosan/PA membrane 5A and 5B

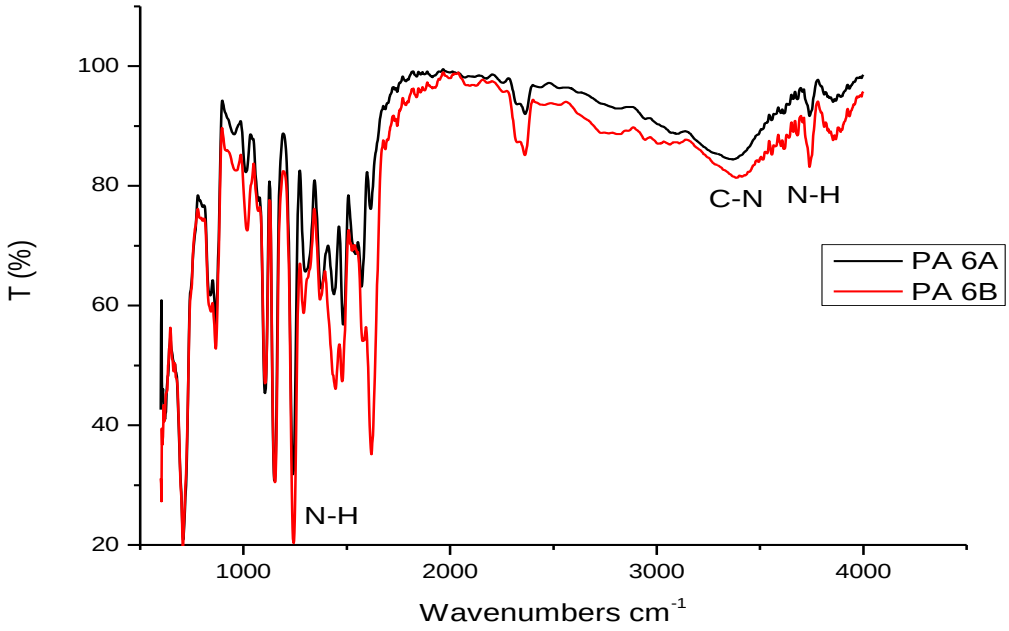


Figure B2 - 4: FTIR graph for PES/chitosan/PA membrane 6A and 6B

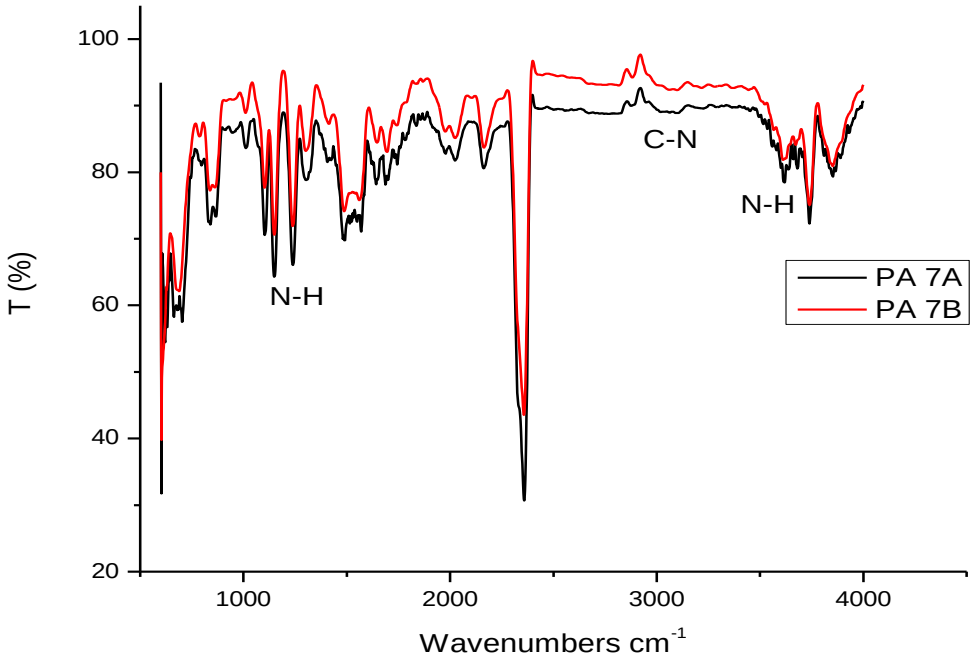


Figure B2 - 5: FTIR graph for PES/chitosan/PA membrane 7A and 7B

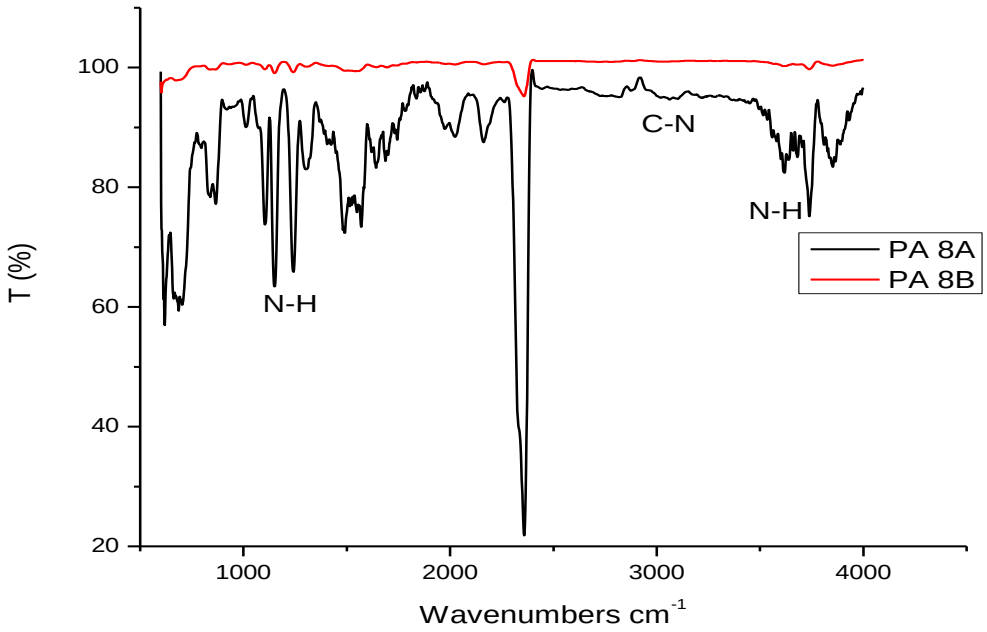


Figure B2 - 6: FTIR graph for PES/chitosan/PA membrane 8A and 8B

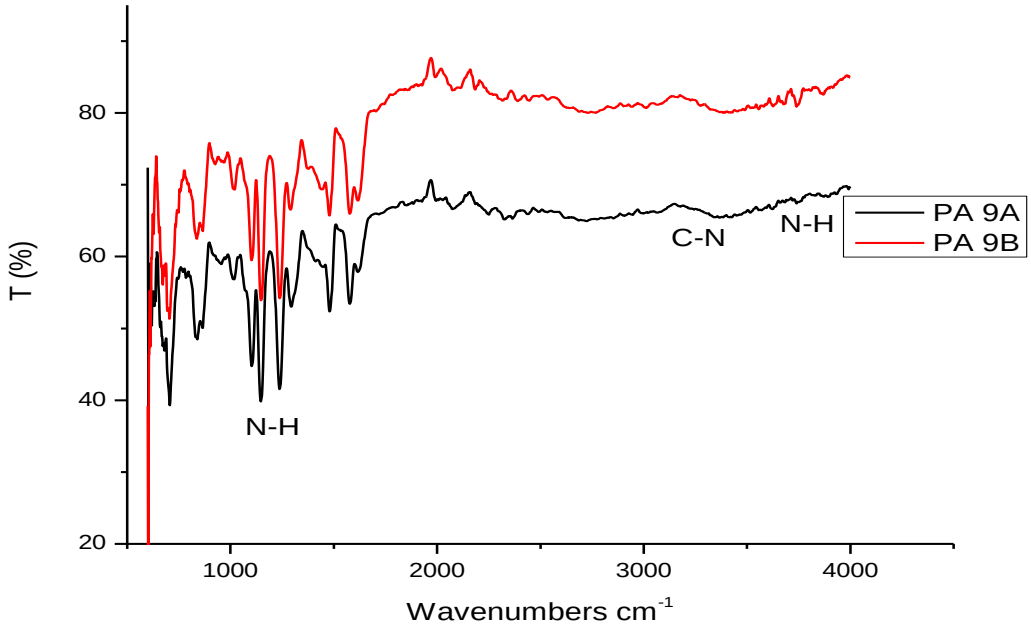


Figure B2 - 7: FTIR graph for PES/chitosan/PA membrane 9A and 9B

B3: TGA Raw data for the PES/chitosan samples

Table B3 - 1: Raw data for PES/chitosan membranes

Time	Pristine PES		PES 1		PES 2		PES 3		PES 4	
(min)	Temp	Weight	Temp	Weight	Temp	Weight	Temp	Weight	Temp	Weight
0	53,02	100	41,02	100	45,02	100	44,02	100	44,82	100
5	79,92	88,97	67,92	92,77	71,92	97,77	70,92	94,57	71,72	96,57
10	99,51	88,12	87,51	91,92	91,51	96,92	90,51	93,72	91,31	95,72
15	124,55	87,89	112,55	91,69	116,55	96,69	115,55	93,49	116,35	95,49
20	148,94	87,82	136,94	91,62	140,94	96,62	139,94	93,42	140,74	95,42
25	174,6	87,66	162,6	91,46	166,6	96,46	165,6	93,26	166,4	95,26
30	200,26	87,38	188,26	91,18	192,26	96,18	191,26	92,98	192,06	94,98
35	225,44	87,03	213,44	90,83	217,44	95,83	216,44	92,63	217,24	94,63
40	250,7	85,88	238,7	89,68	242,7	94,68	241,7	91,48	242,5	93,48
45	276,07	82,84	264,07	86,64	268,07	91,64	267,07	88,44	267,87	90,44
50	302,12	75,23	290,12	79,03	294,12	84,03	293,12	80,83	293,92	82,83
55	334,14	46,24	322,14	50,04	326,14	55,04	325,14	51,84	325,94	53,84
60	354,83	30,75	342,83	34,55	346,83	39,55	345,83	36,35	346,63	38,35
65	377,42	27,57	365,42	31,37	369,42	36,37	368,42	33,17	369,22	35,17
70	401,83	24,98	389,83	28,78	393,83	33,78	392,83	30,58	393,63	32,58
75	426	22,23	414	26,03	418	31,03	417	27,83	417,8	29,83
80	451	19,11	439	22,91	443	27,91	442	24,71	442,8	26,71
85	476	15,55	464	19,35	468	24,35	467	21,15	467,8	23,15
90	501,15	11,86	489,15	15,66	493,15	20,66	492,15	17,46	492,95	19,46
95	525,93	8,37	513,93	12,17	517,93	17,17	516,93	13,97	517,73	15,97
100	550,69	5,24	538,69	9,04	542,69	14,04	541,69	10,84	542,49	12,84

105	575,42	2,45	563,42	6,25	567,42	11,25	566,42	8,05	567,22	10,05
110	600,24		588,24	3,75	592,24	8,75	591,24	5,55	592,04	7,55
115	623,9		611,9	3,35	615,9	8,35	614,9	5,15	615,7	7,15
120	648,77		636,77	3,32	640,77	8,32	639,77	5,12	640,57	7,12
125	673,64		661,64	3,3	665,64	8,3	664,64	5,1	665,44	7,1
130	695,16		683,16	3,3	687,16	8,3	686,16	5,1	686,96	7,1

Time	PES 5		PES 6		PES 7		PES 8		PES 9	
(min)	Temp	Weight	Temp	Weight	Temp	Weight	Temp	Weight	Temp	Weight
0	51,22	100	47,02	100	46,02	100	49,22	100	47,22	100
5	78,12	101,27	73,92	98,87	72,92	98,97	76,12	99,47	74,12	99,17
10	97,71	99,92	93,51	98,02	92,51	98,12	95,71	98,62	93,71	98,32
15	122,75	99,69	118,55	97,79	117,55	97,89	120,75	98,39	118,75	98,09
20	147,14	99,62	142,94	97,72	141,94	97,82	145,14	98,32	143,14	98,02
25	172,8	99,46	168,6	97,56	167,6	97,66	170,8	98,16	168,8	97,86
30	198,46	99,18	194,26	97,28	193,26	97,38	196,46	97,88	194,46	97,58
35	223,64	98,83	219,44	96,93	218,44	97,03	221,64	97,53	219,64	97,23
40	248,9	98,68	244,7	95,78	243,7	95,88	246,9	96,38	244,9	96,08
45	274,27	95,64	270,07	92,74	269,07	92,84	272,27	94,34	270,27	93,04
50	300,32	88,03	296,12	85,13	295,12	85,23	298,32	86,73	296,32	85,43
55	332,34	59,04	328,14	56,14	327,14	56,24	330,34	57,74	328,34	56,44
60	353,03	43,55	348,83	40,65	347,83	40,75	351,03	42,25	349,03	40,95
65	375,62	40,37	371,42	37,47	370,42	37,57	373,62	39,07	371,62	37,77
70	400,03	37,78	395,83	34,88	394,83	34,98	398,03	36,48	396,03	35,18
75	424,2	35,03	420	32,13	419	32,23	422,2	33,73	420,2	32,43

80	449,2	31,91	445	29,01	444	29,11	447,2	30,61	445,2	29,31
85	474,2	28,35	470	25,45	469	25,55	472,2	27,05	470,2	25,75
90	499,35	24,66	495,15	21,76	494,15	21,86	497,35	23,36	495,35	22,06
95	524,13	21,17	519,93	18,27	518,93	18,37	522,13	19,87	520,13	18,57
100	548,89	18,04	544,69	15,14	543,69	15,24	546,89	16,74	544,89	15,44
105	573,62	15,25	569,42	12,35	568,42	12,45	571,62	13,95	569,62	12,65
110	598,44	12,75	594,24	9,85	593,24	9,95	596,44	11,45	594,44	10,15
115	622,1	12,35	617,9	9,45	616,9	9,55	620,1	11,05	618,1	9,75
120	646,97	12,32	642,77	9,42	641,77	9,52	644,97	11,02	642,97	9,72
125	671,84	12,3	667,64	9,4	666,64	9,5	669,84	11	667,84	9,7
130	693,36	12,3	689,16	9,4	688,16	9,5	691,36	11	689,36	9,7

B4: TGA Raw data for the PES/chitosan/PA samples

Table B4 - 1: Raw data for PES/chitosan/PA membranes

Time	PES/PA		PA 1		PA 2		PA 3		PA 4	
(min)	Weight (%)	Temp	Temp	Weight	Temp	Weight	Temp	Weight	Temp	Weight
0	147,02	100	100	99,18	100	100	100	100	100	100
5	159	149,75	148,75	97,76	157,55	97,11	158	97,56	157,8	97,36
10	339,51	210,76	209,26	97	218,06	96,35	218,51	96,8	218,31	96,6
15	364,55	235,8	234,3	96,09	243,1	95,44	243,55	95,89	243,35	95,69
20	388,94	260,19	258,69	95,86	267,49	95,21	267,94	95,66	267,74	95,46
25	414,6	285,85	284,35	94,86	293,15	94,21	293,6	94,66	293,4	94,46
30	440,26	311,51	310,01	94,52	318,81	93,87	319,26	94,32	319,06	94,12

35	465,44	336,69	335,19	94,5	343,99	93,85	344,44	94,3	344,24	94,1
40	490,7	361,95	360,45	94	369,25	93,35	369,7	93,8	369,5	93,6
45	516,07	387,32	385,82	93,35	394,62	92,7	395,07	93,15	394,87	92,95
50	542,12	413,37	411,87	92,55	420,67	91,9	421,12	92,35	420,92	92,15
55	574,14	445,39	443,89	92,4	452,69	91,75	453,14	92,2	452,94	92
60	594,83	466,08	464,58	91,1	473,38	90,45	473,83	90,9	473,63	90,7
65	617,42	488,67	487,17	90,6	495,97	89,95	496,42	90,4	496,22	90,2
70	641,83	513,08	511,58	89,5	520,38	88,85	520,83	89,3	520,63	89,1
75	666	537,25	535,75	87,8	544,55	87,15	545	87,6	544,8	87,4
80	691	562,25	560,75	85,6	569,55	84,95	570	85,4	569,8	85,2
85	716	587,25	585,75	83,8	594,55	83,15	595	83,6	594,8	83,4
90	741,15	612,4	610,9	77,55	619,7	76,9	620,15	77,35	619,95	77,15
95	765,93	637,18	635,68	65,2	644,48	64,55	644,93	65	644,73	64,8
100	790,69	661,94	660,44	44,2	669,24	43,55	669,69	44	669,49	43,8
105	815,42	686,67	685,17	14,76	693,97	14,11	694,42	14,56	694,22	14,36
110	840,24	711,49	709,99	6,15	718,79	5,5	719,24	5,95	719,04	5,75
115	863,9	735,15	733,65	5,75	742,45	5,1	742,9	5,55	742,7	5,35
120	888,77	760,02	758,52	5,72	767,32	5,07	767,77	5,52	767,57	5,32
125	913,64	784,89	783,39	5,7	792,19	5,05	792,64	5,5	792,44	5,3
130	935,16	806,41	804,91	5,7	813,71	5,05	814,16	5,5	813,96	5,3

Time	PA 5		PA 6		PA 7		PA 8		PA 9	
(min)	Temp	Weight	Temp	Weight	Temp	Weight	Temp	Weight	Temp	Weight
0	100	100	100	100	100	100	100	100	100	100
5	148,18	87,74	154,17	93,73	156,1	95,66	150,06	89,62	152,62	92,18

10	208,69	86,98	214,68	92,97	216,61	94,9	210,57	88,86	213,13	91,42
15	233,73	86,07	239,72	92,06	241,65	93,99	235,61	87,95	238,17	90,51
20	258,12	85,84	264,11	91,83	266,04	93,76	260	87,72	262,56	90,28
25	283,78	84,84	289,77	90,83	291,7	92,76	285,66	86,72	288,22	89,28
30	309,44	84,5	315,43	90,49	317,36	92,42	311,32	86,38	313,88	88,94
35	334,62	84,48	340,61	90,47	342,54	92,4	336,5	86,36	339,06	88,92
40	359,88	83,98	365,87	89,97	367,8	91,9	361,76	85,86	364,32	88,42
45	385,25	83,33	391,24	89,32	393,17	91,25	387,13	85,21	389,69	87,77
50	411,3	82,53	417,29	88,52	419,22	90,45	413,18	84,41	415,74	86,97
55	443,32	82,38	449,31	88,37	451,24	90,3	445,2	84,26	447,76	86,82
60	464,01	81,08	470	87,07	471,93	89	465,89	82,96	468,45	85,52
65	486,6	80,58	492,59	86,57	494,52	88,5	488,48	82,46	491,04	85,02
70	511,01	79,48	517	85,47	518,93	87,4	512,89	81,36	515,45	83,92
75	535,18	77,78	541,17	83,77	543,1	85,7	537,06	79,66	539,62	82,22
80	560,18	75,58	566,17	81,57	568,1	83,5	562,06	77,46	564,62	80,02
85	585,18	73,78	591,17	79,77	593,1	81,7	587,06	75,66	589,62	78,22
90	610,33	67,53	616,32	73,52	618,25	75,45	612,21	69,41	614,77	71,97
95	635,11	55,18	641,1	61,17	643,03	63,1	636,99	57,06	639,55	59,62
100	659,87	34,18	665,86	40,17	667,79	42,1	661,75	36,06	664,31	38,62
105	684,6	4,74	690,59	10,73	692,52	12,66	686,48	6,62	689,04	9,18
110	709,42		715,41	2,12	717,34	4,05	711,3		713,86	0,57
115	733,08		739,07	1,72	741	3,65	734,96		737,52	0,17
120	757,95		763,94	1,69	765,87	3,62	759,83		762,39	0,14
125	782,82		788,81	1,67	790,74	3,6	784,7		787,26	0,12
130	804,34		810,33	1,67	812,26	3,6	806,22		808,78	0,12

Appendix C: Information about membrane performance evaluation

C1: Effect of chitosan degree of deacetylation on rejection of PES/chitosan membranes

Table C1 – 1: Effect of chitosan degree of deacetylation on rejection of PES/chitosan membranes

Manganese(%)

DD%	33,93	73,05	60,82	61,94	95,97	82,92	79,92	90,17	85,55
Membrane	PES 1	PES 2	PES 3	PES 4	PES 5	PES 6	PES 7	PES 8	PES9
Run 1	69,75	86	78,5	78,9	98	88,58	88,58	93,58	88,58
Run 2	74,8	85,58	82,98	85,3	98,58	92,58	87,58	95,56	93,58
Run 3	65,9	78,58	73,89	77	97,58	83,58	79,58	87,58	85,58
Mean	70,15	83,39	78,46	80,40	98,05	88,25	85,25	92,24	89,25
Std Dev	4,46	4,17	4,55	4,35	0,50	4,51	4,93	4,16	4,04

Iron(%)

DD%	33,93	73,05	60,82	61,94	95,97	82,92	79,92	90,17	85,55
Membrane	PES 1	PES 2	PES 3	PES 4	PES 5	PES 6	PES 7	PES 8	PES9
Run 1	66,58	80,8	70,8	75,3	96,8	85,8	82	90,9	88,9
Run 2	54,58	77,2	72,8	74	98,8	79,58	77,58	85,8	92,5
Run 3	71,58	84,2	68,8	83,2	96,58	88,8	86,8	94,2	82,8
Mean	64,25	80,73	70,80	77,50	97,39	84,73	82,13	90,30	88,07
Std Dev	8,74	3,50	2,00	4,98	1,22	4,70	4,61	4,23	4,90

Magnesium(%)

DD%	33,93	73,05	60,82	61,94	95,97	82,92	79,92	90,17	85,55
Membrane	PES 1	PES 2	PES 3	PES 4	PES 5	PES 6	PES 7	PES 8	PES9
Run 1	60,25	78,58	67,58	75,58	98,58	86,58	80,58	89,58	87,98
Run 2	53,58	82,58	62,58	79,58	97,58	83,58	84,58	91,58	90,2
Run 3	65,58	75	75,58	73,58	92,58	80,25	76,58	84,58	83,25
Mean	59,80	78,72	68,58	76,25	96,25	83,47	80,58	88,58	87,14
Std Dev	6,01	3,79	6,56	3,06	3,21	3,17	4,00	3,61	3,55

Calcium(%)

DD%	33,93	73,05	60,82	61,94	95,97	82,92	79,92	90,17	85,55
Membrane	PES 1	PES 2	PES 3	PES 4	PES 5	PES 6	PES 7	PES 8	PES9
Run 1	55,58	75,58	61,58	77,58	92,58	84,58	75,58	87,89	85,58
Run 2	65,58	65,58	74,89	70,89	96,58	80,89	79,89	86,58	80,89
Run 3	48,58	78,85	58,59	72,89	96,56	80,58	78,58	83,58	88,69
Mean	56,58	73,34	65,02	73,79	95,24	82,02	78,02	86,02	85,05
Std Dev	8,54	6,91	8,68	3,43	2,30	2,23	2,21	2,21	3,93

Sulphates(%)

DD%	33,93	73,05	60,82	61,94		95,97	82,92	79,92	90,17	85,55
Membrane	PES 1	PES 2	PES 3	PES 4	PES 5	PES 6	PES 7	PES 8	PES9	
Run 1	45,58	65,51	50,25	60,45	80,25	74,58	69,58	77,9	73,89	
Run 2	40,89	60,58	46,58	64,56	84,2	70,89	63,59	81,58	79,52	
Run 3	50,12	69,58	55,58	55,58	76,58	78,89	75	73,58	69	
Mean	45,53	65,22	50,80	60,20	80,34	74,79	69,39	77,69	74,14	
Std Dev	4,62	4,51	4,53	4,50	3,81	4,00	5,71	4,00	5,26	

C2: Effect of chitosan degree of deacetylation on rejection of PES/chitosan membranes

Table C2 – 1: Effect of chitosan degree of deacetylation on rejection of PES/chitosan/PA membranes

Manganese(%)

DD%	33,93	73,05	60,82	61,94	95,97	82,92	79,92	90,17	85,55
Membrane	PES 1	PES 2	PES 3	PES 4	PES 5	PES 6	PES 7	PES 8	PES9
Run 1	75,58	88,58	80,58	86,59	99,99	88,89	87,89	90,4	89,88
Run 2	79,58	86,58	85,59	84,2	96,58	91,28	88,58	96,58	90,58
Run 3	71,58	82,58	80,59	83,58	98,58	88,58	85,58	93,25	92,58
Mean	75,58	85,91	82,25	84,79	98,38	89,58	87,35	93,41	91,01
Std Dev	4,00	3,06	2,89	1,59	1,71	1,48	1,57	3,09	1,40

Iron(%)

Membrane	PES 1	PES 2	PES 3	PES 4	PES 5	PES 6	PES 7	PES 8	PES9
Run 1	65,58	82,8	70,58	78,58	90,58	85,8	82	88,3	86,8
Run 2	58,59	77,58	72,8	73,58	88,59	83,2	76,8	85,5	93,2
Run 3	62,58	72,8	66,58	85,59	90,58	88,5	85,8	92	80,2
Mean	62,25	77,73	69,99	79,25	89,92	85,83	81,53	88,60	86,73
Std Dev	3,51	5,00	3,15	6,03	1,15	2,65	4,52	3,26	6,50

Magnesium(%)

DD%	33,93	73,05	60,82	61,94	95,97	82,92	79,92	90,17	85,55
Membrane	PES 1	PES 2	PES 3	PES 4	PES 5	PES 6	PES 7	PES 8	PES9
Run 1	58,59	71,58	73,58	75,58	90,25	82,58	80,58	86,3	84,58
Run 2	63,58	74,59	63,58	68,58	86,58	84,58	85,89	78,58	80,58
Run 3	59,58	78,58	58,98	78,59	88,58	79,58	75,56	94,58	88,52
Mean	60,58	74,92	65,38	74,25	88,47	82,25	80,68	86,49	84,56
Std Dev	2,64	3,51	7,46	5,14	1,84	2,52	5,17	8,00	3,97

Calcium(%)

DD%	33,93	73,05	60,82	61,94	95,97	82,92	79,92	90,17	85,55
Membrane	PES 1	PES 2	PES 3	PES 4	PES 5	PES 6	PES 7	PES 8	PES9
Run 1	55,59	70,58	60,58	72,59	89,59	77,58	75,59	82,58	77,89
Run 2	65,85	66,58	63,58	66,59	85	76,58	82,59	78,88	84,59
Run 3	50,58	75,58	60,58	64,58	86,59	81,58	78,58	86,58	78,58
Mean	57,34	70,91	61,58	67,92	87,06	78,58	78,92	82,68	80,35
Std Dev	7,78	4,51	1,73	4,17	2,33	2,65	3,51	3,85	3,69

Sulphates(%)

DD%	33,93	73,05	60,82	61,94	95,97	82,92	79,92	90,17	85,55
Membrane	PES 1	PES 2	PES 3	PES 4	PES 5	PES 6	PES 7	PES 8	PES9
Run 1	50,58	68,87	55,58	63,51	83,89	74,58	71,88	78,88	76,58
Run 2	45,89	73,58	51,58	68	87,89	70,58	65,89	83,58	80,58
Run 3	53,89	65,58	58,89	58,88	79,58	78,58	77,58	73,58	73,58
Mean	50,12	69,34	55,35	63,46	83,79	74,58	71,78	78,68	76,91
Std Dev	4,02	4,02	3,66	4,56	4,16	4,00	5,85	5,00	3,51

C3: Effect of feed pH on the rejection of PES/chitosan membranes

Table C3 – 1: Effect of feed pH on rejection of PES/chitosan membranes

Manganese(%)

Feed pH	1st run	2nd Run	3rd Run	Mean	Std Dev
2,40	98,50	90,58	95,58	94,89	4,01
3,50	73,80	66,58	75,58	71,99	4,77
4,70	65,80	61,58	71,58	66,32	5,02
5,50	41,52	37,65	46,58	41,92	4,48
6,80	48,80	55,58	45,58	49,99	5,10
8,60	44,20	39,52	48,58	44,10	4,53

Iron(%)

Feed pH	1st run	2nd Run	3rd Run	Mean	Std Dev
2,40	95,89	90,58	91,25	92,57	2,89
3,50	69,58	62,58	71,58	67,91	4,73
4,70	60,52	57,58	64,58	60,89	3,51
5,50	38,58	33,52	42,58	38,23	4,54
6,80	55,58	52,21	60,96	56,25	4,41
8,60	59,80	63,58	55,58	59,65	4,00

Magnesium (%)

Feed pH	1st run	2nd Run	3rd Run	Mean	Std Dev
2,40	92,85	85,58	85,58	88,00	4,20
3,50	55,60	60,58	51,25	55,81	4,67
4,70	45,63	48,58	41,25	45,15	3,69
5,50	33,50	30,58	36,58	33,55	3,00
6,80	36,58	34,58	32,25	34,47	2,17
8,60	35,89	30,58	42,85	36,44	6,15

Calcium(%)

Feed pH	1st run	2nd Run	3rd Run	Mean	Std Dev
2,40	89,52	85,25	83,52	86,10	3,09
3,50	55,52	53,21	46,52	51,75	4,67
4,70	47,00	43,25	38,52	42,92	4,25
5,50	30,52	28,58	35,85	31,65	3,76
6,80	26,52	30,56	35,52	30,87	4,51
8,60	34,58	30,85	38,58	34,67	3,87

C4: Effect of feed pH on the rejection of PES/chitosan/PA membranes

Table C4 – 1: Effect of feed pH on rejection of PES/chitosan/PA membranes

Manganese(%)

Feed pH	1st run	2nd Run	3rd Run	Mean	Std Dev
2,40	98,50	95,56	97,58	97,21	1,50
3,50	73,80	79,58	70,58	74,65	4,56
4,70	65,80	61,58	71,58	66,32	5,02
5,50	41,52	48,85	39,56	43,31	4,90
6,80	40,58	45,00	50,58	45,39	5,01
8,60	50,58	58,58	53,58	54,25	4,04

Iron(%)

Feed pH	1st run	2nd Run	3rd Run	Mean	Std Dev
2,40	95,89	97,56	90,52	94,66	3,68
3,50	69,58	75,58	70,58	71,91	3,21
4,70	60,52	60,85	68,58	63,32	4,56
5,50	35,56	43,25	39,58	39,46	3,85
6,80	48,80	43,25	50,52	47,52	3,80
8,60	59,80	55,58	65,53	60,30	4,99

Magnesium (%)

Feed pH	1st run	2nd Run	3rd Run	Mean	Std Dev
2,40	92,85	88,58	95,58	92,34	3,53
3,50	58,58	61,58	66,58	62,25	4,04
4,70	50,58	55,58	58,59	54,92	4,05
5,50	38,25	40,25	32,58	37,03	3,98
6,80	30,58	40,00	35,58	35,39	4,71
8,60	40,25	48,59	45,58	44,81	4,22

Calcium(%)

Feed pH	1st run	2nd Run	3rd Run	Mean	Std Dev
2,40	87,58	88,58	95,58	90,58	4,36
3,50	58,60	65,25	53,25	59,03	6,01
4,70	50,36	53,25	45,58	49,73	3,87
5,50	37,58	35,58	30,58	34,58	3,61
6,80	30,58	33,89	30,85	31,77	1,84
8,60	39,69	44,85	35,85	40,13	4,52

Sulphates(%)

Feed pH	1st run	2nd Run	3rd Run	Mean	Std Dev
2,40	50,25	55,52	60,25	55,34	5,00
3,50	66,80	70,58	73,58	70,32	3,40
4,70	74,58	72,50	70,25	72,44	2,17
5,50	38,52	45,58	40,58	41,56	3,63
6,80	83,25	88,52	85,58	85,78	2,64
8,60	85,86	90,85	93,58	90,10	3,91

C5: Effect of feed pH on the flux of PES/chitosan membranes

Table C5 – 1: Effect of feed pH on flux of PES/chitosan membranes

Permeate Flux(l/m^2.hr)

Feed pH	1st run	2nd Run	3rd Run	Mean	Std Dev
2,40	84,25	89,58	93,55	89,13	4,67
3,50	89,89	93,58	90,58	91,35	1,96
4,70	93,25	93,58	96,58	94,47	1,83
5,50	101,00	108,00	105,00	104,67	3,51
6,80	83,89	86,58	88,56	86,34	2,34
8,60	78,58	83,58	81,58	81,25	2,52

C6: Effect of feed pH on the flux of PES/chitosan/PA membranes

Table C6 – 1: Effect of feed pH on flux of PES/chitosan/PA membranes

	Permeate Flux(l/m^2.hr)				
Feed pH	1st run	2nd Run	3rd Run	Mean	Std Dev
2,40	38,59	34,58	36,58	36,58	2,01
3,50	38,59	42,58	35,58	38,92	3,51
4,70	38,59	43,58	40,58	40,92	2,51
5,50	40,89	38,59	43,58	41,02	2,50
6,80	36,58	32,58	35,58	34,91	2,08
8,60	33,58	28,85	38,52	33,65	4,84

C7: Effect of initial concentration and feed pressure for PES/chitosan membrane

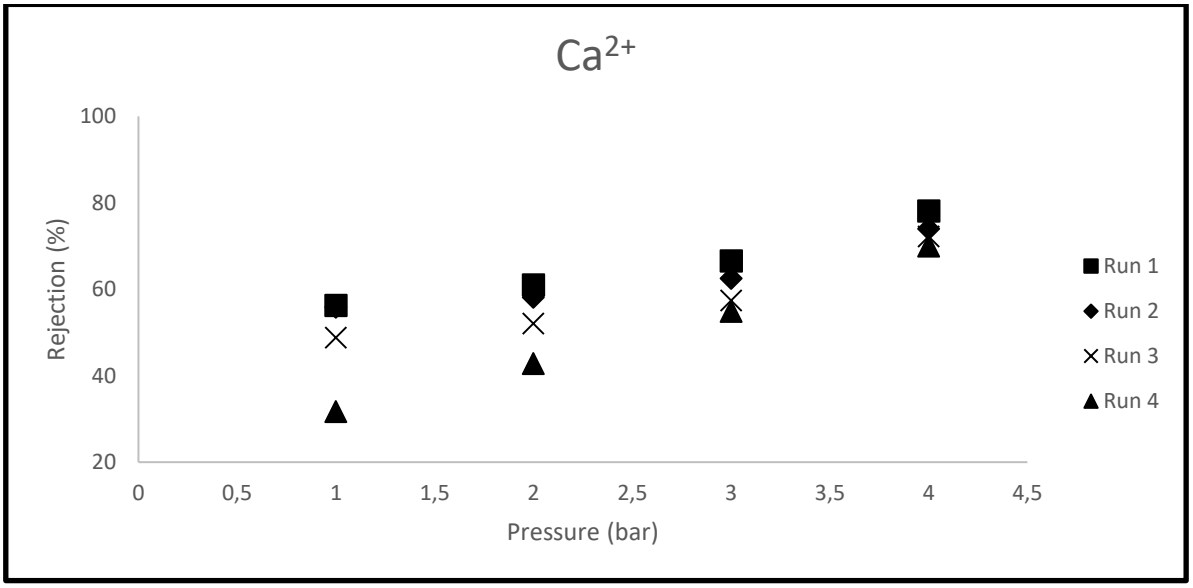


Figure C7 – 1:The effect of feed pressure on the rejection of calcium ion (Ca^{2+}) solution by PES/chitosan membrane

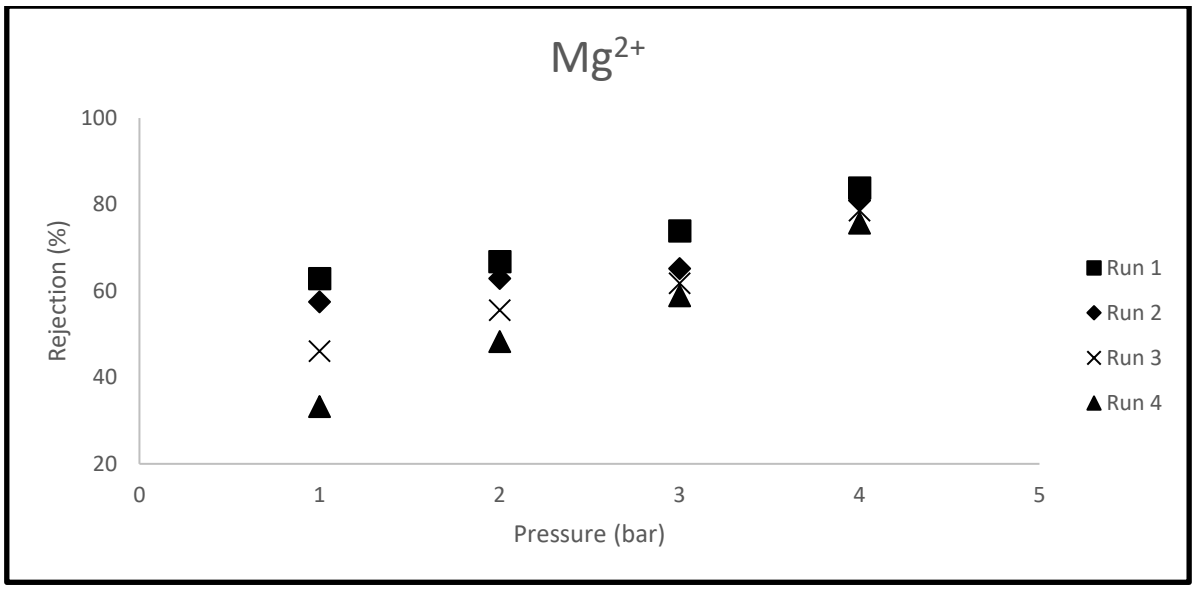


Figure C7 – 2:The effect of feed pressure on the rejection of calcium ion (Mg^{2+}) solution by PES/chitosan membrane

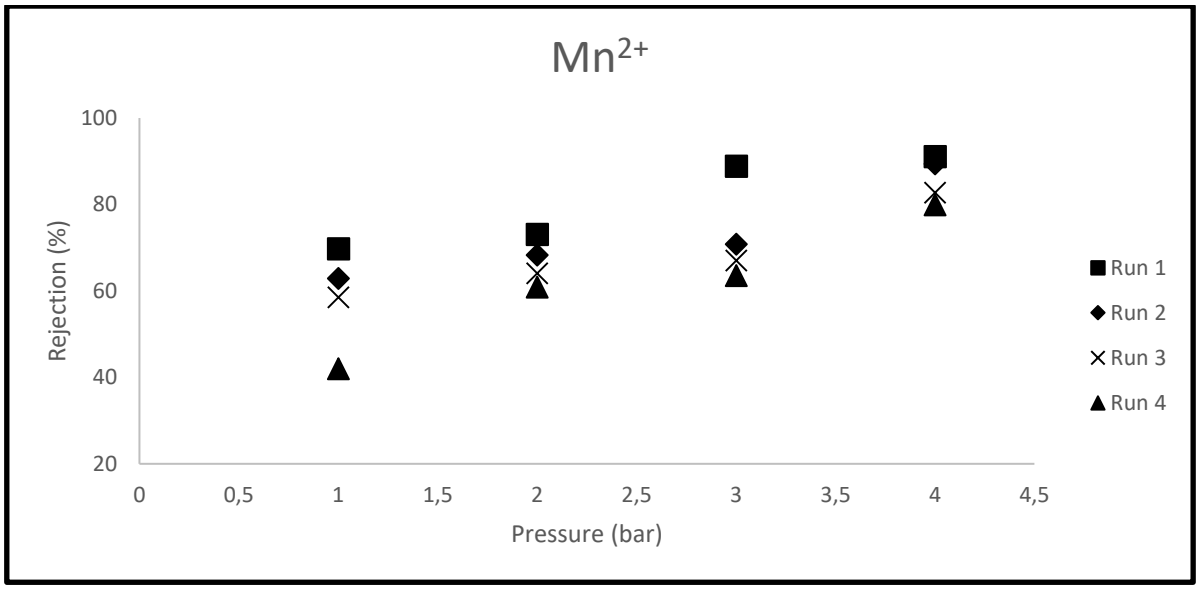


Figure C7 – 3:The effect of feed pressure on the rejection of calcium ion (Mn^{2+}) solution by PES/chitosan membrane

C8: Effect of initial concentration and feed pressure for PES/chitosan/PA membrane

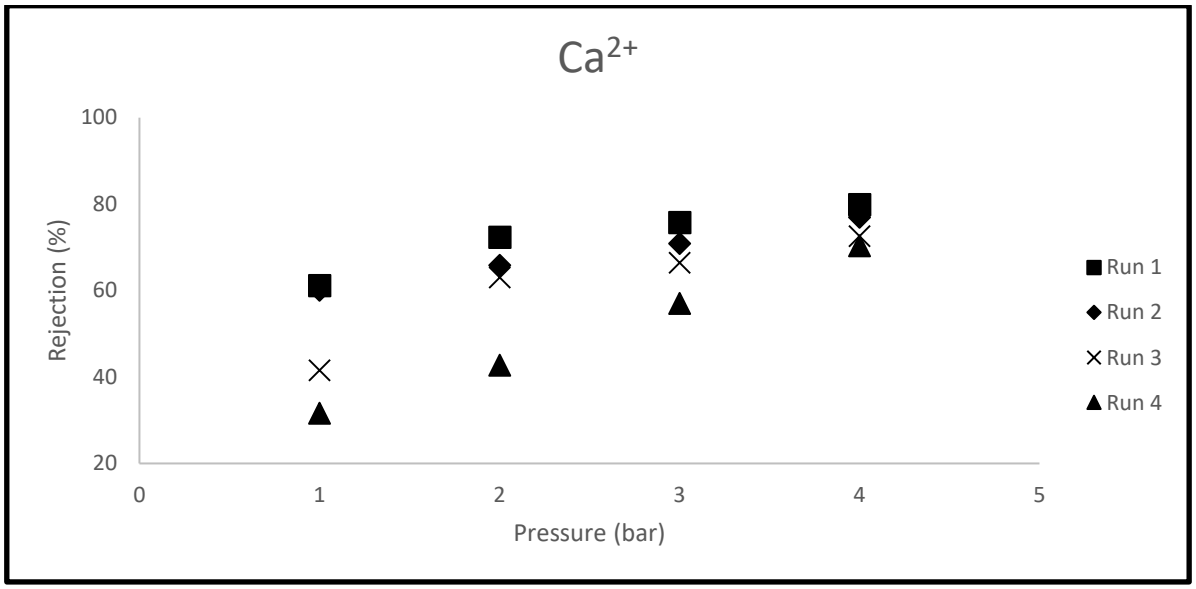


Figure C8 – 1:The effect of feed pressure on the rejection of calcium ion (Ca^{2+}) solution by PES/chitosan/PA membrane

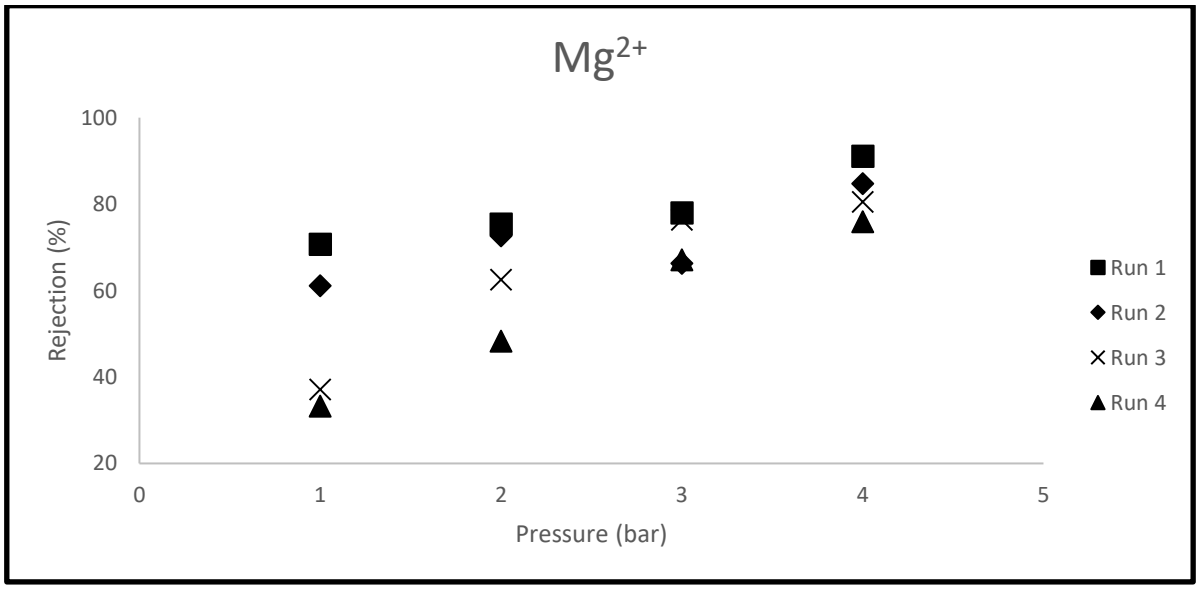


Figure C8 – 2:The effect of feed pressure on the rejection of calcium ion (Mg^{2+}) solution by PES/chitosan/PA membrane

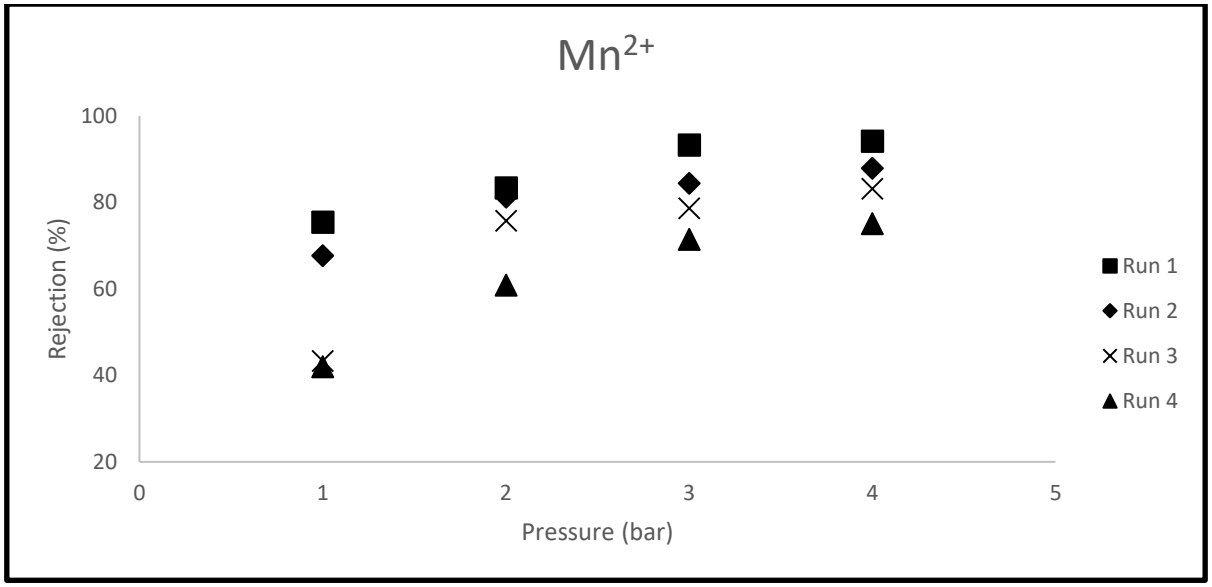


Figure C8 – 3: The effect of feed pressure on the rejection of calcium ion (Mn^{2+}) solution by PES/chitosan/PA membrane

C9: The pumping station in western basin which real industrial AMD was collected



Figure D1-1: Site which real industrial AMD was collected in the western basin, Randfontein

Appendix D: Plagiarism report

SYNTHESIS AND PERFORMANCE OF CHITOSAN-MODIFIED POLYMER COMPOSITE MEMBRANE FOR ACID MINE DRAINAGE TREATMENT MATHABA MJ 1259086

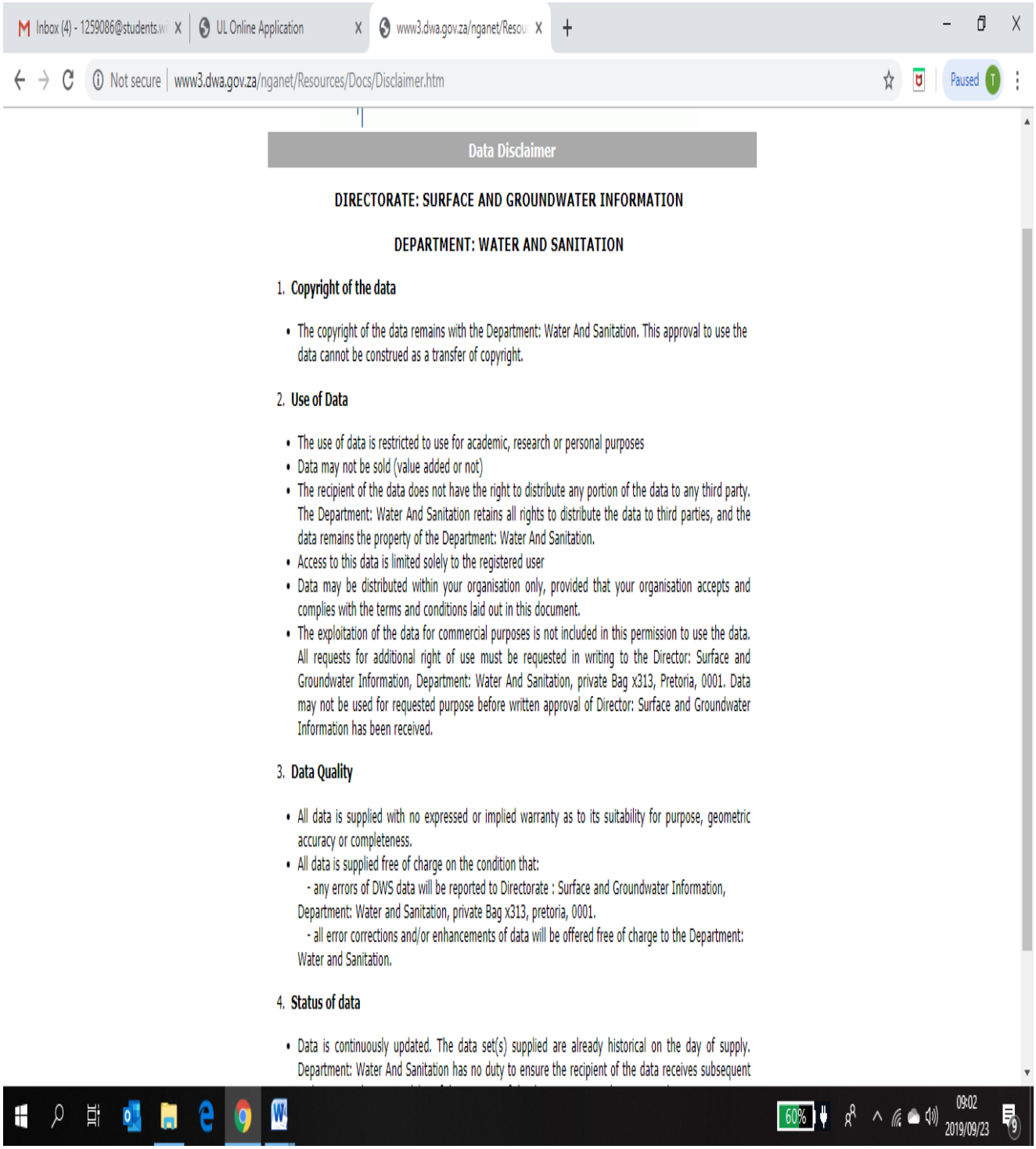
ORIGINALITY REPORT

9%	4%	7%	4%
SIMILARITY INDEX	INTERNET SOURCES	PUBLICATIONS	STUDENT PAPERS

PRIMARY SOURCES

1	Cristina-Veronica Gherasim, Jiří Cuhorka, Petr Mikulášek. "Analysis of lead(II) retention from single salt and binary aqueous solutions by a polyamide nanofiltration membrane: Experimental results and modelling", Journal of Membrane Science, 2013 Publication	<1%
2	link.springer.com Internet Source	<1%
3	Abbas Shockravi, Vahid Vatanpour, Zahra Najjar, Saedeh Bahadori, Ali Javadi. "A new high performance polyamide as an effective additive for modification of antifouling properties and morphology of asymmetric PES blend ultrafiltration membranes", Microporous and Mesoporous Materials, 2017 Publication	<1%
4	Akbari, Ahmad, Zahra Derikvandi, and Sayed Majid Mojallali Rostami. "Influence of chitosan	<1%

Appendix E: Permission to use Material in the thesis


Inbox (4) - 1259086@students.wi
UL Online Application
www3.dwa.gov.za/nganet/Resou
Not secure
www3.dwa.gov.za/nganet/Resources/Docs/Disclaimer.htm
Paused
Data Disclaimer
DIRECTORATE: SURFACE AND GROUNDWATER INFORMATION
DEPARTMENT: WATER AND SANITATION
1. Copyright of the data
• The copyright of the data remains with the Department: Water And Sanitation. This approval to use the data cannot be construed as a transfer of copyright.
2. Use of Data
• The use of data is restricted to use for academic, research or personal purposes
• Data may not be sold (value added or not)
• The recipient of the data does not have the right to distribute any portion of the data to any third party. The Department: Water And Sanitation retains all rights to distribute the data to third parties, and the data remains the property of the Department: Water And Sanitation.
• Access to this data is limited solely to the registered user
• Data may be distributed within your organisation only, provided that your organisation accepts and complies with the terms and conditions laid out in this document.
• The exploitation of the data for commercial purposes is not included in this permission to use the data. All requests for additional right of use must be requested in writing to the Director: Surface and Groundwater Information, Department: Water And Sanitation, private Bag x313, Pretoria, 0001. Data may not be used for requested purpose before written approval of Director: Surface and Groundwater Information has been received.
3. Data Quality
• All data is supplied with no expressed or implied warranty as to its suitability for purpose, geometric accuracy or completeness.
• All data is supplied free of charge on the condition that:
- any errors of DWS data will be reported to Directorate : Surface and Groundwater Information, Department: Water and Sanitation, private Bag x313, pretoria, 0001.
- all error corrections and/or enhancements of data will be offered free of charge to the Department: Water and Sanitation.
4. Status of data
• Data is continuously updated. The data set(s) supplied are already historical on the day of supply. Department: Water And Sanitation has no duty to ensure the recipient of the data receives subsequent
60%
09:02
2019/09/23

ELSEVIER LICENSE
TERMS AND CONDITIONS

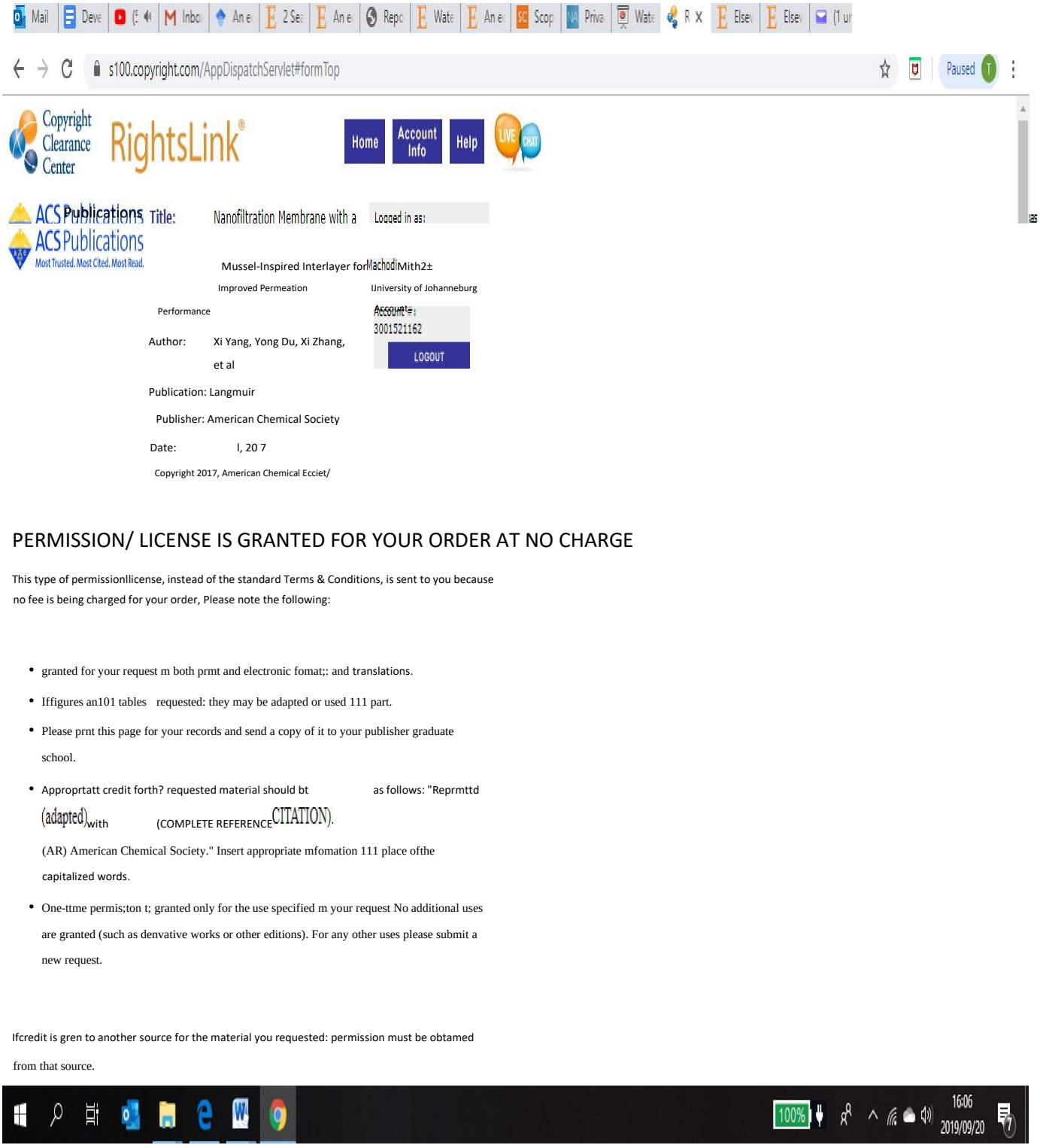
Sep 20, 2019

This Agreement between University of Johanneburg -- Machodi Mathaba ("You") and Elsevier ("Elsevier") consists of your license details and the terms and conditions provided by Elsevier and Copyright Clearance Center.

License Number	4673080623959
License date	Sep 20, 2019
Licensed Content Publisher	Elsevier
Licensed Content Publication	Environmental Pollution
Licensed Content Title	An ecotoxicological screening tool to prioritise acid mine drainage impacted streams for future restoration
Licensed Content Author	P.J. Oberholster,B. Genthe,P. Hobbs,P.H. Cheng,A.R. de Klerk,A.-M. Botha
Licensed Content Date	May 1, 2013
Licensed Content Volume	176
Licensed Content Issue	n/a
Licensed Content Pages	10
Start Page	244
End Page	253
Type of Use	reuse in a thesis/dissertation
Portion	figures/tables/illustrations
Number of figures/tables/illustrations	2
Format	both print and electronic
Are you the author of this Elsevier article?	No
Will you be translating?	No
Original figure numbers	Figure 1,2
Title of your thesis/dissertation	Synthesis and Evaluation of Chitosan-Modified Polymer Composite Membrane for Acid Mine Drainage Treatment
Expected completion date	Nov 2019
Estimated size (number of pages)	298
Requestor Location	University of Johanneburg Unit 92 Montrose avenue Northgate Johannesburg, Gauteng 2162 South Africa Attn: Machodi Mathaba
Publisher Tax ID	ZA 4110266048
Total	0.00 USD
Terms and Conditions	

INTRODUCTION

1. The publisher for this copyrighted material is Elsevier. By clicking "accept" in connection with completing this licensing transaction, you agree that the following terms and conditions


s100.copyright.com/AppDispatchServlet#formTop
Paused
Copyright Clearance Center
RightsLink
Home
Account Info
Help
LIVE CHAT
ACS Publications
Most Trusted. Most Cited. Most Read.
Title:
Nanofiltration Membrane with a Mussel-Inspired Interlayer for Improved Permeation Performance
Logged in as:
Machodi Mith2±
University of Johanneburg
Account #:
3001521162
LOGOUT
Author: Xi Yang, Yong Du, Xi Zhang, et al
Publication: Langmuir
Publisher: American Chemical Society
Date: l, 20 7
Copyright 2017, American Chemical Ecciet/
PERMISSION/ LICENSE IS GRANTED FOR YOUR ORDER AT NO CHARGE
This type of permissionllicense, instead of the standard Terms & Conditions, is sent to you because no fee is being charged for your order, Please note the following:
granted for your request m both prmt and electronic fomat;: and translations.
Iffigures an101 tables requested: they may be adapted or used 111 part.
Please prnt this page for your records and send a copy of it to your publisher graduate school.
Approprtatt credit forth? requested material should bt as follows: "Reprmttd (adapted)with (COMPLETE REFERENCECITATION). (AR) American Chemical Society." Insert appropriate mfomation 111 place ofthe capitalized words.
One-ttme permis;ton t; granted only for the use specified m your request No additional uses are granted (such as denvative works or other editions). For any other uses please submit a new request.
Ifcredit is gren to another source for the material you requested: permission must be obtamed from that source.
100%
16:06
2019/09/20

ELSEVIER LICENSE
TERMS AND CONDITIONS

Sep 20, 2019

This Agreement between University of Johanneburg -- Machodi Mathaba ("You") and Elsevier ("Elsevier") consists of your license details and the terms and conditions provided by Elsevier and Copyright Clearance Center.

License Number	4673100294323
License date	Sep 20, 2019
Licensed Content Publisher	Elsevier
Licensed Content Publication	Journal of Membrane Science
Licensed Content Title	Impact of chemical cleaning on properties and functioning of polyethersulfone membranes
Licensed Content Author	Elizabeth Arkhangelsky,Denis Kuzmenko,Vitaly Gitis
Licensed Content Date	Nov 15, 2007
Licensed Content Volume	305
Licensed Content Issue	1-2
Licensed Content Pages	9
Start Page	176
End Page	184
Type of Use	reuse in a thesis/dissertation
Intended publisher of new work	other
Portion	figures/tables/illustrations
Number of figures/tables/illustrations	1
Format	both print and electronic
Are you the author of this Elsevier article?	No
Will you be translating?	No
Original figure numbers	Figure 1
Title of your thesis/dissertation	Synthesis and Evaluation of Chitosan-Modified Polymer Composite Membrane for Acid Mine Drainage Treatment
Expected completion date	Nov 2019
Estimated size (number of pages)	298
Requestor Location	University of Johanneburg Unit 92 Montrose avenue Northgate Johannesburg, Gauteng 2162 South Africa Attn: Machodi Mathaba
Publisher Tax ID	ZA 4110266048
Total	0.00 USD
Terms and Conditions	

INTRODUCTION

ELSEVIER LICENSE
TERMS AND CONDITIONS

Sep 20, 2019

This Agreement between University of Johanneburg -- Machodi Mathaba ("You") and Elsevier ("Elsevier") consists of your license details and the terms and conditions provided by Elsevier and Copyright Clearance Center.

License Number	4673160058313
License date	Sep 20, 2019
Licensed Content Publisher	Elsevier
Licensed Content Publication	International Journal of Biological Macromolecules
Licensed Content Title	Chitosan-based nanomaterials: A state-of-the-art review
Licensed Content Author	Sudheesh K. Shukla,Ajay K. Mishra,Omotayo A. Arotiba,Bhekie B. Mamba
Licensed Content Date	Aug 1, 2013
Licensed Content Volume	59
Licensed Content Issue	n/a
Licensed Content Pages	13
Start Page	46
End Page	58
Type of Use	reuse in a thesis/dissertation
Intended publisher of new work	other
Portion	figures/tables/illustrations
Number of figures/tables/illustrations	1
Format	both print and electronic
Are you the author of this Elsevier article?	No
Will you be translating?	No
Original figure numbers	Figure 1
Title of your thesis/dissertation	Synthesis and Evaluation of Chitosan-Modified Polymer Composite Membrane for Acid Mine Drainage Treatment
Expected completion date	Nov 2019
Estimated size (number of pages)	298
Requestor Location	University of Johanneburg Unit 92 Montrose avenue Northgate Johannesburg, Gauteng 2162 South Africa Attn: Machodi Mathaba
Publisher Tax ID	ZA 4110266048
Total	0.00 USD
Terms and Conditions	

INTRODUCTION

ELSEVIER LICENSE
TERMS AND CONDITIONS

Sep 20, 2019

This Agreement between University of Johanneburg -- Machodi Mathaba ("You") and Elsevier ("Elsevier") consists of your license details and the terms and conditions provided by Elsevier and Copyright Clearance Center.

License Number	4673160314384
License date	Sep 20, 2019
Licensed Content Publisher	Elsevier
Licensed Content Publication	Journal of Industrial and Engineering Chemistry
Licensed Content Title	Influence of chitosan coating on the separation performance, morphology and anti-fouling properties of the polyamide nanofiltration membranes
Licensed Content Author	Ahmad Akbari,Zahra Derikvandi,Sayed Majid Mojallali Rostami
Licensed Content Date	Aug 25, 2015
Licensed Content Volume	28
Licensed Content Issue	n/a
Licensed Content Pages	9
Start Page	268
End Page	276
Type of Use	reuse in a thesis/dissertation
Intended publisher of new work	other
Portion	figures/tables/illustrations
Number of figures/tables/illustrations	1
Format	both print and electronic
Are you the author of this Elsevier article?	No
Will you be translating?	No
Original figure numbers	Figure 3
Title of your thesis/dissertation	Synthesis and Evaluation of Chitosan-Modified Polymer Composite Membrane for Acid Mine Drainage Treatment
Expected completion date	Nov 2019
Estimated size (number of pages)	298
Requestor Location	University of Johanneburg Unit 92 Montrose avenue Northgate Johannesburg, Gauteng 2162 South Africa Attn: Machodi Mathaba
Publisher Tax ID	ZA 4110266048
Total	0.00 USD
Terms and Conditions	

INTRODUCTION

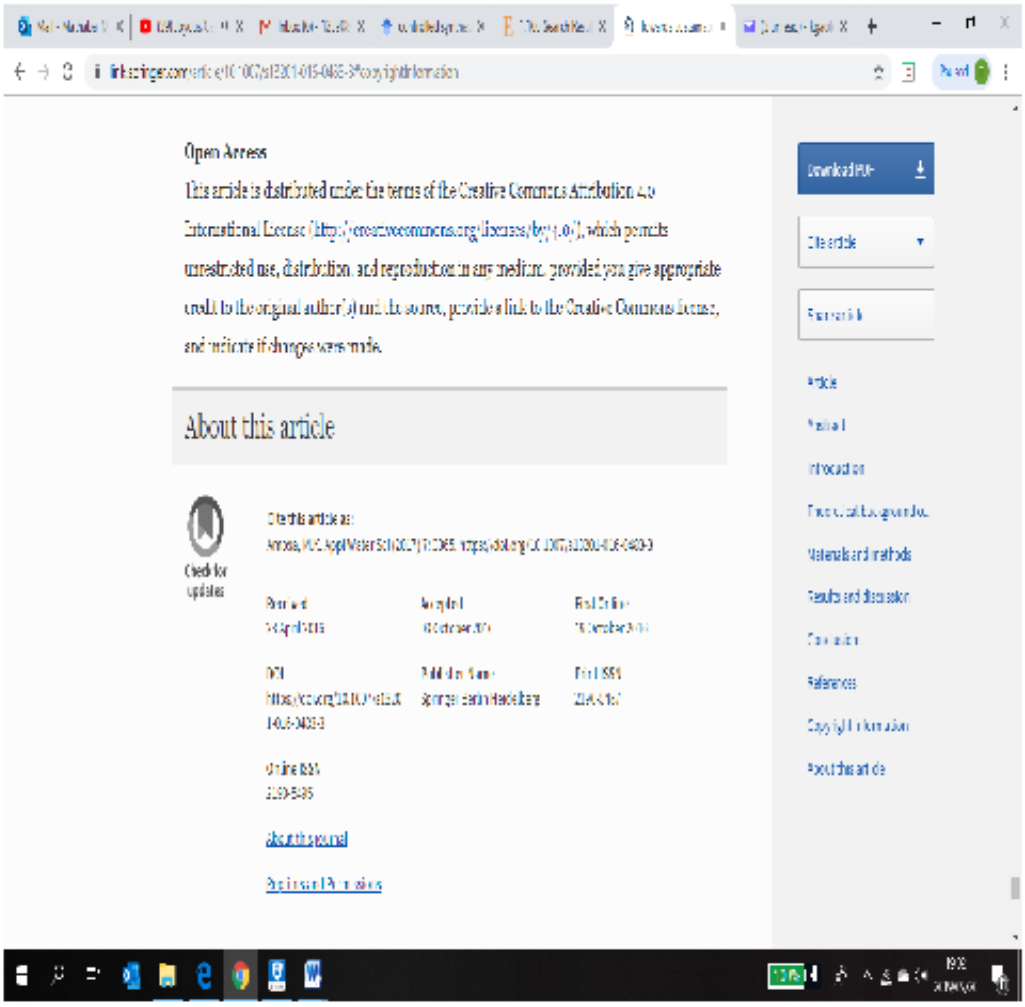
ELSEVIER LICENSE
TERMS AND CONDITIONS

Sep 20, 2019

This Agreement between University of Johanneburg -- Machodi Mathaba ("You") and Elsevier ("Elsevier") consists of your license details and the terms and conditions provided by Elsevier and Copyright Clearance Center.

License Number	4673160743090
License date	Sep 20, 2019
Licensed Content Publisher	Elsevier
Licensed Content Publication	Journal of Membrane Science
Licensed Content Title	Controlled synthesis of high performance polyamide membrane with thin dense layer for water desalination
Licensed Content Author	Chunlong Kong,Masakoto Kanezashi,Tetsuya Yamomoto,Takuji Shintani,Toshinori Tsuru
Licensed Content Date	Oct 15, 2010
Licensed Content Volume	362
Licensed Content Issue	1-2
Licensed Content Pages	5
Start Page	76
End Page	80
Type of Use	reuse in a thesis/dissertation
Intended publisher of new work	other
Portion	figures/tables/illustrations
Number of figures/tables/illustrations	1
Format	both print and electronic
Are you the author of this Elsevier article?	No
Will you be translating?	No
Original figure numbers	Figure 1
Title of your thesis/dissertation	Synthesis and Evaluation of Chitosan-Modified Polymer Composite Membrane for Acid Mine Drainage Treatment
Expected completion date	Nov 2019
Estimated size (number of pages)	298
Requestor Location	University of Johanneburg Unit 92 Montrose avenue Northgate Johannesburg, Gauteng 2162 South Africa Attn: Machodi Mathaba
Publisher Tax ID	ZA 4110266048
Total	0.00 USD
Terms and Conditions	

INTRODUCTION


Open Access
This article is distributed under the terms of the Creative Commons Attribution 4.0 International License (http://creativecommons.org/licenses/by/4.0/), which permits unrestricted use, distribution, and reproduction in any medium, provided you give appropriate credit to the original author(s) and the source, provide a link to the Creative Commons license, and indicate if changes were made.
About this article
Check for updates
Download PDF
Cite article
Article
Introduction
Materials and methods
Results and discussion
Conclusion
References
Copyright information
About this article

Appendix F: Publications

10 Sodalite- and Chitosan-Based Composite Membrane Materials for Treatment of Metal-Containing Wastewater in Mining Operations

Machodi Mathaba and Michael O. Daramola

CONTENTS

10.1 Introduction 169
10.2 Prevention of Formation of AMD and Treatment of Metal-Containing Wastewater 171
10.3 Membranes for Treatment of Metal-Containing Wastewater in Mining Operations 172
10.3.1 Organic and Inorganic Membranes 172
10.3.2 Mixed-Matrix Membranes 174
10.3.2.1 Chitosan-Based Composite Materials 176
10.3.2.2 Sodalite-Based MMMs 179
10.4 Conclusions and Future Outlook 183
References 185

10.1 INTRODUCTION

The major environmental challenge associated with mining industry is acid mine drainage (AMD), which forms when sulfide rocks are exposed to air and water for prolonged periods (Nordstrom et al., 2015). The formation of AMD is a natural process, but reaction caused by exposing sulfide-containing rocks to the environment through mining operations are often catalyzed by bacterial activity. The natural process of AMD formation takes close to 15 years in the absence of bacteria for ferric iron to produce acid, but the presence of bacteria shortens the reaction time down to 8 min (Metesh et al., 1998). Typical characteristics of AMD are very low pH (often from 3 to 2) and elevated concentration of metals and sulfates (Meschke et al., 2015). If left untreated, AMD has a significant negative environmental impact, including the mineralization of affected areas and acidification of receiving ground and surface waters. The solubility of transition metals is greater in low pH media, so AMD carries with it a high concentration of metals such as Al, As, and Mg and other transition metals such as Cu, Zn, Pb, Co, Mn, and Cd depending on the host rock (Hallberg, 2010). It uncontrollably enters the aquatic environment and poses a threat to humans, domesticated animals, and the ecosystem (Durand, 2012). According to Ford (2003), there are four commonly-accepted chemical reactions that represent the chemistry of pyrite weathering to form AMD (Equations 10.1 through 10.4); Equation 10.5 represents the oxidation of pyrite by unhydrolyzed ferric iron.

SCIENTIFIC REPORTS
nature research

OPEN

Synthesis and performance evaluation of PES/chitosan membranes coated with polyamide for acid mine drainage treatment

Mathaba J. Machodi & Michael O. Daramola*

In this article, performance evaluation of PES membrane infused with chitosan and coated with polyamide layer for treatment of acid mine drainage (AMD) is reported. PES/chitosan membranes were fabricated by varying chitosan concentration (0, 0.5, 0.75 and 1 wt%) using phase inversion method. PES/chitosan membranes were coated with polyamide (PA) via co-solvent assisted interfacial polymerization technique (CAIP). Scanning electron microscopy (SEM) and contact angle analysis show that chitosan and polyamide could enhance permeability without affecting rejection of the membrane. The permeability was improved with increasing chitosan content. Atomic absorption spectroscopy (AAS) was used to quantitatively determine cations in the permeate and the sulphate ions were analysed using ultraviolet and visible (UV-VIS) spectrophotometer. Pure water flux of PES/PA membrane was significantly improved from 56 to 93 l/m^2.hr with 1 wt% chitosan addition. Cation rejection (90.4, 88.3, 89.3 and 75.7% for Mn^{2+},Fe^{2+}, Mg^{2+} and Ca^{2+}, respectively) was observed to be higher than anion rejection (56.33% for SO_4^{2-}), when chitosan content was 0.75 wt%. These results indicate that the positively charged membranes under acidic condition had strong repulsive forces with the cations than attractions forces with anions. Polyethersulphone membrane modified with chitosan and coated with polyamide layer displayed potential for application in treatment of AMD.

Membrane technology application and research for treatment of wastewater has been growing rapidly due to global environmental concerns and the need for high quality water demand[1]. Amongst other polymeric membranes, polyethersulphone (PES) and polysulphone (PSf) have gained significant progress in acid mine drainage (AMD) treatment because of their high chemical and thermal resistance, mechanical stability in hot and wet conditions, and high permeability[2]. Although PES exhibits higher degree of hydrophilicity compared to PSf, its inherent hydrophobic character results in serious membrane fouling which leads to deterioration in permeation flux, shortened membrane lifespan and unpredictable separation efficiency[3]. The inevitable normal significance of semi-permeability and selectivity during membrane operation is the accumulation of particles and solutes on the membrane surface, within the matrix and porous structure[4]. The accumulated molecules form a layer on the surface of the membrane which hinders solvent movement across the membrane and generates osmotic back pressure which diminishes the effective transmembrane pressure (TMP) of the system[5]. Particulates, ions, macromolecules and biological substances are common foulants causing trouble during membrane operation. Organic matter is the most challenging and causes both reversible and irreversible fouling because it is common in natural water[6]. The relative resistance to cleaning is a distinguishing factor between reversible and irreversible fouling. Reversible fouling is the type that can be cleaned, and irreversible fouling remains even after cleaning. Irreversible fouling that remains after hydraulic cleaning technique is termed hydraulically irreversible fouling and that which remain after chemical cleaning is called chemically irreversible fouling[7].

Several interventions have been used to increase the hydrophilicity of PES during wastewater treatment to avoid quick membrane replacement caused by irreversible surface fouling and internal fouling[8]. Pure polymeric and modified membranes that feature low fouling character and ability to restore water flux after cleaning would lower the replacement and maintenance cost of the technology during wastewater treatment. One approach to creating such membranes is blending and coating PES membranes with hydrophilic polymers[2]. The advantage of

School of Chemical and Metallurgical Engineering, Faculty of Engineering and the Built Environment, University of the Witwatersrand, Private Bag X3, Wits, 2050, Johannesburg, South Africa. *email: Michael.Daramola@wits.ac.za

Water SA 44(1) 114–122 / Jan 2018
https://doi.org/10.4314/wsa.v44i1.13

Research paper

Synthesis of PES and PES/chitosan membranes for synthetic acid mine drainage treatment

Mathebe J Machodi* and Michael O Daramola

School of Chemical and Metallurgical Engineering, Faculty of Engineering and the Built Environment, University of the Witwatersrand, Private Bag X3, Wits 2050, Johannesburg, South Africa

In this study, chitosan was synthesized from chitin and used to modify polyethersulphone (PES) membrane prepared by the phase inversion method. PES membrane was blended with various concentrations of chitosan to produce PES/0.5 wt% chitosan, PES/0.75 wt% chitosan and PES/1 wt% chitosan membranes. The membranes were tested for metal and sulphate removal from acid mine drainage (AMD). The fabricated membranes were characterized using scanning electron microscopy (SEM), contact angle analyser, Fourier transform infrared (FTIR), porosity determination and pure water flux measurements. Separation performance was conducted on a dead-end filtration cell and metal ions were determined by atomic absorption spectroscopy (AAS), and ultraviolet and visible (UV-vis) spectrophotometry was used for sulphates. Pure water flux of the pristine PES membrane increased from 102 $Lm^{-2}h^{-1}$ to 109 $Lm^{-2}h^{-1}$ and 133 $Lm^{-2}h^{-1}$ for PES/0.5 wt% and PES/0.75 wt%, respectively. Further addition of chitosan to 1 wt% created a dense structure on the membrane surface, thereby reducing the flux to 120 $Lm^{-2}h^{-1}$. The rejection of cations and sulphate ions significantly improved for chitosan-modified membranes due to the creation of adsorptive and/or repulsive sites on the chitosan biopolymer as a result of amine group protonation. The results reveal that chitosan has potential to improve performance of PES membranes as a hydrophilic agent during AMD treatment.

CORRESPONDENCE
Michael O Daramola

EMAIL
Michael.Daramola@wits.ac.za

DATES
Received: 14 March 2019
Accepted: 13 November 2019

KEYWORDS
polyethersulphone
acid mine drainage
chitin
membrane flux

COPYRIGHT
© The Author(s)
Published under a Creative Commons Attribution 4.0 International License (CC BY 4.0)

INTRODUCTION

The discharge of acidic wastewater from active and abandoned mines pose significant water quality and environmental problems globally (Lennox et al., 2016). During mining operations, sulphide-containing rocks such as pyrites (FeS_2) get exposed to water, air and microbial activities, which makes them vulnerable to oxidation. Pyrite will react with oxygen and water to produce acidic discharge which acts as a leaching agent of toxic metals and trace elements available in the host rocks (Kefeni et al., 2018). Equations 1 to 4 show the formation of acid drainage in the presence of air (oxygen), water and bacteria (Bosman et al., 2017; Ohimain et al., 2017; Kaur et al., 2018). The pyrite (FeS_2) oxidation releases hydrogen, sulphate and ferrous irons (Fe^{2+}) (Eq. 1). Further oxidation of ferrous iron (Fe^{2+}) releases ferric iron (Fe^{3+}) (Eq. 2) which either acts as an oxidizing agent and oxidizes more pyrite (Eq. 3) or will precipitate as iron hydroxide ($Fe(OH)_3$) (Eq. 4).

$$2FeS_{2(s)} + 2H_2O_{(l)} + 7O_{2(g)} \rightarrow 2Fe^{2+}_{(aq)} + 4SO_4^{2-}{}_{(aq)} + 4H^+_{(aq)} \quad (1)$$

$$2Fe^{2+}_{(aq)} + 2H^+_{(aq)} + \tfrac{1}{2}O_{2(g)} \rightarrow 2Fe^{3+}_{(aq)} + H_2O_{(l)} \quad (2)$$

$$FeS_{2(s)} + 14Fe^{3+}_{(aq)} + 8H_2O_{(l)} \rightarrow 15Fe^{2+}_{(aq)} + 2SO_4^{2-}{}_{(aq)} + 16H^+_{(aq)} \quad (3)$$

$$Fe^{3+}_{(aq)} + 3H_2O_{(l)} \rightarrow Fe(OH)_{3(s)} + 3H^+_{(aq)} \quad (4)$$

Membrane separation process (MSP) has been successfully applied to treat AMD due to the high salt and metal retention capacity of membranes (Ritchie and Bladergroen, 2008; Gohe et al., 2018; Rhemrich and Phillip, 2011; Daramola et al., 2015). Nanofiltration (NF) membrane is the most preferred because of its low required pressure and energy consumption, high selectivity and permeate flux. NF membranes which are intermediate membranes between ultrafiltration (UF) and reverse osmosis (RO) membranes have higher permitted flux compared to other pressure-driven membranes and can retain dissolved molecules with molecular weight greater than 200 to 300 $gmol^{-1}$, as well as inorganic ions through electrostatic interaction between membrane charge and the ions combined with size exclusion (Carvalho et al., 2011). A study by Aguiar et al. (2016) showed NF membranes to be more suitable for AMD treatment than RO which had high permeate flux and solute rejection. Most commercial NF membranes available in the market are constructed using polyethersulphone (PES) material prepared through phase inversion methods (Zhao et al., 2013).

A significant challenge confronting NF membrane application is fouling, which is caused by suspended or dissolved organic and/or inorganic matter migrating from the liquid phase and forming deposits on the membrane surface, at the pore openings or within the membrane matrix (Aguiar et al., 2016). For economically feasible operation, membrane fouling must be controlled since it reduces permeability, increases energy consumption and shortens membrane lifespan. Although membrane fouling is considered inevitable, the rate and extent is highly impacted by membrane properties, feed characteristics and operational conditions (Wei et al., 2010). Although PES and PSF-based membranes have been widely used, the main disadvantage is related to its

Effect of chitosan's degree of deacetylation on the performance of PES membrane infused with chitosan

MJ. Mathaba[1,2], MO Daramola[1,*]

[1]School of Chemical and Metallurgical Engineering, Faculty of Engineering and the Built Environment, University of the Witwatersrand, Private Bag X3, Wits 2050, Johannesburg, South Africa.

[2]Department of Chemical Engineering, University of Johannesburg, P.O. Box 17011, Doornfontein 2028, Johannesburg, South Africa

*Corresponding author: Michael.Daramola@wits.ac.za

Abstract

This study focuses on the treatment of acid mine drainage using polyethersulphone membrane infused with chitosan having various degree of deacetylation. Chitosan was produced from chitin using varying synthesis process conditions and was infused within polyethersulphone membrane. The results obtained showed that chitosan having high degree of deacetylation was achieved with temperature of 100 °C and NaOH concentration of 40 wt%. Increasing the temperature above 100 °C started degrading the already formed or exposed amine groups, thus reducing the DD of the chitosan sample. The contact angle and porosity analysis indicated that the hydrophilic nature of the membrane was enhanced with increasing chitosan's degree of deacetylation. The performance of the membranes was conducted on a Dead-end filtration cell using synthetic acid mine drainage. The results showed that the flux and rejection of the membrane was enhanced with increasing degree of deacetylation. PES 5 and PES 1 were blended with chitosan having the highest (95.97%) and lowest (33.93%) degree of deacetylation, respectively. PES 5 reported pure water flux of 123 l/m^2.hr and PES 1 was recorded as 104 l/m^2.hr. Similarly, the rejection of the membrane was improved with increasing chitosan's degree of deacetylation. PES 5 had higher rejection and PES 1 had the least rejection. Maximum rejection for the contaminants was determined as 98.05, 97.39, 96.25, 95.24 and 80.34% for Mn^{2+}, Fe^{2+}, Mg^{2+} and Ca^{2+} and SO_4^{2-},respectively. The results obtained showed that chitosan's degree of deacetylation has a positive effect on the performance of polyethersulphone membrane during the treatment of acid mine drainage.

Keywords: polyethersulphone membrane, chitosan, degree of deacetylation, hydrophilic, acid mine drainage

1. Introduction

Membrane technology has gained significant attention for application in wastewater treatment due to high quality water requirements and environmental concerns. Membrane technology has emerged as a proven alternative to conventional processes due to its high separation efficiency and inexpensiveness [1]. However, during operation, membrane fouling restricts full performance of the membrane due to accumulation and deposition of contaminants on the membrane surface and within the pores. Numerous studies deduced that membrane fouling is directly related to hydrophobicity [2,3]. Therefore, hydrophilic modification of membranes during wastewater treatment is essential in membrane science and technology [4]. Natural or synthetic polymeric materials have attracted vast attention to be employed as membrane materials. Polymeric materials are attractive due to their non-toxic, and biodegradable properties and they cost effective [5]. Polyethersulphone (PES) has emerged as one of the most important polymeric material due to its high thermal and chemical resistance and mechanical stability [6].The main disadvantage characterising PES and PES based membranes is related to its hydrophobic character generated by the sulfonyl group linking the two phenylene rings [7]. Several alterations such as chemical, physical and surface modification and blending have been researched to improve the hydrophilic property of PES membranes [8]. The ultimate aim of membrane modification with hydrophilic agents is to localize the hydrophilic material on the membrane surface and within the pores to positively influence membrane permselectivity and reduce fouling [4].

This study opted to blend hydrophilic chitosan within the PES membrane matrix to not only modify the membrane surface but also inside the pores. Chitosan is obtained from chitin which is a higher molecular weight linear polymer and is the second most abundant natural fiber after cellulose. Chitin is found in many different living organisms such as shellfish, crabs, insects, crustacean shells and arthropods [9].Chitosan is obtained by partial N-deacetylation of chitin and it contains one primary amino and two free hydroxyl functional groups [10].The large number of amino (-NH$_2$) and hydroxyl (-OH) groups which can act as contaminate binding sites makes chitosan attractive as it will improve both the membrane's hydrophilic property and permselectivity. Under acidic medium, the amino group gets protonated and attract anions which repel cations through electrostatic repulsion [11].Microporous chitosan/polyethylene glycol mixed matrix membrane was tested by Reiad et al. [12] for the removal of iron and manganese from aqueous solution. The study showed improved iron and manganese rejection by the blend membrane and the authors concluded that its reusable after successful desorption of the rejected metal ions. Boricha and Murthy [13] synthesised and compared PES membrane coated chitosan and acrylonitrile butadiene styrene. It was found that increased chitosan content had a positive effect on the amorphous nature of the membrane.

Chitosan is obtained from chitin through a deacetylation process, that is treating chitin with a strong alkaline solution. The most important parameter characterizing chitosan sample is the degree of deacetylation [14]. Chitosan which is a principal derivative of chitin refers to partially or fully deacetylated chitin, which means the degree of acetylation is around or lower than 50%. Also means the degree of deacetylation is around or higher than 50%. Degree of deacetylation influences the physical, biological and chemical properties of the synthesised chitosan. Degree of deacetylation determines the free amino groups exposed due to the removal of the acetyl groups from the molecular chain of chitin, hence deacetylation name. It is a